

On Continuous Fractional Calculus and its Application to Epidemic Models

*Thesis submitted to the
Jadavpur University, Kolkata
for the award of the degree of*

DOCTOR OF PHILOSOPHY (SCIENCE)



Submitted by

Subrata Paul

(Index No. 10/22/Maths./27)

Supervisor:

Dr. Prakash Chandra Mali

**Professor, Department of Mathematics
Jadavpur University, Kolkata-700032, India**

Co-supervisor:

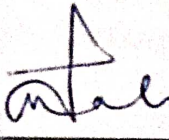
Dr. Banamali Roy

**Associate Professor, Department of Mathematics
Bangabasi Evening College, Kolkata-700009, India**

This thesis is dedicated to my beloved daughter Samriddhi

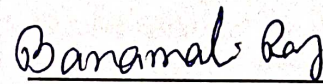
Certificate from the supervisors

This is to certify that the thesis entitled "On Continuous Fractional Calculus and its Application to Epidemic Models" submitted by Sri Subrata Paul who got his name registered on 10th February, 2022 (Index No. 10/22/Maths./27) for the award of Ph.D. (Science) degree of Jadavpur University, is absolutely based upon his own work under the supervision of Prof. (Dr.) Prakash Chandra Mali and Dr. Banamali Roy and that neither this thesis nor a part of it has been submitted for any degree/diploma or any academic award anywhere before.

 13.3.2024

Dr. Prakash Chandra Mali
Professor
Department of Mathematics
Jadavpur University
Kolkata – 700032, West Bengal

Professor
DEPARTMENT OF MATHEMATICS
Jadavpur University
Kolkata – 700 032, West Bengal

 13.3.24

Dr. Banamali Roy
Associate Professor
Department of Mathematics
Bangabasi Evening College
Kolkata – 700009, West Bengal

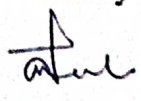
Dr. Banamali Roy
Associate Professor
Dept. of Mathematics
Bangabasi Evening College
Kol - 700 009

Abstract of thesis

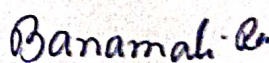
Index No. 10/22/Maths./27

Thesis title: On Continuous Fractional Calculus and its Application to Epidemic Models
Submitted by: Subrata Paul

In this thesis, we have studied the analysis of seven different epidemic models under various conditions. In Chapters 2 – 6, epidemic models of some infectious diseases (COVID-19, Dengue) are analyzed and in Chapter 7 – 8, general epidemic models are studied. In the beginning, the dynamics of COVID-19 transmission is described, using a fractional order $SIQR$ model. To obtain semi-analytic solutions to the model, the Iterative Laplace Transform Method [ILTM] is implemented. Considering COVID-19 cases data in India and Brazil, collected upto 1st August, 2020, the basic reproduction number R_0 is estimated to be 1.7824 and 2.767 respectively. In Chapter 3, a fractional order $SEIR$ model with vaccination has been studied. It has been found that introduction of the vaccination parameter η reduces the reproduction number R_0 . Based on the COVID-19 cases data in India, collected upto 1st August, 2021, the basic reproduction number R_0 without vaccinations estimated to be 3.67 and with vaccination to be 1.55. As is evident from this study that vaccination is an effective method in control and prevention of the COVID-19 disease. Chapter 4 presents a study of an $SEIRV$ epidemic model with optimal control in the context of Caputo fractional derivative of order $0 < \alpha \leq 1$. A comparative study of the model values and real scenario of Brazil starting from 10th April 2021 through 100 days has been performed. It has been observed that the model fits with $\alpha = 0.85$ with realistic data. In Chapter 5, the fractional order $SEIQRD$ compartmental model of COVID-19 is explored with six different categories in the Caputo approach. From 1st of January 2022 to 31st of January 2022, we have compared model values with real data in Italy. This study looked at the many consequences of wearing face masks, and it was discovered that wearing face masks consistently can help reduce the propagation of COVID-19 disease. In Chapter 6, a four compartment host population and a three compartment vector population is considered in a fractional order dengue model in the Caputo sense with a consideration of three control parameters. Two of the control parameters are related to the host population and one is related to the vector population. The fractional order SIR model with a Holling type II saturated incidence rate and treatment rate are explored in Chapter 7 in the Caputo order fractional derivative approach. For $R_0 = 1$ at E_0 the model exhibits a forward bifurcation. In Chapter 8, we analyze a fractional order SIR mathematical model with nonlinear incidence rate of infection as Holling type II and the treatment rate is considered as Monod-Haldane (MH) type. The existence and uniqueness criteria as well as the non-negativity and boundedness have been established. The model's fundamental reproduction number (R_0) was also calculated using the next generation matrix technique. The stability of all proposed model systems at all equilibrium points are demonstrated. The sensitivity analysis, which allows the determination of key parameters in the proposed different models have been carried out. Different numerical methods like Adam-Bashforth-Moulton predictor-corrector, Euler and Taylor's are utilized to approximate the solution to fractional order proposed models. Graphical demonstrations and numerical simulations have been presented using MATLAB. Modeling using fractional-order derivatives is often more efficient than modeling with integer-order derivatives because the option of derivative order gives one more degree of freedom, resulting in a better fit to real-time data with less inaccuracy than the integer-order model.

 13.3.2024

Prof. Prakash Chandra Mali

 13.3.24

Dr. Banamali Roy

 13.3.24

Subrata Paul

Professor
DEPARTMENT OF MATHEMATICS
Jadavpur University
Kolkata - 700 032, West Bengal

Dr. Banamali Roy
Associate Professor
Dept. of Mathematics
Bangabasi Evening College
Kol - 700 009

Acknowledgements

This Ph.D. thesis is a work on "*On Continuous Fractional Calculus and its Application to Epidemic Models*". Without the earnest assistance of many people, it would not have been possible to come to this stage to finish it. Naturally, I am indebted to all of them who stood by me for inspiration, encouragement and persistently pushed me to this venture.

First of all, I have to shower my gratitude and indebtedness to my Ph.D. supervisor **Prof. Prakash Chandra Mali**, Department of Mathematics, Jadavpur University, Kolkata - 700032, West Bengal, India and co-supervisor **Dr. Banamall Roy**, Department of Mathematics, Bangabasi Evening College, Kolkata-700009, West Bengal, India for their guidance as well as encouragement. Their inspiration as well as way of thinking give me a lot of experience not only in research field but also in my personal life.

Likewise, the gratitude and thankfulness go to all the faculty members of Mathematics department of Jadavpur University, namely Prof. Sangik Sinha, Prof. Sujit Kumar Sardar for their support to complete my thesis.

It would be ungrateful if the contribution and insistence of my co-researchers are not acknowledged. In this connection, I want to express my sincere gratitude to my co-researchers Dr. Supriya Mukherjee, Dr. Animesh Mahata, Mr. Balaram Manna, Mr. Ashish Archrya, Mr. Manas Karak and others who provided me a friendly environment in the department to carry out my research work.

My high esteems and gratefulness go to all the members of the Ph.D. Committee for their precious remarks, comments and feedbacks. The necessary assistances that that I have got from the University Authority for successful completion of my Ph.D. work are also acknowledged.

My parents deserve special recognition for their encouragement, intercession and demonstration of the joy of academic endeavor to me. My better half Mrs. Sujata Mandal upholds me constantly and gets me far from any sort of issue and holds my motivation on research work constantly. I also express my deep appreciation to my beloved daughter Samriddhi Paul.

At long last, I want to express my gratitude to the authors of the articles from which I gained a lot of knowledge and used it to write my thesis.

Date: 13/3/24
Place: Kolkata

Subrata Paul
(Subrata Paul) 13.3.24

List of Tables

2.1	The parameters of the model and their descriptions.	17
2.2	In the instance of COVID-19 in India, the estimated parametric values are as follows.	24
2.3	The estimated parametric values are as follows in Brazil.	28
3.1	The parameters of the model and their descriptions.	37
3.2	Estimated values of parameters.	43
4.1	The parameters of the model and their descriptions.	51
4.2	Estimated values of parameters for India.	62
4.3	The estimated parametric values are as follows in Brazil.	67
4.4	Day wise Infected population of Brazil from 10th April, 2021 to 19th July, 2021.	67
5.1	The parameters of the model and their descriptions.	73
5.2	Estimated values of parameters for India.	79
5.3	Numerical simulation of the varying effects of α .	82
5.4	The number of Infected cases in Italy, from 1st January 2022 to 31st January 2022.	84
6.1	Significance of the relevant parameters.	89
6.2	Parameter values for numerical study.	100
6.3	Week wise infected human population of Singapore from 18th week, 2020 to 23rd week, 2020.	107
6.4	Sensitivity indices of R_0 versus model parameters.	108
7.1	Significance of the relevant parameters.	115
7.2	Parameter values for numerical study.	122
8.1	Significance of the relevant parameters	132
8.2	Parameter values for numerical study.	141

List of Figures

2.1	The Diagram of the $SIQR$ model.	16
2.2	Dynamical behavior of susceptible individuals $S(t)$ with regard to time (days) for various values of α .	25
2.3	Dynamical behavior of infected individuals $I(t)$ with regard to time (days) for various values of α .	26
2.4	Dynamical behavior of quarantine individuals $Q(t)$ with regard to time (days) for various values of α .	26
2.5	Dynamical behavior of recovered individuals $R(t)$ with regard to time (days) for various values of α .	27
2.6	The dynamics of recovered individuals for different values of δ with respect to time (days).	27
2.7	The behavior susceptible individuals $S(t)$ with respect to time (days) with a change in the values of α .	29
2.8	The behavior of infected individuals $I(t)$ with regard to time (days) when α changes.	30
2.9	The behavior quarantine individual $Q(t)$ with regard to time (days) when α changes.	30
2.10	The behavior recovered individuals $R(t)$ with regard to time (days) when α changes.	31
2.11	Variation of total quarantine individuals and recovered individuals of system (2.3) corresponding to Table 2.3 for $\alpha = 0.9$ with respect to time (days).	31
2.12	Plot of the infected individuals of the system (2.3) and real time data.	32
2.13	Plot of the recovered individuals of the system (2.3) and real time data.	32
3.1	The $SEIR$ model is depicted as a diagram.	37
3.2	Plots of $S(t)$ for different values of $\alpha = 0.6, 0.8, 1.0$ with respect to time (days) with vaccination and without vaccination.	43
3.3	Plots of $E(t)$ for different values of $\alpha = 0.6, 0.8, 1.0$ with respect to time (days) with vaccination and without vaccination.	44

3.4	Plots of $I(t)$ for various values of $\alpha = 0.6, 0.8, 1.0$ with respect to time (days) with vaccination and without vaccination.	45
3.5	Plots of $R(t)$ for different values of $\alpha = 0.6, 0.8, 1.0$ with respect to time (days) with vaccination and without vaccination.	45
3.6	Time series plot of all individuals with vaccination and various initial conditions, parameter values are given in Table 3.2.	46
4.1	The $SEIRV$ model is represented schematically.	50
4.2	Comparison of dynamical behaviour of all individuals with respect to time for fractional order $\nu = 0.82, \delta = 0$ and $\delta = 0.01$.	63
4.3	Dynamical behaviour of all individuals with respect to time with a vaccination rate, $\delta = 0.01$ and fractional order $\nu = 0.8, 0.9, 1$.	64
4.4	With respect to time, the time series of the model system (4.4) corresponds to Table 4.2.	65
4.5	Time series of optimal control variable w^* and optimal cost J^* with parameter values corresponding to Table 4.2.	66
4.6	Time series solution of Infected population of the system (4.4) for Table 4.3 taking $\nu = 0.8, 0.85, 0.9$.	66
5.1	Depicts a flow chart of the proposed $SEIQRD$ model.	73
5.2	Time series of all classes correspondence to Table 5.2 taking $\phi = 0.98$ of system (5.3).	80
5.3	Dynamic of all classes over time for various values of $\phi = 0.8, 0.85, 0.90, 0.95$.	81
5.4	Variation of $R_{Covid\ 19}$ under α .	82
5.5	Dynamics of $I(t)$ under α and ϕ .	83
5.6	Graph of the infected class of the proposed model (5.3) and real infected data.	83
6.1	Flow diagram of the dengue model.	89
6.2	Time series of human sub-populations for $\alpha = 0.94, 0.96, 0.98$.	101
6.3	Time series solution of mosquitoes sub-populations for $\alpha = 0.94, 0.96, 0.98$.	101
6.4	Impact of β_H and β_M on I_H for $\alpha = 0.98$.	102
6.5	(a) Influence of γ_H and γ_M on R_0 . (b) Influence of d_H and d_M on R_0 .	102
6.6	(a) Contour plot of R_0 for d_H versus d_M . (b) Contour plot of R_0 for γ_H versus γ_M with $\alpha = 0.98$.	103
6.7	Time series solution with optimal control of the model system (6.1) for $\alpha = 0.98$.	104
6.8	Time series solution of optimal cost J and control variables p_1, p_2, p_3 .	105
6.9	Time series solution of I_H of the model (6.1) for $\alpha = 0.7, 0.8, 0.85, 0.9$.	106
6.10	Dynamics of I_H for different values of p_1, p_2 and p_3 with $\alpha = 0.85$.	106

6.11	Dynamics of I_M for different values of p_1 , p_2 and p_3 with $\alpha = 0.85$.	107
6.12	Plot of Sensitivity indices of R_0 versus each model parameters.	109
7.1	The proposed SIR model's flow diagram.	114
7.2	Time series solution of all individuals for values of $\alpha = 0.90, 0.94, 0.98$.	123
7.3	Phase portrait diagram for values of $\alpha = 0.90, 0.94, 0.98$.	123
7.4	Impact of β on I for $\alpha = 0.95, 0.98$.	124
7.5	Nature of I with control and without control for $\alpha = 0.98$.	124
7.6	Impact of γ on I for $\alpha = 0.95, 0.98$.	125
7.7	Impact of δ on I for $\alpha = 0.95, 0.98$.	126
7.8	Contour plots of R_0 for β versus m with $\alpha = 0.87, 0.92$ and 0.97 .	126
8.1	The proposed SIR model's flow diagram.	131
8.2	The behavior of all individuals for values of $\alpha = 0.90, 0.94, 0.98$.	141
8.3	Time series solution of all individuals for values of $\alpha = 0.90, 0.94, 0.98$.	142
8.4	Phase portrait diagram for values of $\alpha = 0.90, 0.94, 0.98$.	142
8.5	Dynamics of S and I under α .	142
8.6	Mean density of S and I under γ for $\alpha = 0.90, 0.94, 0.98$.	143
8.7	Mean density of S and I under δ for $\alpha = 0.90, 0.94, 0.98$.	143
8.8	Variation of γ under S and I for $\alpha = 0.98$.	144
8.9	Variation of δ under S and I for $\alpha = 0.98$.	144
8.10	When $\alpha = 0.9$, the time series of the model system (8.1) corresponds to	
	Table 8.2.	144
8.11	With parameter values matching to Table 8.2 for $\alpha = 0.9$, a time series of	
	the ideal control variable v^* and the ideal cost J^* is produced.	145

Contents

1 Introduction and Preliminaries	1
1.1 General introduction	1
1.2 Basic concept of mathematical epidemiology	3
1.3 Motivation and Research Background	4
1.4 Preliminaries	5
1.5 Organization of the thesis	7
2 Dynamics of $SIQR$ epidemic model with fractional order derivative	13
2.1 Introduction	14
2.1.1 Research background and motivation	14
2.2 Model formulation	16
2.3 Analysis of the model	17
2.3.1 Non-negativity and boundedness of solutions	17
2.3.2 Basic reproduction number, Disease-free equilibrium, Epidemic equilibrium state	18
2.3.3 Iterative scheme	18
2.4 Stability analysis	19
2.5 The $SIQR$ model's Adam - Bashforth - Moulton predictor - corrector scheme	21
2.6 Numerical simulation and discussion	23
2.7 Data fitting and model validation	29
2.8 Conclusion	33
3 Study of fractional order $SEIR$ epidemic model and effect of vaccination on the spread of COVID-19	34
3.1 Introduction	35
3.2 Model formulation	36
3.3 Analysis of the model	38
3.3.1 Non-negativity and boundedness of solutions	38
3.3.2 Basic reproduction number	38
3.4 Stability analysis	38

3.5	Predictor-corrector technique for the <i>SEIR</i> model	40
3.6	Numerical simulation and discussion	42
3.7	Conclusion	44
4	Dynamics of Caputo fractional order <i>SEIRV</i> epidemic model with optimal control and stability analysis	47
4.1	Introduction	48
4.1.1	Research background and motivation	49
4.2	Model formulation	50
4.3	Analysis of the model	52
4.3.1	Positivity and boundedness of solutions	52
4.3.2	Existence and uniqueness	52
4.3.3	Equilibrium points and Basic reproduction number	55
4.3.4	Significance of sensitivity parameters	55
4.4	Stability analysis	56
4.5	<i>SEIRV</i> model with optimal control	58
4.6	Adam-Bashforth-Moulton predictor-corrector scheme for the <i>SEIRV</i> model	59
4.7	Numerical simulation and discussion	61
4.8	Data fitting and model validation	62
4.9	Conclusion	67
5	Fractional order <i>SEIQRD</i> epidemic model of Covid-19: a case study of Italy	69
5.1	Introduction	70
5.1.1	Motivation and research background	71
5.1.2	Structure of the chapter	72
5.2	Model formulation	72
5.3	Analysis of the model	74
5.3.1	Existence and uniqueness	74
5.3.2	Positivity and boundedness of solutions	75
5.3.3	The equilibrium points of the system	76
5.3.4	The basic reproduction number of the system	76
5.3.5	Stability behavior at E_0	76
5.4	Numerical procedure	78
5.5	Numerical study	79
5.6	Conclusion	84
6	Optimal Control Analysis of Fractional Order Dengue Model - A Case Study of Singapore	86
6.1	Introduction	87

6.1.1	Arrangement of the chapter	88
6.2	Model formulation	88
6.3	Fundamental mathematical results	90
6.3.1	Existence and uniqueness	90
6.3.2	Non-negativity and boundedness	91
6.3.3	Equilibrium points	93
6.3.4	Basic Reproduction Number	93
6.4	Stability analysis	94
6.4.1	Local stability	94
6.5	Sensitivity analysis	96
6.6	Optimal control	96
6.7	Numerical procedure	99
6.8	Numerical discussion	99
6.9	Conclusion	108
7	Dynamical behavior of a fractional order SIR model with stability analysis	111
7.1	Introduction	112
7.1.1	Motivation and research background	113
7.1.2	Structure of the chapter as follows	113
7.2	Model formulation	114
7.3	Analysis of the system	115
7.3.1	Positivity and boundedness	115
7.3.2	Existence and uniqueness	116
7.3.3	Equilibria of system (7.2)	118
7.3.4	The basic reproduction number of the system	118
7.3.5	Dynamic behavior	118
7.3.6	Local stability	119
7.3.7	Global stability	119
7.4	Forward bifurcation	121
7.5	Numerical procedure	121
7.6	Numerical simulation and discussion	122
7.7	Conclusion	125
8	Study of fractional order SIR model with M-H type treatment rate and its stability analysis	128
8.1	Introduction	129
8.1.1	Motivation and Research Background	130
8.1.2	Chapter structure	130
8.2	Formulation of the model system	131

8.3	Analysis of the system	132
8.3.1	Model existence and model uniqueness	132
8.3.2	Boundedness and non-negativity	133
8.3.3	Equilibrium points of the model (8.2)	135
8.3.4	The basic reproduction number	135
8.3.5	Stability analysis at E_0	135
8.3.6	Stability analysis at E_1	136
8.4	SIR model with optimal control	138
8.5	Numerical procedure	140
8.6	Numerical discussion	140
8.7	Conclusion	145
9	Summary and future scopes	147

Chapter 1

Introduction and Preliminaries

“The most beautiful thing we can experience is the mysterious. It is the source of all true art and science.”

- Albert Einstein

1.1 General introduction

Mathematical modelling in epidemiology is an important branch of basic science. Epidemiology is the branch of science where the patterns and determinants of health, illness, disease conditions and associated factors at population level are studied. The meaning of the Greek terms epi, demos, and logos are respectively upon, people and study [1]. So the word epidemiology means the study of what is upon the people. The Greek physician

Hippocrates (460 - 377 B.C.E.) who described the connection between environment and disease, is considered the father of epidemiology [2].

Although the history of epidemiology is very lengthy, but the mathematical study and analysis of infectious diseases is only about three hundreds and fifty years old. John Graunt (1620 - 1674) was honoured for first statistical study of infectious diseases. Daniel Bernoulli worked on smallpox by using mathematical methods in 1766 [3 - 4]. In the early twentieth century, William Hamer did commanding work on measles. He was the first to use the mass action law in mathematical modelling of infectious diseases. Sir Ronald Ross is considered as the father of modern mathematical epidemiology for his commanding work on malaria. He discovered that malaria transmits from mosquitoes to humans and then humans to mosquitoes. He worked for the prevention of malaria and derived a threshold number, which is nothing but the basic reproduction number that provides whether the disease can persist or not. For his work on malaria, the Nobel prize was awarded to Sir Ronald Ross in 1902. But, the mathematical epidemic model proposed by Kermack and McKendrick in 1927 [5] has helped to reach the subject mathematical epidemiology to a new level. They proposed a deterministic epidemic model for the first time and provided biological interpretation by analysing the model using mathematical tools. More developments and progresses have been particularly made during the past three decades. Numerous mathematical models have been formulated by the researchers to study the dynamical behavior of various infectious diseases which show rich non-linear phenomena [6 - 7]. Mathematical modelling in epidemiology has become powerful and important tool to understand the infectious disease dynamics and to improve control of infection in the population. A good epidemic model is an intelligent model which is able to predict any possible outbreak of the disease and is effective in reducing the transmission of the disease. It is a simplest version of reality in Biology [8 - 9].

The novel coronavirus disease (COVID-19) is a worldwide infectious disease in the current time [10 - 14]. Including this year the world faces severe attack by coronavirus several times, some of those are: (i) SARSCoV occurred in China and then spread many neighbouring countries in 2002 - 2003 [15], (ii) MERS-CoV appeared in 2012 throughout the Middle East [16 - 17], (iii) SARS-CoV-2 was first identified in China in December 2019 and the whole world has been suffering from it [18]. Though the infection of COVID-19 was first reported in Wuhan, China in December 2019, due to human movement it spread throughout the world. The emergence of COVID-19 occurred in a crucial time because that time was the spring festival time in China, so a large number of people moved from one place to another places [19] and the disease started to spread to huge number of people who moved from their working place to their home land as a consequence the disease spreads to the whole world. COVID-19 have killed enormous people throughout the world.

The plague of Athens is the first serious epidemic mentioned by the historians that hurt

the city of Athens in 430-426 B.C.E. [20 - 21]. The Black Death is the one of the most well documented epidemics that struck the Mediterranean and Europe and killed 50-100 million people in 1348-1350 [22]. The Bombay plague in the years 1905-1906, the influenza pandemic in the early twentieth century, the H1N1 swine flu pandemic in the year 2009 are some of other notable epidemic all over the world.

1.2 Basic concept of mathematical epidemiology

Mathematical models have become extremely important tools in understanding and analyzing the spread and control of infectious diseases. Though the SIR model is one of the simplest epidemiological models, it is still one of the most popular and mainly used to study infant viral and bacterial infections. There are few models, used for childhood disease is *SEIR* model, one which adds a class of exposed (*E*) individuals. Similar models like *SAIR*, introducing asymptomatic class (*A*) are fruitful for analyzing epidemic like COVID-19. There are many modifications of the *SIR* model, including those that include births and deaths, where upon recovery there is no immunity (*SIS* model), where immunity lasts only for a short period of time (*SIRS*), where there is a latent period of the disease where the person is not infectious (*SEIS* and *SEIR*), and where infants can be born with immunity (MSIR).

In the modeling of infectious illnesses, the incidence rate is crucial in determining the behavior of phenomena. Kermack and Mckendrick proposed the transmission rate as βSI in 1927. Capasso et al. [23] proposed a nonlinear occurrence $g(I)S$ for $g'(I) < 0$ that permits for particular “behavioral” effects. With behavioral modifications, Capasso and Serio inspired their approach. The potential damage of infection may become extra ordinarily high during times of high occurrence, leading to major behavioral modifications that minimize the actual risk of illness [24]. Goel and Nilam [25], Wei and Chen [26], Capasso et al. [27 - 28], Zhang et al. [29], Anderson and May [30], including Kumar and Nilam [31 - 32], only a few writers have drawn attention towards the significance of taking nonlinear incidence rates into account while studying the relationship between infectious transmission and illness [33]. Li et al. [34] presented a *SIR* model with $f(S, I) = \frac{\beta SI}{1+\gamma I}$. Wang and Ruan [35] proposed the following SIR transmission dynamics with a fixed treatment rate:

$$h(I) = \begin{cases} n & \text{for } I > 0, \\ 0 & \text{for } I = 0. \end{cases}$$

Zhang and Liu [36], who also provided a superior treatment rate (Holling type II) as a continuously differentiable function that populates at the largest benefit, as shown below: $h(I) = \frac{mI}{1+nI}$ for $I \geq 0, m > 0, n > 0$, where m is the cure rate and n is the rate of limitation in the availability of treatment.

The basic reproduction number [37] of a system gives a threshold which can be interpreted as the number of secondary infections that one infectious individual produces in a population consisting only of susceptible individuals. It is a measure of the disease transmissibility in the population. How rapidly the disease spreads that depends on the value of the basic reproduction number. Generally the basic reproduction number is denoted by R_0 . The definition of R_0 states that it must be non-negative (i.e. zero or positive). If there is no transmission of infection then R_0 must be zero. Again the stability of disease free equilibrium point (the point at which the population remains in disease free state) is strongly dependent on the value of R_0 . It has been well established that the disease free equilibrium point is stable if $R_0 < 1$ and unstable if $R_0 > 1$. So making R_0 less than unity is very effective for controlling any infectious disease which can be possible if proper controlling measures like awareness, vaccination and treatment are taken into account. To control an outbreak, it is important to identify the most important parameters which strongly influence R_0 that can help the public health authorities to prevent and control the spreading of infectious diseases in population.

1.3 Motivation and Research Background

A mathematical modelling of infectious disease is critical for better understanding the transmission patterns of the disease and evaluating control strategies. It serves as motivation for mathematical and biological experts to investigate and evaluate the dynamical systems that regulate such diseases in order to anticipate their spread and control in the long term. Fractional order modeling is a useful tool that has been used to explore the nature of diseases since the fractional derivative is an extension of the integer-order derivative. In order to replicate real-world issues, several innovative fractional operators with various properties have been designed. In addition, the integer derivative has a local identity, whereas the fractional derivative has a global character. Numerous varieties of fractional derivatives, both with and without singular kernels, are available today. Leibniz's query from 1695 marks the beginning of the fractional derivative. The fractional derivative also improves in the improvement of the system's consistency domain. We have the derivatives of Caputo, Riemann-Liouville, and Katugampola for singular kernels. There are two varieties of fractional derivatives without singular kernels: the Caputo-Fabrizio fractional derivative, which has an exponential kernel, and the Atangana-Baleanu fractional derivative, which has a Mittag-Leffler kernel. While memory and genetic properties are involved, working with fractional-order derivatives is crucial because it provides a more accurate technique to describe COVID-19 outbreaks. Numerous academic articles, monographs, and novels have provided evidence to support this claim; for instance. Over these years, several types of fractional calculus, for example, Riemann-Liouville, Caputo, Caputo-Fabrizio, Katugampola, Atangana-Baleanu, Hadamard etc. have been introduced

to study the dynamics of the epidemic models, each displaying certain advantages and disadvantages. We have used the Caputo–Fabrizio operator because of its possession of a nonlocal and nonsingular exponential kernel and is found to be best suited to analyze the dynamics of COVID-19. The dynamics of COVID-19 transmission are described using a fractional order SIQR model. We investigate the disease’s impact using an appropriate mathematical model in context of the Caputo–Fabrizio fractional differential equation, motivated by early research. One of the several variations of the conventional *SIR* model is the *SIQR* model. It has been observed that quarantining the infected individuals is a better measure to control the spread of the disease. Motivated by the current research, we present and analyze different models using fractional derivative. The Caputo derivative is particularly useful for discussing real-world situations since it permits traditional beginning and boundary conditions to be used in the derivation, and the derivative of a constant is zero, whereas the Riemann–Liouville fractional derivative does not. It is quite challenging to genuinely create an appropriate mathematical model using classical differentiation in the situation of COVID-19 because to the large number of uncertainties, unknowns, and disinformation. Generally, non-local operators are better suited for such circumstances because, depending on whether power law, fading memory, or overlap effects are taken into account, they can represent non-localities and certain memory effects.

1.4 Preliminaries

We provide the reader with some useful definitions and characteristics of fractional derivatives [38 – 49].

Definition 1.4.1. *Let $f \in C^n([t_0, \infty+), \mathbb{R})$, the Caputo derivative of fractional order $\alpha > 0$ is defined by*

$${}^C D_t^\alpha f(t) = \frac{1}{\Gamma(n-\alpha)} \int_{t_0}^t \frac{f^{(n)}(s)}{(t-s)^{\alpha-n+1}} ds,$$

where $\Gamma(\cdot)$ represents the Gamma function, $t \geq t_0$, $n \in \mathbb{Z}^+$ and $\alpha \in (n-1, n)$.

Definition 1.4.2. *Let $f \in C^n([t_0, \infty+), \mathbb{R})$, the Caputo-Fabrizio fractional derivative of order $0 < \alpha \leq 1$ is defined by*

$${}^{CF} D_t^\alpha f(t) = \frac{M(\alpha)}{(1-\alpha)} \int_{t_0}^t \exp\left[-\frac{\alpha(1-x)}{(1-\alpha)}\right] \frac{d}{dx}(f(x)) dx,$$

where $M(\alpha)$ is a normalization function which depends on α and satisfies $M(0) = M(1) = 1$.

Definition 1.4.3. *The Laplace transform for the fractional operator of order $0 < \alpha \leq 1$ for $m = 0, 1, 2, \dots$ is defined as $L\{ {}^{CF} D_t^{m+\alpha} f(t) \} (p) = \frac{1}{(1-\alpha)} L(f^{(m+1)}(t)) L(\exp(-\frac{\alpha t}{(1-\alpha)}))$.*

Lemma 1.4.1. *The Laplace transform of the derivative of Caputo*

$$L \{ {}^C D_t^\alpha f(t) \} = p^\alpha F(p) - \sum_{j=0}^{n-1} p^{\alpha-j-1} f^{(j)}(t_0),$$

where $F(p) = L \{ f(t) \}$.

Lemma 1.4.2. *For any $B \in \mathbb{C}^{n \times n}$ where \mathbb{C} be the complex plane and $c, d > 0$, the Laplace transform of Mittag-Leffler function is defined as $L \{ t^{d-1} E_{c,d}(Bt^c) \} = s^{c-d} (s^c - B)^{-1}$, for $\text{Re}(s) > \|B\|^{\frac{1}{c}}$, where $\text{Re}(s)$ denotes the real portion of s .*

Lemma 1.4.3. *One parametric and two parametric Mittag-Leffler functions are described as follows: $E_\alpha(z) = \sum_{j=0}^{\infty} \frac{z^j}{\Gamma(\alpha j + 1)}$ and $E_{\alpha_1, \alpha_2}(z) = \sum_{j=0}^{\infty} \frac{z^j}{\Gamma(\alpha_1 j + \alpha_2)}$, where $\alpha, \alpha_1, \alpha_2 \in \mathbb{R}_+$.*

Lemma 1.4.4. *Consider the system ${}^C D_t^\alpha u(t) = g(t, x), t_0 > 0$ with initial condition $u(t_0) = u_0$, where $\alpha \in (0, 1]$, $g : [t_0, \infty) \times \Omega \rightarrow \mathbb{R}^n$, $\Omega \in \mathbb{R}^n$, if Lipschitz condition is satisfied by $g(t, x)$ with respect to x , then there exists a solution of the above system on $[t_0, \infty) \times \Omega$ which is unique.*

Lemma 1.4.5. *Let $0 < \alpha \leq 1$, $\phi(t) \in C[a, b]$. If ${}^C D_t^\alpha f(t) \geq 0$ (${}^C D_t^\alpha f(t) \leq 0$), $t \in (a, b)$ then $\phi(t)$ is a increasing (decreasing) function for $t \in [a, b]$.*

Lemma 1.4.6. *Consider the following fractional-order system:*

$${}^C D_t^\alpha X(t) = \Phi(X), X_{t_0} = (x_{t_0}^1, x_{t_0}^2, \dots, x_{t_0}^n), x_{t_0}^i > 0, i = 1, 2, \dots, n,$$

with $0 < \alpha \leq 1$, $X(t) = (x^1(t), x^2(t), \dots, x^n(t))$ and $\Phi(X) : [t_0, \infty) \rightarrow \mathbb{R}^{n \times n}$. The equilibrium points of the above system are evaluated by solving the following system of equations: $\Phi(X) = 0$. These equilibrium points are locally asymptotically stable iff each eigenvalue λ of the Jacobian matrix $J(X) = \frac{\partial(\Phi_1, \Phi_2, \dots, \Phi_n)}{\partial(x^1, x^2, \dots, x^n)}$ calculated at the equilibrium points satisfy $|\arg(\lambda_i)| > \frac{\alpha\pi}{2}$.

Lemma 1.4.7. *Suppose $g(t) \in \mathbb{R}_+$ be a differentiable function. Then, for any $t \geq t_0$, ${}^C D_t^\alpha \left[g(t) - g^* - g^* \ln \frac{g(t)}{g^*} \right] \leq \left(1 - \frac{g^*}{g(t)} \right) {}^C D_t^\alpha g(t)$, $g^* \in \mathbb{R}_+$, $\forall \alpha \in (0, 1)$.*

Lemma 1.4.8. *The applications of Fractional ordered optimal control problem (FOCP) have grown in recent decades [50 – 52]. Agrawal [51] has introduced general form of FOCPs in the Riemann-Liouville sense and suggests a numerical method to solve FOCP using Lagrange multiplier technique. In traditional integer order optimal control problems, the calculus of variations is the common method. Pontryagins principle is one of the most useful approaches to solve optimal control problem. There are several works where these*

methods are employed in Fractional ordered optimal control problems. Let u be a pseudo-state vector and $X = [x^1, x^2, \dots, x^n] \in R^n$ is the input vector and X is the admissible control of the dynamical system ${}_{t_0}^C D_t^\alpha u = f(u, x, t)$, $u(0) = u_0$. The system's pseudo-state is supposed to reach final condition u_g in the unknown final time T_g . The control $x \in X$ must be chosen for all $t \in [0, T_g]$ to minimize the objective functional J which is defined by the application and can be abstracted as $J = A(u(T_g)) + \int_0^{T_g} F[u(t), x(t)]dt$.

The constraints on the system dynamics can be adjoined to the Lagrangian F by introducing time-varying Lagrange multiplier vector λ , whose elements are called the co-states of the system. This motivates the construction of the Hamiltonian H defined for all $t \in [0, T_g]$.

$H(u(t), x(t), \lambda(t)) = \lambda^T(t)f(u(t), x(t)) + f(u(t), x(t))$. Where λ^T stands for transpose of λ . Pontryagin's minimum principle states that the optimal state trajectory u^* , optimal control x^* , and corresponding Lagrange multiplier vector λ^* must minimize the Hamiltonian H so that [53]:

$$(i) H(u^*(t), x^*(t), \lambda^*(t)) \leq H(u^*(t), x(t), \lambda^*(t)),$$

$$(ii) \frac{\partial A(u)}{\partial T_g} + H(T_g) = 0 \text{ for } u = u(T_g),$$

$$(iii) {}^{RL}D_{T_g}^\alpha \lambda^T = \frac{\partial H}{\partial u} \text{ at } u = u^*,$$

$$(iv) \frac{\partial H}{\partial x} \text{ at } x = x^* \text{ and } \frac{\partial^2 H(u^*(t), x^*(t), \lambda^*(t))}{\partial x^2} \leq 0, \text{ where } {}^{RL}D_t^\alpha f(t) = \frac{-1}{\Gamma(1-\alpha)} \frac{d}{dz} \int_{T_g}^t \frac{f(z)dz}{(t-z)^\alpha} \text{ is the Right-Liouville derivative of order } \alpha. \text{ These four conditions are the necessary conditions for optimal control.}$$

1.5 Organization of the thesis

Based on the above mentioned factors, we have formulated and analyzed seven different epidemic models in seven chapters (Chapter 2 to Chapter 8). In Chapter 2 to 6, we have formulated and analyzed the epidemic models for some particular infectious diseases (COVID-19, Dengue) whereas in Chapter 7 to 8, we have studied the general epidemic models.

Chapter 1: In this chapter, we have studied brief introduction of epidemiology with some mathematical preliminaries.

Chapter 2: In this chapter, the dynamics of COVID-19 transmission are described using a fractional order $SIQR$ model. The stability analysis of the model is performed. To obtain semi-analytic solutions to the model, the Iterative Laplace Transform Method [ILTM] is implemented. Real-time data from COVID-19 cases in India and Brazil is employed to estimate the parameters of the fractional order $SIQR$ model. Numerical solutions obtained using Adam-Bashforth-Moulton predictor-corrector technique is com-

pared with those obtained by ILTM. Based on the COVID-19 cases data in India and Brazil, collected upto 1st August, 2020, we estimated the basic reproduction number R_0 to be 1.7824 and 2.767 respectively. We observe that the proposed *SIQR* model with fractional order derivatives comply with the real time data in case of infected and recovered individuals. It is observed that the fractional order of the derivatives is more effective in studying the dynamics of the spread of COVID-19 in comparison to integral order of the *SIQR* model. Modeling using fractional-order derivatives is often more efficient than modeling with integer-order derivatives because the option of derivative order gives one more degree of freedom, resulting in a better fit to real-time data with less inaccuracy than the integer-order model. According to our understanding of the challenges, the incidence of disease transmission must be reduced, or a large part of the population would be afflicted in a very short span of time. For successful isolation and control of the disease's transmission, common preventative methods include lockdown, curfews, and the designation of containment zones.

Chapter 3: In the present chapter, a fractional order SEIR model with vaccination has been proposed. The positivity and boundedness of the solutions have been verified. The stability analysis of the model shows that the system is locally as well as globally asymptotically stable at disease-free equilibrium point E_0 when $R_0 < 1$ and at epidemic equilibrium E_1 when $R_0 > 1$. We have demonstrated the global stability of the equilibrium points by constructing the Lyapunov function. It has been found that introduction of the vaccination parameter η reduces the reproduction number R_0 . Based on the COVID-19 cases data in India, collected upto 1st August, 2021, we estimated the basic reproduction number R_0 without vaccination to be 3.67 and with vaccination to be 1.55. The parameters are identified using real-time data from COVID-19 cases in India. To numerically solve the *SEIR* model with vaccination, the Adam-Bashforth-Moulton technique is used. MATLAB (2018a) was used for graphical presentation and numerical simulations. It has been observed that the *SEIR* model with fractional order derivatives of the dynamical variables is much more effective in studying the effect of vaccination than the integral model. As is evident from our study that vaccination is an effective method in control and prevention of the COVID-19 disease. The model described in this research may be used to investigate the dynamics of various epidemic illnesses, as well as the function of vaccination in successful transmission control. Our investigation suggests that the primary task of health officials, policymakers, and experts should be to implement the most appropriate vaccination plan to fight against the disease. It is very important that the transmission of diseases is controlled at an early stage to avoid a massive impact on the population.

Chapter 4: This chapter presents a study of an *SEIRV* epidemic model with optimal control in the context of the Caputo fractional derivative of order $0 < \alpha \leq 1$. The stability analysis of the model is performed. The stability analysis of the model shows that the system is locally as well as globally asymptotically stable at disease-free equilibrium point E_0 when $R_0 < 1$ and at epidemic equilibrium E_1 when $R_0 > 1$. Sensitivity analysis shows that R_0 is directly proportional to the birth rate of susceptible individuals Λ , the rate of infection of susceptible individuals β and the rate of progression from exposed to infected individuals δ_1 , all of which may be controlled with the effective execution of vaccination drives. Also we have discussed the optimal control of fractional order *SEIRV* model with vaccination as the control parameter w . We have used the Pontryagin's Maximum Principle to provide the necessary conditions needed for the existence of the optimal solution to the optimal control problem. It is evident that if the control measure w is employed then the transmission of the disease may be checked and eradicated. Additionally, the optimal control value w^* has been determined to minimize the cost of vaccination. We have assumed a final time $t_g = 100$ for optimal control. The Adam-Bashforth-Moulton predictor-corrector method is implemented to solve the *SEIRV* model numerically. Numerical simulations are presented using MATLAB to validate the efficacy and impact of the control parameter. We have comparatively studied the model values and real scenario of Brazil starts from 10th April 2021 and continues up to 100 days. It has been observed that our model fits with $\alpha = 0.85$ with realistic data. For analyzing COVID-19 transmission dynamics, the fractional order of the *SEIRV* model is found to be better than the integral order. The order of derivative can differ from region to region. If we vary the order of derivatives while keeping other parametric values fixed, the results will be different.

Chapter 5: In this chapter, the fractional order *SEIQRD* compartmental model of COVID-19 is explored with six different categories in the Caputo approach. A few findings for the new model's existence and uniqueness criterion, as well as non-negativity and boundedness of the solution, have been established. The model's fundamental reproduction number $R_{Covid19}$ was also calculated using the next generation matrix technique. The Routh-Hurwitz consistency criteria and La-Salle invariant principle are used to analyze the dynamics of the equilibrium. When $R_{Covid-19} < 1$ at infection-free equilibrium, we prove that the system is locally asymptotically stable and unstable if $R_{Covid-19} > 1$. We also observed that $R_{Covid-19} < 1$, the system is globally asymptotically stable. The main objective of this study is to investigate the COVID-19 transmission dynamics in Italy, in which the first case of Coronavirus infection 2019 (COVID-19) was identified on January 31st in 2020. In addition, the fractional-order Taylor's approach is utilized to approximate the solution to the proposed model. The model's validity is demonstrated by comparing real-world data with simulation outcomes. From the 1st of January 2022 to the 31st of

January 2022, we have compared model values with real-world scenarios in Italy. Real data was also used to fit the model in order to forecast infected population instances in real life. In real-world dynamical processes, such as epidemic propagation, fractional calculus plays a vital role. Currently, research on a vaccine to avert the COVID-19 pandemic is showing promising results, with Pfizer claiming that their vaccine has a 95 effectiveness rate. However, it will be some time before the vaccinations are widely distributed around the world. This study looked at the many consequences of wearing face masks, and it was discovered that wearing face masks on a consistent and suitable basis can help reduce the propagate of the COVID-19 disease. As a result, wearing a face mask should be made mandatory until everyone has access to vaccinations.

Chapter 6: Dengue is a vector borne disease caused by the dengue viruses of four serotypes, DEN 1 to DEN 4 and is a mosquito borne disease. After malaria, the Dengue and is transmitted into human population by the bite of female adult Aedes mosquitoes. In this chapter, we have analyzed the dynamics of dengue transmission in a four compartment host population and a three compartment vector population with two control parameters pertaining to measures taken to prevent mosquito bites and measures of treatment techniques and a three compartment mosquito population with a control parameter characterizing the inhibition of breeding of mosquitoes. The basic reproduction number is obtained using the Next Generation Matrix method. Stability of the equilibrium points and sensitivity analysis of model parameters are discussed. The dengue fever free equilibrium is locally and globally stable when $R_0 < 1$ and unstable when $R_0 > 1$. The sensitivity analysis, which allows us to determine the key parameters in the proposed model. The Euler method is utilized to approximate the solution to the fractional order dengue model. Numerical simulations are carried out to illustrate the impact of control measures in the disease transmission regarding the case study of Singapore. The case study of Singapore is used to validate the findings and it is observed that the model system fits the realistic data for Caputo order $\alpha = 0.85$. Thus, we may be convinced that the fractional order Caputo derivatives are more effective in studying epidemic models with real time data than integral order derivatives. The basic reproduction number R_0 is obtained by next generation matrix method. The objective of our work has been to construct the objective function $J(p_1, p_2, p_3)$ is to minimize the cost of implementation of the control parameters. Hence, as the use of mosquito repellents and other personal prophylactic measures along with treatment efforts for infected individuals increases there is a considerable decrease in the number of infected human population. This is also the case with the use of certain biological and chemical controls over the detection and elimination of vector breeding sources. With an increase in the environmental management programs and source reduction methods there is a decrease in the infected vector population which in turn causes a decrease in the infected human population.

Chapter 7: In this chapter, the fractional order *SIR* model with a Holling type II saturated incidence rate and treatment rate are explored in the Caputo order fractional derivative approach. The existence and uniqueness criterion, as well as non-negativity and boundedness of the solution of the new model have been established. The stability analysis of the model shows that the system is locally as well as globally asymptotically stable at disease-free equilibrium point E_0 when $R_0 < 1$ and at epidemic equilibrium E^* when $R_0 > 1$. For $R_0 = 1$ at E_0 the model exhibits a forward bifurcation. We discovered via numerical simulations that managing the treatment of infectious in accordance with the Holling type II treatment rate can result in more efficient management of the new infection. The stability of the endemic equilibrium in the model has been tested using the Routh-Hurwitz criterion. The simulation results predict that the infection will worsen as the rate of transmission rises, but that it will stabilize due to the accessibility of treatment centres. Additionally, when the amount of inhibition used by the infected increases, infection will also decline. Using simulation results, we also discovered that the population's treatment must be carefully coordinated with the resources that are available in order to completely eradicate the virus. An essential tool for understanding the dynamics of epidemics is epidemic modelling. When there is forward bifurcation, the disease-free equilibrium loses stability as R_0 approaches unity and a stable endemic equilibrium emerges. The graphical depiction of the efficiency of theoretical solutions is displayed by the numerical simulations. Effectively reducing the infection from society will need knowledge, adequate treatment for infectious diseases, and the availability of health resources. Moreover, by using the appropriate Lyapunov function, we were able to show that the equilibrium was globally stable. We have also noticed that fractional order is crucial to population dynamics. Fractional-order Taylor's approach is utilized to approximate the solution of the proposed model. Graphical demonstrations and numerical simulations have been presented using MATLAB.

Chapter 8: In this chapter, we analyze a fractional order susceptible-infected-recovered (*SIR*) mathematical model with nonlinear incidence rate and nonlinear treatment rate for the control of infectious illness. The incidence rate of infection is considered as Holling type II and the treatment rate is considered as Monod-Haldane (MH) type. The existence and uniqueness criteria for the new model, as well as the non-negativity and boundedness have been established. The stability of the model demonstrates that the system is locally and globally asymptotically stable at the disease-free equilibrium point E_0 when $R_0 < 1$ and the epidemic equilibrium E_1 when $R_0 > 1$. We also provide an ideal control strategy for the *SIR* model using the treatment rate as a control parameter. The R-H criteria has been used to examine the stability of the model's endemic equilibrium. Numerical simulations provide the visualisation of the efficacy of theoretical solutions. Comprehen-

sive information, suitable infectious disease treatment methods, and the availability of healthcare services are required for the successful decrease of infection within society. In addition, we showed the global stability of the equilibrium state by choosing an appropriate Lyapunov function. The optimum solution to the optimal control issue must meet certain requirements, which we have established using the Pontryagin's Maximum Principle. It is obvious that the disease's spread can be stopped and eliminated if the control measure v^* is used. Additionally, we have the ideal control value v^* to reduce the cost of vaccination. The solution of the suggested model is approximated using the fractional order Taylor's method. With the help of MATLAB (2018a), we have performed numerical simulations and have illustrated the results through graphical representations. As a consequence, changing the derivatives' order may change the stability requirements for equilibrium locations without changing any other parametric variables.

Chapter 9: The final chapter includes summary with a brief discussion on the scope for future research work.

Chapter 2

Dynamics of $SIQR$ epidemic model with fractional order derivative

“Life is a school of probability.”

- Walter Bagehot

This chapter is based on the paper
Dynamics of $SIQR$ epidemic model with fractional order derivative, Partial Differ. Equ. Appl. Math., 5, 100216, 2022.

2.1 Introduction

The first case of corona virus infection in human species with symptoms similar to common cold [54] were reported in 1965 by Tyrrell and Bynoe. However, after numerous mutations, the virus has ultimately proved to be catastrophic in Wuhan, Hubei Province, China, in 2019. Henceforth, the virus was named SARS-CoV-2 and the disease was declared to be COVID-19. The devastation spread quickly throughout multiple nations, prompting the World Health Organization to identify a pandemic on March 11, 2020 [55]. No sooner had the futile efforts of the doctors and the administrative heads of states succumbed to the wrath of the virus, researchers from all areas of science sprang to activity. Along with medical researches going on in full swing, the study of the transmission of the disease, effect of preventive measures, prediction of future outbreaks and potential control strategies were also investigated extensively. The simple epidemic model by Kermack and Mckendrick in 1927 [56] is among the initial works on mathematical modelling of infectious diseases which later on proved to be the building block of further research [56, 57, 79]. In order to study such mathematical models, the entire population is primarily divided into subclasses, namely, susceptible individuals $S(t)$, infected individuals $I(t)$, the quarantined individuals $Q(t)$ and the recovered individuals $R(t)$. Integral order ordinary differential equations are common among epidemiological modelling of biological systems [58, 59]. However, there are certain reservations regarding the integral order of the differential equations in such models. Such restrictions are taken into account by a comparatively new and emerging area of mathematical calculus, namely the fractional-order differential equations [60 - 64]. In fact, fractional-order differential equations (FODEs) and their applications have been intensively investigated and used in biology, physics, chemistry, biochemistry, hydrology, engineering and medicine [65 - 69]. The stability results of the fractional order dengue model have been discussed in [70]. Some interesting results are obtained in [71] on modelling the Hepatitis-C Virus replications by a fractional-order differential mathematical model. Particularly, fractional calculus has been applied in studying epidemic models related to different infectious diseases [72 - 73]. Thus, extensive studies have evolved various techniques to construct real and approximate solutions to such fractional order differential equations [74 - 76].

2.1.1 Research background and motivation

A mathematical modelling of infectious disease [77] is critical for better understanding the transmission patterns of the disease and evaluating control strategies. It serves as motivation for mathematical and biological experts to investigate and evaluate the dynamical systems that regulate such diseases in order to anticipate their spread and control in the long term. The four epidemiological divisions that assess the susceptible part of individuals, the infected, the quarantine, and the recovered, have characterized basic definitions

of infectious diseases. One of the several variations of the conventional *SIR* model is the *SIQR* model. It has been observed that quarantining the infected individuals is a better measure to control the spread of the disease. Over these years, several types of fractional calculus, for example, Riemann–Liouville, Caputo, Caputo–Fabrizio, Katugampola, Atangana–Baleanu, Hadamard etc. have been introduced to study the dynamics of the epidemic models, each displaying certain advantages and disadvantages. Zhang et al. [78] developed the unique asymptotic stability criteria for fractional-order gene regulation systems with time delay. Wu et al. [79] investigated global uniform asymptotical stability for fractional-order gene regulatory networks with time-varying delays and structured uncertainties. Based on the vector Lyapunov function, Zhang et al. [80] presented a unique stability condition for fractional-order composite systems with time delay. We have used the Caputo–Fabrizio operator because of its possession of a nonlocal and nonsingular exponential kernel and is found to be best suited to analyze the dynamics of COVID-19 [38 - 47]. The dynamics of COVID-19 (Coronavirus Disease-2019) transmission are described using a fractional order *SIQR* model. We investigate the disease’s impact using an appropriate mathematical model [*SIQR* model] in context of the Caputo–Fabrizio fractional differential equation, motivated by early research.

The purpose of the present chapter is to:

- To study local stability as well as global stability of the model system.
- The Iterative Laplace Transform Method has been used to generate semi-analytic solutions to the model system.
- Determination of the Basic Reproduction number and Equilibrium points.
- To confirm the Iterative Laplace Transform Method’s predictions, the Adam-Bashforth scheme is applied to the *SIQR* model.
- To confirm the findings and prevent the growth of COVID-19, a numerical simulation was used.

The following is an overview of the chapter’s structure: Mathematical model with fractional order derivative is discussed in Section 2.2. Section 2.3 discusses some fundamental results of the proposed model system. Section 2.4 is focused to a description of the Model’s stability analysis and stability criterion. In Section 2.5, we perform Adam-Bashforth-Moulton predictor-corrector scheme for the *SIQR* model. In Section 2.6, numerical simulation and discussion are presented via MATLAB. Section 2.7 includes the validation of the model with real time data. Finally, Section 2.8 constitutes the conclusion of the chapter.

2.2 Model formulation

Let us consider the case of a Susceptible – Infected – Quarantine – Removed (*SIQR*) epidemic. The *SIQR* disease transmission model is derived assuming several strong assumptions [81]. The population (N) is divided into four classes: the susceptible individuals (S), the infected individuals (I), the quarantine individuals (Q) and the recovered individuals (R) at any time $t \geq 0$. Now

$$N(t) = S(t) + I(t) + Q(t) + R(t). \quad (2.1)$$

Individuals who are Susceptible in this model are those who are at risk of becoming infected. Quarantine is defined as an infected person who exhibits signs of the disease and is isolated. Quarantined individuals who recover from the disease are considered as Recovered. The differential equations governing the *SIQR* model are given as:

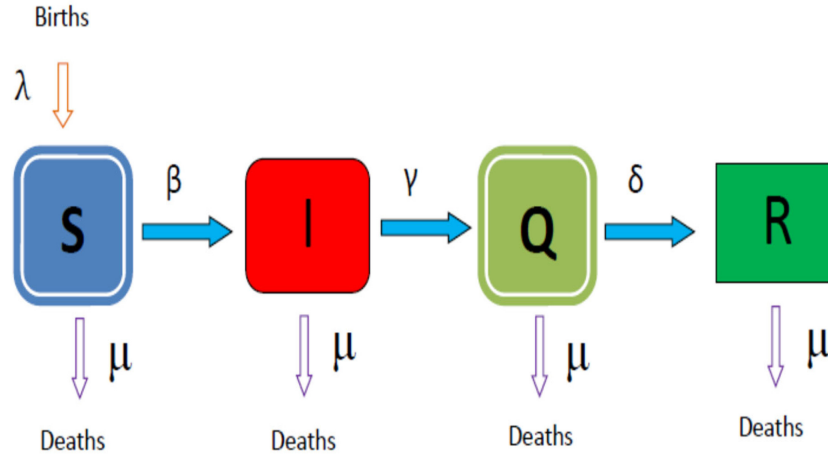


Figure 2.1: The Diagram of the *SIQR* model.

$$\begin{aligned} D_t S(t) &= \lambda - \beta SI - \mu S, \\ D_t I(t) &= \beta SI - (\gamma + \mu)I, \\ D_t Q(t) &= \gamma I - (\delta + \mu)Q, \\ D_t R(t) &= \delta Q - \mu R. \end{aligned} \quad (2.2)$$

The model (2.2) having fractional order derivatives with the Caputo-Fabrizio (CF)

operator of order $0 < \alpha \leq 1$ have been proposed as follows:

$$\begin{aligned}
{}^{CF}D_t^\alpha S(t) &= \lambda - \beta SI - \mu S, \\
{}^{CF}D_t^\alpha I(t) &= \beta SI - (\gamma + \mu)I, \\
{}^{CF}D_t^\alpha Q(t) &= \gamma I - (\delta + \mu)Q, \\
{}^{CF}D_t^\alpha R(t) &= \delta Q - \mu R,
\end{aligned} \tag{2.3}$$

with initial condition $S(0) = S_0 > 0, I(0) = I_0 \geq 0, Q(0) = Q_0 \geq 0, R(0) = R_0 \geq 0$.

λ	Natural birth rate
μ	Natural death rate
β	Contact rate between S and I
γ	Infection rate of Q class
δ	Recovery rate

Table 2.1: The parameters of the model and their descriptions.

2.3 Analysis of the model

2.3.1 Non-negativity and boundedness of solutions

Proposition 2.3.1. *All the variables are positive for all $t \geq 0$. The closed region $\Omega = \{(S, I, Q, R) \in \mathbb{R}^4 : 0 < N \leq \frac{\lambda}{\mu}\}$ is positive consistent for the model (2.3).*

Proof. From the model (2.3), ${}^{CF}D_t^\alpha S(t) = \lambda - \beta SI - \mu S \geq -(\beta I + \mu)S$.

Therefore, $S(t) \geq S(0)\exp(-\int_0^t (\beta I + \mu) dp) > 0$.

Now, ${}^{CF}D_t^\alpha I(t) = \beta SI - (\gamma + \mu)I \geq -(\gamma + \mu)I$.

Therefore, $I(t) \geq I(0)\exp(-\int_0^t (\gamma + \mu) dp) > 0$.

Also, ${}^{CF}D_t^\alpha Q(t) = \gamma I - (\delta + \mu)Q \geq -(\delta + \mu)Q$.

We have, $Q(t) \geq Q(0)\exp(-\int_0^t (\delta + \mu) dp) > 0$.

Again, ${}^{CF}D_t^\alpha (S + I + Q + R)(t) = \lambda - \mu(S + I + Q + R)$.

Therefore, ${}^{CF}D_t^\alpha N(t) = \lambda - \mu N$.

Thus, $\lim_{t \rightarrow \infty} \sup N(t) \leq \frac{\lambda}{\mu}$.

Therefore, the model (2.3) is bounded by $\frac{\lambda}{\mu}$. Thus S , I and Q are positive functions and Ω is positively consistent of the system (2.3).

2.3.2 Basic reproduction number, Disease-free equilibrium, Epidemic equilibrium state

The basic reproduction number, indicated by R_0 , is defined as the predicted number of secondary cases created by a single Susceptible individual's infection. The disease-free equilibrium point is locally asymptotically stable when $R_0 < 1$ and unstable when $R_0 > 1$. Since the considered model has disease-free equilibrium at $(\frac{\lambda}{\mu}, 0, 0, 0)$. So, an effective strategy should be developed, when a pandemic breaks out so that R_0 reduces to less than 1 as soon as possible. Using next generation matrix method [37, 49], the leading eigen value of the matrix FV^{-1} may be used to calculate the reproduction number (R_0) where,

$$F = \begin{bmatrix} \frac{\beta\lambda}{\mu} & 0 \\ 0 & 0 \end{bmatrix} \text{ and } V = \begin{bmatrix} \mu + \gamma & 0 \\ -\gamma & \mu + \delta \end{bmatrix}.$$

Therefore, the reproduction number (R_0) = $\frac{\beta\lambda}{\mu(\mu+\gamma)}$.

2.3.3 Iterative scheme

Consider the model (2.3) along with initial conditions. Applying the Laplace transform to both sides of model (2.3), we derive

$$\begin{aligned} \frac{pLS(t) - S(0)}{p + \alpha(1-p)} &= L(\lambda - \beta SI - \mu S), \\ \frac{pLI(t) - I(0)}{p + \alpha(1-p)} &= L(\beta SI - (\gamma + \mu)I), \\ \frac{pLQ(t) - Q(0)}{p + \alpha(1-p)} &= L(\gamma I - (\delta + \mu)Q), \\ \frac{pLR(t) - R(0)}{p + \alpha(1-p)} &= L(\delta Q - \mu R). \end{aligned} \tag{2.4}$$

Rearranging, we get

$$\begin{aligned}
LS(t) &= \frac{S(0)}{p} + \frac{p + \alpha(1-p)}{p} L(\lambda - \beta SI - \mu S), \\
LI(t) &= \frac{I(0)}{p} + \frac{p + \alpha(1-p)}{p} L(\beta SI - (\gamma + \mu)I), \\
LQ(t) &= \frac{Q(0)}{p} + \frac{p + \alpha(1-p)}{p} L(\gamma I - (\delta + \mu)Q), \\
LR(t) &= \frac{R(0)}{p} + \frac{p + \alpha(1-p)}{p} L(\delta Q - \mu R).
\end{aligned} \tag{2.5}$$

Using inverse Laplace transform of the equations (2.5), we get

$$\begin{aligned}
S(t) &= S(0) + L^{-1}\left[\frac{p + \alpha(1-p)}{p}\right] L(\lambda - \beta SI - \mu S), \\
I(t) &= I(0) + L^{-1}\left[\frac{p + \alpha(1-p)}{p}\right] L(\beta SI - (\gamma + \mu)I), \\
Q(t) &= Q(0) + L^{-1}\left[\frac{p + \alpha(1-p)}{p}\right] L(\gamma I - (\delta + \mu)Q), \\
R(t) &= R(0) + L^{-1}\left[\frac{p + \alpha(1-p)}{p}\right] L(\delta Q - \mu R).
\end{aligned} \tag{2.6}$$

Using initial conditions, we get the recursive equations given by,

$$\begin{aligned}
S_{n+1}(t) &= S_n(0) + L^{-1}\left[\frac{p + \alpha(1-p)}{p}\right] L(\lambda - \beta S_n I_n - \mu S_n), \\
I_{n+1}(t) &= I_n(0) + L^{-1}\left[\frac{p + \alpha(1-p)}{p}\right] L(\beta S_n I_n - (\gamma + \mu)I_n), \\
Q_{n+1}(t) &= Q_n(0) + L^{-1}\left[\frac{p + \alpha(1-p)}{p}\right] L(\gamma I_n - (\delta + \mu)Q_n), \\
R_{n+1}(t) &= R_n(0) + L^{-1}\left[\frac{p + \alpha(1-p)}{p}\right] L(\delta Q_n - \mu R_n).
\end{aligned} \tag{2.7}$$

2.4 Stability analysis

To obtain the equilibrium points of the system (2.3) we have,
i.e., ${}^{CF}D_t^\alpha S(t) = {}^{CF}D_t^\alpha I(t) = {}^{CF}D_t^\alpha Q(t) = {}^{CF}D_t^\alpha R(t) = 0$.

We have two equilibrium points given by $E_0(\frac{\lambda}{\mu}, 0, 0, 0)$ and $E_1(S^*, I^*, Q^*, R^*)$ where $S^* = \frac{\beta}{\mu+\gamma}$, $I^* = \frac{\lambda}{\mu+\gamma} - \frac{\beta\mu}{(\mu+\gamma)^2}$, $Q^* = \frac{\gamma I^*}{\mu+\delta}$, $R^* = \frac{\delta Q^*}{\mu}$.

For further analysis, the Jacobian matrix of the system (2.3) at any equilibrium point (S, I, Q, R) is given by

$$J = \begin{bmatrix} -\beta I - \mu & -\beta S & 0 & 0 \\ \beta I & \beta S - (\mu + \gamma) & 0 & 0 \\ 0 & \gamma & -(\mu + \delta) & 0 \\ 0 & 0 & \delta & -\mu \end{bmatrix}.$$

Theorem 2.4.1. *The disease-free equilibrium of the system (2.3) is locally stable if $R_0 < 1$ and unstable if $R_0 > 1$.*

Proof. At the equilibrium point $E_0(\frac{\lambda}{\mu}, 0, 0, 0)$, the Jacobian matrix becomes,

$$J(E_0) = \begin{bmatrix} -\mu & -\frac{\beta\lambda}{\mu} & 0 & 0 \\ 0 & \frac{\beta\lambda}{\mu} - (\mu + \gamma) & 0 & 0 \\ 0 & \gamma & -(\mu + \delta) & 0 \\ 0 & 0 & \delta & -\mu \end{bmatrix}.$$

The characteristic roots of the matrix $J(E_0)$ are $-\mu$, $-\mu$, $-(\mu + \delta)$ and $(\mu + \gamma)(R_0 - 1)$. Since the first three roots are negative and other will be negative if $R_0 < 1$ and positive if $R_0 > 1$. Thus the equilibrium point E_0 is locally asymptotically stable if $R_0 < 1$ and unstable if $R_0 > 1$.

Theorem 2.4.2. *If $R_0 > 1$, the epidemic equilibrium $E_1(S^*, I^*, Q^*, R^*)$ is locally asymptotically stable.*

Proof. At the equilibrium point $E_1(S^*, I^*, Q^*, R^*)$, the Jacobian matrix becomes,

$$J(E_1) = \begin{bmatrix} -\beta I^* - \mu & -\beta S^* & 0 & 0 \\ \beta I^* & \beta S^* - (\mu + \gamma) & 0 & 0 \\ 0 & \gamma & -(\mu + \delta) & 0 \\ 0 & 0 & \delta & -\mu \end{bmatrix}.$$

The characteristic equation of the matrix $J(E_1)$ is $(-\mu - x)(-\mu - \delta - x)(x^2 - ax + b) = 0$. Where, $a = \beta S^* - \beta I^* - (2\mu + \gamma)$ and $b = \beta I^*(\mu + \gamma) + \mu(\mu + \gamma) - \beta\mu S^*$.

The roots of the characteristic equations $J(E_1)$ are $x_1 = -\mu < 0$, $x_2 = (\mu + \delta) < 0$ and other two satisfies the following quadratic equation,

$$x^2 - ax + b = 0. \quad (2.8)$$

It is noted that the roots of (2.8) will be negative if $a < 0$ and $b > 0$.

Theorem 2.4.3. *The disease-free equilibrium point of the system (2.3) is globally asymptotically stable if $R_0 < 1$ and unstable if $R_0 > 1$.*

Proof. Considering the suitable Lyapunov function as $F = I$.

Calculative the time fractional derivative of the above function

$${}^{CF}D_t^\alpha F(t) = {}^{CF}D_t^\alpha I(t).$$

Utilizing system (3.3) we get,

$${}^{CF}D_t^\alpha F(t) = \beta SI - (\gamma + \mu)I \leq [\beta S - (\gamma + \mu)]I.$$

Since, $S = \frac{\lambda}{\mu} \leq N$, it follows that,

$${}^{CF}D_t^\alpha F(t) \leq I(\gamma + \mu)[R_0 - 1].$$

Hence if $R_0 < 1$, then ${}^{CF}D_t^\alpha F(t) < 0$. By LaSalle's extension to Lyapunov's principle, the disease-free equilibrium point is globally asymptotically stable and unstable if $R_0 > 1$.

Theorem 2.4.4. If $R_0 > 1$, the epidemic equilibrium E_1 is globally asymptotically stable if $(2I - \frac{I^*Q}{Q^*} - \frac{IQ^*}{Q}) \leq 0$.

Proof. Consider the model (2.3) and $R_0 > 1$, so that the epidemic equilibrium E_1 of model exists.

We consider the following non-linear Lyapunov function of Goh-Volterra type:

$$V = (S - S^* - S^* \log \frac{S}{S^*}) + (I - I^* - I^* \log \frac{I}{I^*}) + (Q - Q^* - Q^* \log \frac{Q}{Q^*}).$$

The time fractional derivative of the above function is,

$${}^{CF}D_t^\alpha V(t) = (1 - \frac{S^*}{S}) {}^{CF}D_t^\alpha S(t) + (1 - \frac{I^*}{I}) {}^{CF}D_t^\alpha I(t) + (1 - \frac{Q^*}{Q}) {}^{CF}D_t^\alpha Q(t).$$

Utilizing system (2.3) we get,

$${}^{CF}D_t^\alpha V(t) = (\lambda - \beta SI - \mu S - \frac{S^*(\lambda - \beta SI - \mu S)}{S}) + ((\beta SI - (\gamma + \mu)I) - \frac{I^*(\beta SI - (\gamma + \mu)I)}{I}) + ((\gamma I - (\delta + \mu)Q) - \frac{Q^*(\gamma I - (\delta + \mu)Q)}{Q}).$$

At steady state from equation (2.3), we have

$$\lambda = \beta S^* I^* + \mu S^*, \quad (\gamma + \mu) = \beta S^*, \quad (\delta + \mu) = \frac{\gamma I^*}{Q^*}.$$

Using the condition of steady state of the above equation, we have

$${}^{CF}D_t^\alpha V(t) = (\beta S^* I^* + \mu S^* - \beta SI - \mu S - \frac{S^*(\beta S^* I^* + \mu S^* - \beta SI - \mu S)}{S}) + ((\beta SI - \beta S^* I^*) - \frac{I^*(\beta SI - \beta S^* I^*)}{I}) + ((\gamma I - (\frac{\gamma I^*}{Q^*})Q) - \frac{Q^*(\gamma I - (\frac{\gamma I^*}{Q^*})Q)}{Q}).$$

Further simplification gives,

$${}^{CF}D_t^\alpha V(t) = -\frac{\mu}{S}(S - S^*)^2 - \frac{\beta I^*}{S}(S - S^*)^2 + \gamma(2I - \frac{I^*Q}{Q^*} - \frac{IQ^*}{Q}).$$

Thus, ${}^{CF}D_t^\alpha V(t) \leq 0$ if $(2I - \frac{I^*Q}{Q^*} - \frac{IQ^*}{Q}) \leq 0$.

By LaSalle's extension to Lyapunov's principle, the epidemic equilibrium E_1 is globally asymptotically stable if $(2I - \frac{I^*Q}{Q^*} - \frac{IQ^*}{Q}) \leq 0$.

2.5 The SIQR model's Adam - Bashforth - Moulton predictor - corrector scheme

For fractional order initial value problems of any variety, the Adams-Bashforth-Moulton technique is the most used numerical method. Consider the fractional differential equation

as follows:

$${}^C D_t^\alpha W_j(t) = f_j(t, W_j(t)), W_j^r(t)(0) = W_{j0}^r, r = 0, 1, 2, \dots, [\alpha], j \in N. \quad (2.9)$$

where W_{j0}^r is the arbitrary real number, $\alpha > 0$ and in the Caputo interpretation, D_t^α is the fractional differential operator, which is equal to the well-known Volterra integral equation

$$W_j(t) = \sum_{j=0}^n W_{j0}^r \frac{t^n}{n!} + \frac{1}{\Gamma(\alpha)} \int_0^t (t-v)^{\alpha-1} f_j(v, W_j(v)) dv. \quad (2.10)$$

We use Adam's-Bashforth-Moulton predictor-corrector technique to understand the numerical solution of a nonlinear fractional *SIQR* model. The algorithm is represented in the following way.

Let $h = \frac{T}{m}$, $t_n = nh$, $n = 0, 1, 2, \dots, m$.

The corrector values are defined as,

$$\begin{aligned} S_{n+1}(t) &= S(0) + \frac{h^{\alpha_1}}{\Gamma(\alpha_1 + 2)} (\lambda - \beta S_{n+1}^p I_{n+1}^p - \mu S_{n+1}^p) \\ &+ \frac{h^{\alpha_1}}{\Gamma(\alpha_1 + 2)} \sum_{j=0}^n \alpha_{1,j,n+1} (\lambda - \beta S_j I_j - \mu S_j), \\ I_{n+1}(t) &= I(0) + \frac{h^{\alpha_2}}{\Gamma(\alpha_2 + 2)} (\beta S_{n+1}^p I_{n+1}^p - (\gamma + \mu) I_{n+1}^p) \\ &+ \frac{h^{\alpha_2}}{\Gamma(\alpha_2 + 2)} \sum_{j=0}^n \alpha_{2,j,n+1} (\beta S_j I_j - (\gamma + \mu) I_j), \\ Q_{n+1}(t) &= Q(0) + \frac{h^{\alpha_3}}{\Gamma(\alpha_3 + 2)} (\gamma I_{n+1}^p - (\delta + \mu) Q_{n+1}^p) \\ &+ \frac{h^{\alpha_3}}{\Gamma(\alpha_3 + 2)} \sum_{j=0}^n \alpha_{3,j,n+1} (\gamma I_j - (\delta + \mu) Q_j), \\ R_{n+1}(t) &= R(0) + \frac{h^{\alpha_4}}{\Gamma(\alpha_4 + 2)} (\delta Q_{n+1}^p - \mu R_{n+1}^p) + \frac{h^{\alpha_4}}{\Gamma(\alpha_4 + 2)} \sum_{j=0}^n \alpha_{4,j,n+1} (\delta Q_j - \mu R_j). \end{aligned} \quad (2.11)$$

The corresponding predictor values are given as,

$$\begin{aligned}
S_{n+1}^p &= S(0) + \frac{1}{\Gamma(\alpha_1)} \sum_{j=0}^n \beta_{1,j,n+1} (\lambda - \beta S_j I_j - \mu S_j), \\
I_{n+1}^p &= I(0) + \frac{1}{\Gamma(\alpha_2)} \sum_{j=0}^n \beta_{2,j,n+1} (\beta S_j I_j - (\gamma + \mu) I_j), \\
Q_{n+1}^p &= Q(0) + \frac{1}{\Gamma(\alpha_3)} \sum_{j=0}^n \beta_{3,j,n+1} (\gamma I_j - (\delta + \mu) Q_j), \\
R_{n+1}^p &= R(0) + \frac{1}{\Gamma(\alpha_4)} \sum_{j=0}^n \beta_{4,j,n+1} (\delta Q_j - \mu R_j),
\end{aligned} \tag{2.12}$$

where,

$$\alpha_{i,j,n+1} = \begin{cases} n^{(\alpha+1)} - (n - \alpha)(n + 1)^\alpha, & \text{if } j = 0, \\ (n - j + 2)^{(\alpha+1)} + (n - j)^{(\alpha+1)} - 2(n - j + 1)^{(\alpha+1)}, & \text{if } 0 \leq j \leq n, \\ 1, & \text{if } j = 1, \end{cases}$$

and

$$\beta_{i,j,n+1} = \frac{h^{\alpha_1}}{\alpha} [(n + 1 - j)^{\alpha_1} - (n - j)^{\alpha_1}], 0 \leq j \leq n \text{ and } i = 1, 2, 3, 4.$$

2.6 Numerical simulation and discussion

We will explore into numerical simulations of the Caputo-Fabrizio Coronavirus model (2.3) in this section. From the data given in [55], we use the total initial population of India $N(0) = 1382339513$. At $t = 0$, we have $N(0) = S(0) + I(0) + Q(0) + R(0)$. From the data given in [55], $I(0) = 1401737$, $Q(0) = 350435$, $R(0) = 1184321$ as on 1st August, 2020. Therefore, initial susceptible individuals are determined as $S(0) = N(0) - I(0) - Q(0) - R(0) = 1379403021$.

We can achieve an approximate solution to (2.3) by using ILTM up to four terms as given below:

$$\begin{aligned}
S(t) &= 1.348475481619412 \times 10^9 + (2.06157397629214 \times 10^7 - 2.06157397629214 \times \\
&10^7 t) \alpha + (9979277.478555693 - 9979277.478555693 t) \alpha^2 + \\
&(213892.1387878844 - 427784.2775757688 t + 106427.94759027788 t^2) \alpha^2 +
\end{aligned}$$

Parameter	Value	Reference
λ	0.0182	Estimated
μ	0.0073	[55]
β	0.25172	Estimated
γ	0.3448	Estimated
δ	0.05	[55]

Table 2.2: In the instance of COVID-19 in India, the estimated parametric values are as follows.

$$\begin{aligned}
& (4908.80807228498 - 14726.42421685494t + 7861.062639637445t^2 - 983.7531468944577t^3)\alpha^3 + \\
& (268.45068326930414 - 805.3520498079124t + 536.9013665386083t^2 - 89.48356108976805t^3)\alpha^3 + \\
& (-11.689062445747911 + 46.7562497829916t - 13.32137452984554t^2 - 7.364625025553762t^3 + \\
& 1.5207065071168033t^4)\alpha^4 + (-0.7335655572328584 + 3.667827786164292t - 5.125093038775163t^2 + \\
& 3.0050236604151244t^3 - 0.7090605251997234t^4 + 0.05244550408194907t^5)\alpha^5 \\
& + (-0.00492636944404962 + 0.029558216664297716t - 0.05415069498430903t^2 + \\
& 0.04259896675896235t^3 - 0.015321087824711106t^4 + 0.0024426254074567154t^5 \\
& - 0.00013502096139782384t^6)\alpha^6 + (-0.000013122966745592261 + 0.00009186076721914583t - \\
& 0.00020996746792947618t^2 + 0.00022309043467506846t^3 - 0.00012029386183459572t^4 + \\
& 0.00003324484908883373t^5 - 0.000004374322248530754t^6 + 2.083010594538454 \times 10^{(-7)}t^7)\alpha^7,
\end{aligned}$$

$$\begin{aligned}
I(t) = & 1012335.068983295 + (258876.91049060074 - 258876.91049060074t)\alpha + \\
& (95516.35617971071 - 95516.35617971071t)\alpha + (12420.173869269402 - 24840.347738538803t + \\
& 6344.312276269353t^2)\alpha^2 + (22551.882711126695 - 45103.76542225339t + 11747.782261432008t^2)\alpha^2 + \\
& (385.19267736198077 - 1155.5780320859421t + 172.50028042425208t^2 + 70.56575675621251t^3)\alpha^3 + \\
& (-268.45068326930414 + 805.3520498079124t - 536.9013665386083t^2 + 89.48356108976805t^3)\alpha^3 + \\
& (-80.87273314550815 + 323.4909325820326t - 310.64491003955067t^2 + 99.92642061680984t^3 - \\
& 9.234189473054808t^4)\alpha^4 + (0.7335655572328584 - 3.667827786164292t + 5.125093038775163t^2 - \\
& 3.0050236604151244t^3 + 0.7090605251997234t^4 - 0.05244550408194907t^5)\alpha^5 + \\
& (0.00492636944404962 - 0.029558216664297716t + 0.05415069498430903t^2 - 0.04259896675896235t^3 + \\
& 0.015321087824711106t^4 - 0.0024426254074567154t^5 + 0.00013502096139782384t^6)\alpha^6 + \\
& (0.000013122966745592261 - 0.00009186076721914583t + 0.00020996746792947618t^2 - \\
& 0.00022309043467506846t^3 + 0.00012029386183459572t^4 - 0.00003324484908883373t^5 + \\
& 0.000004374322248530754t^6 - 2.083010594538454 \times 10^{-7}t^7)\alpha^7,
\end{aligned}$$

$$\begin{aligned}
Q(t) = & 1226844.644274208 - 232197.10714117886\alpha + \\
& (-306048.1919000001 + 306048.1919000001t)\alpha - 89257.51364467504\alpha^2 + (-231367.0251 + \\
& 462734.0502t - 115683.51255t^2)\alpha^2 - 17632.368283945347\alpha^3 + 92.56179559125607\alpha^4 + \\
& 7.713482965938004t^4\alpha^4 + \frac{1}{6}t^3(17817.49187512786\alpha^3 - 555.3707735475364\alpha^4) +
\end{aligned}$$

$$t(232197.10714117886\alpha + 178515.02728935008\alpha^2 + 52897.10485183604\alpha^3 - 370.2471823650243\alpha^4) + \frac{1}{2}t^2(-89164.9518490838\alpha^2 - 53082.228443018554\alpha^3 + 647.9325691387925\alpha^4),$$

$$R(t) = 1624099.713711325 - 43416.78594852515\alpha + (-638557.57078218 + 638557.57078218t)\alpha - 2617.7612636548674\alpha^2 + (231554.70369109 - 463109.40738218t + 115777.351845545t^2)\alpha^2 + 13258.700591944958\alpha^3 - 2209.783431990826t^3\alpha^3 + t(43416.78594852515\alpha + 5235.522527309735\alpha^2 - 39776.101775834875\alpha^3) + \frac{1}{2}t^2(-2617.7612636548674\alpha^2 + 39776.101775834875\alpha^3).$$

Figure 2.2 shows the behavior between susceptible individuals versus time for different fractional order α . We observe that number of susceptible individuals decreases with time because they are getting into infected class. Figure 2.3 is indicating the relation between infected individuals versus time with different fractional order α . An increases in the value of α leads to decreases in the infection rate in the infected individuals. We see in Figure 2.4 that number of quarantine individuals increases with time for changes in the values of the fractional order α . The number of recovered individuals grows exponentially, as shown in Figure 2.5 when α decreases. Figure 2.6 shows the behavior of recovered individuals

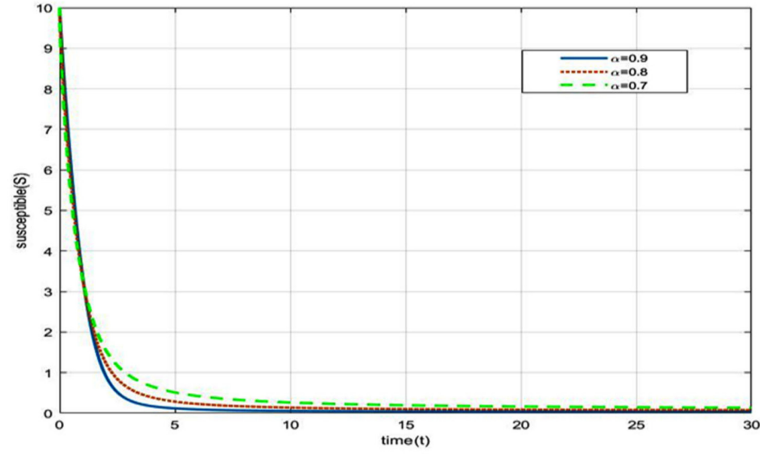


Figure 2.2: Dynamical behavior of susceptible individuals $S(t)$ with regard to time (days) for various values of α .

for different recovery rate δ versus time with $\alpha = 0.9$. A decreases in the recovery rate δ causes a decreases in the number of recovered individuals as expected. We now study effect of the COVID -19 pandemic on the Brazilian population [131]. From the data given in [131] the total initial population of Brazil $N(0) = 209500000$ as on 1st August 2020. Using (2.1) at $t = 0$ we have $N(0) = S(0) + I(0) + Q(0) + R(0)$. From the data given in [131], $I(0) = 2167100, Q(0) = 541775, R(0) = 2152361$ as on 1st August, 2020. Therefore, initial susceptible population is determined as $S(0) = N(0) - I(0) - Q(0) - R(0) = 204638764$.

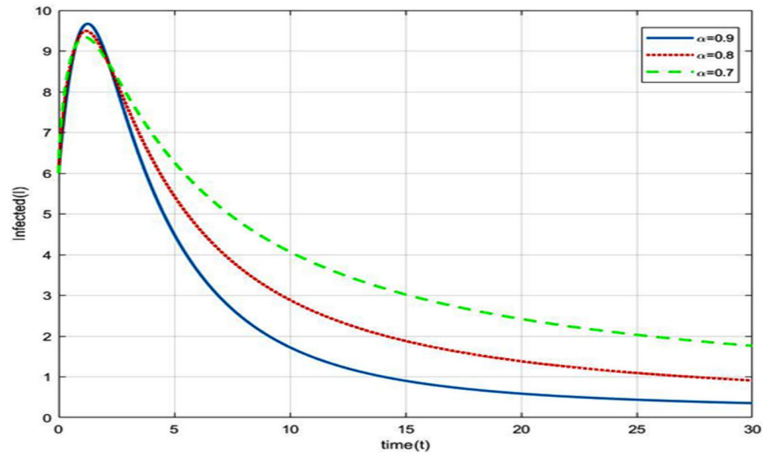


Figure 2.3: Dynamical behavior of infected individuals $I(t)$ with regard to time (days) for various values of α .

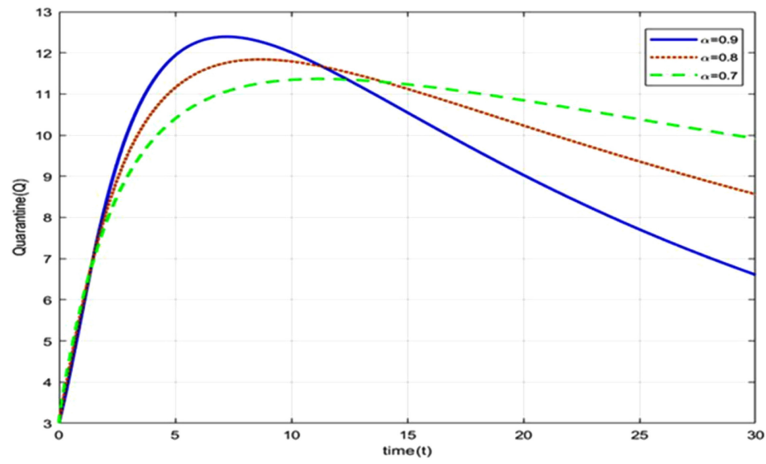


Figure 2.4: Dynamical behavior of quarantine individuals $Q(t)$ with regard to time (days) for various values of α .

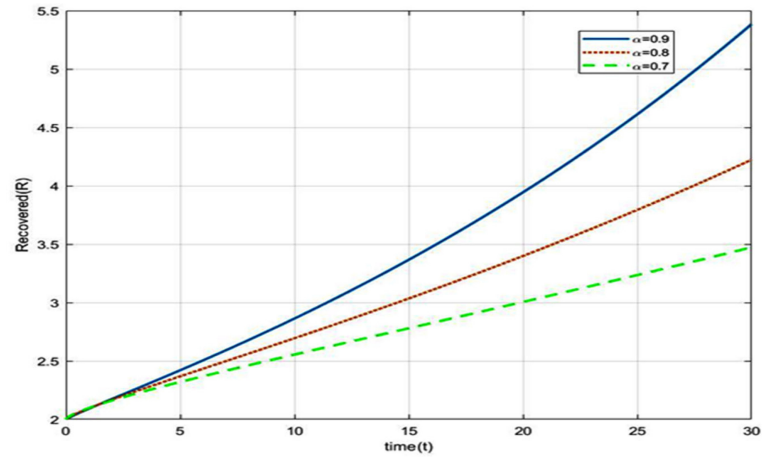


Figure 2.5: Dynamical behavior of recovered individuals $R(t)$ with regard to time (days) for various values of α .

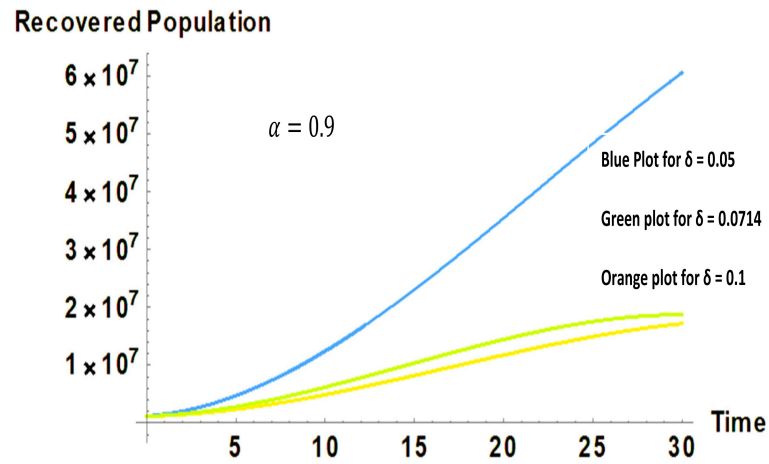


Figure 2.6: The dynamics of recovered individuals for different values of δ with respect to time (days).

Parameter	Value	Reference
λ	0.01867	Estimated
μ	0.00626	[131]
β	0.315	Estimated
γ	0.3333	Estimated
δ	0.04	[131]

Table 2.3: The estimated parametric values are as follows in Brazil.

We achieve an approximate fractional order solution by applying ILTM to four terms in a succession, as shown below:

$$\begin{aligned}
S(t) = & 1.988324783119671 \times 10^8 + (5766154.964132981 - 5766154.964132981t)\alpha \\
& + (42994.313931732555 - 85988.62786346511t + 21575.945826256426t^2)\alpha^2 + (-2886.972994182714 + \\
& 8660.918982548143t - 4384.476770316121t^2 + 498.7743044475575t^3)\alpha^3 + (4.17314911233352 - \\
& 16.692596449334072t - 14.670688294784533t^2 + 16.130469846513165t^3 - 2.3387206164314174t^4)\alpha^4 + \\
& (1.2076687365300693 - 6.038343682650347t + 8.449330559097664t^2 - 4.81440661545906t^3 + \\
& 1.0993855080902668t^4 - 0.07968347888673288t^5)\alpha^5 + (0.0022060561968627744 - \\
& 0.01323633718117665t + 0.02445116550820208t^2 - 0.0195702694327723t^3 + 0.00723995188278034t^4 - \\
& 0.0011994028218474224t^5 + 0.00006982319726061211t^6)\alpha^6 + (-0.00006151578090385235 + \\
& 0.0004306104663269664t - 0.0009842524944616376t^2 + 0.00104576827536549t^3 - \\
& 0.0005638946582853133t^4 + 0.0001558399782897593t^5 - 0.00002050526030128412t^6 + \\
& 9.764409667278152 \times 10^{-7}t^7)\alpha^7,
\end{aligned}$$

$$\begin{aligned}
I(t) = & 2076914.236797711 + (111128.28717407388 - 111128.28717407388t)\alpha + \\
& (-20702.38871722496 + 41404.77743444992t - 10396.275037363199t^2)\alpha^2 + (-302.1686554503082 + \\
& 906.5059663509248t - 466.65206741227087t^2 + 55.221424917565585t^3)\alpha^3 + (63.243214166524844 - \\
& 252.9728566660994t + 250.6279597707888t^2 - 83.54683312537152t^3 + 7.956750889669616t^4)\alpha^4 + \\
& (-1.2076687365300693 + 6.038343682650347t - 8.449330559097664t^2 + 4.81440661545906t^3 - \\
& 1.0993855080902668t^4 + 0.07968347888673288t^5)\alpha^5 + (-0.0022060561968627744 + \\
& 0.01323633718117665t - 0.02445116550820208t^2 + 0.0195702694327723t^3 - 0.00723995188278034t^4 + \\
& 0.0011994028218474224t^5 - 0.00006982319726061211t^6)\alpha^6 + (0.00006151578090385235 - \\
& 0.0004306104663269664t + 0.0009842524944616376t^2 - 0.00104576827536549t^3 + \\
& 0.0005638946582853133t^4 - 0.0001558399782897593t^5 + 0.00002050526030128412t^6 - \\
& 9.764409667278152 \times 10^{-7}t^7)\alpha^7,
\end{aligned}$$

$$\begin{aligned}
Q(t) = & 2556591.201558373 + (-1936032.837279405 + 1936032.837279405t)\alpha + \\
& (-81404.66029879282 + 162809.32059758564t - 40736.007990638325t^2)\alpha^2 + (2688.651702308761 - \\
& 8065.9551069262825t + 4100.333235946969t^2 - 470.56051121273583t^3)\alpha^3 + (-67.3556824838279 +
\end{aligned}$$

$$269.4227299353116t - 235.74488869339768t^2 + 67.3556824838279t^3 - 5.6129735403189915t^4)\alpha^4,$$

$$R(t) = 2259922.883515276 + (-189988.44328005833 + 189988.44328005833t)\alpha + (81882.89643428754 - 163765.79286857508t + 40941.44821714377t^2)\alpha^2 + (543.6633304944202 - 1630.9899914832604t + 815.4949957416302t^2 - 90.61055508240335t^3)\alpha^3.$$

Figure 2.7 depicts the behavior of susceptible individuals over time and Figure 2.8 indicates the relation between infected individuals and time for different values of α . Figure 2.9 depicts that the number of quarantined individuals grows with time for changes in the values of α . Figure 2.10 depicts that the number of recovered individuals will increase with time and a decrease in the fractional order α leads to a drop in the number of recovered individuals in the Brazilian population.

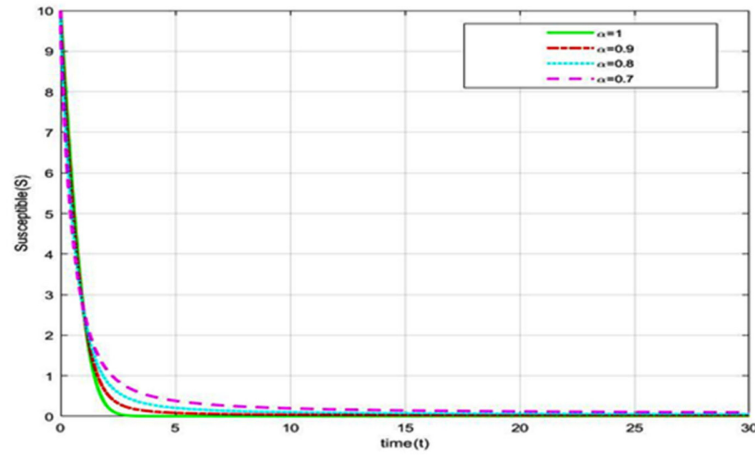


Figure 2.7: The behavior susceptible individuals $S(t)$ with respect to time (days) with a change in the values of α .

2.7 Data fitting and model validation

The data fitting and model validation of the system (2.3) for infected and recovered cases are described in this section. The parametric values are given in Table 2.2. Figure 2.12 and Figure 2.13 depict the graphical representation of the infected and the recovered individuals respectively of the system (2.3) and the real time data of the same reported in India from 1st July to 15th July 2020 [55]. The results of model (2.3) thus obtained are in complete agreement with the real time data.

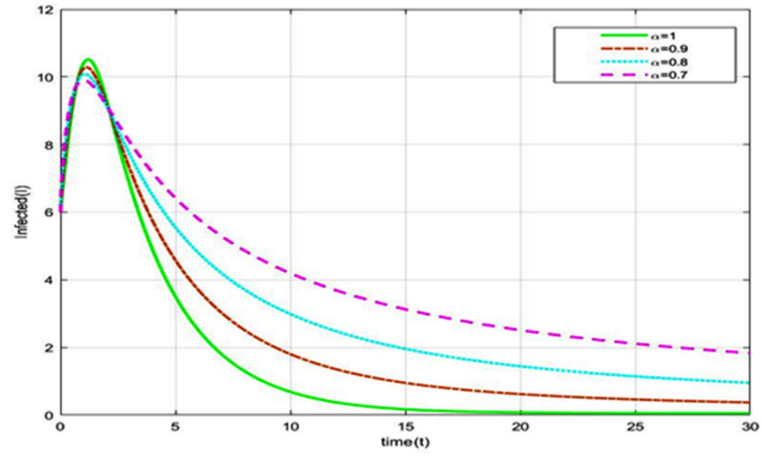


Figure 2.8: The behavior of infected individuals $I(t)$ with regard to time (days) when α changes.

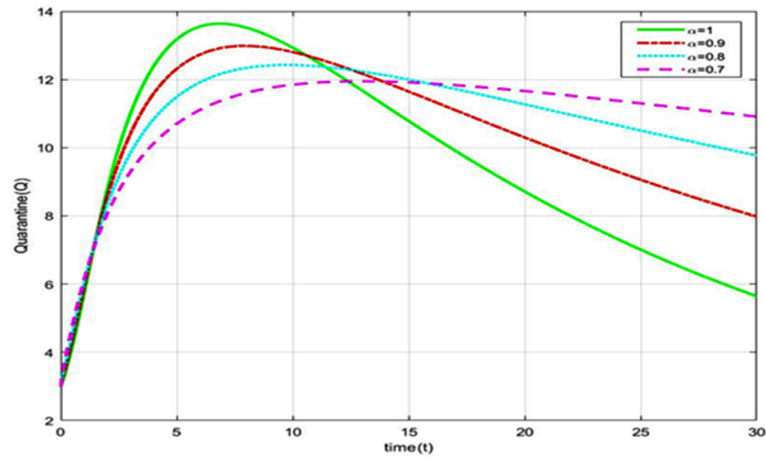


Figure 2.9: The behavior quarantine individual $Q(t)$ with regard to time (days) when α changes.

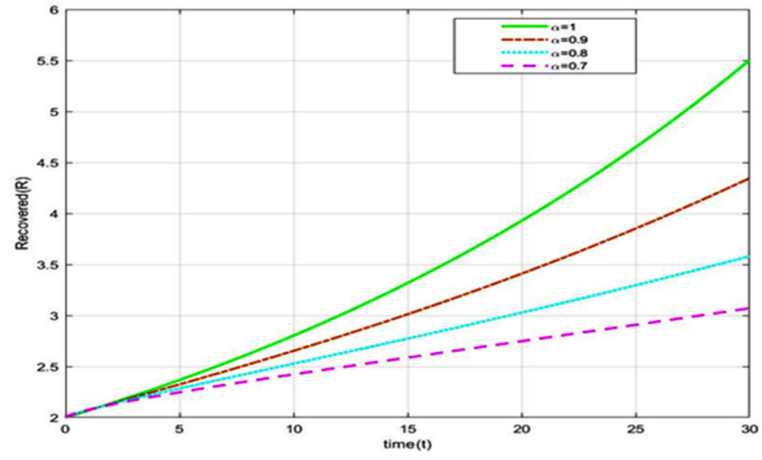


Figure 2.10: The behavior recovered individuals $R(t)$ with regard to time (days) when α changes.

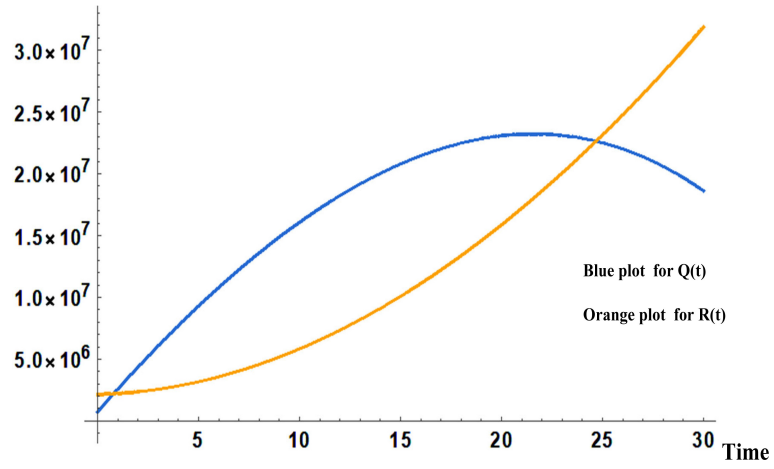


Figure 2.11: Variation of total quarantine individuals and recovered individuals of system (2.3) corresponding to Table 2.3 for $\alpha = 0.9$ with respect to time (days).

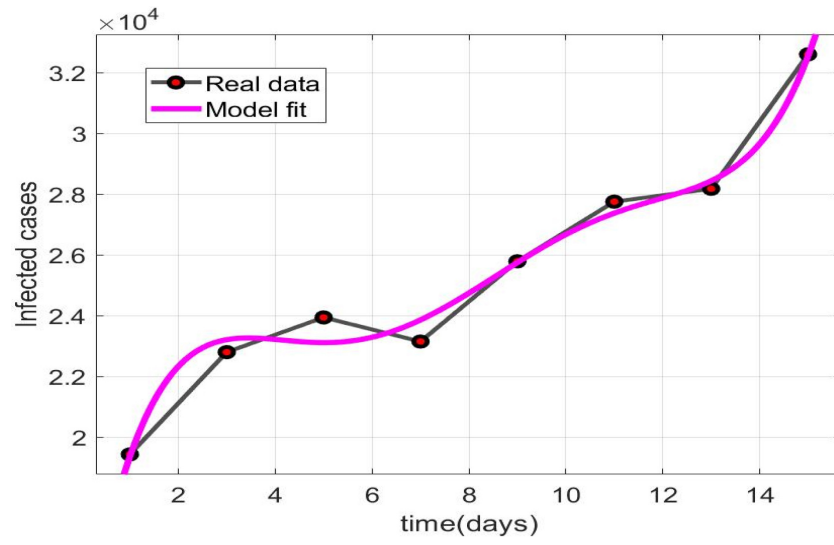


Figure 2.12: Plot of the infected individuals of the system (2.3) and real time data.

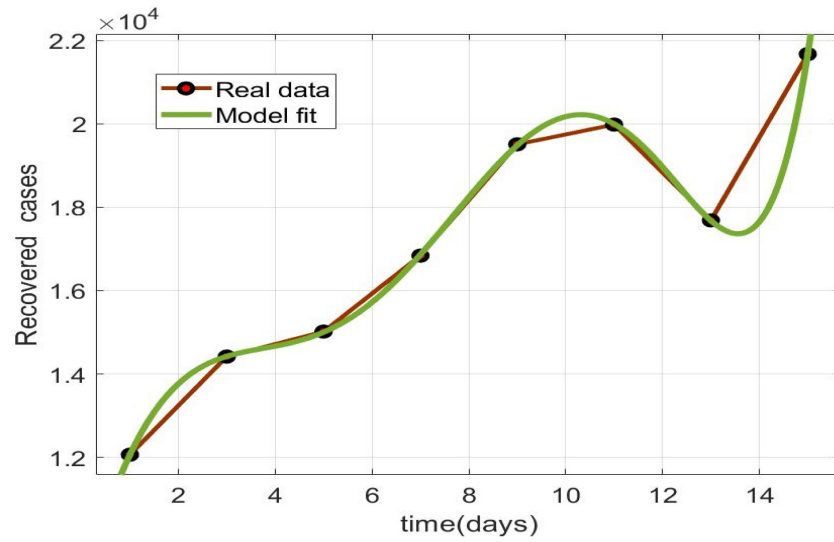


Figure 2.13: Plot of the recovered individuals of the system (2.3) and real time data.

2.8 Conclusion

The fractional order derivatives using the Caputo-Fabrizio of order $0 < \alpha \leq 1$ of the *SIQR* model were explored in this chapter. Based on the COVID-19 cases data in India and Brazil, collected upto 1st August, 2020, we estimated the basic reproduction number R_0 to be 1.7824 and 2.767 respectively. Modeling using fractional-order derivatives is often more efficient than modelling with integer-order derivatives because the option of derivative order gives one more degree of freedom, resulting in a better fit to real-time data with less inaccuracy than the integer-order model. We used the Iterated Laplace Transform Method to solve our proposed model and compared the results to numerical solutions obtained utilizing the Adams–Bashforth–Moulton predictor corrector technique. The parameter values in (2.3) have been estimated using the real time data given in [55, 131] and is presented in Table 2.2 and Table 2.3. In section 2.4, E_0 and E_1 are determined, along with their stability analysis. In section 2.7, we observe that the proposed *SIQR* model with fractional order derivatives comply with the real time data in case of infected and recovered individuals. Thus, it may be considered to be an effective model to study contagious diseases. According to our understanding of the challenges, the incidence of disease transmission must be reduced, or a large part of the population would be afflicted in a very short span of time. For successful isolation and control of the disease's transmission, common preventative methods include lockdown, curfews, and the designation of containment zones.

Chapter 3

Study of fractional order $SEIR$ epidemic model and effect of vaccination on the spread of COVID-19

“To us probability is the very guide of life.”

- Bishop Butler

This chapter is based on the paper

Study of Fractional Order SEIR Epidemic Model and Effect of Vaccination on the Spread of COVID-19, Int. J. Appl. Comput. Math., 8(237), 2022.

3.1 Introduction

Since its inception, human race has encountered and battled deadly epidemics and pandemics due to mass infection caused by viruses, for example SARS, HIV, AIDS, H5N1, Chicken pox and Small pox, etc. Modelling and analysis of such epidemic behavior has been an integral part of research in the areas of Biological and Physical Sciences [82-86]. Though the *SIS*, *SIR* or *SIRS* models [58, 59] have been employed to study illness transmission, the incubation time has been thought to be insignificant. Hence, a new kind of model called *SEIR* was introduced. Similar other factors may influence the population dynamics of certain infectious diseases. Vaccination is one such component that plays an important role in the prevention and control of such illnesses. In 2006, Gumel, McCluskey and Watmough [87] considered an *SVEIR* model to discuss the significance of an anti-SARS vaccine, where *V* accounts for the vaccinated population. In 2016, Wang et al. [88] studied the stability of an *SVEIR* model. However, both the studies and many others, were guided by integral order differential operators of the dynamical variables. In this communication we have considered Caputo order fractional derivatives of a four compartmentalized population with vaccination.

At present times an extensive investigation [89 - 102] of the spread of the highly contagious Coronavirus disease with alarming fatality rate is being carried out. Different models exist in epidemiology to forecast and explain the complexities of an epidemic. Kermack and McKendrick developed one such epidemic model in 1927 [5]. Tang, Wang, Li, and Bragazzi [95] proposed a compartmental deterministic model that took illness progression, patient epidemiological status, and prevention approaches into account. The *SIR* model is most widely used for analyzing and forecasting disease progression adopted in 1991 [103] by Anderson et al. However, all these models were based on integral order derivatives. Differential equations using fractional differential operators have been found to be useful in depicting epidemic scenarios for a variety of infectious diseases [63, 64, 104 - 106]. Several approaches for generating precise and approximate solutions to fractional order differential equations have been developed as a result of extensive research [74, 75, 167, 168]. Several fractional operators have been devised to explore the dynamics of epidemic systems, including Caputo–Fabrizio, Riemann–Liouville, Caputo, Hadamard, Atangana–Baleanu, Katugampola, and others. We employed the Caputo operator to examine the dynamics of COVID-19, since it has a nonlocal and nonsingular exponential kernel [38, 44, 109 - 112]. The dynamical and nonstandard computational study of a heroin epidemic model is discussed by Raza et al. [113]. For more related publications, see Refs. [114 - 120].

As stated earlier, vaccination is a crucial method for eradicating infectious diseases. Covid-19 vaccination has recently been confirmed as a successful method of preventing the spread of the disease. Theoretical findings indicate that the Covid-19 vaccination approach dif-

fers from traditional vaccination methods in terms of achieving disease eradication at low vaccination doses. India started administering COVID-19 vaccines on January 16, 2021. 170,153,432 doses have been administered in this country as of 10 May 2021 [121- 122]. Covishield (a Serum Institute of India-manufactured version of the Oxford–AstraZeneca vaccine) and Covaxin, which were utilised in India at the start of the programme, are now licensed vaccinations (developed by Bharat Biotech). In April 2021, Sputnik V has been licensed as a third vaccination, with delivery beginning in late May 2021. The objective of the current chapter is:

- The model’s dynamical behavior and stability are investigated.
- The Basic Reproduction Number and Equilibrium Points are calculated.
- Numerical simulation to confirm the results and regulate the spread of COVID-19.
- In India, the model was validated and discussed in the COVID-19 instances.

The chapter is structured as follows: Section 3.2 discusses a mathematical model with a fractional order derivative. Section 3.3 discusses some fundamental results of the proposed model system. Section 3.4 is devoted to the discussion of stability analysis and stability criterion of the Model. For the *SEIR* model with vaccination parameter, we use the Adam-Bashforth-Moulton scheme in Section 3.5. The numerical simulation and discussion are given in Section 3.6 using MATLAB. The conclusion of the chapter is presented in Section 3.7.

3.2 Model formulation

At time $t \geq 0$, the total population (N) is divided into four classes, namely, the susceptible (S), the exposed (E), the infected (I) and the recovered (R) class. Thus

$$N(t) = S(t) + E(t) + I(t) + R(t). \quad (3.1)$$

The *SEIR* model with integer order [123, 124] is expressed as follows:

$$\begin{aligned} D_t S(t) &= \lambda - \beta SI - \mu S - \eta S, \\ D_t E(t) &= \beta SI - (k + \mu)E, \\ D_t I(t) &= kE - (\gamma + \mu)I, \\ D_t R(t) &= \gamma I - \mu R + \eta S. \end{aligned} \quad (3.2)$$

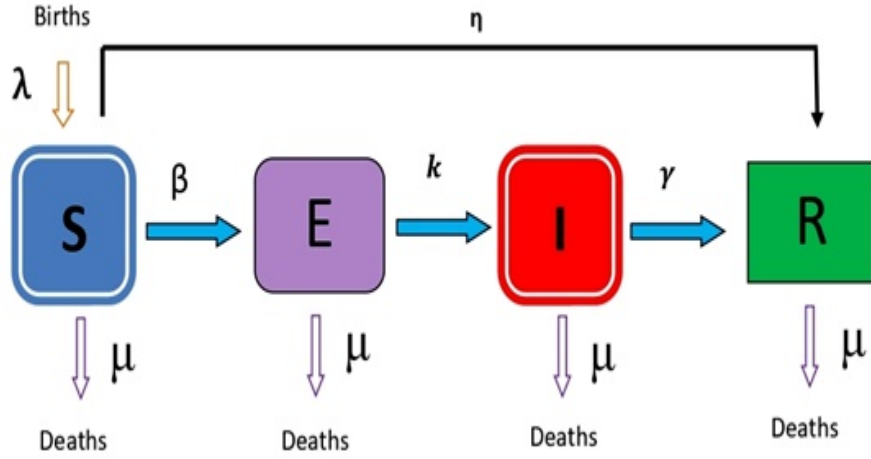


Figure 3.1: The *SEIR* model is depicted as a diagram.

We analyze the SEIR model with vaccination in this presentation, utilizing the Caputo operator of order $0 < \alpha \leq 1$.

$$\begin{aligned}
 {}^C D_t^\alpha S(t) &= \lambda - \beta SI - \mu S - \eta S, \\
 {}^C D_t^\alpha E(t) &= \beta SI - (k + \mu)E, \\
 {}^C D_t^\alpha I(t) &= kE - (\gamma + \mu)I, \\
 {}^C D_t^\alpha Q(t) &= \gamma I - \mu R + \eta S.
 \end{aligned} \tag{3.3}$$

The initial conditions are $S(0) = S_0 > 0$, $E(0) = E_0 > 0$, $I(0) = I_0 > 0$, $R(0) = R_0 \geq 0$.

λ	birth rate of susceptible individuals
μ	death rate
β	contact rate from S to E
γ	recovery rate
k	progression rate exposed to infected
η	vaccination rate

Table 3.1: The parameters of the model and their descriptions.

3.3 Analysis of the model

3.3.1 Non-negativity and boundedness of solutions

Proposition 3.3.1. *The region $\Omega = \{(S, E, I, R) \in \mathbb{R}^4 : 0 < N \leq \frac{\lambda}{\mu}\}$ is non-negative invariant for the model (3.3) for $t \geq 0$.*

Proof. *We have*

$${}^C D_t^\alpha (S + E + I + R)(t) = \lambda - \mu(S + E + I + R)(t).$$

$$\text{Therefore, } {}^C D_t^\alpha N(t) + \mu N = \lambda.$$

Taking Laplace transform [125], we have

$$p^\alpha L(N(t)) - p^{\alpha-1} N(0) + \mu L(N(t)) = \frac{\lambda}{p}.$$

$$\text{So, } L(N(t)) = \frac{p^{\alpha-1} N(0)}{p^{\alpha+1} + \mu} + \frac{\lambda}{p^{\alpha+1} + \mu}.$$

Applying inverse Laplace transform [126 - 128], we get

$$N(t) = N(0)E_{\alpha,1}(-\mu t^\alpha) + \lambda t^\alpha E_{\alpha,\alpha+1}(-\lambda t^\alpha).$$

According to Mittag-Leffler function,

$$E_{c,d}(z) = zE_{c,c+d}(z) + \frac{1}{\Gamma(d)}.$$

$$\text{Thus, } \lim_{t \rightarrow \infty} \sup N(t) \leq \frac{\lambda}{\mu}.$$

As a result, the functions S, E, I , and R are all non-negative.

3.3.2 Basic reproduction number

The basic reproduction number R_0 may be obtained from the maximum eigenvalue of the matrix FV^{-1} where,

$$F = \begin{bmatrix} 0 & \frac{\beta\lambda}{\mu+\eta} \\ 0 & 0 \end{bmatrix} \text{ and } V = \begin{bmatrix} \mu+k & 0 \\ -k & \mu+\gamma \end{bmatrix}.$$

Therefore, the reproduction number $(R_0) = \frac{k\beta\lambda}{(\mu+\eta)(\mu+k)(\mu+\gamma)}$.

3.4 Stability analysis

The system's equilibrium may be found by solving the system (3.3). The disease-free equilibrium points E_0 and the epidemic equilibrium point E_1 of the system (3.3) are obtained from

$$\text{i.e., } {}^C D_t^\alpha S(t) = {}^C D_t^\alpha E(t) = {}^C D_t^\alpha I(t) = {}^C D_t^\alpha R(t) = 0.$$

The mode (3.3) has two equilibrium points namely $E_0(\frac{\lambda}{\mu+\eta}, 0, 0, \frac{\lambda\eta}{\mu(\mu+\eta)})$ and $E_1(S^*, E^*, I^*, R^*)$ where

E_0 is the disease-free equilibrium point and E_1 is the unique epidemic equilibrium point of the system (2.3), where

$$S^* = \frac{(\mu+\gamma)(\mu+k)}{\beta k}, E^* = \frac{(\mu+\gamma)I^*}{k}, I^* = \frac{\lambda k}{(\mu+\gamma)(\mu+k)} - \frac{(\mu+\eta)}{\beta}, R^* = \frac{\gamma I^* + \eta S^*}{\mu}.$$

The Jacobian matrix (J) of the system (3.3) at (S, E, I, R) is given by

$$J = \begin{bmatrix} -\beta I - \mu - \eta & 0 & -\beta S & 0 \\ \beta I & -(\mu + k) & \beta S & 0 \\ 0 & k & -(\mu + \gamma) & 0 \\ 0 & 0 & \gamma & -\mu \end{bmatrix}.$$

Theorem 3.4.1. *When $R_0 < 1$, the point E_0 of the system (3.3) is locally asymptotically stable, and when $R_0 > 1$, it is unstable.*

Proof. The Jacobian matrix (J) at E_0 becomes,

$$J(E_0) = \begin{bmatrix} -\mu - \eta & 0 & -\frac{\lambda\beta}{\mu+\eta} & 0 \\ 0 & -(\mu + k) & \frac{\lambda\beta}{\mu+\eta} & 0 \\ 0 & k & -(\mu + \gamma) & 0 \\ 0 & 0 & \gamma & -\mu \end{bmatrix}.$$

Now $(-\mu - \eta)$, $-\mu$, $-(\mu + \gamma)$ and $(\mu + k)(R_0 - 1)$ are the roots of the characteristic equation. The equilibrium point E_0 is locally asymptotically stable or unstable according as $R_0 < 1$ or $R_0 > 1$.

Theorem 3.4.2. *If $R_0 > 1$, the epidemic equilibrium $E_1(S^*, E^*, I^*, R^*)$ is locally asymptotically stable.*

Proof. The Jacobian matrix J at E_1 becomes,

$$J(E_1) = \begin{bmatrix} -\beta I^* - \mu - \eta & 0 & -\beta S^* & 0 \\ \beta I^* & -(\mu + k) & \beta S^* & 0 \\ 0 & k & -(\mu + \gamma) & 0 \\ 0 & 0 & \gamma & -\mu \end{bmatrix}.$$

The characteristic equation is $(-\mu - x)(x^3 + ax^2 + bx + c) = 0$.

Where, $a = \beta I^* + 3\mu + k + \gamma + \eta$,

$b = (\beta I^* + \mu + \eta)(2\mu + k + \gamma) + (\mu + k)(\mu + \gamma) - \beta k S^*$,

$c = (\beta I^* + \mu)(\mu + k)(\mu + \gamma) - (\mu + \eta)\beta k S^*$.

Applying Routh-Hurwitz condition, the model (3.3) is locally asymptotically stable at E_1 as $a > 0, b > 0, ab > c$.

Theorem 3.4.3. *When $R_0 < 1$, the system (3.3) is globally asymptotically stable and unstable if $R_0 > 1$ at E_0 .*

Proof. Using the appropriate Lyapunov function as $F = B_1 E + B_2 I$.

The aforementioned function's time fractional derivative is

$${}^C D_t^\alpha F(t) = B_1 {}^C D_t^\alpha E(t) + B_2 {}^C D_t^\alpha I(t).$$

Utilizing system (3.3) we get,

$${}^C D_t^\alpha F(t) = B_1(\beta SI - (k + \mu)E) + B_2(kE - (\gamma + \mu)I).$$

Using little perturbation from (3.3), we have

$$B_1 = \lambda k, B_2 = (\mu + k)(\mu + \eta).$$

Since, $S = \frac{\lambda}{\mu + \eta} \leq N$, It follows that,

$${}^C D_t^\alpha F(t) \leq I(\gamma + \mu)(\mu + k)(\mu + \eta)[R_0 - 1].$$

Hence if $R_0 < 1$, then ${}^C D_t^\alpha F(t) < 0$. As a result of LaSalle's use of Lyapunov's concept [38, 129], the point E_0 is globally asymptotically stable and unstable if $R_0 > 1$.

Theorem 3.4.4. The equilibrium point E_1 is globally asymptotically stable if $R_0 > 1$.

Proof. The non-linear Lyapunov function of Goh-Volterra form is as follows:

$$V = (S - S^* - S^* \log \frac{S}{S^*}) + (E - E^* - E^* \log \frac{E}{E^*}) + Q(I - I^* - I^* \log \frac{I}{I^*}).$$

Taking Caputo derivative, we get

$${}^C D_t^\alpha V(t) = (1 - \frac{S^*}{S}) {}^C D_t^\alpha S(t) + (1 - \frac{E^*}{E}) {}^C D_t^\alpha E(t) + Q(1 - \frac{I^*}{I}) {}^C D_t^\alpha I(t).$$

Using system (3.3) we get,

$${}^C D_t^\alpha V(t) \leq (\lambda - \beta SI - \mu S - \eta S - \frac{S^*(\lambda - \beta SI - \mu S - \eta S)}{S}) + ((\beta SI - (k + \mu)E) - \frac{E^*(\beta SI - (k + \mu)E)}{E}) + Q((kE - (\gamma + \mu)I) - \frac{I^*(kE - (\gamma + \mu)I)}{I}).$$

At steady state from equation (2.3), we have

$$\lambda = \beta S^* I^* + \mu S^* + \eta S^*$$

Using the condition of steady state of the above equation, we have

$${}^C D_t^\alpha V(t) \leq (\beta S^* I^* + \mu S^* + \eta S^* - \beta SI - \mu S - \eta S - \frac{S^*(\beta S^* I^* + \mu S^* + \eta S^* - \beta SI - \mu S - \eta S)}{S}) + ((\beta SI - (k + \mu)E) - \frac{E^*(\beta SI - (k + \mu)E)}{E}) + Q((kE - (\gamma + \mu)I) - \frac{I^*(kE - (\gamma + \mu)I)}{I}).$$

Taking all infected classes that do not have a single star (*) from the above equation and equal to zero:

$$S^* \beta I - (\mu + k)E + Q(kE - (\mu + \gamma)I) = 0.$$

The steady state was slightly perturbed between (3.3) and the above equation, resulting in:

$$Q = \frac{S^* \beta}{(\mu + \gamma)}, (\mu + k) = \frac{I^* S^* \beta}{E^*}, k = \frac{(\mu + \gamma)I}{E^*}.$$

Further simplification gives,

$${}^C D_t^\alpha V(t) \leq (\beta S^* I^* + \mu S^* + \eta S^* - \mu S - \frac{S^*(\beta S^* I^* + \mu S^* - \mu S - \eta S)}{S}) + (-\frac{\beta S I E^*}{E} + \beta S^* I^*) + (-\frac{\beta S^* I^* E I^*}{I E^*} + \beta S^* I^*).$$

Using A.M \geq G.M., we have

$$(2 - \frac{S}{S^*} - 2\frac{S^*}{S}) \leq 0, (3 - \frac{S}{S^*} - \frac{I^* E}{I E^*} - \frac{S E^* I}{E}) \leq 0. \text{ Thus, } {}^C D_t^\alpha V(t) \leq 0 \text{ for } R_0 > 1.$$

The point E_1 is globally asymptotically stable if $R_0 > 1$.

3.5 Predictor-corrector technique for the SEIR model

The Adams-Bashforth-Moulton approach is the most extensively employed numerical approach for fractional order initial value circumstances. Let us consider

$${}^C D_t^\alpha L_j(t) = g_j(t, L_j(t)), L_j^r(t)(0) = L_{j0}^r, r = 0, 1, 2, \dots, [\alpha], j \in N, \quad (3.4)$$

where $L_{j0}^r \in R$ is equal to the well-known Volterra integral equation

$$L_j(t) = \sum_{j=0}^n L_{j0}^r \frac{t^n}{n!} + \frac{1}{\Gamma(\alpha)} \int_0^t (t-u)^{\alpha-1} g_j(u, L_j(u)) du. \quad (3.5)$$

The algorithm is explained as follows

Let $h = \frac{T}{m}$, $t_n = nh$, $n = 0, 1, 2, \dots, m$.

Corrector formulae:

$$\begin{aligned} S_{n+1}(t) &= S(0) + \frac{h^{\alpha_1}}{\Gamma(\alpha_1 + 2)} (\lambda - \beta S_{n+1}^p I_{n+1}^p - \mu S_{n+1}^p - \eta S_{n+1}^p) \\ &+ \frac{h^{\alpha_1}}{\Gamma(\alpha_1 + 2)} \sum_{j=0}^n \alpha_{1,j,n+1} (\lambda - \beta S_j I_j - \mu S_j - \eta S_j), \\ E_{n+1}(t) &= I(0) + \frac{h^{\alpha_2}}{\Gamma(\alpha_2 + 2)} (\beta S_{n+1}^p I_{n+1}^p - (k + \mu) E_{n+1}^p) \\ &+ \frac{h^{\alpha_2}}{\Gamma(\alpha_2 + 2)} \sum_{j=0}^n \alpha_{2,j,n+1} (\beta S_j I_j - (k + \mu) E_j), \\ I_{n+1}(t) &= Q(0) + \frac{h^{\alpha_3}}{\Gamma(\alpha_3 + 2)} (k E_{n+1}^p - (\gamma + \mu) I_{n+1}^p) \\ &+ \frac{h^{\alpha_3}}{\Gamma(\alpha_3 + 2)} \sum_{j=0}^n \alpha_{3,j,n+1} (k E_j - (\gamma + \mu) I_j), \\ R_{n+1}(t) &= R(0) + \frac{h^{\alpha_4}}{\Gamma(\alpha_4 + 2)} (\gamma I_{n+1}^p - \mu R_{n+1}^p + \eta S_{n+1}^p) \\ &+ \frac{h^{\alpha_4}}{\Gamma(\alpha_4 + 2)} \sum_{j=0}^n \alpha_{4,j,n+1} (\gamma I_j - \mu R_j + \eta S_j). \end{aligned} \quad (3.6)$$

Predictor formulae:

$$\begin{aligned}
S_{n+1}^p &= S(0) + \frac{1}{\Gamma(\alpha_1)} \sum_{j=0}^n \beta_{1,j,n+1} (\lambda - \beta S_j I_j - \mu S_j - \eta S_j), \\
E_{n+1}^p &= I(0) + \frac{1}{\Gamma(\alpha_1)} \sum_{j=0}^n \beta_{1,j,n+1} (\beta S_j I_j - (k + \mu) E_j), \\
I_{n+1}^p &= Q(0) + \frac{1}{\Gamma(\alpha_1)} \sum_{j=0}^n \beta_{1,j,n+1} (k E_j - (\gamma + \mu) I_j), \\
R_{n+1}^p &= R(0) + \frac{1}{\Gamma(\alpha_1)} \sum_{j=0}^n \beta_{1,j,n+1} (\gamma I_j - \mu R_j + \eta S_j),
\end{aligned} \tag{3.7}$$

where,

$$\alpha_{i,j,n+1} = \begin{cases} n^{(\alpha+1)} - (n - \alpha)(n + 1)^\alpha, & \text{if } j = 0, \\
(n - j + 2)^{(\alpha+1)} + (n - j)^{(\alpha+1)} - 2(n - j + 1)^{(\alpha+1)}, & \text{if } 0 \leq j \leq n, \\
1, & \text{if } j = 1, \end{cases}$$

and

$$\beta_{i,j,n+1} = \frac{h^{\alpha_1}}{\alpha} [(n + 1 - j)^{\alpha_1} - (n - j)^{\alpha_1}], 0 \leq j \leq n \text{ and } i = 1, 2, 3, 4.$$

3.6 Numerical simulation and discussion

In this part, we use the mathematical software MATLAB (2018a) to do rigorous numerical simulations of the findings produced by Adam's Bashforth-Moulton predictor-corrector system. The model has been discussed in both the cases of without vaccine corresponding to $\eta = 0$ and with vaccine corresponding to $\eta = 0.1$

Figure 3.2 shows the behavior of susceptible individuals with time for different fractional order α in both cases of with and without vaccination. We observe that number of susceptible individuals decreases with time for all values of α . At a given period, however, the number of susceptible individuals grows as the value of decreases, suggesting that the fractional order derivatives of the dynamical variables produce greater benefits in determining the number of susceptible individuals. Moreover, the administration of vaccine shows that the number of susceptible individuals is always less than those in the case of without vaccination for different values of α as expected.

Figure 3.3 indicates the relation between exposed individuals and time for different frac-

Parameter	Value [without vaccination]	Value [with vaccination]	Reference
λ	0.0182	0.0182	Estimated
μ	0.0073	0.0073	Estimated
β	0.476	0.476	Estimated
η	0.0	0.01	Model to fit
γ	0.286	0.286	[131, 132]
k	0.071	0.071	[131, 132]
R_0	3.67	1.55	Estimated

Table 3.2: Estimated values of parameters.

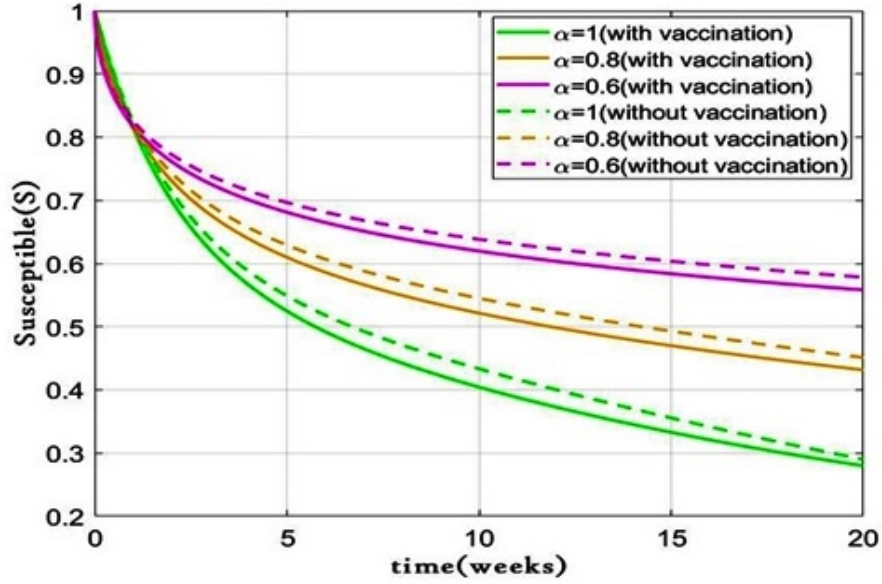


Figure 3.2: Plots of $S(t)$ for different values of $\alpha = 0.6, 0.8, 1.0$ with respect to time (days) with vaccination and without vaccination.

tional order α in both cases of with and without vaccination. We observe that the number of exposed individuals increases with time for all values of α . However, at a fixed time t the number of exposed individuals decreases with a decrease in the value of α . Furthermore, the introduction of vaccination shows that the number of exposed individuals is less than those in the case of without vaccination for different values of α as expected.

Figure 3.4 represents the behavior of the number of infected individuals with time for different fractional order α in both cases of with and without vaccination. We observe that the number of infected individuals decreases consistently with time for different fractional values of α which further decreases with the use of vaccines.

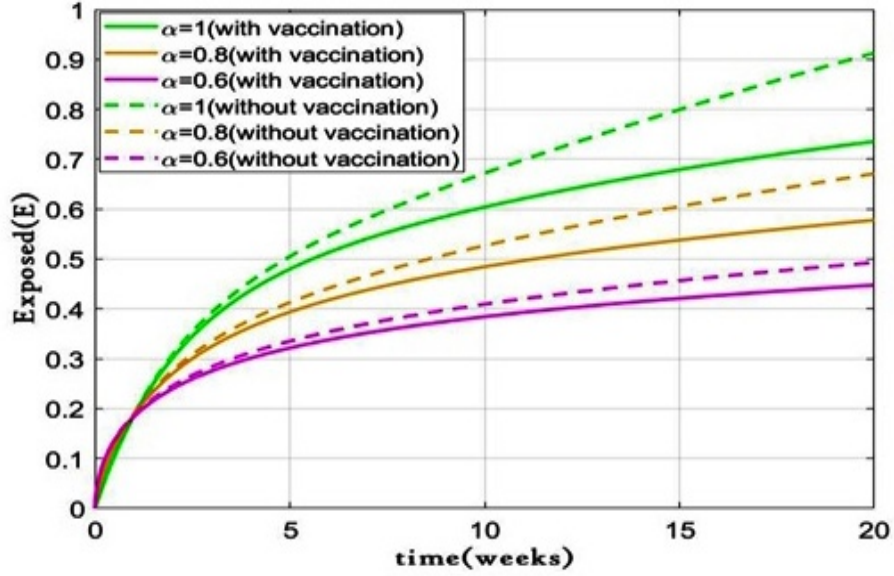


Figure 3.3: Plots of $E(t)$ for different values of $\alpha = 0.6, 0.8, 1.0$ with respect to time (days) with vaccination and without vaccination.

The behavior of recovered individuals with time is shown in Figure 3.5. It is evident from the graph that the number of recovered individuals increases with time for all values of α . It may also be deduced that the recovered individuals increases because of the impact of vaccines.

Figure 3.6 shows the time series analysis of the $SEIR$ model with vaccination for $R_0 = 1.55$ and parameter values given in Table 3.2. The two equilibrium points are $E_0 = (1.0520, 0, 0, 1.4411)$ and $E_1 = (0.6795, 0.0825, 0.0199, 1.7104)$. It shows that with varying initial values, model system (3.3) has an endemic equilibrium and is globally asymptotically stable, confirming our theoretical results in Theorem 3.4.4.

3.7 Conclusion

In this chapter, we have discussed the fractional order derivatives with the Caputo operator of order $0 < \alpha \leq 1$ of $SEIR$ model with vaccination. Based on the COVID-19 cases data in India, collected upto 1st August, 2021, we estimated the basic reproduction number R_0 without vaccination to be 3.67 and with vaccination to be 1.55. Thus, it shows that introduction of the vaccination parameter η reduces the reproduction number R_0 . The parameter values in (3.3) have been estimated using the real time data given in

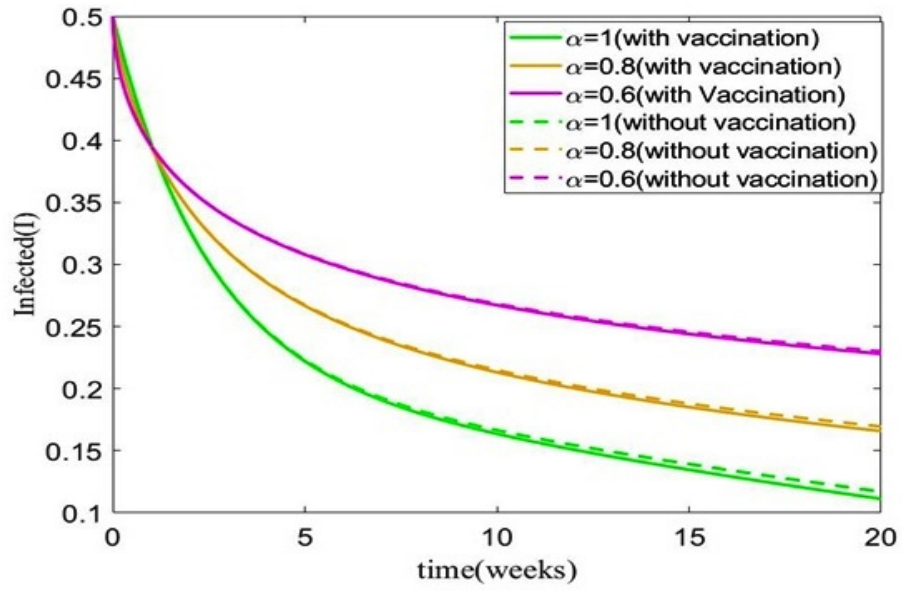


Figure 3.4: Plots of $I(t)$ for various values of $\alpha = 0.6, 0.8, 1.0$ with respect to time (days) with vaccination and without vaccination.

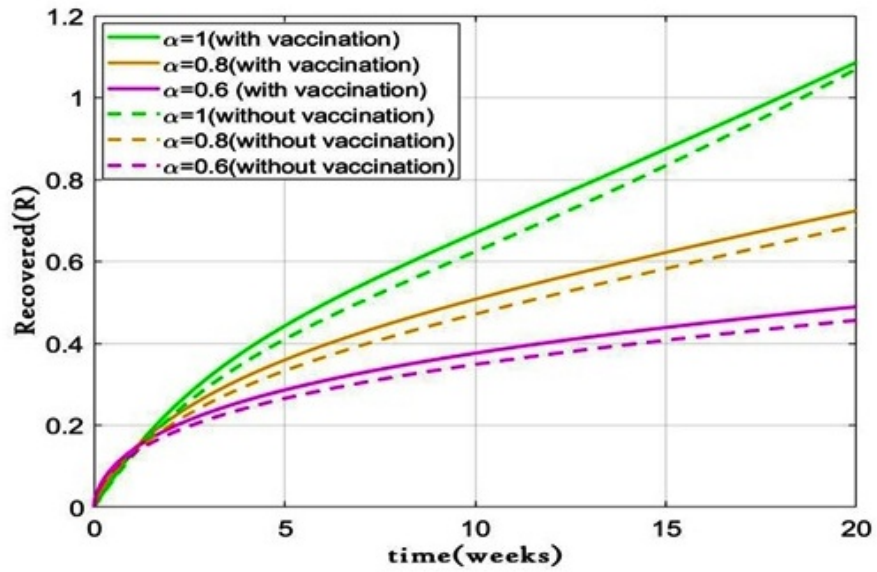


Figure 3.5: Plots of $R(t)$ for different values of $\alpha = 0.6, 0.8, 1.0$ with respect to time (days) with vaccination and without vaccination.

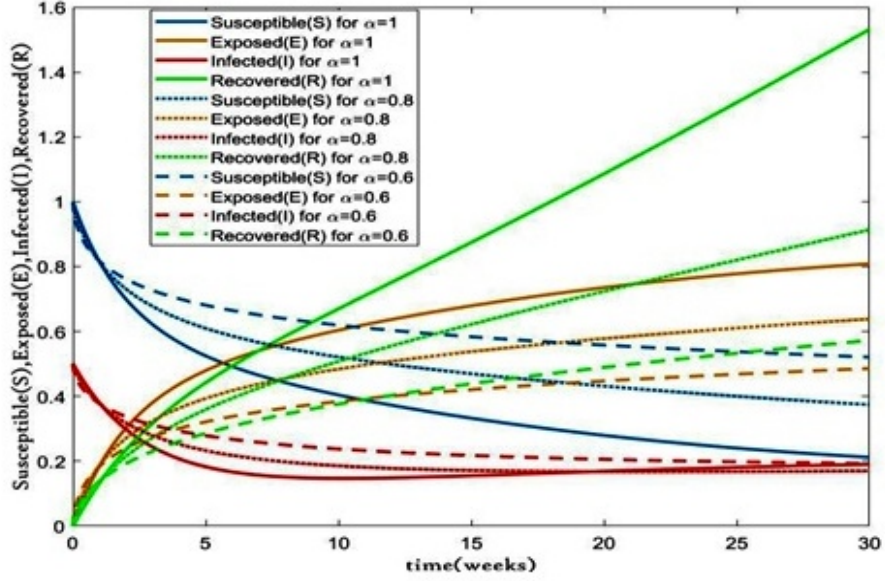


Figure 3.6: Time series plot of all individuals with vaccination and various initial conditions, parameter values are given in Table 3.2.

[131, 1321] and are presented in Table 3.2. We have demonstrated the global stability of the equilibrium points by constructing the Lyapunov function. The choice of a derivative order is often more appropriate for modeling complex data due to its freedom and reduced error. This benefit can be utilized in real time data since the data is typically less accurate than the integer-ordered model. As is evident from our study that vaccination is an effective method in control and prevention of the COVID-19 disease. The model described in this research may be used to investigate the dynamics of various epidemic illnesses, as well as the function of vaccination in successful transmission control. Our investigation suggests that the primary task of health officials, policymakers, and experts should be to implement the most appropriate vaccination plan to fight against the disease. It is very important that the transmission of diseases is controlled at an early stage to avoid a massive impact on the population. Some of the preventive measures that can be utilized are the enforcement of curfews, checkpoints, and containment zones. These can be used to prevent the spread of contamination.

Chapter 4

Dynamics of Caputo fractional order $SEIRV$ epidemic model with optimal control and stability analysis

“The important thing is not to stop questioning. Curiosity has its own reason for existing.”
- Albert Einstein

This chapter is based on the paper
Dynamics of Caputo Fractional Order $SEIRV$ Epidemic Model with Optimal Control and Stability Analysis, Int. J. Appl. Comput. Math. 8(1), 1-25, 2022.

4.1 Introduction

The first instances of corona virus infection in humans in 1965, with symptoms that were comparable to the common cold were first reported by Tyrrell and Bynoe [54]. From December 2019, a new coronavirus known as SARS-COV-2 has been identified in a number of nations, infecting thousands of individuals worldwide with a higher mortality rate. The virus, however, proved deadly in Wuhan, Hubei Province, China, in 2019, after multiple modifications [133]. Henceforth, the virus was named SARS-CoV-2 and the disease was declared to be COVID-19. The spread of the disease with fatal consequences soon accelerated in several countries and was declared a pandemic by World Health Organization on 11th March 2020. It can harm the respiratory tract in a variety of ways, from a typical cold to more serious diseases like SARS [134]. COVID-19 has recently engulfed most of the world's countries, infecting a huge number of individuals. COVID-19 has had a significant impact on people's lives and has resulted in significant economic losses. Coronavirus (formally known as COVID-19) has killed 4,336,797 individuals and infected 205,468,881 individuals throughout the world since it first emerged in China (as on Aug 12, 2021) [83].

Epidemic mathematical models may help in various aspects, including analyzing the role of epidemic propagation and suggesting effective control measures. The idea that epidemic disease transmission patterns may be expressed mathematically dates back to 1766, when Daniel Bernoulli published an article describing the impact of smallpox variolization on lifespan [135]. The epidemiological model created by Kermack and Mckendrick during 1927 is an example of a mathematical model that can be useful in studying the development and prevention of infectious illness [5]. Differential equations of integral order are commonly used in epidemiology modelling of biological processes [58, 59, 136, 137]. Many studies have been conducted in this field of mathematics, and it has been shown that differential equations using fractional operators are effective in demonstrating epidemic models linked to many infectious illnesses [63, 64, 103 - 105]. Tang, Wang, Li, and Bragazzi [95] proposed a compartmental mathematical approach that would combine the disease's clinical progression, the patient's epidemiological state, and intervention measures. There are several concerns, however, about the integral order of the differential equations in such models. Fractional order differential equations, a relatively new and growing topic of mathematical calculus, takes into account such constraints. Various approaches for constructing actual and approximate solutions to fractional order differential equations have emerged throughout time as a result of extensive research [74, 75, 76, 108, 138, 139]. Because of its memory effects, fractional-order models have been investigated for mimicking actual occurrences in recent decades [140]. In [141], the SEIRA mathematical model is analyzed using the Atangana–Baleanu fractional derivative method with the Mittag-Leffler kernel. Furthermore, because fractional models have been shown to

be capable of accurately representing chaotic systems, they have surfaced in a variety of domains dealing with chaos, including physics, biology, and finances [142 - 144].

4.1.1 Research background and motivation

Fractional derivatives are a powerful tool for describing memory and heredity features in a wide range of systems and phenomena. Fractional-order differential equations preserve the function's fundamental information in stacked form. We have such an additional variable (order of the derivative) in fractional-order modeling that is beneficial for numerical methods. Fractional-order modeling has been used to investigate the disease transmission dynamics. In addition, the integer-order differentiation is local, whereas the fractional differentiation is not so. This behavior helps in the simulation of epidemic situations. Furthermore, the fractional derivative has the capability to improve the system's stability zone. The calculus of fractional order system adds an additional parameter to the modeling framework, which helps in numerical simulations. When talking about real problems, the Caputo derivative is highly useful since it allows traditional starting and boundary conditions be included in the derivation, and the derivative of a constant is zero, that is not the case with the Riemann–Liouville fractional derivative. In this study, a fractional SEIRV model with optimum control has been created using Caputo fractional-order differential equations, motivated by the aforementioned studies and the benefits of Caputo fractional-order differential equations.

The objectives of this chapter are:

- Investigate the SEIRV model's dynamical behavior and stability.
- Determine the Basic Reproduction number and Equilibrium points.
- The model system is subjected to an optimal control analysis by controlling 'vaccination rate' parameter.
- Application of the Adam-Bashforth-Moulton predictor-corrector technique to obtain numerical solution.

The chapter is organized as follows: *SEIRV* model with fractional derivative in Caputo sense is discussed in Section 4.2. The existence and uniqueness of the model solution, including positivity and boundedness are established in Section 4.3. The stability analysis and stability criterion of the model system are discussed in Section 4.4. We also provide an optimal control strategy for an *SEIRV* model using the control parameter "vaccination rate" in Section 4.5. In Section 4.6, we perform Adam-Bashforth-Moulton predictor-corrector scheme for the *SEIRV* model. In Section 4.7, numerical simulation

and discussion are presented via MATLAB. Section 4.8 includes the validation of the model with real time data. Finally, Section 4.9 includes the conclusion of the chapter.

4.2 Model formulation

The entire population (N) is divided into five categories, namely, the susceptible individuals (S), the exposed individuals (E), the infected individuals (I), the recovered individuals (R) and the vaccinated individuals (V) at any time $t \geq 0$. Thus

$$N(t) = S(t) + E(t) + I(t) + R(t) + V(t). \quad (4.1)$$

The $SEIRV$ model with vaccination in the sense of integral order is defined as follows

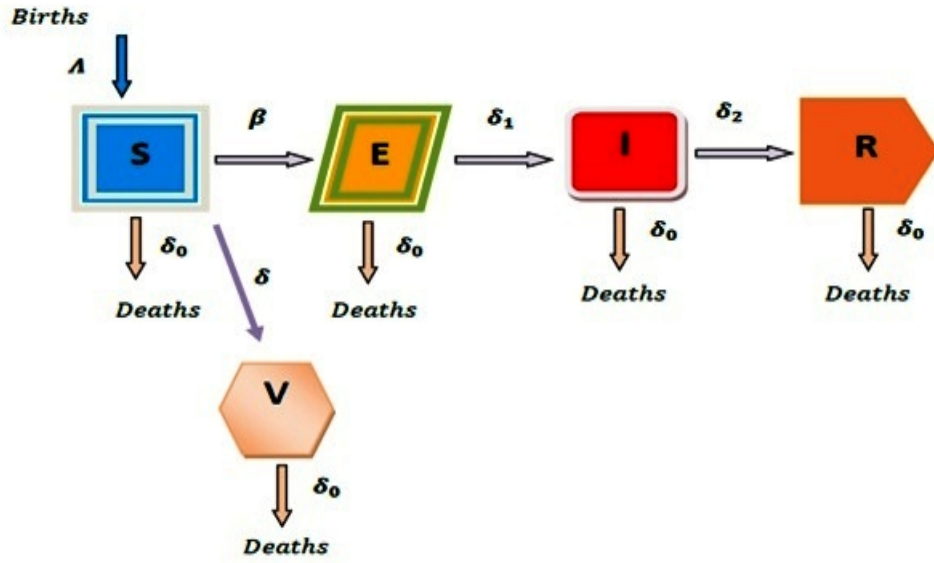


Figure 4.1: The $SEIRV$ model is represented schematically.

on the basis of the flow diagram:

$$\begin{aligned}
 D_t S(t) &= \Lambda - \beta S(t)I(t) - \delta_0 S(t) - \delta S(t), \\
 D_t E(t) &= \beta S(t)I(t) - (\delta_0 + \delta_1)E(t), \\
 D_t I(t) &= \delta_1 E(t) - (\delta_0 + \delta_2)I(t), \\
 D_t R(t) &= \delta_2 I(t) - \delta_0 R(t), \\
 D_t V(t) &= \delta S(t) - \delta_0 V(t).
 \end{aligned} \quad (4.2)$$

In this communication, we consider the $SEIRV$ model using fractional order derivatives [145- 153] with Caputo operator of order $0 < \nu \leq 1$.

$$\begin{aligned}
{}^C D_t^\nu S(t) &= \Lambda^\nu - \beta^\nu S(t)I(t) - \delta_0^\nu S(t) - \delta^\nu S(t), \\
{}^C D_t^\nu E(t) &= \beta^\nu S(t)I(t) - (\delta_0^\nu + \delta_1^\nu)E(t), \\
{}^C D_t^\nu I(t) &= \delta_1^\nu E(t) - (\delta_0^\nu + \delta_2^\nu)I(t), \\
{}^C D_t^\nu R(t) &= \delta_2^\nu I(t) - \delta_0^\nu R(t), \\
{}^C D_t^\nu V(t) &= \delta^\nu S(t) - \delta_0^\nu V(t).
\end{aligned} \tag{4.3}$$

Λ	birth rate of susceptible individuals
δ_0	the rate of mortality of all individuals
β	the rate of infection of susceptible individuals
δ	the rate of vaccination
δ_1	the rate of progression from exposed to infected individuals
δ_2	the recovery rate of infected individuals

Table 4.1: The parameters of the model and their descriptions.

It is found that the model system's time dimension (4.3) is correct as both sides of the model system's equations have dimension $(\text{time})^{-\nu}$ [153]. Next, let us consider $t_0 = 0$ and disregarded the superscript ν of all parameters and the system becomes:

$$\begin{aligned}
{}^C D_t^\nu S(t) &= \Lambda - \beta S(t)I(t) - \delta_0 S(t) - \delta S(t), \\
{}^C D_t^\nu E(t) &= \beta S(t)I(t) - (\delta_0 + \delta_1)E(t), \\
{}^C D_t^\nu I(t) &= \delta_1 E(t) - (\delta_0 + \delta_2)I(t), \\
{}^C D_t^\nu R(t) &= \delta_2 I(t) - \delta_0 R(t), \\
{}^C D_t^\nu V(t) &= \delta S(t) - \delta_0 V(t).
\end{aligned} \tag{4.4}$$

The initial conditions are $S(0) = S_0 > 0, E(0) = E_0 > 0, I(0) = I_0 > 0, R(0) = R_0 \geq 0, V(0) = V_0 \geq 0$.

4.3 Analysis of the model

4.3.1 Positivity and boundedness of solutions

Proposition 4.3.1. *For all $t \geq 0$, the variables are positive. The closed region $\Omega = \{(S, E, I, R, V) \in \mathbb{R}^5 : 0 < N \leq \frac{\Lambda}{\delta_0}\}$ is positive invariant for the system (4.4).*

Proof. *From the model (4.4), we have ${}^C D_t^\nu(S + E + I + R + V)(t) = \Lambda - \delta_0(S + E + I + R + V)(t)$.*

Therefore, ${}^C D_t^\nu N(t) + \delta_0 N = \Lambda$.

Using Laplace transform, we obtain

$$p^\nu L(N(t)) - p^{\nu-1} N(0) + \delta_0 L(N(t)) = \frac{\Lambda}{p}$$

$$\text{So, } L(N(t)) = \frac{p^\nu N(0)}{p^{\nu+1} + \delta_0} + \frac{\Lambda}{p^{\nu+1} + \delta_0}.$$

Applying inverse Laplace transform, we get

$$N(t) = N(0)E_{\nu,1}(-\delta_0 t^\nu) + \Lambda t^\nu E_{\nu,\nu+1}(-\delta_0 t^\nu).$$

According to Mittag-Leffler function,

$$E_{c,d}(z) = zE_{c,c+d}(z) + \frac{1}{\Gamma(d)}.$$

$$\text{Thus, } \lim_{t \rightarrow \infty} \sup N(t) \leq \frac{\Lambda}{\delta_0}.$$

Hence the model (4.4) is bounded above by $\frac{\Lambda}{\delta_0}$. Thus S, E, I, R , and V are all positive functions, and the system (4.4) is positive invariant.

4.3.2 Existence and uniqueness

This section demonstrates that the system (4.4) has a unique solution. To begin with, we rewrite system (4.4) in the following manner:

$${}^C D_t^\nu S(t) = G_1(t, S(t)),$$

$${}^C D_t^\nu E(t) = G_2(t, S(t)),$$

$${}^C D_t^\nu I(t) = G_3(t, S(t)),$$

$${}^C D_t^\nu R(t) = G_4(t, S(t)),$$

$${}^C D_t^\nu V(t) = G_5(t, S(t)),$$

where

$$G_1(t, S(t)) = \Lambda - \beta S(t)I(t) - \delta_0 S(t) - \delta S(t), G_2(t, S(t)) = \beta S(t)I(t) - (\delta_0 + \delta_1)E(t),$$

$$G_3(t, S(t)) = \delta_1 E(t) - (\delta_0 + \delta_2)I(t), G_4(t, S(t)) = \delta_2 I(t) - \delta_0 R(t),$$

$$G_5(t, S(t)) = \delta S(t) - \delta_0 V(t).$$

Taking integral transform on both sides of the above equations, we obtain

$$S(t) - S(0) = \frac{1}{\Gamma(\nu)} \int_0^t (t-p)^{(\nu-1)} G_1(p, S) dp,$$

$$E(t) - E(0) = \frac{1}{\Gamma(\nu)} \int_0^t (t-p)^{(\nu-1)} G_2(p, E) dp,$$

$$I(t) - I(0) = \frac{1}{\Gamma(\nu)} \int_0^t (t-p)^{(\nu-1)} G_3(p, I) dp,$$

$$R(t) - R(0) = \frac{1}{\Gamma(\nu)} \int_0^t (t-p)^{(\nu-1)} G_4(p, R) dp,$$

$$V(t) - V(0) = \frac{1}{\Gamma(\nu)} \int_0^t (t-p)^{(\nu-1)} G_5(p, V) dp.$$

The kernels $G_i, i = 1, 2, 3, 4, 5$, fulfill the Lipschitz condition and contraction, as demonstrated.

Theorem 4.3.1. G_1 satisfies the Lipschitz condition and contraction if the following condition holds: $0 \leq \beta a_1 + \delta_0 + \delta < 1$.

Proof. For S and S_1 ,

$$\begin{aligned} \|G_1(t, S) - G_1(t, S_1)\| &= \|-\beta I(t)(S(t) - S_1(t)) - \delta_0(S(t) - S_1(t)) - \delta(S(t) - S_1(t))\| \\ \Rightarrow \|G_1(t, S) - G_1(t, S_1)\| &\leq (\beta \|I(t)\| + \delta_0 + \delta) \|S(t) - S_1(t)\|. \end{aligned}$$

Suppose $K_1 = \beta a_1 + \delta_0 + \delta$, where $\|I(t)\| \leq a_1$ is a bounded function.

So $\|G_1(t, S) - G_1(t, S_1)\| \leq K_1 \|S(t) - S_1(t)\|$.

For G_1 , the Lipschitz condition is obtained, and if $0 \leq \beta a_1 + \delta_0 + \delta < 1$, then G_1 is a contraction.

In the same manner, $G_j, j = 2, 3, 4, 5$ satisfy the Lipschitz condition as follows:

$$\begin{aligned} \|G_2(t, E) - G_2(t, E_1)\| &\leq K_2 \|E(t) - E_1(t)\|, \\ \|G_3(t, I) - G_3(t, I_1)\| &\leq K_3 \|I(t) - I_1(t)\|, \\ \|G_4(t, R) - G_4(t, R_1)\| &\leq K_4 \|R(t) - R_1(t)\|, \\ \|G_5(t, V) - G_5(t, V_1)\| &\leq K_5 \|V(t) - V_1(t)\|, \end{aligned}$$

where $K_2 = (\delta_1 + \delta_0)$, $K_3 = (\delta_2 + \delta_0)$, $K_4 = \delta_0$, $K_5 = \delta_0$.

For $j = 2, 3, 4, 5$, we obtain $0 \leq K_j < 1$, then G_j are contractions. Consider the following recursive patterns, as suggested by the system (4.4):

$$\begin{aligned} \phi_{1n}(t) &= S_n(t) - S_{n-1}(t) = \frac{1}{\Gamma(\nu)} \int_0^t (t-p)^{(\nu-1)} (G_1(p, S_{n-1}) - G_1(p, S_{n-2})) dp, \\ \phi_{2n}(t) &= E_n(t) - E_{n-1}(t) = \frac{1}{\Gamma(\nu)} \int_0^t (t-p)^{(\nu-1)} (G_2(p, E_{n-1}) - G_2(p, E_{n-2})) dp, \\ \phi_{3n}(t) &= I_n(t) - I_{n-1}(t) = \frac{1}{\Gamma(\nu)} \int_0^t (t-p)^{(\nu-1)} (G_3(p, I_{n-1}) - G_3(p, I_{n-2})) dp, \\ \phi_{4n}(t) &= R_n(t) - R_{n-1}(t) = \frac{1}{\Gamma(\nu)} \int_0^t (t-p)^{(\nu-1)} (G_4(p, R_{n-1}) - G_4(p, R_{n-2})) dp, \\ \phi_{5n}(t) &= V_n(t) - V_{n-1}(t) = \frac{1}{\Gamma(\nu)} \int_0^t (t-p)^{(\nu-1)} (G_5(p, V_{n-1}) - G_5(p, V_{n-2})) dp, \end{aligned}$$

with $S_0(t) = S(0)$, $E_0(t) = E(0)$, $I_0(t) = I(0)$, $R_0(t) = R(0)$ and $V_0(t) = V(0)$.

Throughout the above system, we compute the norm of its first equation, and then

$$\begin{aligned} \|\phi_{1n}(t)\| &= \|S_n(t) - S_{n-1}(t)\| = \left\| \frac{1}{\Gamma(\nu)} \int_0^t (t-p)^{(\nu-1)} (G_1(p, S_{n-1}) - G_1(p, S_{n-2})) dp \right\| \\ \Rightarrow \|\phi_{1n}(t)\| &\leq \frac{1}{\Gamma(\nu)} \sum_0^t \|(t-p)^{(\nu-1)} (G_1(p, S_{n-1}) - G_1(p, S_{n-2})) dp\|. \end{aligned}$$

Possessing Lipschitz's condition, we have

$$\|\phi_{1n}(t)\| \leq \frac{1}{\Gamma(\nu)} K_1 \int_0^t \|(\phi_{1(n-1)}(p))\| dp.$$

In similar aspect, we obtain

$$\begin{aligned} \|\phi_{2n}(t)\| &\leq \frac{1}{\Gamma(\nu)} K_2 \int_0^t \|(\phi_{2(n-1)}(p))\| dp, \\ \|\phi_{3n}(t)\| &\leq \frac{1}{\Gamma(\nu)} K_3 \int_0^t \|(\phi_{3(n-1)}(p))\| dp, \\ \|\phi_{4n}(t)\| &\leq \frac{1}{\Gamma(\nu)} K_4 \int_0^t \|(\phi_{4(n-1)}(p))\| dp, \\ \|\phi_{5n}(t)\| &\leq \frac{1}{\Gamma(\nu)} K_5 \int_0^t \|(\phi_{5(n-1)}(p))\| dp. \end{aligned}$$

As a result, we may write

$$S_n(t) = \sum_{i=0}^n \phi_{1i}(t), E_n(t) = \sum_{i=0}^n \phi_{2i}(t), I_n(t) = \sum_{i=0}^n \phi_{3i}(t), R_n(t) = \sum_{i=0}^n \phi_{4i}(t), V_n(t) = \sum_{i=0}^n \phi_{5i}(t).$$

Theorem 4.3.2. *A system of solutions described by the SEIRV model (4.4) exists if there exists t_1 such that $(\frac{1}{\Gamma(\nu)}t_1 K_j) < 1$.*

Proof. We have

$$\|\phi_{1n}(t)\| \leq \|S_n(0)\| [\frac{1}{\Gamma(\nu)}t K_1]^n,$$

$$\|\phi_{2n}(t)\| \leq \|E_n(0)\| [\frac{1}{\Gamma(\nu)}t K_2]^n,$$

$$\|\phi_{3n}(t)\| \leq \|I_n(0)\| [\frac{1}{\Gamma(\nu)}t K_3]^n,$$

$$\|\phi_{4n}(t)\| \leq \|R_n(0)\| [\frac{1}{\Gamma(\nu)}t K_4]^n,$$

$$\|\phi_{5n}(t)\| \leq \|V_n(0)\| [\frac{1}{\Gamma(\nu)}t K_5]^n.$$

Thus, the system is continuous and has a solution. Now we'll explain how the functions listed above may be used to construct a model solution of (4.4). We make the assumption that

$$S(t) - S(0) = S_n(t) - P_{1n}(t), E(t) - E(0) = E_n(t) - P_{2n}(t), I(t) - I(0) = I_n(t) - P_{3n}(t), \\ R(t) - R(0) = R_n(t) - P_{4n}(t), V(t) - V(0) = V_n(t) - P_{5n}(t).$$

$$\text{So, } \|P_{1n}(t)\| = \left\| \frac{1}{\Gamma(\nu)} \int_0^t (G_1(p, S) - G_1(p, S_{n-1})) dp \right\| \\ \leq \frac{1}{\Gamma(\nu)} t K_1 \|S - S_{n-1}\|.$$

We get the result by repeating the process.

$$\|P_{1n}(t)\| \leq [\frac{1}{\Gamma(\nu)}t]^{n+1} K_1^{n+1} K$$

$$\Rightarrow \|P_{1n}(t)\| \rightarrow 0 \text{ as } n \rightarrow \infty.$$

Similarly, we may establish that

$$\|P_{jn}(t)\| \rightarrow 0, j = 2, 3, 4, 5 \text{ as } n \rightarrow \infty.$$

To examine the uniqueness of the solution, we assume that there is another solution of the system, such as $S_1(t), E_1(t), I_1(t), R_1(t)$ and $V_1(t)$. Then

$$S(t) - S_1(t) = \frac{1}{\Gamma(\nu)} \int_0^t (t-p)^{(\nu-1)} (G_1(p, S) - G_1(p, S_{n-1})) dp.$$

Taking norm we have

$$\|S(t) - S_1(t)\| = \frac{1}{\Gamma(\nu)} \int_0^t \|(G_1(p, S) - G_1(p, S_{n-1}))\| dp.$$

From Lipschitz condition

$$\|S(t) - S_1(t)\| = \frac{1}{\Gamma(\nu)} t K_1 \|S(t) - S_1(t)\|.$$

Thus

$$\|S(t) - S_1(t)\| (1 - \frac{1}{\Gamma(\nu)} t K_1) \leq 0. \quad (4.5)$$

Theorem 4.3.3. *The model system (4.4) has a unique solution, provided that $(1 - \frac{1}{\Gamma(\nu)} t K_1) > 0$.*

Proof. Assuming that condition (4.5) is valid,

$$\|S(t) - S_1(t)\| (1 - \frac{1}{\Gamma(\nu)} t K_1) \leq 0.$$

Then $\|S(t) - S_1(t)\| = 0$. So we have $S(t) = S_1(t)$.

Similarly, we can prove that $E(t) = E_1(t), I(t) = I_1(t), R(t) = R_1(t), V(t) = V_1(t)$.

4.3.3 Equilibrium points and Basic reproduction number

The disease-free equilibrium points E_0 and the epidemic equilibrium point E_1 of the system (4.4) are obtained from

$$\text{i.e., } {}^C D_t^\nu S(t) = {}^C D_t^\nu E(t) = {}^C D_t^\nu I(t) = {}^C D_t^\nu R(t) = {}^C D_t^\nu V(t) = 0.$$

We have $E_0(\frac{\Lambda}{\delta+\delta_0}, 0, 0, 0, \frac{\Lambda\delta}{\delta_0(\delta+\delta_0)})$ and $E_1(S^*, E^*, I^*, R^*, V^*)$ where

$$S^* = \frac{(\delta_1+\delta_0)(\delta_2+\delta_0)}{\beta\delta_1}, E^* = I^* \frac{(\delta_2+\delta_0)}{\delta_1}, I^* = \frac{\Lambda\delta_1}{(\delta_1+\delta_0)(\delta_2+\delta_0)} - \frac{(\delta+\delta_0)}{\beta}, R^* = \frac{\delta_2 I^*}{\delta_0}, V^* = \frac{(\delta_1+\delta_0)(\delta_2+\delta_0)\delta}{\beta\delta_0\delta_1}.$$

The basic reproduction number, indicated by R_0 , is the estimated number of secondary cases generated by infection of a single susceptible individual. Using next generation matrix method [92, 154], the reproduction number (R_0) can be obtained from the leading eigenvalue of the matrix FV^{-1} where,

$$F = \begin{bmatrix} 0 & \frac{\beta\Lambda}{(\delta+\delta_0)} \\ 0 & 0 \end{bmatrix} \text{ and } V = \begin{bmatrix} (\delta+\delta_0) & 0 \\ -\delta_1 & (\delta_2+\delta_0) \end{bmatrix}.$$

Therefore, the reproduction number (R_0) = $\frac{\beta\Lambda\delta_1}{(\delta+\delta_0)(\delta_1+\delta_0)(\delta_2+\delta_0)}$.

Each parameter is obviously dependent on ν . So R_0 is a function of ν . For analysis purpose, we have fixed the value of ν . If we change the value of ν , then all other parametric values will be changed and this will change the value of R_0 .

4.3.4 Significance of sensitivity parameters

This section shows the impact of altering parameter values on the R_0 , reproduction number's perceived usefulness. The crucial parameter, which might be a critical threshold for illness management, must be identified.

The following are the mathematical representations of R_0 's sensitivity index towards the parameters $\Lambda, \beta, \delta, \delta_0, \delta_1, \delta_2$:

$$\begin{aligned} \frac{\partial R_0}{\partial \Lambda} &= \frac{\beta\delta_1}{(\delta+\delta_0)(\delta_1+\delta_0)(\delta_2+\delta_0)}, \frac{\partial R_0}{\partial \beta} = \frac{\delta_1}{(\delta+\delta_0)(\delta_1+\delta_0)(\delta_2+\delta_0)}, \frac{\partial R_0}{\partial \delta} = -\frac{\Lambda\beta\delta_1}{(\delta+\delta_0)^2(\delta_1+\delta_0)(\delta_2+\delta_0)}, \\ \frac{\partial R_0}{\partial \delta_1} &= \frac{\Lambda\beta\delta_0}{(\delta+\delta_0)(\delta_1+\delta_0)^2(\delta_2+\delta_0)}, \frac{\partial R_0}{\partial \delta_2} = -\frac{\Lambda\beta\delta_1}{(\delta+\delta_0)(\delta_1+\delta_0)(\delta_2+\delta_0)^2}, \\ \frac{\partial R_0}{\partial \delta_0} &= -\frac{\Lambda\beta\delta_1[3\delta_0^2+2\delta_0(\delta+\delta_2+\delta_0)+(\delta\delta_1+\delta_1\delta_1+\delta\delta_2)]}{[(\delta+\delta_0)(\delta_1+\delta_0)(\delta_2+\delta_0)]^2}. \end{aligned}$$

It is inferred that some derivatives seem positive, and that the basic reproductive number R_0 increases as any of the aforementioned positive value parameters Λ, β, δ_1 is increased. The proportionate reaction to the proportion stimulation is used to calculate the elasticity. We have

$$E_\Lambda = \frac{\Lambda}{R_0} \frac{\partial R_0}{\partial \Lambda} = 1, E_\beta = \frac{\beta}{R_0} \frac{\partial R_0}{\partial \beta} = 1, E_{\delta_1} = \frac{\delta_1}{R_0} \frac{\partial R_0}{\partial \delta_1} = \frac{\delta_0}{\delta_1+\delta_0}.$$

As a result, we observed that E_Λ, E_β and E_{δ_1} are positive. This means that increasing the values of the parameters Λ, β, δ_1 raises the value of the fundamental reproduction

number R_0 . The fundamental reproduction number might vary a lot depending on how these factors are changed. A highly sensitive component should be computed with care, since even slight variations might result in significant quantitative systemic changes.

4.4 Stability analysis

For stability analysis, the Jacobian matrix of the system (4.4) at disease-free equilibrium point E_0 is given by $J_0 = P$, where

$$J = \begin{bmatrix} P_{11} & 0 & P_{13} & 0 & 0 \\ 0 & P_{22} & P_{23} & 0 & 0 \\ 0 & P_{32} & P_{33} & 0 & 0 \\ 0 & 0 & P_{43} & P_{44} & 0 \\ P_{51} & 0 & 0 & 0 & P_{55} \end{bmatrix},$$

where $P_{11} = -(\delta_0 + \delta)$, $P_{13} = -\beta S_0$, $P_{22} = (\delta_0 + \delta_1)$, $P_{23} = \beta S_0$, $P_{32} = \delta_1$, $P_{33} = (\delta_0 + \delta_2)$, $P_{43} = \delta_2$, $P_{44} = \delta_0$, $P_{51} = \delta$, $P_{55} = \delta_2$.

Theorem 4.4.1. *When $R_0 < 1$, the disease-free equilibrium point of the system (4.4) is locally asymptotically stable, and when $R_0 > 1$, it is unstable.*

Proof. The characteristic equation of J_0 is given by determinant $(P - \lambda I_5) = 0$. The roots of the characteristic equation are $-\delta_0, -\delta_0, -(\delta + \delta_0)$ and $\lambda^2 - \lambda(P_{22} + P_{33}) + (P_{22}P_{33} - P_{23}P_{32}) = 0$. By Routh-Hurwitz Criterion, the roots are negative if $(P_{22} + P_{33}) < 0$ and $(P_{22}P_{33} - P_{23}P_{32}) > 0$.

Now $(P_{22}P_{33} - P_{23}P_{32}) > 0$
 $\Rightarrow (\delta_1 + \delta_0)(\delta_0 + \delta_2) - \frac{\beta\delta_1}{\delta + \delta_0} > 0$
 $\Rightarrow R_0 < 1$.

Since the first three roots are negative and other roots will be negative if $R_0 < 1$ and positive if $R_0 > 1$ Therefore the equilibrium point E_0 is locally asymptotically stable or unstable according as $R_0 < 1$ or $R_0 > 1$.

Theorem 4.4.2. *When $R_0 < 1$, the disease-free equilibrium point E_0 of the system (4.4) is globally asymptotically stable, and unstable when $R_0 > 1$.*

Proof. Taking the appropriate Lyapunov function into consideration.

$$F = \delta_1 E + (\delta_0 + \delta_1) I.$$

The time fractional derivative of the above function is

$${}^C D_t^\nu F(t) = \delta_1 {}^C D_t^\alpha E(t) + (\delta_0 + \delta_1) {}^C D_t^\alpha I(t).$$

From (4.4) we get,

$${}^C D_t^\nu F(t) = \delta_1 (\beta SI - (\delta_0 + \delta_1) E) + (\delta_0 + \delta_1) (\delta_1 E - (\delta_0 + \delta_2) I).$$

Now,

$${}^C D_t^\nu F(t) \leq I(\delta + \delta_0)(\delta_2 + \delta_0)[R_0 - 1].$$

Hence if $R_0 < 1$, then ${}^C D_t^\nu F(t) < 0$. Hence, by LaSalle's extension to Lyapunov's principle [129, 130], the disease-free equilibrium point E_0 is globally asymptotically stable and unstable if $R_0 > 1$.

Theorem 4.4.3. *If $R_0 > 1$, the epidemic equilibrium $E_1 = (S^*, E^*, I^*, R^*, V^*)$ is locally asymptotically stable.*

Proof. The characteristic equation is $(-\delta_0 - \lambda)(-\delta_0 - \lambda)(\lambda^3 + A\lambda^2 + B\lambda + C) = 0$.

Where, $A = -(G_{11} + G_{22} + G_{33})$, $B = G_{11}(G_{22} + G_{33}) + (G_{22}G_{33} - G_{23}G_{32} + G_{13}G_{21}G_{32})$, $C = -G_{11}(G_{22}G_{33} - G_{23}G_{32} + G_{13}G_{21}G_{32})$,

where $G_{11} = -\beta I^* - \delta - \delta_0$, $G_{22} = -\delta_1 - \delta_0$, $G_{22} = -\delta_2 - \delta_0$, $G_{23} = \beta S^*$, $G_{32} = \delta_1$, $G_{13} = -\beta S^*$, $G_{23} = \beta I^*$, $G_{21} = \beta I^*$.

Since $A > 0$, $C > 0$, $AB > C$, by Routh-Hurwitz Criterion, the system (4.4) is locally asymptotically stable at E_1 .

Theorem 4.4.4. *The epidemic equilibrium E_1 is globally asymptotically stable if $R_0 > 1$.*

Proof. The Goh-Volterra form's non-linear Lyapunov function is defined as

$$W = (S - S^* - S^* \log \frac{S}{S^*}) + (E - E^* - E^* \log \frac{E}{E^*}) + Q(I - I^* - I^* \log \frac{I}{I^*}).$$

Using Lemma 1.4.7 and then the above function's time fractional derivative is,

$${}^C D_t^\nu W(t) \leq (1 - \frac{S^*}{S})^C D_t^\alpha S(t) + (1 - \frac{E^*}{E})^C D_t^\alpha E(t) + Q(1 - \frac{I^*}{I})^C D_t^\alpha I(t).$$

Using system (4.4) we get,

$${}^C D_t^\nu W(t) \leq (\Lambda - \beta SI - \delta_0 S - \delta S - \frac{S^*(\Lambda - \beta SI - \delta_0 S - \delta S)}{S}) + ((\beta SI - (\delta_0 + \delta_1)E) - \frac{E^*(\beta SI - (\delta_0 + \delta_1)E)}{E}) + Q((\delta_1 E - (\delta_0 + \delta_2)I) - \frac{I^*(\delta_1 E - (\delta_0 + \delta_2)I)}{I}).$$

At steady state from equation (4.4), we have

$$\Lambda = \beta S^* I^* + \delta_0 S^* + \delta S^*$$

Using the condition of steady state of the above equation, we have

$${}^C D_t^\nu W(t) \leq (\beta S^* I^* + \delta_0 S^* + \delta S^* - \beta SI - \delta_0 S - \delta S - \frac{S^*(\beta S^* I^* + \delta_0 S^* + \delta S^* - \beta SI - \delta_0 S - \delta S)}{S}) + ((\beta SI - (\delta_0 + \delta_1)E) - \frac{E^*(\beta SI - (\delta_0 + \delta_1)E)}{E}) + Q((\delta_1 E - (\delta_0 + \delta_2)I) - \frac{I^*(\delta_1 E - (\delta_0 + \delta_2)I)}{I}).$$

Adding all infected classes without a single star (*) from the above equation to zero:

$$S^* \beta I - (\delta_0 + \delta_1)E + Q(\delta_1 E - (\delta_0 + \delta_2)I) = 0.$$

The steady state was somewhat perturbed between (4.4) and the above equation, yielding:

$$Q = \frac{S^* \beta}{(\delta_0 + \delta_2)}, (\delta_0 + \delta_1) = \frac{I^* S^* \beta}{E^*}, \delta_1 = \frac{(\delta_0 + \delta_2) I^*}{E^*}.$$

Further simplification gives,

$${}^C D_t^\nu W(t) \leq (\beta S^* I^* + \delta_0 S^* + \delta S^* - \delta_0 S - \frac{S^*(\beta S^* I^* + \delta_0 S^* + \delta S^* - \delta_0 S)}{S}) + (-\frac{\beta S I E^*}{E} + \beta S^* I^*) + (-\frac{\beta S^* I^* E I^*}{I E^*} + \beta S^* I^*).$$

We have an arithmetic mean that is greater than the geometric mean.

$$(2 - \frac{S}{S^*} - \frac{S^*}{S} \leq 0, (3 - \frac{S^*}{S} - \frac{I^* E}{I E^*} - \frac{S E^* I}{E} \leq 0. \text{ Hence, } {}^C D_t^\nu W(t) \leq 0 \text{ for } R_0 > 1.$$

Hence W is a Lyapunov function. If $R_0 > 1$, the epidemic equilibrium E_1 is globally asymptotically stable, according to LaSalle's Invariance Principle [129].

4.5 $SEIRV$ model with optimal control

Vaccination is an important tool in the fight against infectious illnesses. The vaccine against Covid-19 has recently been proven to be an effective means of stopping the disease's transmission. Ding et al. [50] and Agarwal et al. [51] have contributed on optimum control theory in fractional calculus. Pontryagin's maximal principle [52] strikes at the core of the concept of optimal control in fractional calculus. Our goal is to incorporate the effectiveness of vaccination through a control measure namely w ($0 \leq w(t) \leq 1$) and to identify the best control w^* to minimize the cost function $J(w)$ of the control strategy. The cost function

$$J(w^*) = \min (J(w(t))) \text{ with } J(w) = \left(\int_0^{t_g} [E + I + A_1 w^2] dt \right), \quad (4.6)$$

subject to

$$\begin{aligned} {}^C D_t^\nu S(t) &= \Lambda - \beta S(t)I(t) - \delta_0 S(t) - \delta S(t), S(0) = S_0 > 0, \\ {}^C D_t^\nu E(t) &= \beta S(t)I(t) - (\delta_0 + \delta_1)E(t), E(0) = E_0 \geq 0, \\ {}^C D_t^\nu I(t) &= \delta_1 E(t) - (\delta_0 + \delta_2)I(t), I(0) = I_0 \geq 0, \\ {}^C D_t^\nu R(t) &= \delta_2 I(t) - \delta_0 R(t), R(0) = R_0 \geq 0, \\ {}^C D_t^\nu V(t) &= \delta S(t) - \delta_0 V(t), V(0) = V_0 \geq 0, \end{aligned} \quad (4.7)$$

where $0 \leq w(t) \leq 1$.

Theorem 4.5.1. *Let $w(t)$ be a measurable control function on $[0, t_g]$. Then an optimal control w^* to minimize the objective function $J(w)$ of (4.6) with $w^* = \max [\min(\bar{w}, 1), 0]$, $\bar{w} = \frac{(\epsilon_1 - \epsilon_5)S}{2A_1}$. where (S, E, I, R, V) is the corresponding solution of the system (4.7).*

Proof. *The Hamiltonian has been analyzed in the following manner:*

$H = [E + I + A_1 w^2] + \epsilon_1(\Lambda - \beta S(t)I(t) - \delta_0 S(t) - wS(t)) + \epsilon_2(\beta S(t)I(t) - (\delta_0 + \delta_1)E(t)) + \epsilon_3(\delta_1 E(t) - (\delta_0 + \delta_2)I(t)) + \epsilon_4(\delta_1 E(t) - (\delta_0 + \delta_2)I(t)) + \epsilon_5(wS(t) - \delta_0 V(t)),$
with $\epsilon_i(t), i = 1, 2, 3, 4, 5$ are the adjoint variables with $\epsilon_i(t_g) = 0$, expressed in the canon-

ical equations:

$$\begin{aligned}
{}^{RL}D_t^\nu \epsilon_1(t) &= -\frac{\partial H}{\partial S} = \epsilon_1(\beta I(t) + \delta_0 - w) - \epsilon_2(\beta I(t)) - \epsilon_5(w), \\
{}^{RL}D_t^\nu \epsilon_2(t) &= -\frac{\partial H}{\partial E} = -1 + \epsilon_2((\delta_1 + \delta_0)E(t)) - \epsilon_3(\delta_1), \\
{}^{RL}D_t^\nu \epsilon_3(t) &= -\frac{\partial H}{\partial I} = -1 + \epsilon_1(\beta S(t)) - \epsilon_2(\beta S(t)) + \epsilon_3(\delta_2 + \delta_0) - \epsilon_4(\delta_2), \\
{}^{RL}D_t^\nu \epsilon_4(t) &= -\frac{\partial H}{\partial R} = \epsilon_4\delta_0, \\
{}^{RL}D_t^\nu \epsilon_5 V(t) &= -\frac{\partial H}{\partial V} = \epsilon_5\delta_0.
\end{aligned} \tag{4.8}$$

As a result, the issue of determining w^* that minimizes H in the presence of (4.7) is recast as minimizing the Hamiltonian with regard to the control. We then establish the following optimum condition using the Pontryagin principle:

$$\frac{\partial H}{\partial w} = 2A_1 w + (\epsilon_1 - \epsilon_5)S = 0,$$

which may be solved using state and adjoint variables to yield

$$\bar{w} = \frac{(\epsilon_1 - \epsilon_5)S}{2A_1}.$$

For the best control w^* , take into account the control constraints as well as the sign of $\frac{\partial H}{\partial w}$.

As a result, we get

$$w^* = \begin{cases} 0 & \text{if } \frac{\partial H}{\partial w} < 0, \\ \bar{w} & \text{if } \frac{\partial H}{\partial w} = 0, \\ 1 & \text{if } \frac{\partial H}{\partial w} > 0. \end{cases}$$

By substituting w^* to the equation, the optimal condition may be determined for the system (4.7).

4.6 Adam-Bashforth-Moulton predictor-corrector scheme for the $SEIRV$ model

The Adams-Bashforth-Moulton strategy is the most widely used numerical technique for addressing any fractional order initial value problems. Let's look at the fractional differential equation below.

$${}^C D_t^\nu F_j(t) = g_j(t, F_j(t)), F_j^r(t)(0) = F_{j0}^r, r = 0, 1, 2, \dots, [\alpha], j \in N. \tag{4.9}$$

where $F_{j0}^r \in R$ is equal to the well-known Volterra integral equation

$$F_j(t) = \sum_{n=0}^{\nu} F_{j0}^r \frac{t^n}{n!} + \frac{1}{\Gamma(\nu)} \int_0^t (t-u)^{\nu-1} g_j(u, F_j(u)) du. \quad (4.10)$$

The algorithm is explained as follows

Let $h = \frac{T}{m}$, $t_n = nh$, $n = 0, 1, 2, \dots, m$.

Corrector formulae:

$$\begin{aligned} S_{n+1}(t) &= S(0) + \frac{h^\nu}{\Gamma(\nu+2)} (\Lambda - \beta S_{n+1}^p I_{n+1}^p - \delta_0 S_{n+1}^p - \delta S_{n+1}^p) \\ &+ \frac{h^\nu}{\Gamma(\nu+2)} \sum_{j=0}^n \alpha_{1,j,n+1} (\Lambda - \beta S_j I_j - \delta_0 S_j - \delta S_j), \\ E_{n+1}(t) &= E(0) + \frac{h^\nu}{\Gamma(\nu+2)} (\beta S_{n+1}^p I_{n+1}^p - (\delta_0 + \delta_1) E_{n+1}^p) \\ &+ \frac{h^\nu}{\Gamma(\nu+2)} \sum_{j=0}^n \alpha_{1,j,n+1} (\beta S_j I_j - (\delta_0 + \delta_1) E_j), \\ I_{n+1}(t) &= I(0) + \frac{h^\nu}{\Gamma(\nu+2)} (\delta_1 E_{n+1}^p - (\delta_0 + \delta_2) I_{n+1}^p) \\ &+ \frac{h^\nu}{\Gamma(\nu+2)} \sum_{j=0}^n \alpha_{1,j,n+1} (\delta_1 E_j - (\delta_0 + \delta_2) I_j), \\ R_{n+1}(t) &= R(0) + \frac{h^\nu}{\Gamma(\nu+2)} (\delta_2 I_{n+1}^p - \delta_0 R_{n+1}^p) + \frac{h^\nu}{\Gamma(\nu+2)} \sum_{j=0}^n \alpha_{1,j,n+1} (\delta_2 I_j - \delta_0 R_j), \\ V_{n+1}(t) &= V(0) + \frac{h^\nu}{\Gamma(\nu+2)} (\delta S_{n+1}^p - \delta_0 V_{n+1}^p) + \frac{h^\nu}{\Gamma(\nu+2)} \sum_{j=0}^n \alpha_{1,j,n+1} (\delta S_j - \delta_0 V_j). \end{aligned} \quad (4.11)$$

Predictor formulae:

$$\begin{aligned}
S_{n+1}^p &= S(0) + \frac{1}{\Gamma(\nu)} \sum_{j=0}^n \Theta_{j,n+1} (\Lambda - \beta S_j I_j - \delta_0 S_j - \delta S_j), \\
E_{n+1}^p &= I(0) + \frac{1}{\Gamma(\nu)} \sum_{j=0}^n \Theta_{j,n+1} (\beta S_j I_j - \delta_0 + \delta_1) E_j, \\
I_{n+1}^p &= Q(0) + \frac{1}{\Gamma(\nu)} \sum_{j=0}^n \Theta_{j,n+1} (\delta_0 + \delta_2) I_j, \\
R_{n+1}^p &= R(0) + \frac{1}{\Gamma(\nu)} \sum_{j=0}^n \Theta_{j,n+1} (\delta_2 I_j - \delta_0 R_j), \\
V_{n+1}^p &= V(0) + \frac{1}{\Gamma(\nu)} \sum_{j=0}^n \Theta_{j,n+1} (\delta S_j - \delta_0 V_j),
\end{aligned} \tag{4.12}$$

where,

$$\nu_{j,n+1} = \begin{cases} n^{(\nu+1)} - (n - \nu)(n + 1)^\nu, & \text{if } j = 0, \\
(n - j + 2)^{(\nu+1)} + (n - j)^{(\nu+1)} - 2(n - j + 1)^{(\nu+1)}, & \text{if } 0 \leq j \leq n, \\
1, & \text{if } j = 1, \end{cases}$$

and

$$\Theta_{j,n+1} = \frac{h^\nu}{\nu} [(n + 1 - j)^\nu - (n - j)^\nu], 0 \leq j \leq n.$$

4.7 Numerical simulation and discussion

In this section, we perform rigorous numerical simulations to evaluate and verify the analytical results of our model system (4.4). Using mathematical software MATLAB (2018a version), we have employed Adam's-Bashforth-Moulton predictor-corrector scheme to obtain numerical solution to the system (4.4).

We investigate numerical simulations of the model system (4.4) for India in the Caputo sense, using the parameters listed in Table 4.2. We estimate and anticipate the progression of the COVID-19 pandemic using recent Indian data up to the 10th of August 2021 [83]. In the India scenario, Table 2 is utilized for simulation. The following figures were produced to examine the behavior of the model (4.4) under various initial conditions.

Parameter	Value	Reference
Λ	0.0182	[123]
δ	0.01	Model to fit
β	0.476	[155]
δ_0	0.0073	[123]
δ_1	0.071	[156]
δ_2	0.286	[155]

Table 4.2: Estimated values of parameters for India.

Figure 4.2 demonstrates the dynamical behavior of all individuals for fractional order $\nu = 0.82$. The comparison of the number of susceptible, infected, exposed and recovered individuals in case of $\delta = 0$ and $\delta = 0.01$ is quite obvious. The number of susceptible individuals is more for $\delta = 0$ than $\delta = 0.01$. Similar is the case with exposed individuals and infected individuals. However, in case of recovered individuals, it is just the opposite, due to obvious reasons. Now, the recovered individuals will be more in case of $\delta = 0.01$ than in case of $\delta = 0$. Figure 4.3 depicts the dynamical behavior of all individuals with a vaccination rate of 0.01 at fractional orders of $\nu = 0.8, 0.9, 1$ and the value of R_0 is 1.55. The purpose of this study is to demonstrate the importance of the COVID-19 vaccination rate. When we enforced a vaccination rate, the basic reproduction number decreases. Figure 4.4(a) to 4.4(e) shows the time series of susceptible individuals, exposed individuals, infected individuals, recovered individuals and vaccinated individuals across a time period of $[0, 100]$ with optimal control taking fractional order $\nu = 1$. Vaccination is a critical component in preventing people from COVID-19, and various ideas have been proposed in which vaccination rates are viewed as quite beneficial. As a result, the addition of the vaccination parameter decreases the reproduction number R_0 . For the simulation of the optimal control problem subject to the model (4.4) corresponding to Table 4.2 in the India scenario, we used a final time of $t_g = 100$. Figure 4.5 depicts the time series of optimal control variable w^* and optimal cost J^* .

4.8 Data fitting and model validation

The data fitting and model validation of the system (4.4) for Infected population in Brazil are described in this section. From the 10th of April to the 19th of July, 2021, we compared the model values with the real scenario for Brazil. The total initial population of Brazil is around 209500000 [83]. The parametric values are given in Table 4.3. We have taken $t = 1$ day as time unit and $t = 100$ as final time. Table 4.4 recommends day wise Infected population from 10th April, 2021 to 19th July, 2021. Figure 4.6 depict time series solution of Infected population of the system (4.4) for Table 4.3 taking $\nu = 0.8, 0.85, 0.9$.

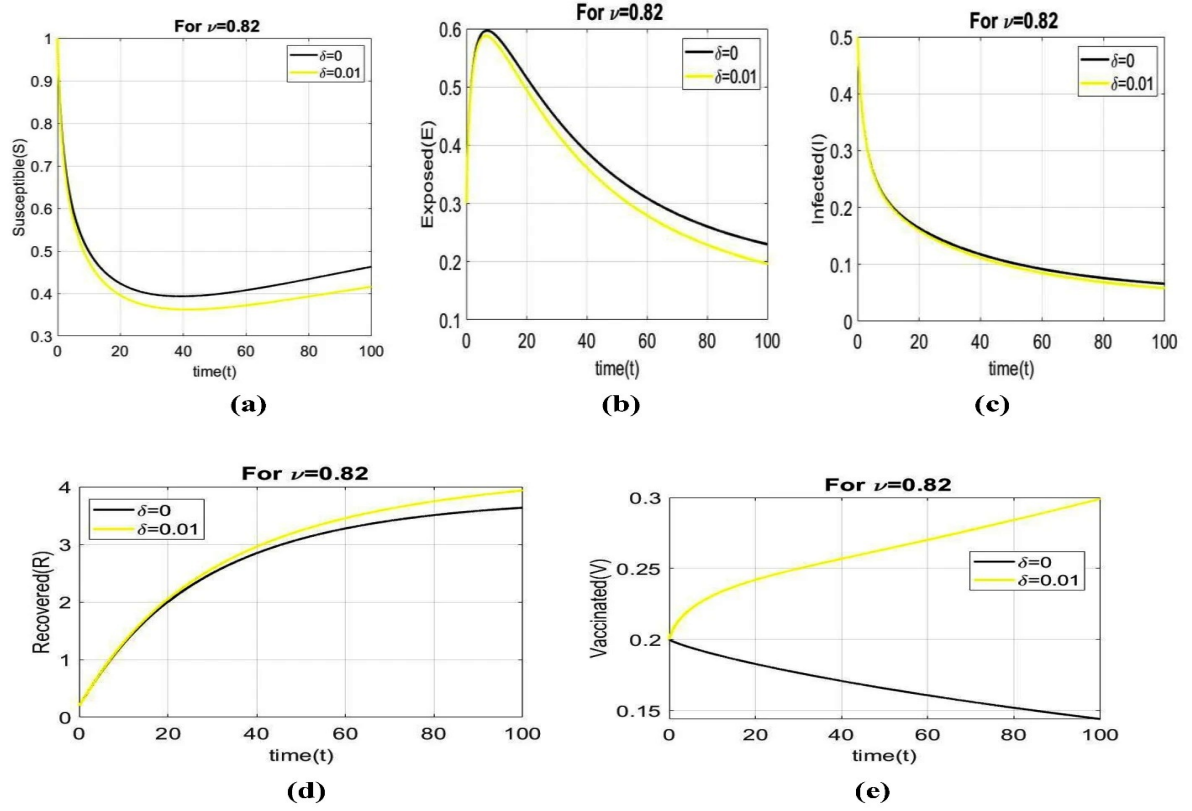


Figure 4.2: Comparison of dynamical behaviour of all individuals with respect to time for fractional order $\nu = 0.82$, $\delta = 0$ and $\delta = 0.01$.

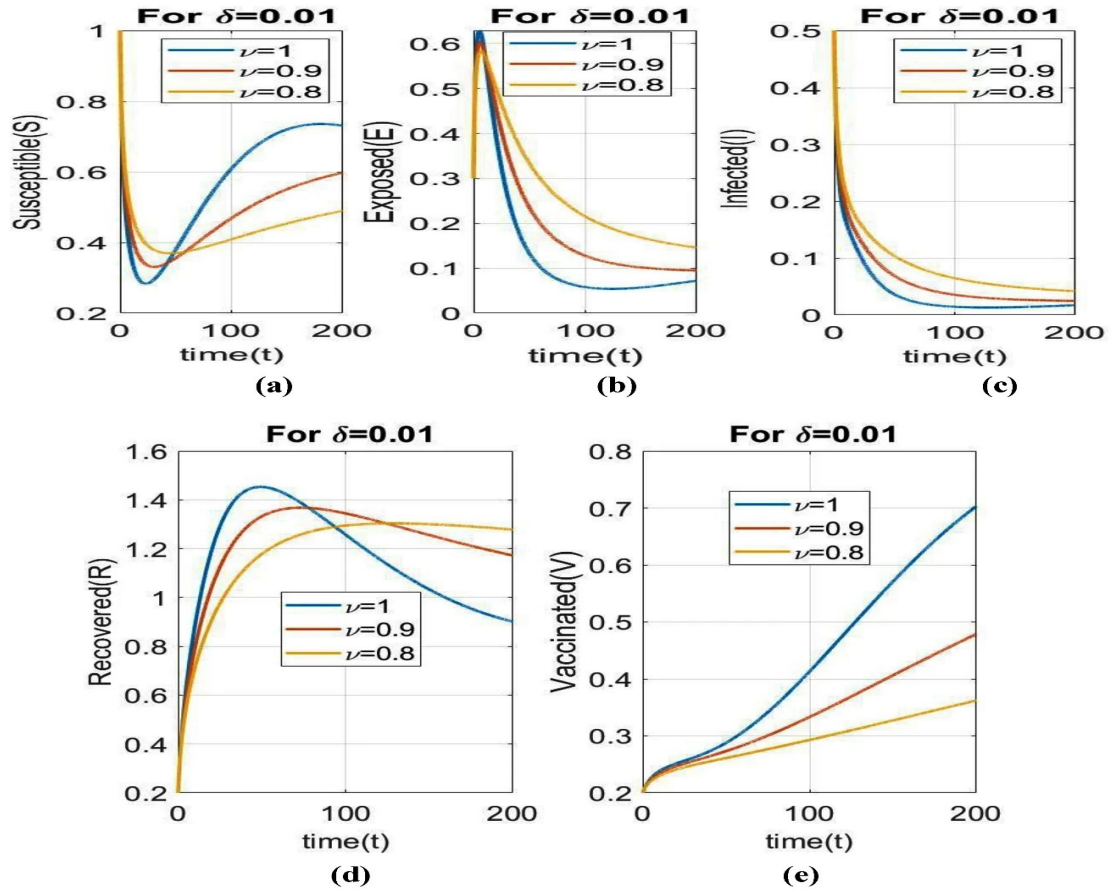


Figure 4.3: Dynamical behaviour of all individuals with respect to time with a vaccination rate, $\delta = 0.01$ and fractional order $\nu = 0.8, 0.9, 1$.

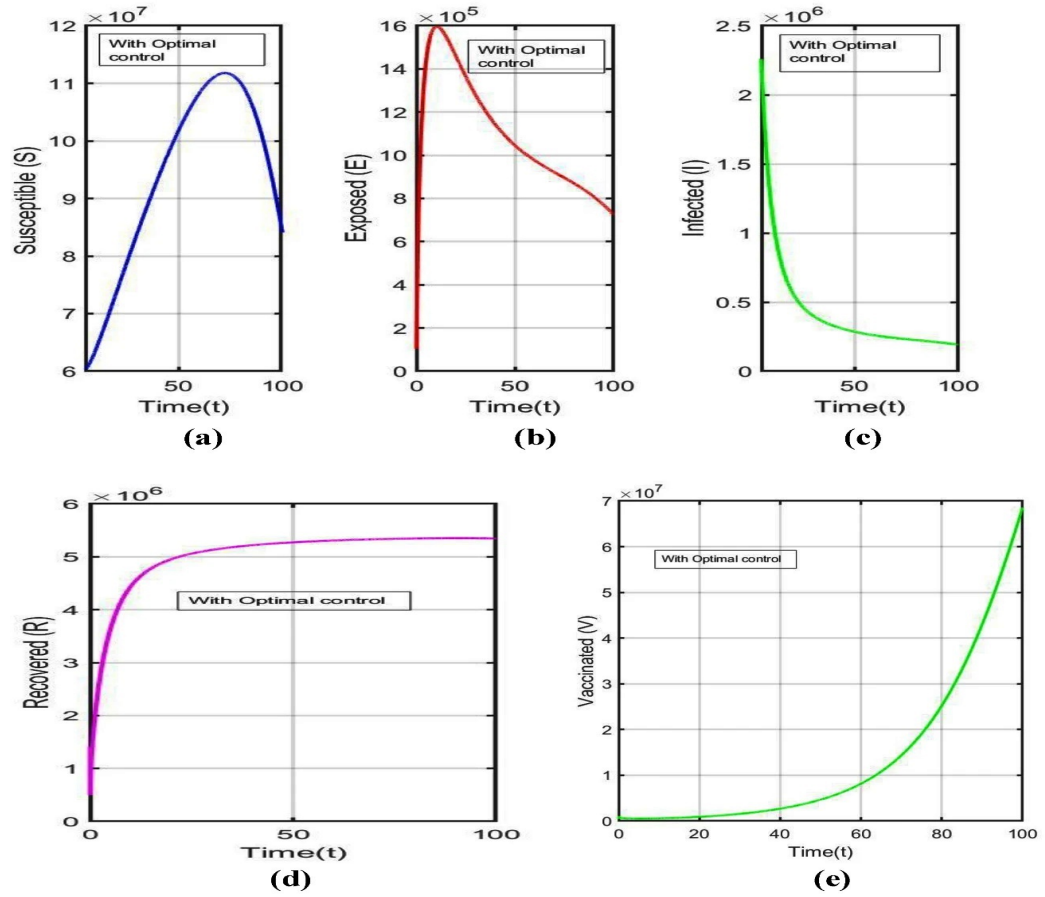


Figure 4.4: With respect to time, the time series of the model system (4.4) corresponds to Table 4.2.

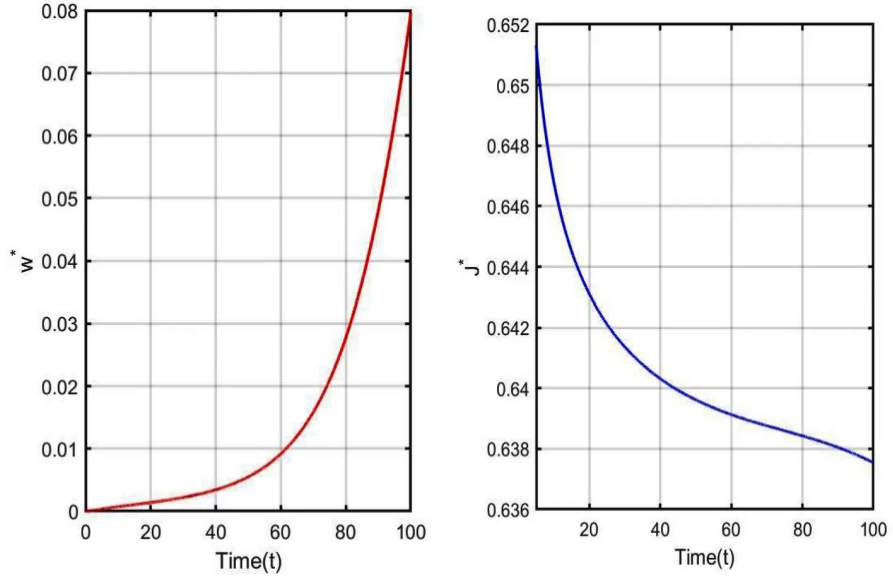


Figure 4.5: Time series of optimal control variable w^* and optimal cost J^* with parameter values corresponding to Table 4.2.

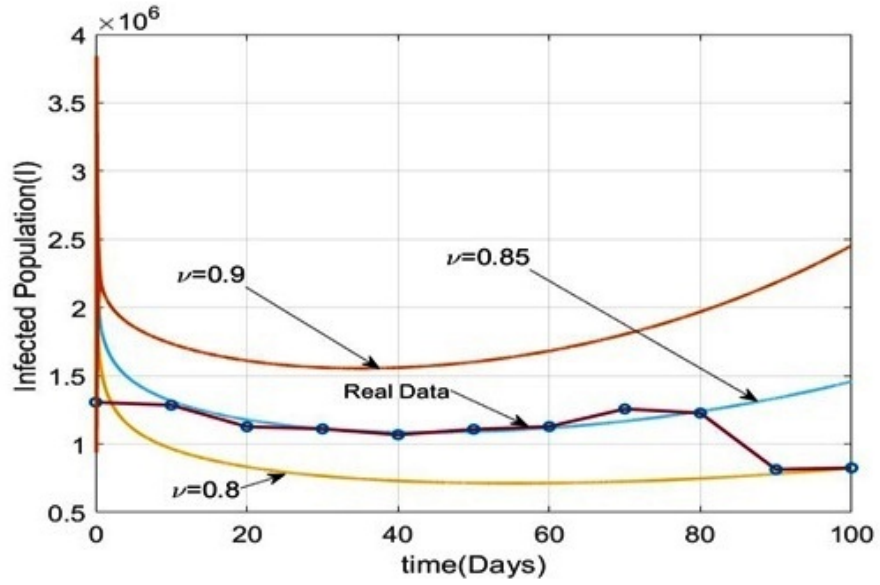


Figure 4.6: Time series solution of Infected population of the system (4.4) for Table 4.3 taking $\nu = 0.8, 0.85, 0.9$.

Parameter	Value	Reference
Λ	0.0187	[123]
δ	0.01	Model to fit
β	0.32	[155]
δ_0	0.0063	[123]
δ_1	0.344	[156]
δ_2	0.041	[155]

Table 4.3: The estimated parametric values are as follows in Brazil.

Day	Infected population
10/04/2021	1,269,000
20/04/2021	1,285,000
30/04/2021	1,270,000
10/05/2021	1,111,000
20/05/2021	1,068,000
30/05/2021	1,108,000
09/06/2021	1,128,000
19/06/2021	1,257,000
29/06/2021	1,227,000
09/07/2021	813,700
19/07/2021	825,000

Table 4.4: Day wise Infected population of Brazil from 10th April, 2021 to 19th July, 2021.

4.9 Conclusion

In this chapter, we have discussed the optimal control of fractional order $SEIRV$ model with vaccination as the control parameter w . Based on the COVID-19 cases data in India, collected upto 10th August, 2021, we estimated the basic reproduction number R_0 without vaccination to be 3.67 and with vaccination to be 1.55. The fractional-order derivatives are usually more suitable in modeling since the choice of the derivative order provides one more degree of freedom and this leads to better fit to the real time data with less error than the integer-order model. A comparison of the number of individuals in different compartments for $\nu = 0.82$ has been presented in Figure 4.2 in case of $\delta = 0$ and $\delta = 0.01$. The stability analysis of the model shows that the system is locally as well as globally asymptotically stable at disease-free equilibrium point E_0 when $R_0 < 1$ and at epidemic equilibrium E_1 when $R_0 > 1$. Sensitivity analysis shows that R_0 is

directly proportional to the birth rate of susceptible individuals Λ , the rate of infection of susceptible individuals β and the rate of progression from exposed to infected individuals δ_1 , all of which may be controlled with the effective execution of vaccination drives. We have used the Pontryagin's Maximum Principle to provide the necessary conditions needed for the existence of the optimal solution to the optimal control problem. Adam-Bashforth-Moulton predictor-corrector technique has been used to obtain numerical solutions to the system. Numerical simulations are presented using MATLAB to validate the efficacy and impact of the control parameter. It is evident that if the control measure w is employed then the transmission of the disease may be checked and eradicated. Additionally, the optimal control value w^* has been determined in Theorem 4.5.1 to minimize the cost of vaccination given by $J(w) = \int_0^{t_g} [E + I + A_1 W^2] dt$. We have assumed a final time $t_g = 100$ for optimal control. The order of derivative can differ from region to region. If we vary the order of derivatives while keeping other parametric values fixed, the results will be different (Figure 4.6). This demonstrates that the order of derivative is important in system simulation. We have comparatively studied the model values and real scenario of Brazil starts from 10th April 2021 and continues up to 100 days. It has been observed that our model fits with $\nu = 0.85$ with realistic data.

Chapter 5

Fractional order $SEIQRD$ epidemic model of Covid-19: a case study of Italy

“Look deep into nature, and then you will understand everything better”

- Albert Einstein

This chapter is based on the paper

Fractional order $SEIQRD$ epidemic model of Covid-19: a case study of Italy, , PLoS ONE, 18(3), e0278880, 2023.

5.1 Introduction

The world is still addressing the Coronavirus illness 2019 (COVID-19), which is caused by the new Coronavirus SARSCoV-2, a highly aggressive virus that attacks the individual respiratory system. The hospitalized individuals' ailments were linked to the marine and moist animal industries in Wuhan, Hubei Province, China [157]. COVID-19 spreads from person to person by touching contaminated surfaces and inhalation of infected persons' respiratory droplets [158]. Those who have been infected with COVID-19 have reported high fever, persistent cough, and exhaustion. Nonetheless, depending on the immune system, COVID-19 symptoms and consequences differ from person to person. People with a strong immune response seem to be more likely to get mild - to - moderate illnesses as well as recover avoid going to the hospital. Various investigations, however, have identified other symptoms such as neurological illnesses and gastroenteritis of different severity [159, 160]. With so many waves of infection, the illness caused numerous deaths in many countries. COVID-19 outbreaks have occurred in Italy, with the population suffering the effects of the consequences. The number of confirmed incidence and mortality in every phase has been published, and there appears to be an increasing incidence. On February 21, 2020, the first Italian victim of COVID-19, a 38-year-old male hospitalized at Codogno Hospital in Lodi, was diagnosed. On the 12th of February, 2022, it has infected over 424,636,034 people over the world, resulting in 5903,485 deaths and 349,857,774 recoveries [161]. According to reports, the mortality rate in waves 1 and 2 was 1 %. Many social programmers and events have been discontinued or extended as a result of the epidemic. The T-20 cricket world cup will be hosted in Australia in 2020, while the Summer Olympics, which were scheduled to be held in Tokyo, have been postponed. The Indian Premier League, one of the most popular cricket events, has been relocated from India to the United Arab Emirates.

Its importance has been demonstrated by the construction of mathematical models in the fields of epidemiology and physics. The Coronavirus infection has been examined by several researchers from various perspectives. While biologists and mathematicians working on the systems of the COVID-19 disease analyzed and constructed mathematical systems based on real-world cases from various countries, and offered information on the infection's peak and clearance. In this context, [160, 161] are some mathematical models that have been developed for this disease. The information from Italy is taken into account, and a mathematical model for the COVID-19 disease is developed, with its study reported in [162]. [163] examines the number of genuine instances from the Mexican population using a mathematical model. [164] proposes a fractional *SEIR* model utilizing the wavelet approach. The authors investigated the influence of social distance and other factors that might be regarded important for the reduction of COVID-19 infection in [165]. The authors used a mathematical modeling technique to evaluate genuine infected patients

from Saudi Arabia and generated results on disease eradication in the nation [166]. [167] describes a comparative study of Coronavirus infection dynamics. In [168, 170, 99, 97, 44] suggests some additional relevant work on COVID-19 modeling and associated illness outcomes. In [123], Paul et al. analyzed the scenario analysis of COVID-19 pandemic using SEIR epidemic model. A deeper understanding of the pandemic dynamics, including the characteristics of Covid-19 transmission, was made possible by the modeling technique [169, 170]. We have previously published research on fractional order phenomena [97, 99, 100]. The novel fractional operator has shown to be quite effective in solving a variety of mathematical modeling problems as well as some recent work on COVID-19 [171 - 174]. From the study of data obtained from Wuhan, Li et al. [14] calculated the epidemiology and discovered the mean incubation time was 5.2 days. The authors of [175, 176] highlighted some interesting outcomes of Corona virus disease. In [177] introduced deeper investigation of modified epidemiological computer virus model containing the Caputo operator. Furthermore, the researchers in [178 - 183] analyzed fractional derivatives of the COVID-19 infection models and presented some recommendations for infection minimization in the form of lockdown and control measures.

5.1.1 Motivation and research background

Fractional order modeling is a useful tool that has been used to explore the nature of diseases since the fractional derivative is an extension of the integer-order derivative. In order to replicate real-world issues, several innovative fractional operators with various properties have been designed. In addition, the integer derivative has a local identity, whereas the fractional derivative has a global character. Numerous varieties of fractional derivatives, both with and without singular kernels, are available today. Leibniz's query from 1695 marks the beginning of the fractional derivative. The fractional derivative also improves in the improvement of the system's consistency domain. We have the derivatives of Caputo, Riemann-Liouville, and Katugampola for singular kernels [126, 184]. There are two varieties of fractional derivatives without singular kernels: the Caputo-Fabrizio fractional derivative [38], which has an exponential kernel, and the Atangana-Baleanu fractional derivative, which has a Mittag-Leffler kernel [185]. While memory and genetic properties are involved, working with fractional-order derivatives is crucial because it provides a more accurate technique to describe COVID-19 outbreaks. Numerous academic articles, monographs, and novels have provided evidence to support this claim; for instance, [186 - 193]. Motivated by the current research, we present and analyze the *SEIQRD* model in Caputo sense. The Caputo derivative is particularly useful for discussing real-world situations since it permits traditional beginning and boundary conditions to be used in the derivation, and the derivative of a constant is zero, whereas the Riemann-Liouville fractional derivative does not. It is quite challenging to genuinely cre-

ate an appropriate mathematical model using classical differentiation in the situation of COVID-19 because to the large number of uncertainties, unknowns, and disinformation. Generally, non-local operators are better suited for such circumstances because, depending on whether power law, fading memory, or overlap effects are taken into account, they can represent non-localities and certain memory effects.

5.1.2 Structure of the chapter

In Section 5.2, we have established the *SEIQRD* epidemic model of Covid-19 in Caputo sense. We have investigated the existence, uniqueness, non-negative, boundedness criterion and stability analysis of the solution of model in Section 5.3. In Section 5.4, the fractional-order Taylor's approach in Caputo derivative is utilized to approximate the solution to the proposed model. The numerical study is given using MATLAB (2018a) in Section 5.5. Finally, the chapter's conclusion is found in Section 5.6.

5.2 Model formulation

The mathematical model of COVID-19 transmission formulated in this study was motivated by the study of [99, 100]. In the present study, the model will be divided into six compartments [see Figure 5.1]. The total human population to be considered is denoted as $N(t)$, and at any time, it comprises of the susceptible (S), exposed (E), infected (I), quarantined (Q), recovered (R), and death (D) compartments, respectively. Thus

$$N(t) = S(t) + E(t) + I(t) + Q(t) + R(t) + D(t). \quad (5.1)$$

Now we formulate the *SEIQRD* model with fractional order derivatives with Caputo operator of order $0 < \phi \leq 1$.

$$\begin{aligned} {}^C D_t^\phi S(t) &= \tilde{a}^\phi - \tilde{b}^\phi(1 - \tilde{\alpha}^\phi \tilde{\beta}^\phi)S(t)I(t) - \tilde{c}^\phi S(t), \\ {}^C D_t^\phi E(t) &= \tilde{b}^\phi(1 - \tilde{\alpha}^\phi \tilde{\beta}^\phi)S(t)I(t) - (\tilde{e}^\phi + \tilde{c}^\phi)E(t), \\ {}^C D_t^\phi I(t) &= \tilde{e}^\phi E(t) - (\tilde{f}^\phi + \tilde{g}^\phi + \tilde{h}^\phi + \tilde{c}^\phi)I(t), \\ {}^C D_t^\phi Q(t) &= \tilde{f}^\phi I(t) - (\tilde{k}^\phi + \tilde{l}^\phi + \tilde{c}^\phi)Q(t), \\ {}^C D_t^\phi R(t) &= \tilde{g}^\phi I(t) + \tilde{k}^\phi Q(t) - \tilde{c}^\phi R(t), \\ {}^C D_t^\phi D(t) &= \tilde{h}^\phi I(t) + \tilde{l}^\phi Q(t). \end{aligned} \quad (5.2)$$

Now for the sake of convenience of calculation, we redefine the parameters [see Table 5.1] as $a = \tilde{a}^\phi, b = \tilde{b}^\phi, \alpha = \tilde{\alpha}^\phi, \beta = \tilde{\beta}^\phi, c = \tilde{c}^\phi, e = \tilde{e}^\phi, f = \tilde{f}^\phi, g = \tilde{g}^\phi, h = \tilde{h}^\phi, l = \tilde{l}^\phi, k =$

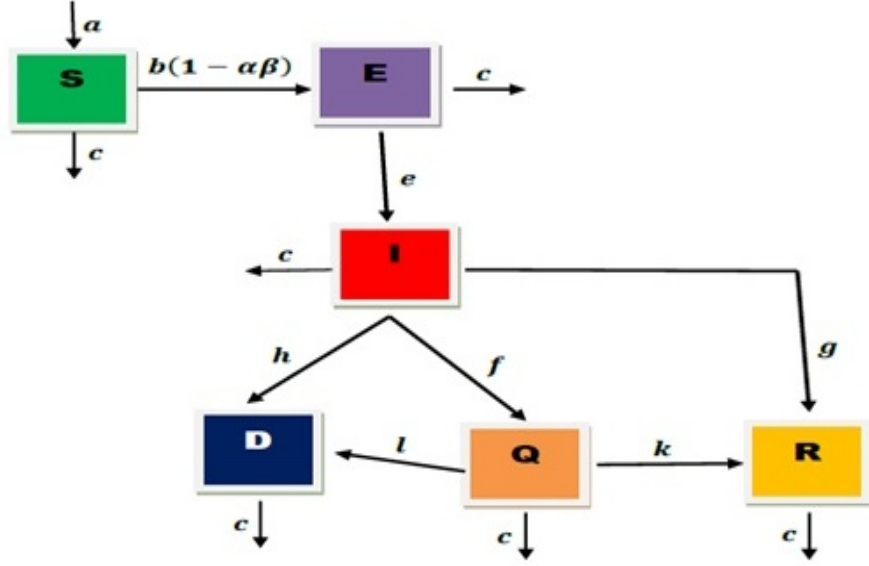


Figure 5.1: Depicts a flow chart of the proposed *SEIQRD* model.

a	Recruitment rate into S
b	Contact rate
α	Percentage of people who use a face mask
β	The efficacy of face masks
c	Mortality rate of all individuals
e	Progression rate from E to I
f	Isolation rate for I
g	Recovery rate of I
h	Death rate of I due to COVID-19 disease
k	Recovery rate of Q
l	Death rate of Q due to COVID-19 disease

Table 5.1: The parameters of the model and their descriptions.

\tilde{k}^ϕ . Thus, the modified model system (5.2) can be finally written in the following form

with initial conditions,

$$\begin{aligned}
{}^C D_t^\phi S(t) &= a - b(1 - \alpha\beta)S(t)I(t) - cS(t), \\
{}^C D_t^\phi E(t) &= b(1 - \alpha\beta)S(t)I(t) - (e + c)E(t), \\
{}^C D_t^\phi I(t) &= eE(t) - (f + g + h + c)I(t), \\
{}^C D_t^\phi Q(t) &= fI(t) - (k + l + c)Q(t), \\
{}^C D_t^\phi R(t) &= gI(t) + kQ(t) - cR(t), \\
{}^C D_t^\phi D(t) &= hI(t) + lQ(t).
\end{aligned} \tag{5.3}$$

The initial conditions are $S(0) > 0, E(0) > 0, I(0) > 0, Q(0) > 0, R(0) > 0, D(0) > 0$.

5.3 Analysis of the model

5.3.1 Existence and uniqueness

The following are the necessary and sufficient conditions for a fractional order system's solution to exist and be unique:

Theorem 5.3.1. *For each initial condition, there exists a unique solution of fractional order system (5.3).*

Proof. *We are looking for a sufficient condition for the presence and uniqueness of system (5.3) solutions in the region $\Pi \times (0, T]$ where*

$\Pi = \{(S, E, I, Q, R, D) \in \mathbb{R}^6 : \max(|S|, |E|, |I|, |Q|, |R|, |D|) \leq M\}$. *The method employed in [194] is used. Denote $Y = (S, E, I, Q, R, D)$ and $\bar{Y} = (\bar{S}, \bar{E}, \bar{I}, \bar{Q}, \bar{R}, \bar{D})$.*

Consider a mapping

$F(Y) = (F_1(Y), F_2(Y), F_3(Y), F_4(Y), F_5(Y), F_6(Y))$, *where*

$$\begin{aligned}
F_1(Y) &= a - b(1 - \alpha\beta)S(t)I(t) - cS(t), \\
F_2(Y) &= b(1 - \alpha\beta)S(t)I(t) - (e + c)E(t), \\
F_3(Y) &= eE(t) - (f + g + h + c)I(t), \\
F_4(Y) &= fI(t) - (k + l + c)Q(t), \\
F_5(Y) &= gI(t) + kQ(t) - cR(t), \\
F_6(Y) &= hI(t) + lQ(t).
\end{aligned}$$

For $Y, \bar{Y} \in \Pi$:

$$\begin{aligned}
& \|F(Y) - F(\bar{Y})\| \\
&= |F_1(Y) - F_1(\bar{Y})| + |F_2(Y) - F_2(\bar{Y})| + |F_3(Y) - F_3(\bar{Y})| + |F_4(Y) - F_4(\bar{Y})| \\
&+ |F_5(Y) - F_5(\bar{Y})| + |F_6(Y) - F_6(\bar{Y})| \\
&= |a - b(1 - \alpha\beta)S(t)I(t) - cS(t) - a + b(1 - \alpha\beta)\bar{S}(t)\bar{I}(t) + c\bar{S}(t)| + \\
&|b(1 - \alpha\beta)S(t)I(t) - (e + c)E(t) - b(1 - \alpha\beta)\bar{S}(t)\bar{I}(t) + (e + c)\bar{E}(t)| + \\
&|eE(t) - (f + g + h + c)I(t) - e\bar{E}(t) + (f + g + h + c)\bar{I}(t)| + \\
&|fI(t) - (k + l + c)Q(t) - f\bar{I}(t) - (k + l + c)\bar{Q}(t)| + \\
&|gI(t) + kQ(t) - cR(t) - g\bar{I}(t) - k\bar{Q}(t) + c\bar{R}(t)| + \\
&|hI(t) + IQ(t) - h\bar{I}(t) - l\bar{Q}(t)| \\
&\leq (c + 2b(1 - \alpha\beta)M) |S - \bar{S}| + (2e + c) |E - \bar{E}| + (2f + 2g + 2h + c) |I - \bar{I}| \\
&+ (2k + 2l + c) |Q - \bar{Q}| + c |R - \bar{R}| \\
&\leq G_1 |S - \bar{S}| + G_2 |E - \bar{E}| + G_3 |I - \bar{I}| + \\
&G_4 |Q - \bar{Q}| + G_5 |R - \bar{R}| \\
&\leq G \|Y - \bar{Y}\|, \text{ where } G = \max\{G_1, G_2, G_3, G_4, G_5\},
\end{aligned}$$

$$G_1 = (c + 2b(1 - \alpha\beta)M), \quad G_2 = (2e + c), \quad G_3 = (2f + 2g + 2h + c), \quad G_4 = (2k + 2l + c), \quad G_5 = c.$$

As a result, $F(Y)$ fulfils the Lipschitz [195] requirement. Hence the system (5.3) exists and is unique.

5.3.2 Positivity and boundedness of solutions

Proposition 5.3.1. *The region $\Omega = \{(S, E, I, Q, R, D) \in R^6 : 0 < N \leq \frac{a}{c}\}$ is non-negative invariant for the model (5.3), for all $t \geq 0$.*

Proof. We have

$${}^C D_t^\phi (S + E + I + Q + R + D)(t) = a - c(S + E + I + Q + R + D)(t).$$

Therefore, ${}^C D_t^\phi N(t) + cN = a$.

Using Laplace transform and Lemma 1.4.1, we have

$$z^\phi L(N(t)) - z^{\phi-1} N(0) + cL(N(t)) = \frac{a}{z}$$

So, $L(N(t)) = \frac{z^\phi N(0)}{z^{\phi+1}+c} + \frac{a}{z^{\phi+1}+c}$.

Applying inverse Laplace transform, we have

$$N(t) = N(0)E_{\phi,1}(-ct^\phi) + at^\phi E_{\phi,\phi+1}(-ct^\phi).$$

According to Mittag-Leffler function,

$$E_{c,d}(x) = xE_{c,c+d}(x) + \frac{1}{\Gamma(d)}.$$

Thus, $\lim_{t \rightarrow \infty} \text{Sup}N(t) \leq \frac{a}{c}$.

As a result, the function S, E, I, Q, R and D are all non-negative.

5.3.3 The equilibrium points of the system

The system's equilibrium may be found by solving the model (5.3) i.e.,

$$\text{i.e., } {}^C D_t^\phi S(t) = {}^C D_t^\phi E(t) = {}^C D_t^\phi I(t) = {}^C D_t^\phi Q(t) = {}^C D_t^\phi R(t) = {}^C D_t^\phi D(t) = 0.$$

The model (5.3) has two equilibrium points namely, the infection free equilibrium

$E_0(\frac{a}{c}, 0, 0, 0, 0, 0)$ and $E_1(S^*, E^*, I^*, Q^*, R^*, D^*)$ where

$$S^* = \frac{(e+c)(f+g+h+c)}{eb(1-\alpha\beta)}, E^* = I^* \frac{(f+g+h+c)}{e}, I^* = \frac{c}{b(1-\alpha\beta)}(R_{Covid\ 19} - 1), Q^* = \frac{f}{k+l+c}I^*, R^* = (g + \frac{kf}{k+l+c})I^*, D^* = 0.$$

5.3.4 The basic reproduction number of the system

The next-generation matrix technique is used to calculate the model's basic reproduction number $R_{Covid\ 19}$, which may be obtained from the maximum eigenvalue of the matrix FV^{-1} [37, 49] where,

$$F = \begin{bmatrix} 0 & \frac{\beta(1-\alpha\beta)a}{c} \\ 0 & 0 \end{bmatrix} \text{ and } V = \begin{bmatrix} (e+c) & 0 \\ -e & (f+g+h+c) \end{bmatrix}.$$

Therefore, $R_{Covid\ 19} = \frac{\beta(1-\alpha\beta)ae}{c(e+c)(f+g+h+c)}$.

5.3.5 Stability behavior at E_0

The Jacobian matrix of the model (5.3) at E_0 is given by $J_{E_0} = A$, where

$$J = \begin{bmatrix} A_{11} & 0 & A_{13} & 0 & 0 \\ 0 & A_{22} & A_{23} & 0 & 0 \\ 0 & A_{32} & A_{33} & 0 & 0 \\ 0 & 0 & A_{43} & A_{44} & 0 \\ P_{51} & 0 & 0 & 0 & A_{55} \end{bmatrix},$$

where $A_{11} = -a, A_{22} = -(e+c), A_{32} = e, A_{13} = -\frac{\beta(1-\alpha\beta)a}{c}, A_{23} = \frac{\beta(1-\alpha\beta)a}{c}A_{33} = -(f+g+h+c), A_{43} = f, A_{53} = g, A_{63} = h, A_{44} = -(k+l+c), A_{54} = k, A_{64} = l, A_{55} = -c$.

Theorem 5.3.2. When $R_{Covid\ 19} < 1$, the system (5.3) is globally asymptotically stable, and unstable when $R_{Covid\ 19} > 1$ at E_0 .

Proof. Using the appropriate Lyapunov function

$$F = eE + (e + c)I.$$

The aforementioned function's time derivative is

$${}^C D_t^\phi F(t) = e {}^C D_t^\phi E(t) + (e + c) {}^C D_t^\phi I(t).$$

From (5.3) we get,

$${}^C D_t^\phi F(t) = e(b(1 - \alpha\beta)SI - (e + c)E) + (e + c)(eE - (f + g + h + c)I).$$

Now,

$${}^C D_t^\phi F(t) \leq I(e + c)(f + g + h + c)[R_{Covid\ 19} - 1].$$

Hence if $R_{Covid\ 19} < 1$, then ${}^C D_t^\phi F(t) < 0$.

As a result of LaSalle's use of Lyapunov's concept [129, 130], the point E_0 is globally asymptotically stable and unstable if $R_{Covid\ 19} > 1$.

Theorem 5.3.3. If $R_{Covid\ 19} > 1$, the system (5.3) is globally asymptotically stable at E_1 .

Proof. The Lyapunov function of the Goh-Volterra form's is as follows:

$$W = (S - S^* - S^* \log \frac{S}{S^*}) + (E - E^* - E^* \log \frac{E}{E^*}) + L(I - I^* - I^* \log \frac{I}{I^*}).$$

Using Lemma 1.4.7 and taking Caputo derivative, we get

$${}^C D_t^\phi W(t) \leq (1 - \frac{S^*}{S}) {}^C D_t^\phi S(t) + (1 - \frac{E^*}{E}) {}^C D_t^\phi E(t) + L(1 - \frac{I^*}{I}) {}^C D_t^\phi I(t).$$

Using (5.3) we get,

$${}^C D_t^\phi W(t) \leq (a - b(1 - \alpha\beta)SI - cS - \frac{S^*(a - b(1 - \alpha\beta)SI - cS)}{S}) + ((b(1 - \alpha\beta)SI - (e + c)E) - \frac{E^*(b(1 - \alpha\beta)SI - (e + c)E)}{E}) + L((eE - (f + g + h + c)I) - \frac{I^*(eE - (f + g + h + c)I)}{I}).$$

Equation (5.3) gives us the steady state,

$$a = b(1 - \alpha\beta)S^*I^* + cS^*.$$

Using the condition of steady state of the above equation, we have

$${}^C D_t^\phi W(t) \leq (b(1 - \alpha\beta)S^*I^* + cS^* - b(1 - \alpha\beta)SI - cS - \frac{S^*(b(1 - \alpha\beta)S^*I^* + cS^* - b(1 - \alpha\beta)SI - cS)}{S}) + ((b(1 - \alpha\beta)SI - (e + c)E) - \frac{E^*(b(1 - \alpha\beta)SI - (e + c)E)}{E}) + L((eE - (f + g + h + c)I) - \frac{I^*(eE - (f + g + h + c)I)}{I}).$$

Taking all infected classes that do not have a single star (*) from the above equation and equal to zero:

$$b(1 - \alpha\beta)S^* - (e + c)E + L(eE - (f + g + h + c)I) = 0.$$

The steady state was slightly perturbed with the above equation, resulting in:

$$L = \frac{b(1 - \alpha\beta)S^*}{(f + g + h + c)}, (e + c) = \frac{I^*b(1 - \alpha\beta)S^*}{E^*}, e = \frac{(f + g + h + c)I^*}{E^*}.$$

Further simplification gives,

$${}^C D_t^\phi W(t) \leq (b(1 - \alpha\beta)S^*I^* + cS^* - cS - \frac{S^*(b(1 - \alpha\beta)S^*I^* + cS^* - cS)}{S}) + (-\frac{E^*(b(1 - \alpha\beta)SI)}{E} + I^*b(1 - \alpha\beta)S^*) + (-\frac{E^*(b(1 - \alpha\beta)S^*I^*)}{IE^*} + I^*b(1 - \alpha\beta)S^*).$$

Using A.M \geq G.M., we have

$$(2 - \frac{S}{S^*} - \frac{S^*}{S}) \leq 0, (3 - \frac{S^*}{S} - \frac{I^*E}{IE^*} - \frac{SE^*I}{E}) \leq 0. \text{ Thus, } {}^C D_t^\phi W(t) \leq 0.$$

The point E_1 is globally asymptotically stable if $R_{Covid\ 19} > 1$.

5.4 Numerical procedure

As discussed in Theorem 5.3.1, the solution of the system (5.3) is unique. To obtain the numerical solution of the system (5.3), Taylor's theorem will be used.

As a result, we proceed with the model's 1st equation as follows:

$${}^C D_t^\phi S(t) = \Lambda_1(t, S, E, I, Q, R, D), S(0) = S_0, t > 0. \quad (5.4)$$

Consider the set of points $[0, A]$ as the points on which we are prepared to approximate the system's solution. Actually, we are unable to calculate $S(t)$, which will be system's necessary solution. We divide $[0, A]$, into P sub-intervals $[t_r, t_{r+1}]$ of length, i.e., $m = \frac{A}{P}$, using the nodes $t_r = rm$, for $r = 0, 1, 2, \dots, P$. We extend the Taylor's theorem at $t = t_0$, we have a constant $k \in [0, A]$, so that

$$S(t) = S(t_0) + {}^C D_t^\phi S(t) \left\{ \frac{m^\phi}{\Gamma(\phi + 1)} \right\} + {}^C D_t^{2\phi} [S(t)]_{t=k} \left\{ \frac{m^{2\phi}}{\Gamma(2\phi + 1)} \right\}. \quad (5.5)$$

Now substitute ${}^C D_t^\phi S(t_0) = \Lambda_1((t_0), S(t_0), E(t_0), I(t_0), Q(t_0), R(t_0), D(t_0)))$ and $t = t_1$ in (5.2), which provides

$$\begin{aligned} S(t_1) &= S(t_0) + \Lambda_1((t_0), S(t_0), E(t_0), I(t_0), Q(t_0), R(t_0), D(t_0))) \left\{ \frac{m^\phi}{\Gamma(\phi + 1)} \right\} \\ &+ {}^C D_t^{2\phi} [S(t)]_{t=k} \left\{ \frac{m^{2\phi}}{\Gamma(2\phi + 1)} \right\}. \end{aligned} \quad (5.6)$$

If m is small, we ignore the higher terms, then (5.3) implies

$$S(t_1) = S(t_0) + \Lambda_1((t_0), S(t_0), E(t_0), I(t_0), Q(t_0), R(t_0), D(t_0))) \left\{ \frac{m^\phi}{\Gamma(\phi + 1)} \right\}. \quad (5.7)$$

A general formula of expanding about $t_r = t_r + m$, is

$$S(t_{r+1}) = S(t_r) + \Lambda_1((t_r), S(t_r), E(t_r), I(t_r), Q(t_r), R(t_r), D(t_r))) \left\{ \frac{m^\phi}{\Gamma(\phi + 1)} \right\}. \quad (5.8)$$

In similar way, we get

$$E(t_{r+1}) = E(t_r) + \Lambda_1((t_r), S(t_r), E(t_r), I(t_r), Q(t_r), R(t_r), D(t_r))) \left\{ \frac{m^\phi}{\Gamma(\phi + 1)} \right\}. \quad (5.9)$$

$$I(t_{r+1}) = I(t_r) + \Lambda_1((t_r), S(t_r), E(t_r), I(t_r), Q(t_r), R(t_r), D(t_r))) \left\{ \frac{m^\phi}{\Gamma(\phi + 1)} \right\}. \quad (5.10)$$

$$Q(t_{r+1}) = Q(t_r) + \Lambda_1(((t_r), S(t_r), E(t_r), I(t_r), Q(t_r), R(t_r), D(t_r)))) \left\{ \frac{m^\phi}{\Gamma(\phi + 1)} \right\}. \quad (5.11)$$

$$R(t_{r+1}) = R(t_r) + \Lambda_1(((t_r), S(t_r), E(t_r), I(t_r), Q(t_r), R(t_r), D(t_r)))) \left\{ \frac{m^\phi}{\Gamma(\phi + 1)} \right\}. \quad (5.12)$$

$$D(t_{r+1}) = D(t_r) + \Lambda_1(((t_r), S(t_r), E(t_r), I(t_r), Q(t_r), R(t_r), D(t_r)))) \left\{ \frac{m^\phi}{\Gamma(\phi + 1)} \right\}. \quad (5.13)$$

5.5 Numerical study

Numerical simulations employing Taylor's theorem are carried out with the help of MATLAB software to support the mathematical study of the system (5.3). This section is divided into four parts. The stability of our proposed model is discussed at E_0 and E_1 in Part 1. Part 2 delves into the dynamical behavior of all individuals of various fractional orders. Part 3 is to explore the varying effects of face masks. Part 4 is to determine whether the model (5.3) fits the data. One of the key components in the verification of an epidemiological model is the fitting of the parameters. We ran numerical simulations to contrast the output of our model with actual data from a number of reports released by the World Health Organization and Worldometer [161, 162]. Italy has a population of about 60,278,248 people [196]. In Italy, there are 7.2 births per 1000 people [197]. The computed recruiting rate is $\frac{7.21 \times 60278248}{1000 \times 365} = 1191$ per day.

Parameters	Value	Source
a	1191	Estimated
b	0.98159	[197]
α	0.1	Estimated
β	0.7	[197]
c	0.0006	[161]
e	0.1×10^{-5}	[162]
f	0.0007	[197]
g	0.05	[197]
h	0.015	Estimated
k	0.053	[197]
l	0.012	Model to fit

Table 5.2: Estimated values of parameters for India:

Part 1:

The stability of our suggested model is discussed in this section. The parameter values

used for the numerical simulations in Part 1 is provided in Table 5.2. Figures 5.2(a) to 5.2(e) depict the nature of all cases corresponding to $\phi = 0.98$. From the following figures, we have observed that the system is locally asymptotically stable at E_0 .

Part 2:

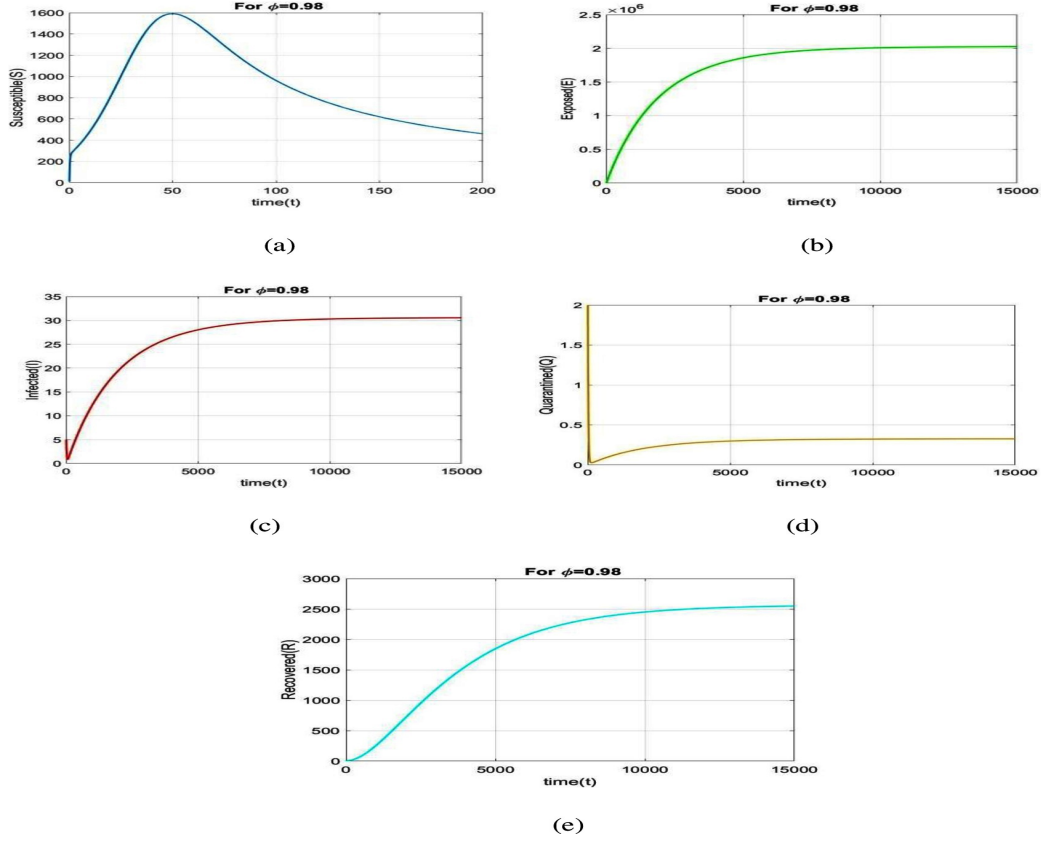


Figure 5.2: Time series of all classes correspondence to Table 5.2 taking $\phi = 0.98$ of system (5.3).

To analyze the dynamical behavior of all people, the values of the parameters in Table 5.2 are employed. Figures 5.3(a) to 5.3(f) depict all individuals' behavior over time for various fractional orders ϕ . Figure 5.3(a) depicts that the number of susceptible individuals increases when ϕ changes from 0.8 to 0.95. An increasing value of ϕ leads to decrease in the exposed rate in the exposed population in Figure 5.3(b). We see in Figure 5.3(c) that number of infected individuals increases when ϕ changes from 0.8 to 0.95. Figure 5.3(d) depicts that the number of quarantined individuals increases with time when ϕ decreases. The number of recovered individuals increases when ϕ changes from 0.8 to 0.95 in Figure 5.3(e). Figure 5.3(f) depicts that the number of death individuals increase with time when ϕ increases.

Part 3:

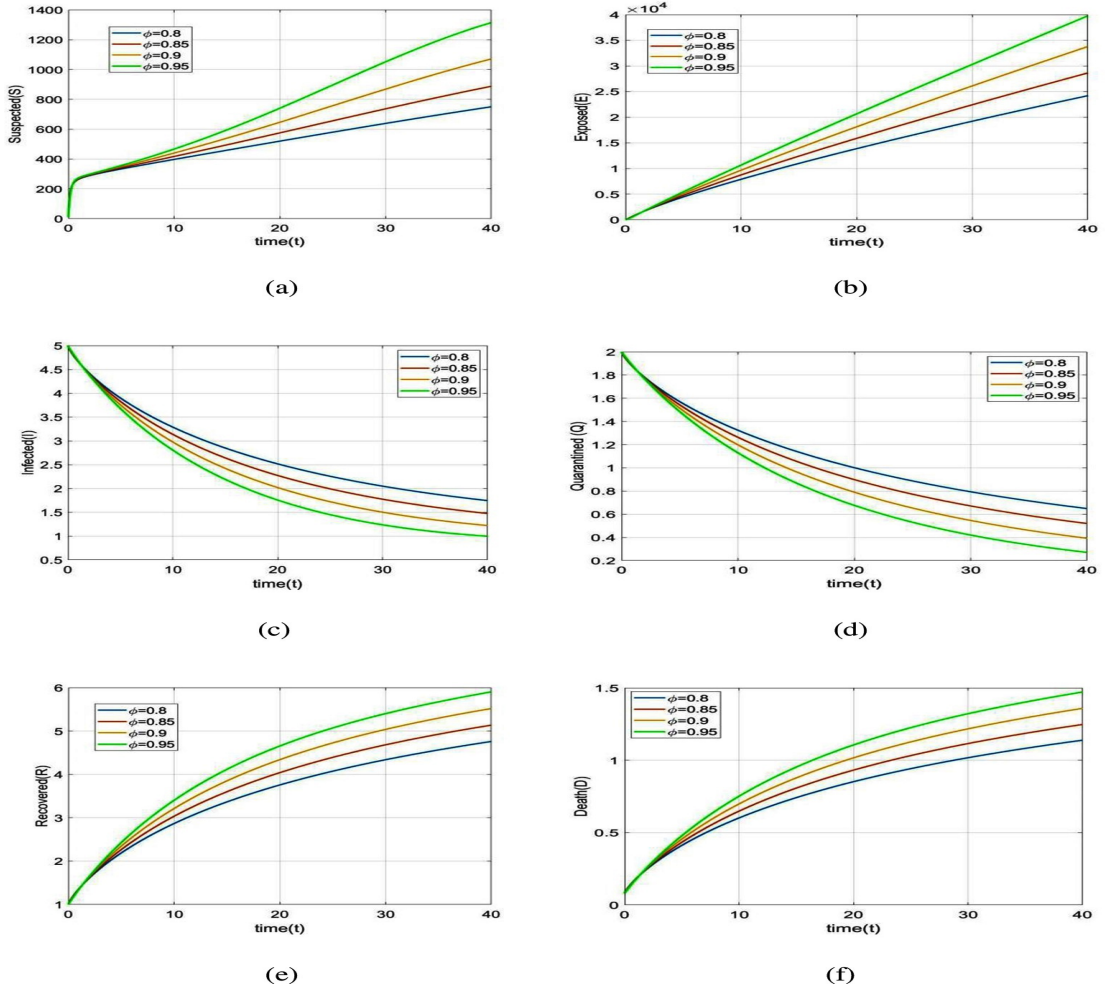


Figure 5.3: Dynamic of all classes over time for various values of $\phi = 0.8, 0.85, 0.90, 0.95$.

Part 3 of the numerical simulation investigates at how changing value impacts the fundamental reproduction number calculated in this work. Table 5.2 shows the parameter values utilized in the numerical simulations for Part 3. The acquired findings are shown in Table 5.3 after computing the fundamental reproduction numbers and utilizing the model parameters from Table 5.2. Table 5.3 shows that if a higher number of individuals in a community constantly utilize face masks, the COVID-19 epidemic can be decreased.

Figure 5.4 depicts that the values of $R_{Covid-19}$ decreases when α increases. The various consequences of wearing face masks were also investigated in this study, and it was discovered that wearing face masks on a consistent and suitable basis can inhibit the spreading of the COVID-19 pandemic. The impact of α and ϕ on the Infected individuals ($I(t)$) is

Parameter	Value	$R_{Covid-19}$
α	0.1 (10%)	1.423 > 1
α	0.5 (50%)	0.973 < 1
α	0.8 (80%)	0.659 < 1

Table 5.3: Numerical simulation of the varying effects of α .

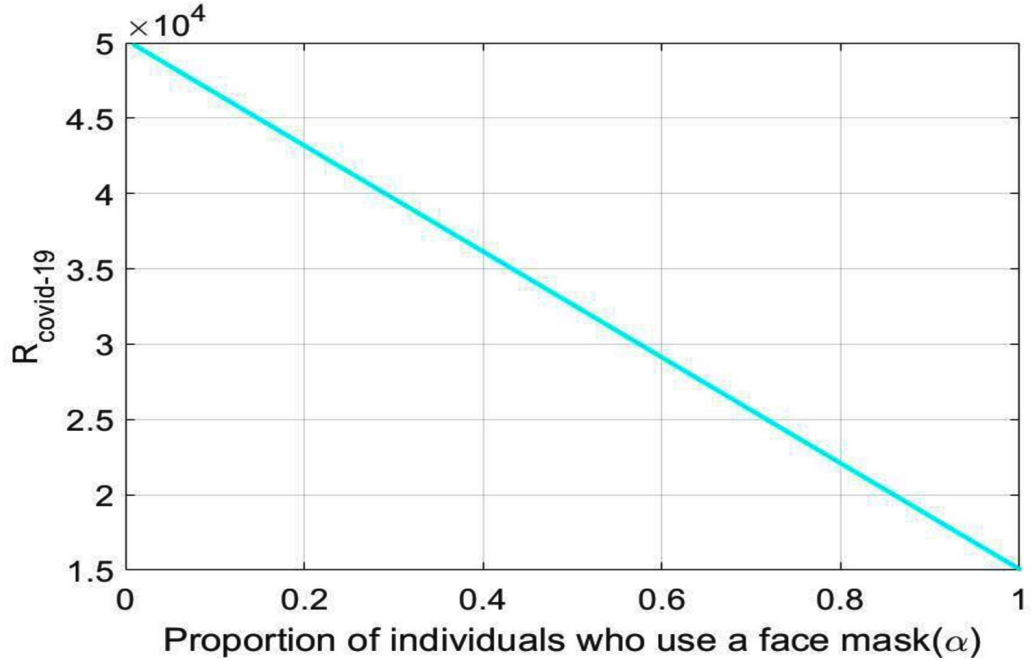


Figure 5.4: Variation of $R_{Covid-19}$ under α .

depicted in Figures 5.5(a) and 5.5(b). Based on the following figures, it can be noted that the implementation of maximum portion of population who use a face masks in order to effectively reduce COVID-19 transmission.

Part 4:

This section describes the data matching and model validation of the system (5.3) for Infected instances. Table 5.2 depicts the parametric values.

Figure 5.6 depicts the graphical representation of the infected cases respectively of the model (5.3) and the real infected cases in Italy [see Table 5.4] from 1st January 2022 to 31st January 2022 [162].

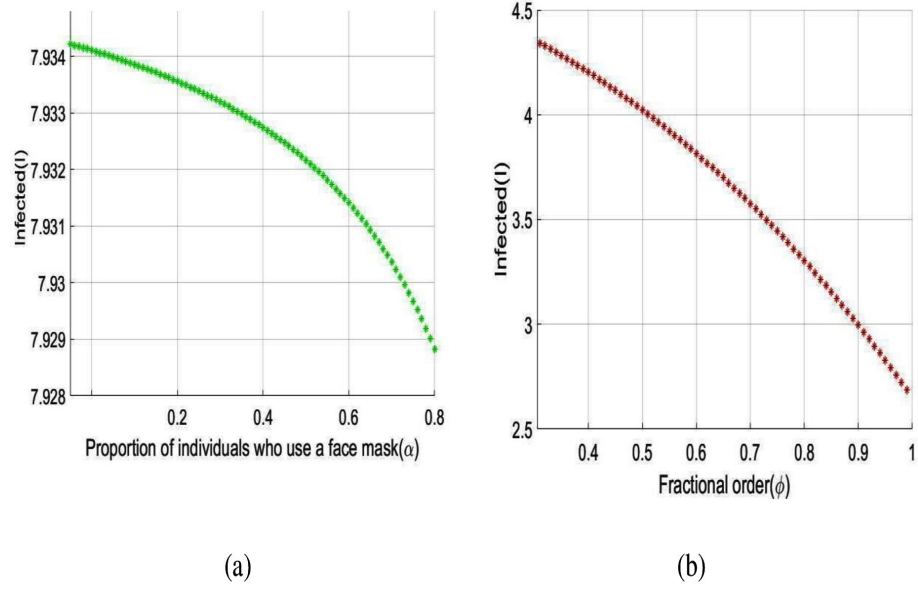


Figure 5.5: Dynamics of $I(t)$ under α and ϕ .

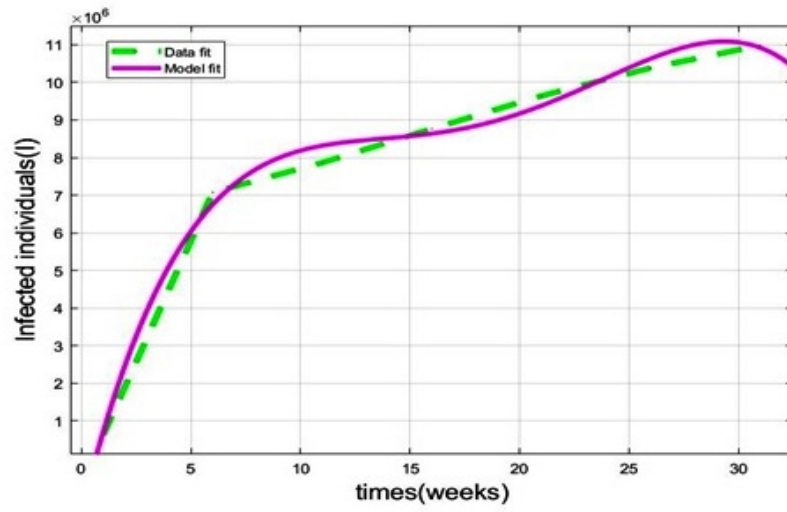


Figure 5.6: Graph of the infected class of the proposed model (5.3) and real infected data.

Day	Total reported data	Source
01/01/2022	635795	[162]
06/01/2022	7077458	[162]
11/01/2022	7864100	[162]
16/01/2022	8763280	[162]
21/01/2022	9637171	[162]
26/01/2022	10383904	[162]
31/01/2022	10983280	[162]

Table 5.4: The number of Infected cases in Italy, from 1st January 2022 to 31st January 2022.

5.6 Conclusion

The present study's possible goal is to develop a mathematical model for studying COVID-19 transmission patterns using actual pandemic cases in Italy, assisted by epidemiological modeling. The fractional order *SEIQRD* model was constructed and explored in this chapter in order to better explain the dynamics of the COVID-19 epidemic in Italy. We employed nonlinear analysis to demonstrate the model's existence and uniqueness. The model's fundamental reproduction number was also calculated using the next generation matrix technique. In order to stop the virus from spreading throughout the nation, our main goal is to establish the fundamental reproductive number and equilibrium. Furthermore, the global stability at the points E_0 and E_1 has been demonstrated. The results reveal that if $R_{Covid-19} < 1$, the point E_0 is globally asymptotically stable. Also if $R_{Covid-19} > 1$, the point E_1 is global asymptotic stable. Furthermore, using the fractional Taylor's approach, numerical analysis was done to establish an approximate solution for the suggested model. From the 1st of January 2022 to the 31st of January 2022, we have compared model values with real-world scenarios in Italy. Real data was also used to fit the model in order to forecast infected population instances in real life. In real-world dynamical processes, such as epidemic propagation, fractional calculus plays a vital role. The strength of memory effects, which is regulated by the order of fractional derivatives, is discovered to be dependent on the system dynamics. If the order of derivatives for the same set of parametric values is changed, the results will be changed (Figure 5.3). This study looked at the many consequences of wearing face masks, and it was discovered that wearing face masks on a consistent and suitable basis can help reduce the propagate of the COVID-19 disease (Figure 5.4 and Figure 5.5). Currently, research on a vaccine to avert the COVID-19 pandemic is showing promising results, with Pfizer claiming that their vaccine has a 95% effectiveness rate. However, it will be some time before the vaccinations are widely distributed around the world. As a result, wearing a face mask should

be made mandatory until everyone has access to vaccinations.

Chapter 6

Optimal Control Analysis of Fractional Order Dengue Model - A Case Study of Singapore

“We can only see a short distance ahead, but we can see plenty there that needs to be done”

- Alan Turing

This chapter is based on the paper
Optimal Control Analysis of Fractional Order Dengue Model - A Case Study of Singapore. (Communicated)

6.1 Introduction

Vector borne diseases (VBD) have posed a constant threat to human livestock and have thus proven to be a potential public health challenge in tropical and sub-tropical countries where climatic conditions are congenial to the growth and transmission of such diseases. There have been various global targets to arrest the spread of such diseases due to their serious effect on the socio-economic development of human population. Vector control strategies are an integral part of all national programs of the affected countries. However, the sustainability of such measures have always been questionable due to prevailing poverty conditions, rapid urbanization, concurrent population growth, changes in climatic conditions etc. Thus, certain holistic approaches aligned to the principle of study for effective prevention of such vector borne diseases are required which in turn demands for a thorough analysis of the dynamics of the mathematical models of these diseases. Research of such mathematical models will help in significant strengthening of entomological pursuits and in the acceleration of vector control measures to reduce the risk and burden on human population. A substantial proportion of the VBDs are contributed by Dengue in the tropical countries [199]. Besides urban localities, there has been an upsurge of dengue incidence in certain rural areas. Dengue fever, mainly caused by the dengue virus has the serotypes, DEN 1 to DEN 4 and is a mosquito borne disease. After malaria, the Dengue fever infection is the deadliest mosquito-borne disease with thousands of deaths and more than 390 million infections [200, 201] worldwide. According to a report published in 2012, more than 100 countries are affected by dengue fever [203]. Mosquito bites are the major transmission routes to human population. Hence, control measures must include certain personal prophylactic measures viz. use of mosquito repellent creams, liquids, coils, mats etc., use of bed nets for sleeping infants and young children during day time to prevent mosquito bite, biological control viz. use of larvivorous fishes in ornamental tanks, fountains, etc., use of biocides, chemical control viz. use of chemical larvicides like abate in big breeding containers, aerosol space spray during day time, environmental management and source reduction methods, health education and sensitizing and involving the community for detection of breeding places and their elimination. Mathematical models that characterize the dynamics of dengue disease have been a field of research for many years [204 - 207]. Modeling is a useful tool in studying the transmission dynamics of the disease and to determine the factors that are responsible for its spread in order to impose effective measures to control its spread. Many researchers [208 - 217] have proposed different epidemic models to study the transmission dynamics of dengue disease where integral order differential equations have been used. However, there are certain reservations regarding the integral order [218, 219] of the differential equations in such models. Such restrictions are taken into account by a comparatively new and emerging area of mathematical calculus, namely the fractional order differential equations. It has been observed that such

models are efficiently demonstrated by differential equations involving fractional operators [104, 220 - 223]. Extensive studies have evolved various techniques to construct real and approximate solutions to such fractional order differential equations [224, 225]. Several types of fractional operators, for example, Caputo–Fabrizio, Riemann–Liouville, Caputo, Hadamard, Atangana–Baleanu, Katugampola, etc. have been introduced to study the dynamics of the epidemic models. We have used the Caputo operator because of its possession of a non-local and non-singular exponential kernel and is found to be best suited to analyze the dynamics of dengue disease.

In this chapter, we have studied the dynamics of dengue transmission in a four compartment human population with two control parameters pertaining to measures taken to prevent mosquito bites and measures of treatment techniques and a three compartment mosquito population with a control parameter characterizing the inhibition of breeding of mosquitoes. Validation of the analytic or numerical results obtained are required to establish the novelty of the work. As is done in other biological models [226, 227], here we have considered case of disease transmission in Singapore [228] to generate the parameter values and compare our results with real time data. It have been observed that the total number of dengue cases in Singapore in 2022 was 31,892. There is an increase of 515% compared to 5182 cases reported during the same epidemiological week (1-51th week) in 2021. In comparison to other South east asian countries in the northern hemisphere, Singapore shows an alarming upsurge.

6.1.1 Arrangement of the chapter

We have formulated a fractional order dengue model in Caputo sense in Section 6.2. The existence, uniqueness, non-negativity, boundedness and stability analysis are discussed in Section 6.3. The sensitivity analysis of the proposed model is discussed in Section 6.4. In Section 6.5, we also provide an optimal control method for a fractional order dengue model using three control parameters. The suggested model's approximate solution is discussed in Section 6.6 using Euler technique in the Caputo derivative. In Section 6.7, the MATLAB-based numerical analysis is presented. Lastly the Section 6.8 covers conclusion of this chapter.

6.2 Model formulation

The total human population (N_H) is divided into four classes: Susceptible (S_H), Exposed (E_H), Infected (I_H), Recovered (R_H) and total mosquito population (N_M) is divided into three classes: Susceptible (S_M), Exposed (E_M), Infected (I_M).

Since a mosquito infected with dengue would carry the virus for the whole of its exis-

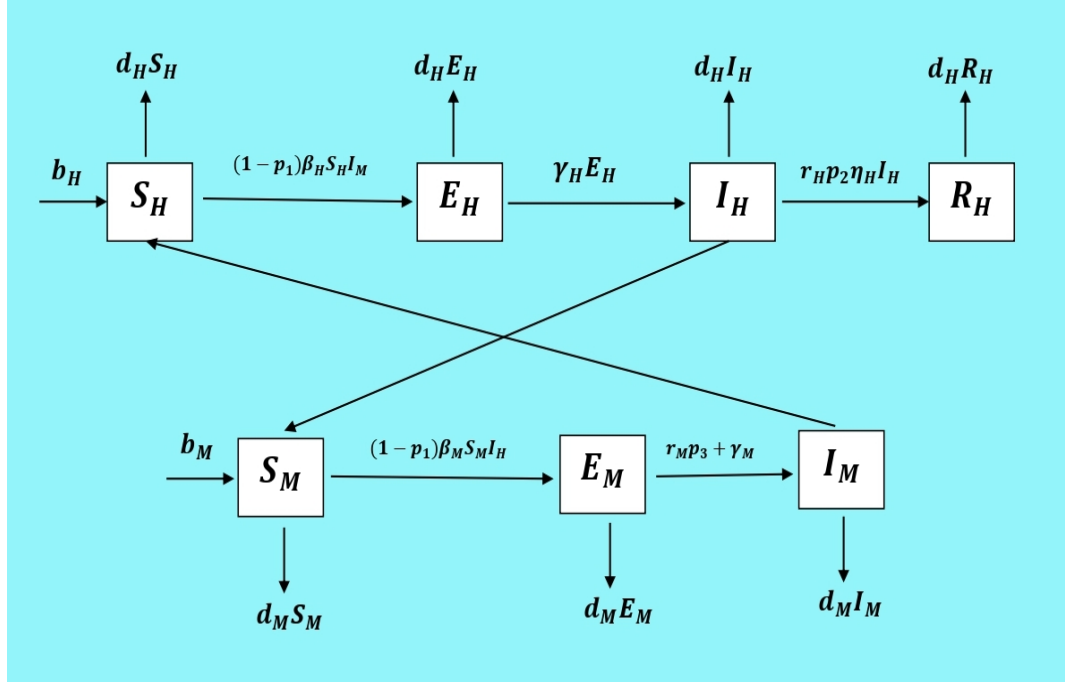


Figure 6.1: Flow diagram of the dengue model.

tence, we have not taken into account any recovered classes in the mosquito population.

Parameters	Biological meaning
b_H	birth rate of human population
b_M	birth rate of mosquito population
d_H	death rate of human population
d_M	death rate of mosquito population
β_H	transmission rate from mosquito to human
β_M	transmission rate from human to mosquito
γ_H	incubation rate of human population
γ_M	incubation rate of mosquito population
η_H	recovery rate of human population
r_H	proportion of effective treatment of dengue
r_M	mosquito killing efficiency

Table 6.1: Significance of the relevant parameters.

Three control functions are used in the proposed model, two of which are for humans

(controls p_1 and p_2) and one for mosquitoes (control p_3). Using mosquito nets or other insect repellents to protect people from mosquito bites is represented by the control p_1 . Therefore, we add $(1-p_1)$ to the rate of illness transmission in order to decrease the infection rate as a result of increased public knowledge. For the purpose of treating sick people, the control p_2 is used. The mosquito-killing operations to lower the mosquito population are represented by the control p_3 . The model's governing differential equations [229 - 233] may be stated in the following format while taking into account all of the aforementioned presumptions:

$$\begin{aligned}
{}^C D_t^\alpha S_H(t) &= b_H - (1 - p_1)\beta_H S_H I_M - d_H S_H; S_H(0) \geq 0, \\
{}^C D_t^\alpha E_H(t) &= (1 - p_1)\beta_H S_H I_M - (d_H + \gamma_H)E_H; E_H(0) \geq 0, \\
{}^C D_t^\alpha I_H(t) &= \gamma_H E_H - r_H p_2 \eta_H I_H - d_H I_H; I_H(0) \geq 0, \\
{}^C D_t^\alpha R_H(t) &= r_H p_2 \eta_H I_H - d_H R_H; R_H(0) \geq 0, \\
{}^C D_t^\alpha S_M(t) &= b_M - (1 - p_1)\beta_M S_M I_H - r_M p_3 S_M - d_M S_M; S_M(0) \geq 0, \\
{}^C D_t^\alpha E_M(t) &= (1 - p_1)\beta_M S_M I_H - (r_M p_3 + \gamma_M + d_M)E_M; E_M(0) \geq 0, \\
{}^C D_t^\alpha I_M(t) &= \gamma_M E_M - (r_M p_3 + d_M)I_M; I_M(0) \geq 0,
\end{aligned} \tag{6.1}$$

and ${}^C D_t^\alpha$ denotes the Caputo operator.

6.3 Fundamental mathematical results

We assert the following outcome.

6.3.1 Existence and uniqueness

Theorem 6.3.1. *The system (6.1) has a unique solution.*

Proof. *Let us take $\Omega \times [0, \tau]$, where*

$\Omega = \{(S_H, E_H, I_H, R_H, S_M, E_M, I_M) \in \mathbb{R}^7 : \max(|S_H|, |E_H|, |I_H|, |R_H|, |S_M|, |E_M|, |I_M|) \leq K\}$ *where τ and K are finite positive real numbers. Denote $X = (S_H, E_H, I_H, R_H, S_M, E_M, I_M)$ and $\bar{X} = (\bar{S}_H, \bar{E}_H, \bar{I}_H, \bar{R}_H, \bar{S}_M, \bar{E}_M, \bar{I}_M)$.*

Let $G(X) = (G_1(X), G_2(X), G_3(X), G_4(X), G_5(X), G_6(X), G_7(X))$, where

$$\begin{aligned}
G_1(X) &= b_H - (1 - p_1)\beta_H S_H I_M - d_H S_H, \\
G_2(X) &= (1 - p_1)\beta_H S_H I_M - (d_H + \gamma_H)E_H, \\
G_3(X) &= \gamma_H E_H - r_H p_2 \eta_H I_H - d_H I_H, \\
G_4(X) &= r_H p_2 \eta_H I_H - d_H R_H, \\
G_5(X) &= b_M - (1 - p_1)\beta_M S_M I_H - r_M p_3 S_M - d_M S_M, \\
G_6(X) &= (1 - p_1)\beta_M S_M I_H - (r_M p_3 + \gamma_M + d_M)E_M, \\
G_7(X) &= \gamma_M E_M - (r_M p_3 + d_M)I_M.
\end{aligned}$$

For $X, \bar{X} \in \Omega$:

$$\begin{aligned}
& \|G(X) - G(\bar{X})\| \\
&= |G_1(X) - G_1(\bar{X})| + |G_2(X) - G_2(\bar{X})| + |G_3(X) - G_3(\bar{X})| + |G_4(X) - G_4(\bar{X})| \\
&+ |G_5(X) - G_5(\bar{X})| + |G_6(X) - G_6(\bar{X})| + |G_7(X) - G_7(\bar{X})| \\
&= |b_H - (1 - p_1)\beta_H S_H I_M - d_H S_H - (b_H - (1 - p_1)\beta_H \bar{S}_H \bar{I}_H - d_H \bar{S}_H)| + \\
&\quad |(1 - p_1)\beta_H S_H I_M - (d_H + \gamma_H)E_H - ((1 - p_1)\beta_H \bar{S}_H \bar{I}_M - (d_H + \gamma_H)\bar{E}_H)| + \\
&\quad |\gamma_H E_H - r_H p_2 \eta_H I_H - d_H I_H - (\gamma_H \bar{E}_H - r_H p_2 \eta_H \bar{I}_H - d_H \bar{I}_H)| + \\
&\quad |r_H p_2 \eta_H I_H - d_H R_H - (r_H p_2 \eta_H \bar{I}_H - d_H \bar{R}_H)| + \\
&\quad |b_M - (1 - p_1)\beta_M S_M I_H - r_M p_3 S_M - d_M S_M - (b_M - (1 - p_1)\beta_M \bar{S}_M \bar{I}_H - r_M p_3 \bar{S}_M - d_M \bar{S}_M)| + \\
&\quad |(1 - p_1)\beta_M S_M I_H - (r_M p_3 + \gamma_M + d_M)E_M - ((1 - p_1)\beta_M \bar{S}_M \bar{I}_H - (r_M p_3 + \gamma_M + d_M)\bar{E}_M)| \\
&\leq d_H |(S_H - \bar{S}_H)| + 2(1 - p_1)\beta_H |(S_H I_M - \bar{S}_H \bar{I}_M)| + (d_H + 2\gamma_H) |E_H - \bar{E}_H| \\
&+ (r_H p_2 \eta_H + d_H) |I_H - \bar{I}_H| + (d_H) |R_H - \bar{R}_H| + 2(1 - p_1)\beta_M |I_H S_M - \bar{I}_H \bar{S}_M| + \\
&d_M |(S_M - \bar{S}_M)| + (r_M p_3 + d_M + 2\gamma_M) |E_M - \bar{E}_M| + (r_M p_3 + d_M) |I_M - \bar{I}_M| \\
&\leq F_1 |S_H - \bar{S}_H| + F_2 |E_H - \bar{E}_H| + F_3 |I_H - \bar{I}_H| + \\
&F_4 |R_H - \bar{R}_H| + F_5 |S_M - \bar{S}_M| + F_6 |E_M - \bar{E}_M| + F_7 |I_M - \bar{I}_M| \\
&\leq F \|X - \bar{X}\|, \text{ where } F = \max\{F_1, F_2, F_3, F_4, F_5, F_6, F_7\},
\end{aligned}$$

$$\begin{aligned}
& F_1 = d_H, \quad F_2 = (d_H + 2\gamma_H), \quad F_3 = (2(1 - p_1)\beta_H + r_H p_2 \eta_H + d_H), \quad F_4 = (d_H), \\
& F_5 = (d_M + 2(1 - p_1)\beta_M), \quad F_6 = (r_M p_3 + d_M + 2\gamma_M) \text{ and } F_7 = (r_M p_3 + d_M).
\end{aligned}$$

Thus, Lipschitz's requirements [150] are met by $G(X)$. As a result, $X(t)$ is the only solution to the model (6.1).

6.3.2 Non-negativity and boundedness

We shall now demonstrate that model solutions are not negative. First, we'll suppose that every model parameter is positive, we have

$$\begin{aligned}
{}^C D_t^\alpha S_H(t)|_{S_H=0} &= b_H > 0, \\
{}^C D_t^\alpha E_H(t)|_{E_H=0} &= (1 - p_1)\beta_H S_H I_M \geq 0, \\
{}^C D_t^\alpha I_H(t)|_{I_H=0} &= \gamma_H E_H \geq 0, \\
{}^C D_t^\alpha R_H(t)|_{R_H=0} &= r_H p_2 \eta_H I_H \geq 0, \\
{}^C D_t^\alpha S_M(t)|_{S_M=0} &= b_M > 0, \\
{}^C D_t^\alpha E_M(t)|_{E_M=0} &= (1 - p_1)\beta_M S_M I_H \geq 0, \\
{}^C D_t^\alpha I_M(t)|_{I_M=0} &= \gamma_M E_M \geq 0.
\end{aligned}$$

As a result, the model's whole set of solutions remains positive.

Theorem 6.3.2. *All solutions of system (6.1) are bounded.*

Proof. Now $N(t) = S_H(t) + E_H(t) + I_H(t) + R_H(t) + S_M(t) + E_M(t) + I_M(t)$, then

$${}^C D_t^\alpha N(t) \leq (b_H + b_M) - d_H N_H(t) - d_M N_M(t).$$

Therefore,

$${}^C D_t^\alpha N(t) + (d_H + d_M)N(t) \leq (b_H + b_M).$$

Using the preceding equation's Laplace transform:

$$\begin{aligned}
z^\alpha F(z) - z^{\alpha-1}N(0) + (d_H + d_M)F(z) &\leq \frac{(b_H + b_M)}{z}, \text{ where } F(z) = L\{N(t)\} \\
\Rightarrow F(z)(z^{\alpha+1} + z(d_H + d_M)) &\leq z^\alpha N(0) + (b_H + b_M) \\
\Rightarrow F(z) &\leq \frac{z^\alpha N(0) + (b_H + b_M)}{z^{\alpha+1} + z(d_H + d_M)} \\
&= \frac{z^\alpha N(0)}{z^{\alpha+1} + z(d_H + d_M)} + \frac{(b_H + b_M)}{z^{\alpha+1} + z(d_H + d_M)}.
\end{aligned}$$

Using inverse Laplace transform:

$$N(t) \leq N(0)E_{\alpha,1}(-(d_H + d_M)t^\alpha) + (b_H + b_M)t^\alpha E_{\alpha,\alpha+1}(-(d_H + d_M)t^\alpha).$$

Using the results of Mittag Leffler function [235, 236], we get

$$E_{c,d}(x) = xE_{c,c+d}(x) + \frac{1}{\Gamma(d)}.$$

Hence,

$$N(t) \leq (N(0) - \frac{(b_H + b_M)}{(d_H + d_M)})E_{\alpha,1}(-(d_H + d_M)t^\alpha) + \frac{(b_H + b_M)}{(d_H + d_M)}.$$

So the system solutions are bounded.

6.3.3 Equilibrium points

The equilibrium points are obtained from the steady state condition ${}^C D_t^\alpha S_H(t) = 0$, ${}^C D_t^\alpha E_H(t) = 0$, ${}^C D_t^\alpha I_H(t) = 0$, ${}^C D_t^\alpha R_H(t) = 0$, ${}^C D_t^\alpha S_M(t) = 0$, ${}^C D_t^\alpha E_M(t) = 0$ and ${}^C D_t^\alpha I_M(t) = 0$. i.e.,

$$\begin{aligned} b_H - (1 - p_1)\beta_H S_H I_M - d_H S_H &= 0, \\ (1 - p_1)\beta_H S_H I_M - (d_H + \gamma_H)E_H &= 0, \\ \gamma_H E_H - r_H p_2 \eta_H I_H - d_H I_H &= 0, \\ r_H p_2 \eta_H I_H - d_H R_H &= 0, \\ b_M - (1 - p_1)\beta_M S_M I_H - r_M p_3 S_M - d_M S_M &= 0, \\ (1 - p_1)\beta_M S_M I_H - (r_M p_3 + \gamma_M + d_M)E_M &= 0, \\ \gamma_M E_M - (r_M p_3 + d_M)I_M &= 0. \end{aligned} \tag{6.2}$$

The equations (6.2) yield two equilibrium points, namely

The dengue fever free equilibrium (DFFE) $E_0(\frac{b_H}{d_H}, 0, 0, 0, \frac{b_M}{d_M}, 0, 0)$.

The dengue fever endemic equilibrium (DFEE)

$$E_1(S_H^*, E_H^*, I_H^*, R_H^*, S_M^*, E_M^*, I_M^*), \tag{6.3}$$

where

$$S_H^* = \frac{b_H}{(1-p_1)\beta_H I_M^* + d_H}, E_H^* = \frac{(r_H p_2 \eta_H + d_H)I_H^*}{\gamma_H}, R_H^* = \frac{(r_H p_2 \eta_H)I_H^*}{d_H}, S_M^* = \frac{b_M}{(1-p_1)\beta_M I_H^* + d_M + r_M p_3}$$

and $E_M^* = \frac{(r_M p_3 + d_M)I_M^*}{\gamma_M}$.

6.3.4 Basic Reproduction Number

The fundamental reproduction number R_0 of the model, obtained as the largest eigenvalue of the matrix FV^{-1} [90,123], is calculated using the next-generation matrix approach where,

$$F = \begin{bmatrix} 0 & 0 & \frac{(1-p_1)\beta_H b_H}{d_H} & 0 \\ 0 & 0 & 0 & 0 \\ 0 & 0 & \frac{(1-p_1)\beta_M b_M}{d_M} & 0 \\ 0 & 0 & 0 & 0 \end{bmatrix} \text{ and } V = \begin{bmatrix} (\gamma_H + d_H) & 0 & 0 & 0 \\ -\gamma_H & (r_H p_2 \eta_H + d_H) & 0 & 0 \\ 0 & 0 & (r_M p_3 + \gamma_M + d_M) & 0 \\ 0 & 0 & -\gamma_M & (r_M p_3 + d_M) \end{bmatrix}. \text{ Therefore,}$$

$$R_0 = \sqrt{\frac{\gamma_H^2 \beta_M b_M (1 - p_1)}{d_M (r_M p_3 + d_M) (r_M p_3 + d_M + \gamma_M) (\gamma_H + d_H) (r_H p_2 \eta_H + d_H)}}. \tag{6.4}$$

6.4 Stability analysis

The stability study of DFFE and DFEE is performed in this part. Both equilibrium points with reference to local stability are discussed using the fundamental reproduction number (R_0).

The Jacobian matrix (J_0) must be calculated at the equilibrium locations specified in equation (6.1) in order to examine the stability of the system. Now

$$J_0(S_H, E_H, I_H, R_H, S_M, E_M, I_M) = G; \quad (6.5)$$

$$G = \begin{bmatrix} G_{11} & 0 & 0 & 0 & 0 & 0 & G_{17} \\ G_{21} & G_{22} & 0 & 0 & 0 & 0 & G_{27} \\ 0 & G_{32} & G_{33} & 0 & 0 & 0 & 0 \\ 0 & 0 & G_{43} & G_{44} & 0 & 0 & 0 \\ 0 & 0 & G_{53} & 0 & G_{55} & 0 & 0 \\ 0 & 0 & G_{63} & 0 & G_{65} & G_{66} & 0 \\ 0 & 0 & 0 & 0 & 0 & G_{76} & G_{77} \end{bmatrix},$$

where

$$\begin{aligned} G_{11} &= -(1-p_1)\beta_H I_M - d_H, G_{17} = -(1-p_1)\beta_H S_H, G_{21} = (1-p_1)\beta_H I_M, G_{22} = -(\gamma_H + d_H), \\ G_{27} &= (1-p_1)\beta_H S_H, G_{32} = \gamma_H, G_{33} = -r_H p_2 \eta_H - d_H, G_{43} = r_H p_2 \eta_H, G_{44} = -d_H, \\ G_{53} &= -(1-p_1)\beta_M S_M, G_{55} = -(1-p_1)\beta_M I_H - r_M p_3 - d_M, G_{63} = (1-p_1)\beta_M S_M, \\ G_{65} &= (1-p_1)\beta_M I_H, G_{66} = -(r_M p_3 + \gamma_M + d_M), G_{76} = \gamma_M, G_{77} = -(r_M p_3 + d_M). \end{aligned}$$

6.4.1 Local stability

The stability of two equilibrium points, E_0 and E_1 , will be examined in this section. The following theorems illustrate the findings of the stability analysis of various equilibria.

Theorem 6.4.1. E_0 is locally asymptotically stable of the system (6.1) if $R_0 < 1$, otherwise it is unstable.

Proof. At E_0 the Jacobian matrix is given by $J_0(\frac{b_H}{d_H}, 0, 0, 0, \frac{b_M}{d_M}, 0, 0) =$

$$\begin{bmatrix} -b_H & 0 & 0 & 0 & 0 & 0 & -(1-p_1)\beta_H \frac{b_H}{d_H} \\ -(\gamma_H + d_H) & 0 & 0 & 0 & 0 & 0 & (1-p_1)\beta_H \frac{b_H}{d_H} \\ 0 & \gamma_H & r_H p_2 \eta_H - d_H & 0 & 0 & 0 & 0 \\ 0 & 0 & r_H p_2 \eta_H & -d_H & 0 & 0 & 0 \\ 0 & 0 & -(1-p_1)\beta_M \frac{b_M}{d_M} & 0 & -d_M & 0 & 0 \\ 0 & 0 & (1-p_1)\beta_M \frac{b_M}{d_M} & 0 & 0 & -(r_M p_3 + \gamma_M + d_M) & 0 \\ 0 & 0 & 0 & 0 & 0 & \gamma_M & -(r_M p_3 + d_M) \end{bmatrix}.$$

The eigenvalues of the system are $\lambda_1 = -d_H$, $\lambda_2 = -d_H$, $\lambda_3 = -d_M$. As a result, $|\arg(\lambda_i)| = \pi > \frac{\alpha\pi}{2}$ ($i = 1, 2, 3$) where $0 < \alpha < 1$. The following equation provides the six more eigenvalues

$$\lambda^4 + A_1\lambda^3 + A_2\lambda^2 + A_3\lambda + A_4 = 0, \quad (6.6)$$

where

$$A_1 = (d_H + \gamma_H)(r_H p_2 \eta_H + d_H) + (r_M p_3 + d_M)(r_M p_3 \gamma_M + d_M),$$

$$A_2 = (d_H + \gamma_H)(r_H p_2 \eta_H + d_H) + (r_M p_3 + d_M)(r_M p_3 \gamma_M + d_M)(d_H + \gamma_H)(r_H p_2 \eta_H + d_H) + (r_M p_3 + d_M)(r_M p_3 \gamma_M + d_M),$$

$$A_3 = 2(r_M p_3 + d_M)(r_M p_3 \gamma_M + d_M)(d_H + \gamma_H)(r_H p_2 \eta_H + d_H),$$

$$A_4 = (1 - R_0)^2 \frac{(r_M p_3 + d_M)(r_M p_3 \gamma_M + d_M)(d_H + \gamma_H)(r_H p_2 \eta_H + d_H)d_H}{\beta_H \gamma_M b_M}.$$

Thus, E_0 is locally asymptotically stable if $R_0 < 1$, otherwise the DFFE is unstable with the help of Routh–Hurwitz criterion.

Theorem 6.4.2. E_1 is locally asymptotically stable of the system (6.1).

Proof. At E_1 the Jacobian matrix is given by

$$J_1 = U, \quad (6.7)$$

where,

$$U = \begin{bmatrix} U_{11} & 0 & 0 & 0 & 0 & 0 & U_{17} \\ U_{21} & U_{22} & 0 & 0 & 0 & 0 & U_{27} \\ 0 & U_{32} & U_{33} & 0 & 0 & 0 & 0 \\ 0 & 0 & U_{43} & U_{44} & 0 & 0 & 0 \\ 0 & 0 & U_{53} & 0 & U_{55} & 0 & 0 \\ 0 & 0 & U_{63} & 0 & U_{65} & U_{66} & 0 \\ 0 & 0 & 0 & 0 & 0 & U_{76} & U_{77} \end{bmatrix},$$

where

$$\begin{aligned} U_{11} &= -(1 - p_1)\beta_H I_M^* - d_H, U_{17} = -(1 - p_1)\beta_H S_H^*, U_{21} = (1 - p_1)\beta_H I_M^*, U_{22} = -(\gamma_H + d_H), \\ U_{27} &= (1 - p_1)\beta_H S_H^*, U_{32} = \gamma_H, U_{33} = -r_H p_2 \eta_H - d_H, U_{43} = r_H p_2 \eta_H, U_{44} = -d_H, \\ U_{53} &= -(1 - p_1)\beta_M S_M^*, U_{55} = -(1 - p_1)\beta_M I_H^* - r_M p_3 - d_M, U_{63} = (1 - p_1)\beta_M S_M^*, \\ U_{65} &= (1 - p_1)\beta_M I_H^*, U_{66} = -(r_M p_3 + \gamma_M + d_M), U_{76} = \gamma_M, U_{77} = -(r_M p_3 + d_M). \end{aligned}$$

The eigenvalues of the system are $\lambda_1 = -d_H$, it follows that $|\arg(\lambda_1)| = \pi > \frac{\alpha\pi}{2}$ where $0 < \alpha < 1$. The remaining six eigenvalues are given by the following equation $\lambda^6 + B_1\lambda^5 + B_2\lambda^4 + B_3\lambda^3 + B_4\lambda^2 + B_5\lambda + B_6 = 0$, where

$$B_1 = -(U_{11} + U_{22} + U_{33} + U_{55} + U_{66} + U_{77}),$$

$$B_2 = (U_{11} + U_{22})(U_{33} + U_{55}) + (U_{11} + U_{22} + U_{33} + U_{55})(U_{66} + U_{77}) + U_{11}U_{22} + U_{33}U_{55} + U_{66}U_{77},$$

$$B_3 = -[(U_{11} + U_{22})U_{33}U_{55} + (U_{33} + U_{55})U_{11}U_{22} + (U_{66} + U_{77})\{U_{11}U_{22} + U_{33}U_{55}(U_{11} + U_{22})(U_{33} + U_{55})\} + (U_{11} + U_{22} + U_{33} + U_{55})U_{66}U_{77}],$$

$$\begin{aligned}
B_4 &= U_{11}U_{22}U_{33}U_{55} + \{(U_{11} + U_{22}U_{33}U_{55} + U_{11}U_{22}(U_{33} + U_{55})\}(U_{66} + U_{77}) + \{(U_{11} + U_{22})(U_{33} + U_{55}) + U_{11}U_{22} + U_{33}U_{55}\}U_{66}U_{77}, \\
B_5 &= -[U_{11}U_{22}U_{33}U_{55}(U_{66} + U_{77}) + \{(U_{11} + U_{22})U_{33}U_{55} + U_{11}U_{22}(U_{33} + U_{55})\}(U_{66} + U_{77}) - U_{32}U_{27}U_{76}U_{55}U_{65} + U_{27}U_{76}U_{32}U_{63} + U_{32}U_{21}U_{17}U_{63}U_{76}], \\
B_6 &= -[U_{11}U_{22}U_{33}U_{55}U_{66}U_{77} - U_{11}U_{32}U_{27}U_{76}U_{55}U_{66} + U_{55}U_{32}U_{27}U_{76}U_{63} - U_{21}U_{17}U_{76}U_{32}U_{535}U_{65} + U_{21}U_{17}U_{76}U_{32}U_{55}U_{63}].
\end{aligned}$$

By the Routh–Hurwitz criterion, E_1 is locally asymptotically stable.

6.5 Sensitivity analysis

The model parameters that have a financial impact on the fundamental rate of reproduction of different infectious illnesses are identified via sensitivity analysis. Epidemiologists may predict the crucial elements that are essential to the dynamics of disease transmission by using this technique. In order to gain an understanding of the model parameters that need to be retained or monitored in order to avoid or control the effects of the illness, we must discover the values of the sensitivity indices. If we wish to stop the transmission of infection, we must identify the model parameters that are essential for understanding how illnesses spread. We must estimate the change of the fundamental reproduction number R_0 with regard to different model parameters in order to calculate the normalised forward sensitivity index of the fundamental reproduction number R_0 .

The normalized sensitivity index $W_{R_0}^p = \frac{\partial R_0}{\partial p} \cdot \frac{p}{R_0}$ is calculated using the normalized sensitivity index of R_0 where p is the parametric space of R_0 .

The sensitivity index [237] will be used to assess how each parameter affects an outbreak of a disease so that precautions can be taken to stop it from spreading. In this instance, we want to estimate significant model parameters that influence the fundamental reproduction number R_0 . We have,

$$\begin{aligned}
W_{R_0}^{b_M} &= \frac{1}{2}, W_{R_0}^{r_H} = -\frac{1}{2} \frac{r_H p_2 \eta_H}{(r_H p_2 \eta_H + d_H)}, W_{R_0}^{d_H} = -\frac{d_H}{2} \left[\frac{1}{(\gamma_H + d_H)} + \frac{1}{(r_H p_2 \eta_H + d_H)} \right], W_{R_0}^{\beta_M} = \frac{1}{2}, W_{R_0}^{\gamma_H} = \\
&\frac{1}{2} \frac{\gamma_H(\gamma_H + 2d_H)}{(\gamma_H + d_H)}, W_{R_0}^{\gamma_M} = -\frac{\gamma_M}{2} \frac{1}{(r_M p_3 + d_M + \gamma_M)}, W_{R_0}^{\eta_H} = -\frac{1}{2} \frac{r_H p_2 \eta_H}{(r_H p_2 \eta_H + d_H)}, W_{R_0}^{r_M} = -\frac{r_M}{2} \left[\frac{p_3}{(r_M p_3 + d_M)} + \right. \\
&\left. \frac{p_3}{(r_M p_3 + d_M + \gamma_M)} \right], W_{R_0}^{p_1} = -\frac{p_1}{2(1-p_1)}, W_{R_0}^{p_2} = -\frac{1}{2} \frac{r_H p_2 \eta_H}{(r_H p_2 \eta_H + d_H)}, \\
W_{R_0}^{p_3} &= -\frac{p_3}{2} \left[\frac{r_M}{(r_M p_3 + d_M)} + \frac{r_M}{(r_M p_3 + d_M + \gamma_M)} \right], W_{R_0}^{d_M} = -\frac{d_M}{2} \left[\frac{1}{d_M} + \frac{1}{d_M(r_M p_3 + d_M)} + \frac{1}{d_M(r_M p_3 + d_M + \gamma_M)} \right].
\end{aligned}$$

6.6 Optimal control

The area of optimal control theory in fractional derivatives has been improved by Agarwal et al. [51] and Ding et al. [50]. Three control parameters are employed in the proposed model, two of which are for humans p_1 and p_2 , and one for mosquitoes p_3 . The control p_1 depicts the actions taken to use mosquito nets to protect people from mosquito bites. For the purpose of treating sick people, the additional control p_2 is used. In order to lower

the mosquito population, the control p_3 indicates mosquito eradication operations. Here, we make the assumption that all controls, as they are implemented in accordance with requirement, are functions of time t . Our major goal is to reduce the overall loss brought on by diseased hosts and mosquitoes as well as the expense of applying three treatments. Therefore, the goal of the best control is to reduce the number of affected people and mosquitoes while also keeping the three controls' implementation costs to a minimum. In order to minimize costs, we create the cost function as follows:

$J(p_1^*(t), p_2^*(t), p_3^*(t)) = \min (J(p_1(t), p_2(t), p_3(t)))$ with

$$J(p_1, p_2, p_3) = \left(\int_0^{t_f} [B_1 E_H + B_2 I_H + B_3 R_H + B_4 E_M + B_5 I_M + \frac{A_1}{2} p_1^2 + \frac{A_2}{2} p_2^2 + \frac{A_3}{2} p_3^2] dt \right), \quad (6.8)$$

subject to

$$\begin{aligned} {}^C D_t^\alpha S_H(t) &= b_H - (1 - p_1) \beta_H S_H I_M - d_H S_H; S_H(0) \geq 0, \\ {}^C D_t^\alpha E_H(t) &= (1 - p_1) \beta_H S_H I_M - (d_H + \gamma_H) E_H; E_H(0) \geq 0, \\ {}^C D_t^\alpha I_H(t) &= \gamma_H E_H - r_H p_2 \eta_H I_H - d_H I_H; I_H(0) \geq 0, \\ {}^C D_t^\alpha R_H(t) &= r_H p_2 \eta_H I_H - d_H R_H; R_H(0) \geq 0, \\ {}^C D_t^\alpha S_M(t) &= b_M - (1 - p_1) \beta_M S_M I_H - r_M p_3 S_M - d_M S_M; S_M(0) \geq 0, \\ {}^C D_t^\alpha E_M(t) &= (1 - p_1) \beta_M S_M I_H - (r_M p_3 + \gamma_M + d_M) E_M; E_M(0) \geq 0, \\ {}^C D_t^\alpha I_M(t) &= \gamma_M E_M - (r_M p_3 + d_M) I_M; I_M(0) \geq 0, \end{aligned} \quad (6.9)$$

where $0 \leq p_1(t), p_2(t), p_3(t) \leq 1$.

Theorem 6.6.1. *Let $(p_1(t), p_2(t), p_3(t))$ be three measurable control functions on $[0, t_f]$, each with a value in $[0, 1]$. Then the three optimal controls $(p_1^*(t), p_2^*(t), p_3^*(t))$ minimizing the objective function $J(p_1(t), p_2(t), p_3(t))$ of (6.8) are given by $p_1^*(t) = \max [\min(\bar{p}_1, 1), 0]$, $\bar{p}_1 = \frac{(\epsilon_2 - \epsilon_1)(\beta_H S_H I_M) + (\epsilon_6 - \epsilon_5)(\beta_M S_M I_H)}{A_2}$, $p_2^*(t) = \max [\min(\bar{p}_2, 1), 0]$, $\bar{p}_2 = \frac{(\epsilon_3 - \epsilon_4)(\eta_H r_H I_H)}{A_2}$, $p_3^*(t) = \max [\min(\bar{p}_3, 1), 0]$, $\bar{p}_3 = \frac{r_M(\epsilon_5 + \epsilon_6 + \epsilon_7)(I_M + E_M + S_M)}{A_3}$.*

Proof. *The Hamiltonian has been studied using the following approach:*

$H = [B_1 E_H + B_2 I_H + B_3 R_H + B_4 E_M + B_5 I_M + \frac{A_1}{2} p_1^2 + \frac{A_2}{2} p_2^2 + \frac{A_3}{2} p_3^2] + \epsilon_1(b_H - (1 - p_1) \beta_H S_H I_M - d_H S_H) + \epsilon_2((1 - p_1) \beta_H S_H I_M - (d_H + \gamma_H) E_H) + \epsilon_3(\gamma_H E_H - r_H p_2 \eta_H I_H - d_H I_H) + \epsilon_4(r_H p_2 \eta_H I_H - d_H R_H) + \epsilon_5(b_M - (1 - p_1) \beta_M S_M I_H - r_M p_3 S_M - d_M S_M) + \epsilon_6((1 - p_1) \beta_M S_M I_H - (r_M p_3 + \gamma_M + d_M) E_M) + \epsilon_7(\gamma_M E_M - (r_M p_3 + d_M) I_M)$,
the adjoint variables with $\epsilon_i(t), i = 1, \dots, 7$, written in terms of the canonical equation, we

have $\epsilon_i(t_f) = 0$:

$${}^{RL}D_t^\alpha \epsilon_1(t)(t) = -\frac{\partial H}{\partial S_H} = -\epsilon_1((1-p_1)\beta_H I_M - d_H) - \epsilon_2((1-p_1)\beta_H I_M),$$

$${}^{RL}D_t^\alpha \epsilon_2(t)(t) = -\frac{\partial H}{\partial E_H} = -B_1 + \epsilon_2((d_H + \gamma_H)) - \epsilon_3(\gamma_H),$$

$${}^{RL}D_t^\alpha \epsilon_3(t)(t) = -\frac{\partial H}{\partial I_H} = -B_2 + \epsilon_3(r_H p_2 \eta_H + d_H) - \epsilon_4(r_H p_2 \eta_H) + \epsilon_5((1-p_1)\beta_M S_M)$$

$$-\epsilon_6((1-p_1)\beta_M S_M),$$

$${}^{RL}D_t^\alpha \epsilon_4(t)(t) = -\frac{\partial H}{\partial R_H} = -B_3 + \epsilon_4 d_H,$$

$${}^{RL}D_t^\alpha \epsilon_5(t)(t) = -\frac{\partial H}{\partial S_M} = -\epsilon_5((1-p_1)\beta_M I_H - d_M) - \epsilon_6((1-p_1)\beta_M I_H),$$

$${}^{RL}D_t^\alpha \epsilon_6(t)(t) = -\frac{\partial H}{\partial E_M} = -B_4 + \epsilon_6(r_M p_3 + \gamma_M + d_M) - \epsilon_7 \gamma_M,$$

$${}^{RL}D_t^\alpha \epsilon_7(t)(t) = -B_5 + \epsilon_1((1-p_1)\beta_H S_H) - \epsilon_2((1-p_1)\beta_H S_H) + \epsilon_7(r_M p_3 + d_M).$$

Thus, the challenge of decreasing the Hamiltonian with regard to the control instead of finding p_1^*, p_2^*, p_3^* that minimises H in the presence of (6.9) is restated. The Pontryagin principle [52] is then used to create the ideal situation shown below:

$$\frac{\partial H}{\partial p_1} = A_1 p_1 + (\epsilon_1 - \epsilon_2)(\beta_H S_H I_M) + (\epsilon_5 - \epsilon_6)(\beta_M S_M I_H),$$

$$\frac{\partial H}{\partial p_2} = A_2 p_2 + (\epsilon_4 - \epsilon_3)(r_H \eta_H I_H),$$

$$\frac{\partial H}{\partial p_3} = A_3 p_3 - r_M(\epsilon_5 + \epsilon_6 + \epsilon_7)(I_M + E_M + S_M).$$

With adjoint variables and state variables, the following results may be obtained:

$$\overline{p_1} = \frac{(\epsilon_2 - \epsilon_1)(\beta_H S_H I_M) + (\epsilon_6 - \epsilon_5)(\beta_M S_M I_H)}{A_2}, \quad \overline{p_2} = \frac{(\epsilon_3 - \epsilon_4)(r_H \eta_H I_H)}{A_2}, \quad \overline{p_3} = \frac{r_M(\epsilon_5 + \epsilon_6 + \epsilon_7)(I_M + E_M + S_M)}{A_3}.$$

For the optimal control p_i^* for $i = 1, 2, 3$, take into account the control limitations and the sign of the function $\frac{\partial H}{\partial p_i}$.

As a result, we get

$$p_i^* = \begin{cases} 0 & \text{if } \frac{\partial H}{\partial p_i} < 0, \\ \overline{p_i} & \text{if } \frac{\partial H}{\partial p_i} = 0, \\ 1 & \text{if } \frac{\partial H}{\partial p_i} > 0. \end{cases}$$

For the model system (6.9), the ideal circumstance might be determined by using p_i^* .

6.7 Numerical procedure

Using the technique described in [238], we offer the solution to the model (6.1) in this part. We express the model (6.1) in the following format to have a numerical scheme:

$${}^C D_t^\alpha u(t) = U(t, u(t)), u(0) = u_0, t > 0, \quad (6.10)$$

where $u = (S_H, E_H, I_H, R_H, S_M, E_M, I_M) \in \mathbb{R}^7$. In addition to satisfying the Lipschitz requirement, the continuous function $U(t, u(t))$ is employed, where u_0 denotes the starting state vector. When we apply the Caputo integral to both sides of (6.10), we get:

$$u(t) = u_0 + \frac{1}{\Gamma(\alpha)} \int_0^t (t-p)^{\alpha-1} U(p, u(p)) dp. \quad (6.11)$$

We assume a uniform grid on $[0, A]$ with $w = \frac{A}{m}$ as the step size and $m \in N$ as the number of iterations. As a result, after using the Euler technique [239], equation (6.11) has the structure shown below:

$$u_{n+1} = u_0 + \frac{w^\alpha}{\Gamma(\alpha+1)} \sum_{j=0}^n ((n-j+1)^\alpha - (n-j)^\alpha) U(t_j, u(t_j)), n = 0, 1, 2, \dots, m. \quad (6.12)$$

Consequently, using the aforementioned approach, we arrived at the iterative formulas shown below for the relevant classes of the model (6.1),

$$\begin{aligned} S_{H(n+1)} &= S_{H_0} + \frac{w^\alpha}{\Gamma(\alpha+1)} \sum_{j=0}^n ((n-j+1)^\alpha - (n-j)^\alpha) (b_H - (1-p_1)\beta_H S_{Hj} I_{Mj} - d_H S_{Hj}), \\ E_{H(n+1)} &= E_{H_0} + \frac{w^\alpha}{\Gamma(\alpha+1)} \sum_{j=0}^n ((n-j+1)^\alpha - (n-j)^\alpha) ((1-p_1)\beta_H S_{Hj} I_{Mj} - (d_H + \gamma_H) E_{Hj}), \\ I_{H(n+1)} &= I_{H_0} + \frac{w^\alpha}{\Gamma(\alpha+1)} \sum_{j=0}^n ((n-j+1)^\alpha - (n-j)^\alpha) (\gamma_H E_{Hj} - r_H p_2 \eta_H I_{Hj} - d_H I_{Hj}), \\ R_{H(n+1)} &= R_{H_0} + \frac{w^\alpha}{\Gamma(\alpha+1)} \sum_{j=0}^n ((n-j+1)^\alpha - (n-j)^\alpha) (r_H p_2 \eta_H I_{Hj} - d_H R_{Hj}), \\ S_{M(n+1)} &= S_{M_0} + \frac{w^\alpha}{\Gamma(\alpha+1)} \sum_{j=0}^n ((n-j+1)^\alpha - (n-j)^\alpha) (b_M - (1-p_1)\beta_M S_{Mj} I_{Hj} - r_M p_3 S_{Mj} - d_M S_{Mj}), \\ E_{M(n+1)} &= E_{M_0} + \frac{w^\alpha}{\Gamma(\alpha+1)} \sum_{j=0}^n ((n-j+1)^\alpha - (n-j)^\alpha) ((1-p_1)\beta_M S_{Mj} I_{Hj} - (r_M p_3 + \gamma_M + d_M) E_{Mj}), \\ I_{M(n+1)} &= I_{M_0} + \frac{w^\alpha}{\Gamma(\alpha+1)} \sum_{j=0}^n ((n-j+1)^\alpha - (n-j)^\alpha) (\gamma_M E_{Mj} - (r_M p_3 + d_M) I_{Mj}). \end{aligned}$$

6.8 Numerical discussion

In this part, we adopt numerical methods to verify the existence, uniqueness and stability of the solutions of model (6.1) and the impact of the control parameters on the human and mosquito population. We have included Euler's theorem into the numerical system using the mathematics programme MATLAB. The numerical output of model simulations

and related results are divided into the following several categories:

Parameters	Values	Reference
b_H	10	[240]
b_M	3.09	[240]
d_H	0.004	[241]
d_M	0.07	[241]
β_H	0.0005	Assumed
β_M	0.0012	Assumed
γ_H	0.01	[242]
γ_M	0.009	[242]
η_H	0.034	[243]
r_H	0.31	[244]
r_M	0.021	[244]
p_1	0.002	Assumed
p_2	0.05	Assumed
p_3	0.0001	Assumed

Table 6.2: Parameter values for numerical study.

Case 1: Dynamical features of the human sub-population for different fractional orders

To analyze the dynamics of the behaviour of human sub populations, the parameter values in Table 6.2 are employed. All human sub-population behaviour over time for several fractional orders α is shown in Figures 6.2 (a) through 6.2 (c). According to Figure 6.2, the dengue outbreak has caused a fast rise in the susceptible population, whereas the exposed and infectious populations originally increased over time but have then decreased. The high incidence of dengue transmission is the cause of the rise, while many interventions like treatment and other safety measures are the cause of the decline. Because most dengue patients need prompt care, the graph of recovered group shows a rise owing to a high treatment rate, and a reduction due to a decline in dengue cases.

Case 2: Dynamical features of the mosquitoes sub-population for different fractional orders

To analyze the dynamics of the behaviour of the mosquito sub-population, the parameter values in Table 6.2 are employed. All mosquitoes sub-population behaviour over time for several fractional orders α are shown in Figures 6.3 (a) through 6.3 (c). Figure 6.3 illustrates how the dengue outbreak causes susceptible *Aedes aegypti* mosquitoes to

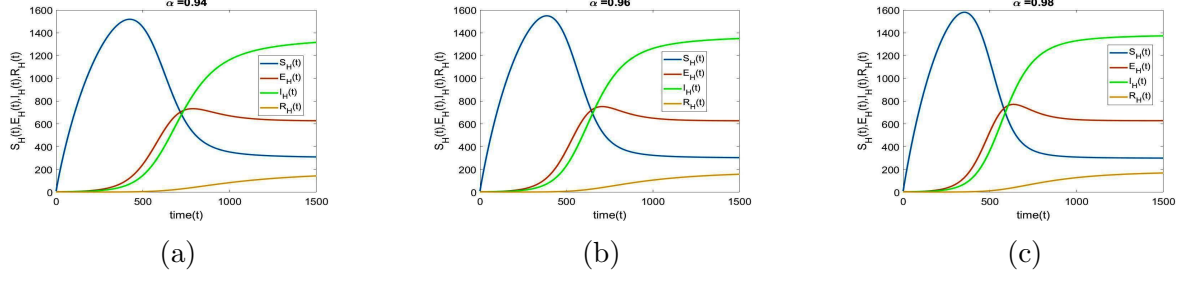


Figure 6.2: Time series of human sub-populations for $\alpha = 0.94, 0.96, 0.98$.

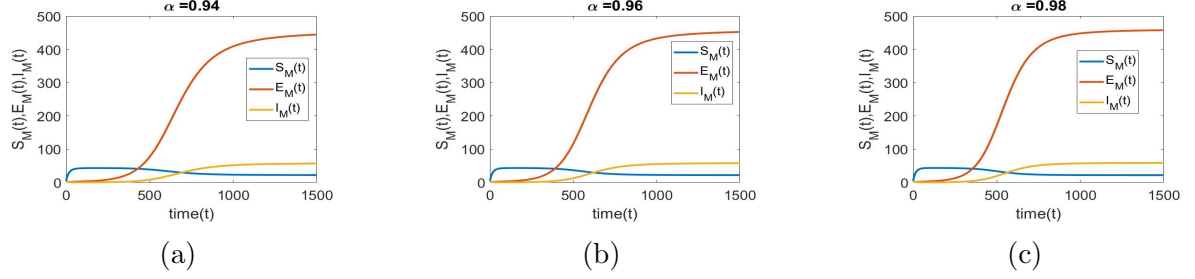


Figure 6.3: Time series solution of mosquitoes sub-populations for $\alpha = 0.94, 0.96, 0.98$.

decline quickly while the infected mosquito population first increases but then gradually declines over time. The high rate of human-to-human transmission of dengue is responsible for both the peaks and troughs of the illness, which are ascribed to both human behaviour and mosquito lifespan. The vertical transmission of the disease by infected *Aedes aegypti* mosquitoes causes a decline in susceptible eggs.

Case 3: Impact of β_H and β_M on I_H for $\alpha = 0.98$

Figure 6.4(a) depicts the impact of β_H on I_H for $\alpha = 0.98$. It is noted that the total number of infected human populations (I_H) rises as the value of β_H increases. The impact of β_M on I_H for $\alpha = 0.98$ is depicted in Figure 6.5(b). It indicates that as β_M rises, so do the populations of infected human people.

Case 4: Impact of control measure to determine the value of R_0

The value of R_0 is calculated using the parameter values in Table 6.2. Simulated Figures 6.5(a) and 6.5(b) show how the control strategies affect the dynamics of dengue illness transmission for $\alpha = 0.98$. Figure 6.5(a) demonstrates that managing the incubation rate of transmission of the disease is crucial if we want to regulate the rate of incubation by showing that γ_H and γ_M have an identical influence on R_0 . From Figure 6.5(b), it is noted that the parameter d_M has more influence on R_0 as compared to d_H .

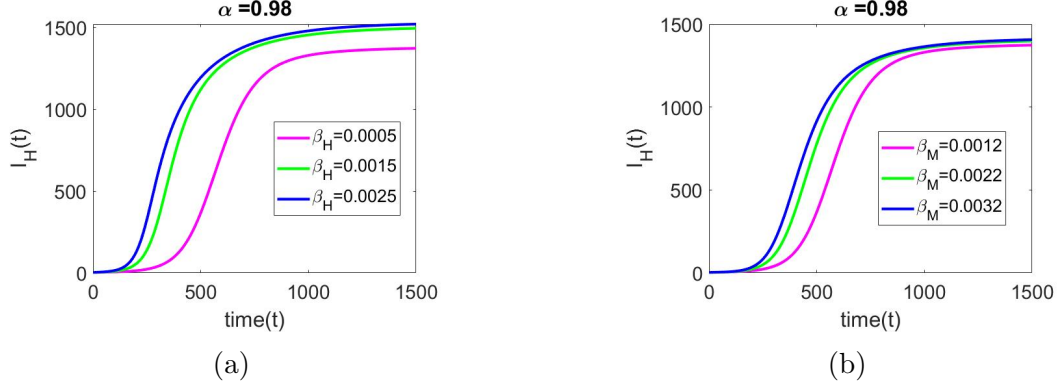


Figure 6.4: Impact of β_H and β_M on I_H for $\alpha = 0.98$.

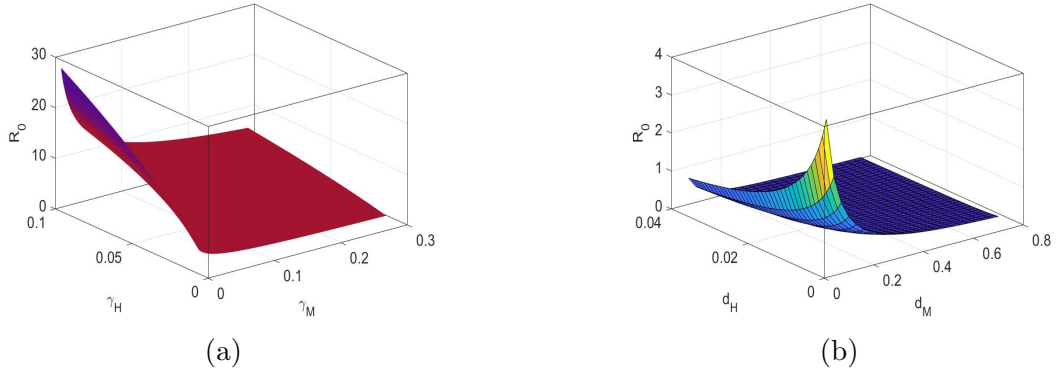


Figure 6.5: (a) Influence of γ_H and γ_M on R_0 . (b) Influence of d_H and d_M on R_0 .

Case 5: Contour plots of R_0 for d_H versus d_M and γ_H versus γ_M with $\alpha = 0.98$

Contour plots of R_0 for d_H versus d_M and γ_H versus γ_M with $\alpha = 0.98$ are shown in Figure 6.6. Figure 6.6(a) shows that when d_H and d_M decline, the value of R_0 decreases. Figure 6.6(b) further shows that when γ_H and γ_M grow in value, the value of R_0 rises.

Case 6: Optimal control

For the study of optimal control, we choose the parameter values $A_1 = 1, A_2 = 10, A_3 = 10, B_1 = 10, B_2 = 10000, B_3 = 1000, B_4 = 100, B_5 = 10, b_H = 0.1, b_M = 0.01, d_H = 0.004, d_M = 0.071, \beta_H = 0.0005, \beta_M = 0.0011, \gamma_H = 0.01, \gamma_M = 0.0092, \eta_H = 0.031, r_H = 0.31, r_M = 0.005$. Figure 6.7 shows the time series solution of all populations with optimal control during time period of $[0, 200]$ days in the system (6.9) taking $\alpha = 0.98$. Figure 6.7 depicts the time series of optimal cost J and the control variables

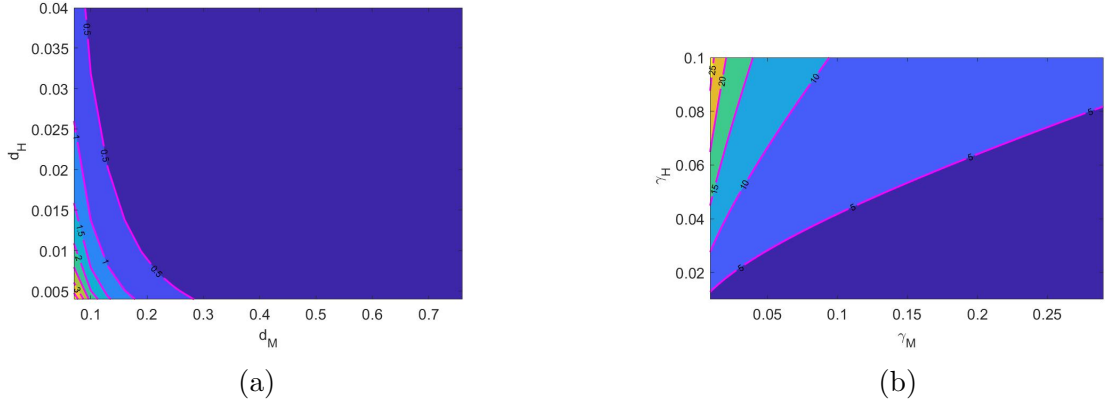


Figure 6.6: (a) Contour plot of R_0 for d_H versus d_M . (b) Contour plot of R_0 for γ_H versus γ_M with $\alpha = 0.98$.

p_1, p_2, p_3 . For optimal control, we selected a final time of $t_f = 200$. To put it in another way, the general public must continue to be very aware of the existence of dengue fever and to take all reasonable precautions to avoid being bitten by mosquitoes and to eliminate them when necessary.

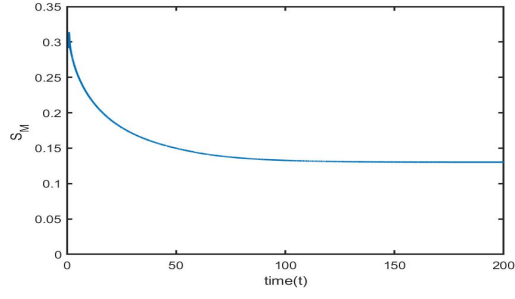
Case 7: Model validation with real data

This section describes model validation of the proposed model (6.1) with real data in Singapore for Infected human population. From 18th week, 2020 to 23rd week, 2020, we contrasted the model results with the actual Singapore reality. The parametric values are given in Table 6.2. Table 6.3 suggests week-by-week infected population estimates from 18th week, 2020 to 23rd week, 2020. Figure 6.9 depicts time series solution of infected human population of the system (6.1) for the parameters values given in Table 6.2 taking $\alpha = 0.7, 0.8, 0.85, 0.9$. It has been noted that our model system matches realistic data with $\alpha = 0.85$.

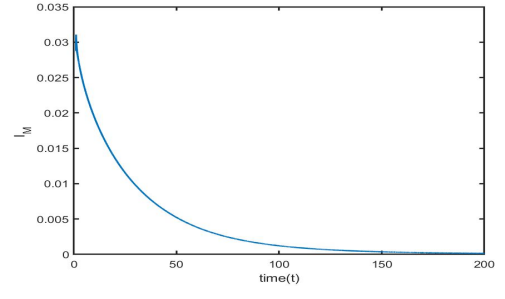
Case 8: Dynamical features of I_H for different values of p_1, p_2 and p_3 with $\alpha = 0.85$.

The parameters values in Table 6.2 are used to examine the effect of p_1, p_2 and p_3 with $\alpha = 0.85$ on I_H . In Figures 6.10(a) to 6.10(c), it is evident that as p_1, p_2 , and p_3 increase, the number of infected human population decreases drastically. Among all control measures, p_1 is seen as more sensitive with respect to p_2 and p_3 on Infected human population (I_H).

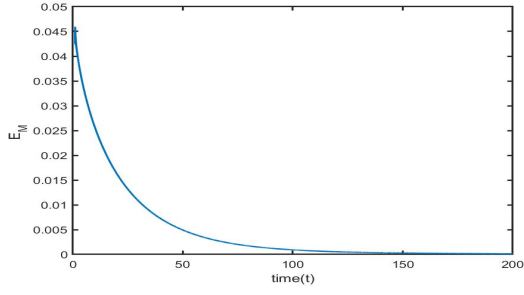
Case 9: Dynamical features of I_M for different values of p_1, p_2 and p_3 with α



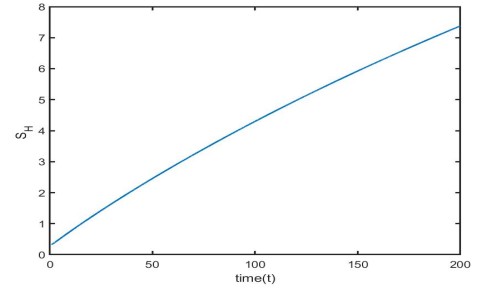
(a)



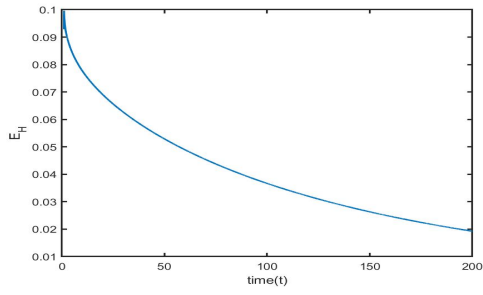
(b)



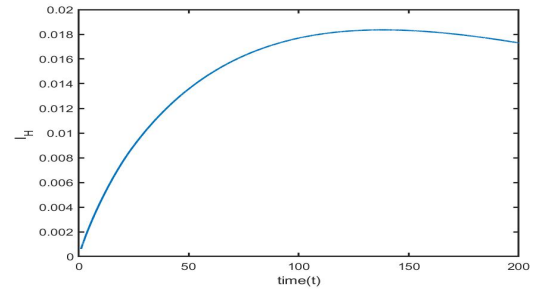
(c)



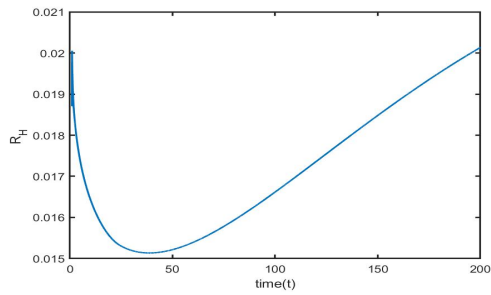
(d)



(e)

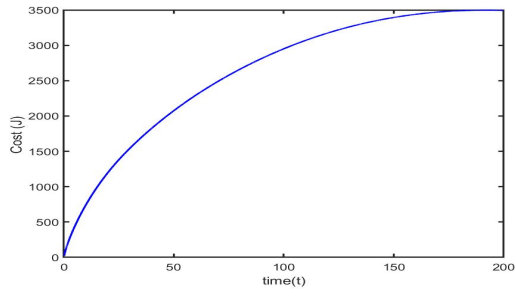


(f)

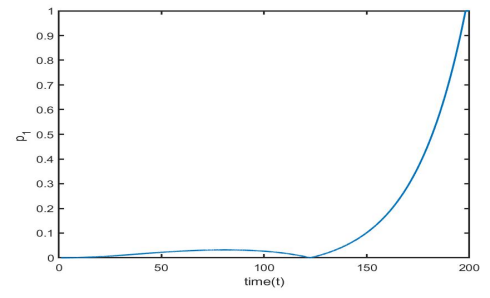


(g)

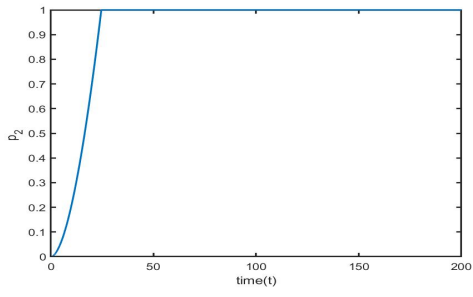
Figure 6.7: Time series solution with optimal control of the model system (6.1) for $\alpha = 0.98$.



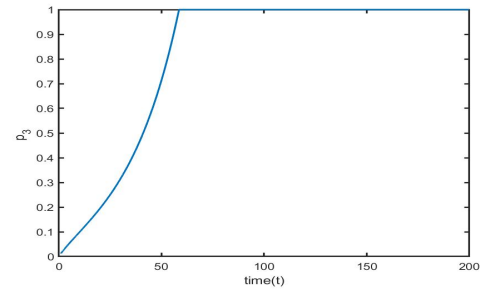
(a)



(b)



(c)



(d)

Figure 6.8: Time series solution of optimal cost J and control variables p_1, p_2, p_3 .

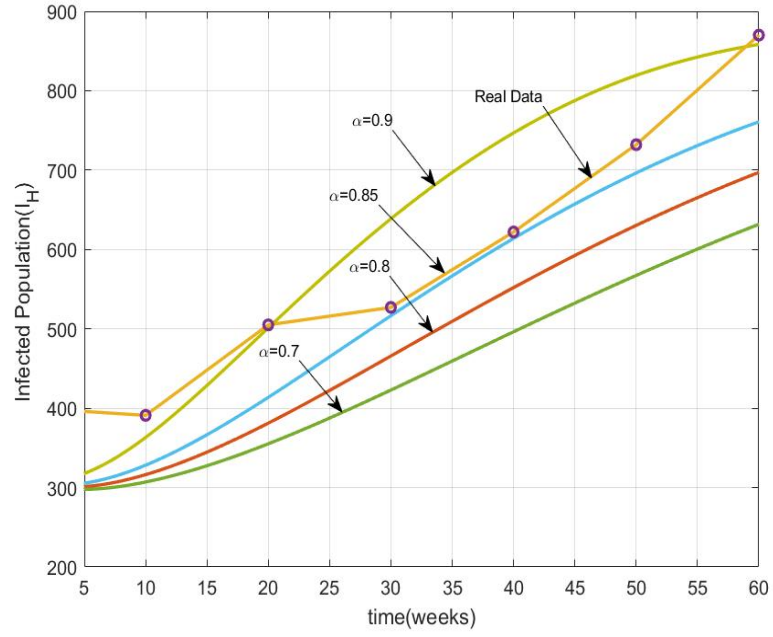
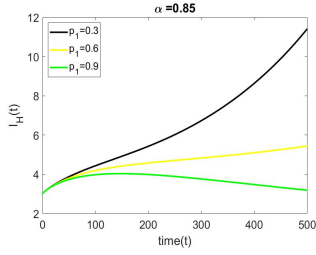
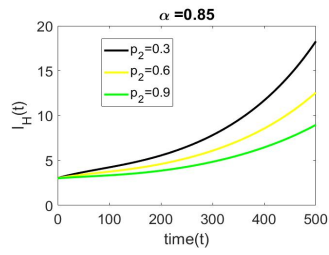


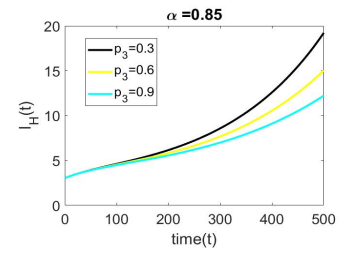
Figure 6.9: Time series solution of I_H of the model (6.1) for $\alpha = 0.7, 0.8, 0.85, 0.9$.



(a)



(b)



(c)

Figure 6.10: Dynamics of I_H for different values of p_1 , p_2 and p_3 with $\alpha = 0.85$.

Week	Infected human population	Reference
18	391	[245]
19	505	[245]
20	527	[245]
21	622	[245]
22	732	[245]
23	870	[245]

Table 6.3: Week wise infected human population of Singapore from 18th week, 2020 to 23rd week, 2020.

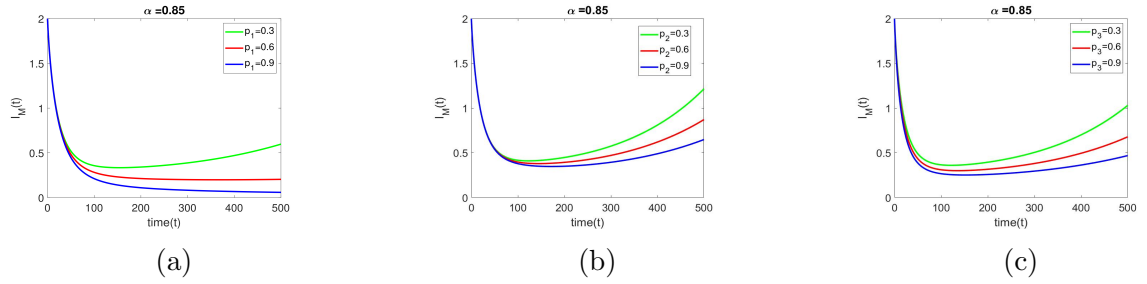


Figure 6.11: Dynamics of I_M for different values of p_1 , p_2 and p_3 with $\alpha = 0.85$.

= 0.85

The parameter values in Table 6.2 are used to examine the effect of p_1 , p_2 and p_3 with $\alpha = 0.85$ on I_M . It is evident from Figures 6.11(a) through 6.11(c) that as p_1 , p_2 and p_3 increase, the number of infected mosquitoes in the population decreases drastically. Among all control measures, p_1 is seen as more sensitive with respect to p_2 and p_3 on Infected mosquito population (I_M).

Case 10: Study of sensitivity

This part explains the sensitivity analysis, which allows us to determine the key parameters in the proposed model. With the help of Table 6.2, the sensitivity indices are visually shown as a bar chart in Figure 6.12 to help identify the dominating parameters whos increase or reduction has a significant impact on the suggested model that is linked to those parameters. The parameters β_M and b_M in the shown bar chart (Figure 6.12) are the most sensitive. The basic reproduction number thus grows together with an increase in the levels of these sensitive factors. Table 6.4 depicts the sensitivity indices of R_0 versus of the proposed model parameters.

Parameters	Sensitivity Index	Values
b_M	$W_{R_0}^{b_M}$	0.5
r_H	$W_{R_0}^{r_H}$	-0.0032
d_H	$W_{R_0}^{d_H}$	-0.22086
β_M	$W_{R_0}^{\beta_M}$	0.5
γ_H	$W_{R_0}^{\gamma_H}$	0.0064
γ_M	$W_{R_0}^{\gamma_M}$	-0.05996
η_H	$W_{R_0}^{\eta_H}$	-0.0032
r_M	$W_{R_0}^{r_M}$	-0.000728
d_M	$W_{R_0}^{d_M}$	-0.48775
p_1	$W_{R_0}^{p_1}$	-0.001
p_2	$W_{R_0}^{p_2}$	-0.0032
p_3	$W_{R_0}^{p_3}$	-0.00073

Table 6.4: Sensitivity indices of R_0 versus model parameters.

6.9 Conclusion

In this chapter, we have analysed the dynamics of dengue transmission in a four compartment host population and a three compartment vector population with two control parameters pertaining to measures taken to prevent mosquito bites and measures of treatment techniques and a three compartment mosquito population with a control parameter characterizing the inhibition of breeding of mosquitoes. The case study of Singapore is used to validate the findings and it is observed in Figure 6.9 that the model system fits the realistic data for Caputo order $\alpha = 0.85$. Thus, we may be convinced that the fractional order Caputo derivatives are more effective in studying epidemic models with real time data than integral order derivatives. As is apparent from Theorem 6.3.1 and 6.3.2, the system possesses a one solution which are positive and bounded. The dengue fever free equilibrium point (E_0) and the dengue fever endemic equilibrium point (E_1) are given by the equation (6.3). The basic reproduction number R_0 given in equation (6.4) is obtained by next generation matrix method. The value of the model parameters given in Table 6.2 are used to determine the numerical value of R_0 . Figures 6.4(a) and 6.4(b) show that the impact of incubation rate in human population γ_H and incubation rate of mosquito population γ_M on the reproduction number is almost the same whereas the impact of death rate of mosquito population d_M is more than the death rate of human population d_H on R_0 . The objective of our work has been to construct the objective function $J(p_1, p_2, p_3)$

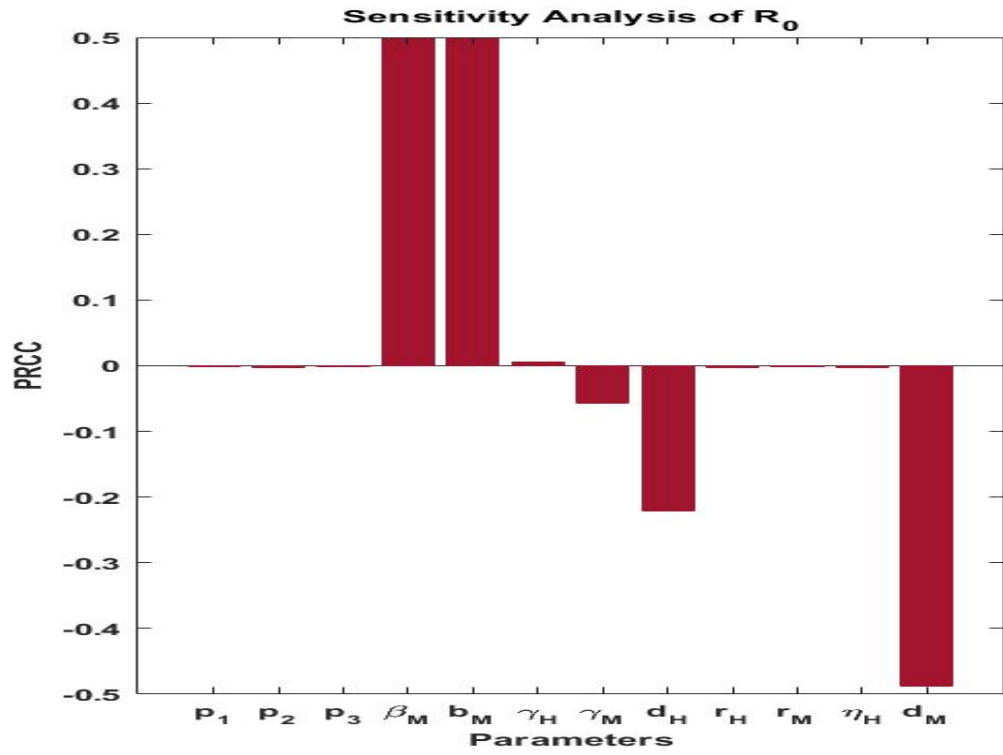


Figure 6.12: Plot of Sensitivity indices of R_0 versus each model parameters.

given in (6.8) to minimise the cost of implementation of the control parameters. The decreasing nature of the objective function for optimal control parameters p_1^*, p_2^*, p_3^* is apparent from the time series plot given in Figure 6.7(a). It is also evident from Figures 6.9 and 6.10 that both the number of infected human population and number of mosquito population decreases significantly for increasing values of p_1, p_2 and p_3 wherein p_1 is more sensitive. Hence, as the use of mosquito repellents and other personal prophylactic measures along with treatment efforts for infected individuals increases there is a considerable decrease in the number of infected human population. This is also the case with the use of certain biological and chemical controls over the detection and elimination of vector breeding sources. With an increase in the environmental management programs and source reduction methods there is a decrease in the infected vector population which in turn causes a decrease in the infected human population.

Chapter 7

Dynamical behavior of a fractional order SIR model with stability analysis

“To isolate mathematics from the practical demands of the sciences is to invite the sterility of a cow shut away from the bulls.”

- Chebyshev

This chapter is based on the paper
Dynamical behavior of a fractional order SIR model with stability analysis,
Results in Control and Optimization, 10, 100212, 2023.

7.1 Introduction

Epidemiology is the study of the prevalence and risk factors for contamination in the human population. It is also frequently referred to as the organism biology of public health. Mathematical models of infectious diseases enable the comprehension of infectious disease transmission and dissemination, the detection of variables influencing transmission in order to pinpoint efficient control techniques, and the evaluation of regard to the goal and intervention strategies. Kermack and McKendrick [5, 246] described deterministic systems for infectious illnesses. Several researchers have explored different types of epidemic systems by examining different models like SI [247], SIS [57], SIR [248 -250], SIRS [31], SEIR [123, 252, 257], SIQR [90], SEIRV [99, 100], and others to better understand the process of disease transmission. Infectious disease management has been harder during the last few decades. Because of its safety and expense, vaccination is one of the most essential health interventions for preventing disease of infectious illnesses. Indeed, A number of vaccine-preventable infectious diseases, including smallpox, have been drastically reduced or even eradicated as a consequence of high vaccination, according to [253].

In the modeling of infectious illnesses, the incidence rate is crucial in determining the behavior of phenomena. Kermack and Mckendrick [5] proposed the transmission rate as βSI in 1927. Capasso et al. [23] proposed a nonlinear occurrence $g(I)S$ for $g'(I) < 0$ that permits for particular “behavioral” effects. With behavioral modifications, Capasso and Serio inspired their approach. The potential damage of infection may become extraordinarily high during times of high occurrence, leading to major behavioral modifications that minimize the actual risk of illness [24]. Goel and Nilam [25], Wei and Chen [26], Capasso et al. [27,28], Zhang et al. [29], Anderson and May [30], including Kumar and Nilam, only a few writers have drawn attention towards the significance of taking nonlinear incidence rates into account while studying the relationship between infectious transmission and illness [33]. Li et al. [34] presented a SIR model with $f(S, I) = \frac{\beta SI}{1+\gamma I}$.

Li et al. [254] investigated non symmetric response of the complex dynamics of Kopel model with between oligopolists. For more publication on this theme, one can see [255 - 258]. It is well known that treatment rates are crucial in avoiding and limiting the spread of illnesses. We are aware that the therapy resources in any community are insufficient. As a result, selecting a successful treatment rate is critical for limiting disease transmission. In the lack of efficient treatment options and vaccinations, epidemic prevention methods focus on efficient preventative measures [259 - 261]. In recent years, many findings involving the study of various issues employing Atangana-Baleanue-Caputo operators, generalised proportional fractional integral operators, have been established. Some recent work can indeed be viewed as [236, 262 - 264]. Wang and Ruan [265] proposed the

following SIR transmission dynamics with a fixed treatment rate:

$$h(I) = \begin{cases} n & \text{for } I > 0, \\ 0 & \text{for } I = 0. \end{cases}$$

Zhang and Liu [266], who also provided a superior treatment rate (Holling type II) as a continuously differentiable function that populates at the largest benefit, as shown below: $h(I) = \frac{mI}{1+nI}$ for $I \geq 0, m > 0, n > 0$,

where m is the cure rate and n is the rate of limitation in the availability of treatment. Zhang et al. [267], Zhou et al. [268] and Dubey et al. [251] have investigated this nonlinear saturation treatment rate in a somewhat different manner. Seidu et al. [269] focused on the thorough cost-effectiveness analysis of Holling's Type II predation form and standard incidence for controlling maize streak virus disease.

Till now a lot of works on fractional order models have been published [270 - 274]. Das et al. [275] considered a Fractional Ordered COVID-19 Model Incorporating Comorbidity and Vaccination. Veisi et al. [276] had explore the novel fractional-order feedback management of COVID-19 prevalence.

7.1.1 Motivation and research background

Fractional order modelling is a powerful method that has been used to study the nature of sickness since it is an extend of the integer-order derivation. Additionally, the fractional order derivation has a global dimension as opposed to the local identity shared by the integer order derivation. The Caputo derivative, as opposed to the Riemann Liouville fractional derivative, permits the use of conventional beginning and steady state in the derivation and has the advantage that the derivative of a constant is 0. Motivated by the current research, the fractional order SIR compartmental model with a Holling type II and saturated treatment rate are explored in this chapter with three different categories in the Caputo approach. A few findings for the new models existence and uniqueness criterion, as well as positivity of the solution, have been established. We have discussed the stability analysis of our proposed model at E_0 as well as E_* . Additionally, the system solution is approximated using the fractional order Taylor's technique. We have studied graphical significance and numerical simulations via MATLAB software.

7.1.2 Structure of the chapter as follows

In Section 7.2, we have established the SIR epidemic model in Caputo sense. We have investigated the existence, uniqueness, non-negativity, boundedness criterion and stability analysis of the solution of model in Section 7.3. We have studied forward bifurcation

theoretically at E_0 of our proposed model in Section 7.4. In Section 7.5, the fractional-order Taylor's approach in Caputo derivative is utilized to approximate the solution to the proposed model. Verification of results numerically of the system in Section 7.6 via MATLAB. Finally the Section 7.7 covers conclusion of the work.

7.2 Model formulation

In this part, we have proposed a mathematical model with an assumption that the whole population size $N(t)$, which is categorised into three classes: susceptible $S(t)$, infected $I(t)$, and recovered $R(t)$. Therefore, we have

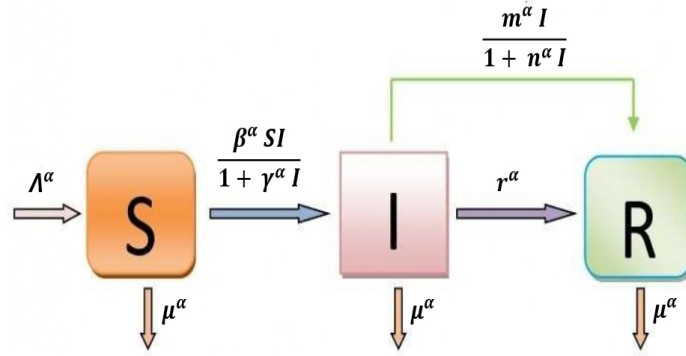


Figure 7.1: The proposed SIR model's flow diagram.

$$\begin{aligned}
 {}^C_{t_0}D_t^\alpha S(t) &= \Lambda^\alpha - \mu^\alpha S(t) - \frac{\beta^\alpha S(t)I(t)}{1 + \gamma^\alpha I(t)}, S(t)|_{t=0} = S(0) > 0, \\
 {}^C_{t_0}D_t^\alpha I(t) &= \frac{\beta^\alpha S(t)I(t)}{1 + \gamma^\alpha I(t)} - \frac{m^\alpha I(t)}{1 + n^\alpha I(t)} - (\mu^\alpha + \delta^\alpha + r^\alpha)I(t), I(t)|_{t=0} = I(0) > 0, \\
 {}^C_{t_0}D_t^\alpha R(t) &= \frac{m^\alpha I(t)}{1 + n^\alpha I(t)} + \delta^\alpha I(t) - \mu^\alpha R(t), R(t)|_{t=0} = R(0) > 0,
 \end{aligned} \tag{7.1}$$

where $0 < \alpha \leq 1$, and ${}^C_{t_0}D_t^\alpha$ denotes the Caputo operator [148, 149, 232, 278]. The term $\frac{\beta^\alpha S(t)I(t)}{1 + \gamma^\alpha I(t)}$ represents Holling type II saturated incidence rate. Also the term $h(I) = \frac{m^\alpha I}{1 + n^\alpha I}$ defines the Holling type II treatment rate.

Λ	recruitment rate
μ	death rate
β	transmission rate
γ	inhabitory rate
m	cure rate
n	rate of limitation in the availability of treatment
δ	recovery rate
r	disease induced mortality rate

Table 7.1: Significance of the relevant parameters.

7.3 Analysis of the system

7.3.1 Positivity and boundedness

Theorem 7.3.1. *All solutions of the model (7.1) initiating from $(S(t_0), I(t_0), R(t_0))$ are non-negative.*

Proof. Suppose, $Y(t_0) = (S(t_0), I(t_0), R(t_0)) \in \Gamma^+ = \{(S, I, R) \in \Gamma^+ : S, I, R \in \mathbb{R}^+\}$ as the initial point of solution of the model (3.1). Firstly, let us consider that there exists a constant τ , $t_0 \leq t < \tau$ such that

$$\begin{cases} S(t) > 0, \text{ for } t_0 \leq t < \tau, \\ S(\tau) = 0, \\ S(\tau^+) < 0. \end{cases}$$

With the help of system (7.1), we have

$${}^C D_t^\alpha S(t)|_{S(\tau)=0} = 0.$$

We have $S(\tau^+) = 0$ with the help of [277], contradicts our assumption that $S(\tau^+) < 0$. Therefore, we get $S(t) \geq 0, \forall t \in [t_0, \infty)$. Similarly, we have $I(t) \geq 0$ and $R(t) \geq 0, \forall t \in [t_0, \infty)$.

Theorem 7.3.2. *All solutions of system (7.1) are bounded.*

Proof. Now $N(t) = S(t) + I(t) + R(t)$, then

$$\begin{aligned} {}^C D_t^\alpha N(t) &= {}^C D_t^\alpha S(t) + {}^C D_t^\alpha I(t) + {}^C D_t^\alpha R(t) \\ &= \Lambda^\alpha - \mu^\alpha N(t) \end{aligned}$$

Therefore,

$${}^C D_t^\alpha N(t) + \mu^\alpha N(t) \leq \Lambda^\alpha.$$

Applying Laplace transform on both sides of the above equation and using Lemma 1.4.1, we have

$$\begin{aligned}
z^\alpha F(z) - z^{\alpha-1}N(0) + \mu^\alpha F(z) &\leq \frac{\Lambda^\alpha}{z}, \text{ where } F(z) = L\{N(t)\} \\
\Rightarrow F(z)(z^{\alpha+1} + z\mu^\alpha) &\leq z^\alpha N(0) + \Lambda^\alpha \\
\Rightarrow F(z) &\leq \frac{z^\alpha N(0) + \Lambda^\alpha}{z^{\alpha+1} + z\mu^\alpha} \\
&= \frac{z^\alpha N(0)}{z^{\alpha+1} + z\mu^\alpha} + \frac{\Lambda^\alpha}{z^{\alpha+1} + z\mu^\alpha}.
\end{aligned}$$

Using inverse Laplace transform on both sides of the above equation,

$$N(t) \leq N(0)L^{-1}\left\{\frac{z^\alpha}{z^{\alpha+1} + z\mu^\alpha}\right\} + \Lambda^\alpha L^{-1}\left\{\frac{1}{z^{\alpha+1} + z\mu^\alpha}\right\}.$$

Applying Lemma 1.4.2 on the above equation, we acquire

$$N(t) \leq N(0)E_{\alpha,1}(-\mu^\alpha t^\alpha) + \Lambda^\alpha t^\alpha E_{\alpha,\alpha+1}(-\mu^\alpha t^\alpha).$$

From the properties of Mittag Leffler function [277], we get

$$E_{c,d}(x) = xE_{c,c+d}(x) + \frac{1}{\Gamma(d)}.$$

Hence,

$$N(t) \leq (N(0) - \frac{\Lambda^\alpha}{\mu^\alpha})E_{\alpha,1}(-\mu^\alpha t^\alpha) + \frac{\Lambda^\alpha}{\mu^\alpha}.$$

As a result, the system solutions are bounded.

7.3.2 Existence and uniqueness

Theorem 7.3.3. The system (7.1) initiating from $(S(t_0), I(t_0), R(t_0)) \in \Gamma^+$ always possess a unique solution in the region Γ^+ , $t \geq t_0$.

Proof. Let us consider the region $\Gamma^+ \times [t_0, \tau]$, where $\Gamma^+ = \{(S, I, R) \in \mathbb{R}^3 : \max(|S|, |I|, |R|) \leq M\}$ and τ is finite. We denote $Y(t) = (S(t), I(t), R(t))$ and $\bar{Y}(t) = (\bar{S}(t), \bar{I}(t), \bar{R}(t))$. Henceforth we denote $Y(t) = Y$ and $\bar{Y}(t) = \bar{Y}$. Consider $F(Y) = (F_1(Y), F_2(Y), F_3(Y))$, where

$$\begin{aligned}
F_1(Y) &= \Lambda^\alpha - \mu^\alpha S(t) - \frac{\beta^\alpha S(t)I(t)}{1 + \gamma^\alpha I(t)}, \\
F_2(Y) &= \frac{\beta^\alpha S(t)I(t)}{1 + \gamma^\alpha I(t)} - \frac{m^\alpha I(t)}{1 + n^\alpha I(t)} - (\mu^\alpha + \delta^\alpha + r^\alpha)I(t), \\
F_3(Y) &= \frac{m^\alpha I(t)}{1 + n^\alpha I(t)} + \delta^\alpha I(t) - \mu^\alpha R(t).
\end{aligned}$$

For any $Y, \bar{Y} \in \Omega$:

$$\begin{aligned}
& \|F(Y) - F(\bar{Y})\| \\
&= |F_1(Y) - F_1(\bar{Y})| + |F_2(Y) - F_2(\bar{Y})| + |F_3(Y) - F_3(\bar{Y})| \\
&= \left| \Lambda^\alpha - \mu^\alpha S(t) - \frac{\beta^\alpha S(t)I(t)}{1 + \gamma^\alpha I(t)} - (\Lambda^\alpha - \mu^\alpha \bar{S}(t) - \frac{\beta^\alpha \bar{S}(t)\bar{I}(t)}{1 + \gamma^\alpha \bar{I}(t)}) \right| + \\
&\quad \left| \frac{\beta^\alpha S(t)I(t)}{1 + \gamma^\alpha I(t)} - \frac{m^\alpha I(t)}{1 + n^\alpha I(t)} - (\mu^\alpha + \delta^\alpha + r^\alpha)I(t) - (\frac{\beta^\alpha \bar{S}(t)\bar{I}(t)}{1 + \gamma^\alpha \bar{I}(t)} - \frac{m^\alpha \bar{I}(t)}{1 + n^\alpha \bar{I}(t)} - (\mu^\alpha + \delta^\alpha + r^\alpha)\bar{I}(t)) \right| \\
&\quad \left| \frac{m^\alpha I(t)}{1 + n^\alpha I(t)} + \delta^\alpha I(t) - \mu^\alpha R(t) - (\frac{m^\alpha \bar{I}(t)}{1 + n^\alpha \bar{I}(t)} + \delta^\alpha \bar{I}(t) - \mu^\alpha \bar{R}(t)) \right| \\
&\leq \mu^\alpha |(S(t) - \bar{S}(t))| + 2\beta^\alpha \left| \left(\frac{S(t)I(t)}{1 + \gamma^\alpha I(t)} - \frac{\bar{S}(t)\bar{I}(t)}{1 + \gamma^\alpha \bar{I}(t)} \right) \right| + 2m^\alpha \left| \frac{I(t)}{1 + n^\alpha I(t)} - \frac{\bar{I}(t)}{1 + n^\alpha \bar{I}(t)} \right| + \\
&\quad (\mu^\alpha + 2\delta^\alpha + r^\alpha) |(I(t) - \bar{I}(t))| + \mu^\alpha |(R(t) - \bar{R}(t))| \\
&\leq (\mu^\alpha + 2\beta^\alpha M) |(S(t) - \bar{S}(t))| + (\mu^\alpha + 2\delta^\alpha + r^\alpha + 2m^\alpha M) |(I(t) - \bar{I}(t))| + \mu^\alpha |(R(t) - \bar{R}(t))| \\
&\leq G_1 |S(t) - \bar{S}(t)| + G_2 |I(t) - \bar{I}(t)| + G_3 |R(t) - \bar{R}(t)| \\
&\leq G \|Y - \bar{Y}\|, \text{ where } G = \max\{G_1, G_2, G_3\},
\end{aligned}$$

$G_1 = (\mu^\alpha + 2\beta^\alpha M)$, $G_2 = (\mu^\alpha + 2\delta^\alpha + r^\alpha + 2m^\alpha M)$ and $G_3 = \mu^\alpha$.

Thus, $F(Y)$ satisfies Lipschitz's criteria [37]. So $Y(t)$ is a unique solution of the model (7.1).

The first two equation of the system (7.1) are free from the effect of $R(t)$. Without loss of generality, it is sufficient to consider first two equations of the system (7.1) for the analysis purpose:

$$\begin{aligned}
{}^C_{t_0} D_t^\alpha S(t) &= \Lambda^\alpha - \mu^\alpha S(t) - \frac{\beta^\alpha S(t)I(t)}{1 + \gamma^\alpha I(t)}, S(t)|_{t=0} = S(0) > 0, \\
{}^C_{t_0} D_t^\alpha I(t) &= \frac{\beta^\alpha S(t)I(t)}{1 + \gamma^\alpha I(t)} - \frac{m^\alpha I(t)}{1 + n^\alpha I(t)} - (\mu^\alpha + \delta^\alpha + r^\alpha)I(t), I(t)|_{t=0} = I(0) > 0.
\end{aligned} \tag{7.2}$$

7.3.3 Equilibria of system (7.2)

Let ${}^C D_t^\alpha S(t) = 0$ and ${}^C D_t^\alpha I(t) = 0$, then the model (7.2) has two equilibrium points namely,

1. The infection free equilibrium $E_0(\frac{\Lambda^\alpha}{\mu^\alpha}, 0)$.
2. The endemic equilibrium $E_*(S^*, I^*)$ where
 $S^* = \frac{\Lambda^\alpha + I^*(\Lambda^\alpha n^\alpha - m^\alpha - \mu^\alpha - \delta^\alpha - r^\alpha) - n^\alpha(\mu^\alpha + \delta^\alpha + r^\alpha)I^{*2}}{\mu^\alpha(1 + n^\alpha I^*)}$ and $XI^{*2} + YI^* + Z = 0$ where
 $X = n^\alpha(\mu^\alpha \gamma^\alpha + \beta^\alpha)(\mu^\alpha + \delta^\alpha + r^\alpha)$,
 $Y = n^\alpha \mu^\alpha(\mu^\alpha \gamma^\alpha + \beta^\alpha) + (\mu^\alpha + \delta^\alpha + r^\alpha)(\Lambda^\alpha n^\alpha - \mu^\alpha - m^\alpha - \delta^\alpha - r^\alpha) - \Lambda^\alpha \mu^\alpha n^\alpha \gamma^\alpha$
and $Z = (\Lambda^\alpha \beta^\alpha - \mu^\alpha - m^\alpha - \delta^\alpha - r^\alpha)$.

7.3.4 The basic reproduction number of the system

The next-generation matrix technique [279] is used to calculate the model's basic reproduction number R_0 , which may be obtained from the maximum eigenvalue of the matrix FV^{-1} where,

$$F = \begin{bmatrix} \frac{\beta^\alpha \Lambda^\alpha}{\mu^\alpha} & 0 \\ 0 & 0 \end{bmatrix} \text{ and } V = \begin{bmatrix} m^\alpha + \mu^\alpha + \delta^\alpha + r^\alpha & 0 \\ \frac{\beta^\alpha \Lambda^\alpha}{\mu^\alpha} & \mu^\alpha \end{bmatrix}.$$

Now, $FV^{-1} = \begin{bmatrix} \frac{\beta^\alpha \Lambda^\alpha}{\mu^\alpha(m^\alpha + \mu^\alpha + \delta^\alpha + r^\alpha)} & 0 \\ 0 & 0 \end{bmatrix}$. The eigenvalues of the matrix FV^{-1} are 0 and $\frac{\beta^\alpha \Lambda^\alpha}{\mu^\alpha(m^\alpha + \mu^\alpha + \delta^\alpha + r^\alpha)}$.

Therefore, $R_0 = \frac{\beta^\alpha \Lambda^\alpha}{\mu^\alpha(m^\alpha + \mu^\alpha + \delta^\alpha + r^\alpha)}$.

7.3.5 Dynamic behavior

At the equilibrium positions calculated below, the Jacobian matrix must be determined to signify the stability locally of the model system.

$$J(S, I) = \begin{bmatrix} A & B \\ C & D \end{bmatrix} \text{ where}$$

$$A = -\mu^\alpha - \frac{\beta^\alpha I}{1 + \gamma^\alpha I},$$

$$B = -\frac{\beta^\alpha S}{(1 + \gamma^\alpha I)^2},$$

$$C = \frac{\beta^\alpha I}{(1 + \gamma^\alpha I)^2},$$

$$D = -\frac{m^\alpha S}{(1 + n^\alpha I)^2} - (\mu^\alpha + \delta^\alpha + r^\alpha).$$

7.3.6 Local stability

At E_0 , we have

$$J\left(\frac{\Lambda^\alpha}{\mu^\alpha}, 0\right) = \begin{bmatrix} -\mu^\alpha & -\frac{\beta^\alpha \Lambda^\alpha}{\mu^\alpha} \\ 0 & -(m^\alpha + \mu^\alpha + \delta^\alpha + r^\alpha) \end{bmatrix}.$$

The eigenvalues of the system are $\lambda_1 = -\mu^\alpha, \lambda_2 = -(m^\alpha + \mu^\alpha + \delta^\alpha + r^\alpha)$. It follows that $|\arg(\lambda_i)| = \pi > \frac{\alpha\pi}{2}$ ($i = 1, 2$) where $0 < \alpha < 1$. Using Lemma 1.4.6, the point E_0 is locally asymptotically stable (LAS).

Now, at $E_*(S^*, I^*)$, we have

$$J(S^*, I^*) = \begin{bmatrix} E & F \\ G & H \end{bmatrix}$$

where

$$\begin{aligned} E &= -\mu^\alpha - \frac{\beta^\alpha I^*}{1 + \gamma^\alpha I^*}, \\ F &= -\frac{\beta^\alpha S^*}{(1 + \gamma^\alpha I^*)^2}, \\ G &= \frac{\beta^\alpha I^*}{(1 + \gamma^\alpha I^*)}, \\ H &= \frac{\beta^\alpha S^*}{(1 + \gamma^\alpha I^*)^2} - \frac{m^\alpha}{(1 + n^\alpha I^*)^2} - (\mu^\alpha + \delta^\alpha + r^\alpha). \end{aligned}$$

The characteristic equation is $\lambda^2 + (E + H)\lambda + (EH - FG) = 0$. We have $-(E + H) < 0$ and the roots are

$$\lambda_{1,2} = \frac{-(E + H)}{2} \pm \frac{\sqrt{(E + H)^2 - 4(EH - FG)}}{2}.$$

If $EH > FG$ then $|\arg(\lambda_{1,2})| = \pi > \frac{\alpha\pi}{2}$; $0 < \alpha < 1$. Since $(E + H)^2 - 4(EH - FG) = (E - H)^2 + 4FG$. Using Lemma 1.4.6, the point E_* is LAS in SI plane.

7.3.7 Global stability

Theorem 7.3.4. *The infection free equilibrium point E_0 of system (7.2) is globally asymptotically stable.*

Proof. Using the appropriate function $L = (S - S_0 - \int_{S_0}^S \lim_{t \rightarrow 0^+} \frac{G(S_0, I)}{G(g, I)} dg) + I$.

$$\begin{aligned} \text{Then } {}^C_{t_0} D_t^\alpha L &= (1 - \frac{S}{S_0}) {}^C_{t_0} D_t^\alpha S + {}^C_{t_0} D_t^\alpha I \\ &= -\frac{\mu^\alpha (S - S_0)^2}{S} + \frac{\beta^\alpha S_0 I}{1 + \gamma^\alpha I} - \frac{m^\alpha I}{1 + n^\alpha I} - (\mu^\alpha + \delta^\alpha + r^\alpha) I \end{aligned}$$

$$= -\frac{\mu^\alpha(S - \frac{\Lambda^\alpha}{\mu^\alpha})^2}{S} + \frac{(\mu^\alpha + \delta^\alpha + r^\alpha + m^\alpha)(R_0 - 1)I}{1 + \gamma^\alpha I} - \frac{[m^\alpha n^\alpha - \gamma^\alpha(\mu^\alpha + \delta^\alpha + r^\alpha + m^\alpha) - n^\alpha \gamma^\alpha(\mu^\alpha + \delta^\alpha + r^\alpha + m^\alpha)I]I^2}{(1 + \gamma^\alpha I)(1 + n^\alpha I)}.$$

Since all parameters of the system are positive, then ${}^C_{t_0}D_t^\alpha L \leq 0$ if $R_0 \leq 1$ and ${}^C_{t_0}D_t^\alpha L = 0$ if $S = S_0 = \frac{\Lambda^\alpha}{\mu^\alpha}, I = I_0 = 0$.

Thus E_0 is globally asymptotically stable (by LaSalle's Lyapunov's concept).

Theorem 7.3.5. The point $E_1(S^*, I^*)$ of system (7.2) is globally asymptotically stable.

Proof. Let us consider the following hypothesis:

$$H(1) : \frac{m^\alpha I^*}{1 + n^\alpha I^*} + \frac{(1 + I)\beta^\alpha S^* I^*}{1 + I\gamma^\alpha I^*} + \frac{m^\alpha}{1 + n^\alpha I^*} \leq \left[\frac{m^\alpha I}{1 + n^\alpha I} + \frac{\beta^\alpha S^{*2}}{S + S\gamma I^*} + I^* \left(\frac{S\beta^\alpha}{1 + \gamma^\alpha} + \frac{m^\alpha}{1 + n^\alpha I I^*} \right) \right].$$

Since (S^*, I^*) is the endemic equilibrium point of model (7.2), then

$$\Lambda^\alpha - \mu^\alpha S^* = \frac{\beta^\alpha S^* I^*}{1 + \gamma^\alpha I^*}, \frac{\beta^\alpha S^* I^*}{1 + \gamma^\alpha I^*} = \frac{m^\alpha I^*}{1 + n^\alpha I^*} + (\mu^\alpha + \delta^\alpha + r^\alpha)I^*.$$

Let us consider the Goh-Volterra form as

$$W(S, I) = \left(S - S^* - S^* \ln \frac{S}{S^*} \right) + \left(I - I^* - I^* \ln \frac{S}{S^*} \right).$$

Now, along the integral curves of (7.2):

$$\begin{aligned} {}^C_{t_0}D_t^\alpha W(S, I) &\leq \frac{S - S^*}{S} {}^C_{t_0}D_t^\alpha S(t) + \frac{I - I^*}{I} {}^C_{t_0}D_t^\alpha I(t), \text{ (using Lemma 1.4.7)} \\ &= \frac{m^\alpha I^*}{1 + n^\alpha I^*} + \frac{(1 + I)\beta^\alpha S^* I^*}{1 + I\gamma^\alpha I^*} + \frac{m^\alpha}{1 + n^\alpha I^*} \\ &\quad - \left[\frac{m^\alpha I}{1 + n^\alpha I} + \frac{\beta^\alpha S^{*2}}{S + S\gamma I^*} + I^* \left(\frac{S\beta^\alpha}{1 + \gamma^\alpha} + \frac{m^\alpha}{1 + n^\alpha I I^*} \right) \right]. \end{aligned}$$

Hence, by $H(1)$, we have

$${}^C_{t_0}D_t^\alpha W(S, I) \leq 0, \forall (S, I) \in \Omega$$

and ${}^C_{t_0}D_t^\alpha W(S, I) = 0$ if $(S, I) = (S^*, I^*)$. So, the point $E_1(S^*, I^*)$ is asymptotically stable globally.

7.4 Forward bifurcation

For $R_0 = 1$. first we assume that $S = u_1$ and $I = u_2$. Then the system (7.2) can be written as

$$\begin{aligned} {}^C D_t^\alpha u_1 &= \Lambda^\alpha - \mu^\alpha u_1 - \frac{\beta^\alpha u_1 u_2}{1 + \gamma^\alpha u_2} \equiv g_1, \\ {}^C D_t^\alpha u_2 &= \frac{\beta^\alpha u_1 u_2}{1 + \gamma^\alpha u_2} - \frac{m^\alpha u_2}{1 + n^\alpha u_2} - (\mu^\alpha + \delta^\alpha + r^\alpha) u_2 \equiv g_2, \end{aligned}$$

Now, the linearized matrix at E_0 and at the bifurcation parameter $\beta^\alpha = \beta_*^\alpha = \frac{\mu^\alpha(m^\alpha + \mu^\alpha + \delta^\alpha + r^\alpha)}{\Lambda^\alpha}$ of the above system is given by

$$J = \begin{bmatrix} -\mu^\alpha & -\frac{\Lambda^\alpha \beta_*^\alpha}{\mu^\alpha} \\ 0 & 0 \end{bmatrix}.$$

At $R_0 = 1$, J has a zero eigen value and another eigen value of J has a negative real part. So, the above system's behaviour cannot be predicted using the linearization method. As a result, we use central manifold theorem [280] to study the system's behaviour at the infection-free equilibrium point. The bifurcation constants

$$c_1 = \sum_{i,j,k=1}^2 \left(\frac{\partial^2 g_k}{\partial u_i \partial u_j} \right)_{E_0} \text{ and}$$

$$c_2 = \sum_{i,j,k=1}^2 \left(\frac{\partial^2 g_k}{\partial u_i (\partial \beta^\alpha)_*} \right)_{E_0}$$

where $x = (x_1, x_2)$ and $y = (y_1, y_2)^t$ are left and right eigenvectors of J corresponding to a zero eigen value respectively. So, we get $x_1 = 0, x_2 = 1$ and $y_1 = -\frac{\beta_*^\alpha \Lambda^\alpha}{(\mu^\alpha)^2}, y_2 = 1$.

The non zero partial derivatives of the function (g'_i) for $i = 1, 2$ of the above system at $R_0 = 1$ and $\beta^\alpha = \beta_*^\alpha$ are $(\frac{\partial^2 g_2}{\partial u_1 \partial u_2})_{E_0} = \beta_*^\alpha, (\frac{\partial^2 g_2}{\partial u_2 \partial u_1})_{E_0} = \beta_*^\alpha$ and $(\frac{\partial^2 g_2}{\partial u_2 \partial \beta_*^\alpha})_{E_0} = \frac{\Lambda^\alpha}{\mu^\alpha}$.

Therefore $c_1 = x_2(2y_1 y_2 \beta_*^\alpha) = -2 \frac{(\beta_*^\alpha)^2 \Lambda^\alpha}{(\mu^\alpha)^2} < 0$ and $c_2 = x_2 y_2 \frac{\Lambda^\alpha}{\mu^\alpha} = \frac{\Lambda^\alpha}{\mu^\alpha} > 0$.

As a result, the bifurcation is forward.

7.5 Numerical procedure

As discussed in Theorem 7.3.3, the system (7.2) obtains a unique solution. To obtain the solution of the system (7.2), Taylor's theorem will be used. As a result, we proceed with the model's 1st equation as follows:

$${}^C D_t^\alpha S(t) = u_1(t, S, I), S(0) = S_0, t > 0. \quad (7.3)$$

Consider the set of points $[0, A]$ as the points on which we are prepared to approximate the system's solution. Actually, we are unable to calculate $S(t)$, which will be the system's

necessary solution. We divide $[0, A]$, into P subintervals $[t_j, t_{j+1}]$ of length, i.e., $w = \frac{A}{P}$, using the nodes $t_j = jw$, for $j = 0, 1, 2, \dots, P$. We extend the Taylor's theorem at $t = t_0$, we have a constant $k \in [0, A]$, so that $S(t) = S(t_0) + {}^C D_t^\alpha S(t) \{ \frac{w^\alpha}{\Gamma(\alpha+1)} \} + {}^C D_t^{2\alpha} [S(t)]_{t=k} \{ \frac{w^{2\alpha}}{\Gamma(2\alpha+1)} \}$. Now substitute ${}^C D_t^\alpha S(t) = u_1(t_0, S(t_0), I(t_0))$ and $t = t_0$ in the above equation which provides

$$S(t_1) = S(t_0) + u_1(t_0, S(t_0), I(t_0)) \{ \frac{w^\alpha}{\Gamma(\alpha+1)} \} + {}^C D_t^{2\alpha} [S(t)]_{t=k} \{ \frac{w^{2\alpha}}{\Gamma(2\alpha+1)} \}.$$

If m is small, we ignore the higher terms, then

$$S(t_1) = S(t_0) + u_1(t_0, S(t_0), I(t_0)) \{ \frac{w^\alpha}{\Gamma(\alpha+1)} \}.$$

A general formula of expanding about $t_j = t_j + w$, is

$$S(t_j + 1) = S(t_j) + u_1(t_j, S(t_j), I(t_j)) \{ \frac{w^\alpha}{\Gamma(\alpha+1)} \}.$$

In similar way, we get

$$I(t_j + 1) = I(t_j) + u_1(t_j, S(t_j), I(t_j)) \{ \frac{w^\alpha}{\Gamma(\alpha+1)} \}.$$

7.6 Numerical simulation and discussion

To access and validate the analytical results of our model system (7.2) in this section, we employ detailed numerical simulations. Approximation and numerical approaches have been developed although most fractional order differential equations do not have exact analytic solutions. In the numerical technique, we have used Taylor's theorem via MATLAB software.

Parameters	Values	Reference
Λ	3	Assumed
μ	0.04	Assumed
β	0.004	Assumed
γ	0.0005	Model to fit
m	0.03	Assumed
n	0.006	Assumed
δ	0.02	Model to fit
r	0.003	Assumed

Table 7.2: Parameter values for numerical study.

Case 1: Stability analysis.

In this situation, the stability of our proposed model is explored. Table 7.2 lists the parameters that were employed in this case's numerical simulations. Figures 7.2(a) to 7.2(c) depict the time series solution of infected individuals corresponding to $\alpha = 0.90, 0.94$ and 0.98 . From the following figures, we have observed that the system (7.2) is LAS at E_0 , confirming our theoretical results. Figures 7.3(a) to 7.3(c) depict the stability globally

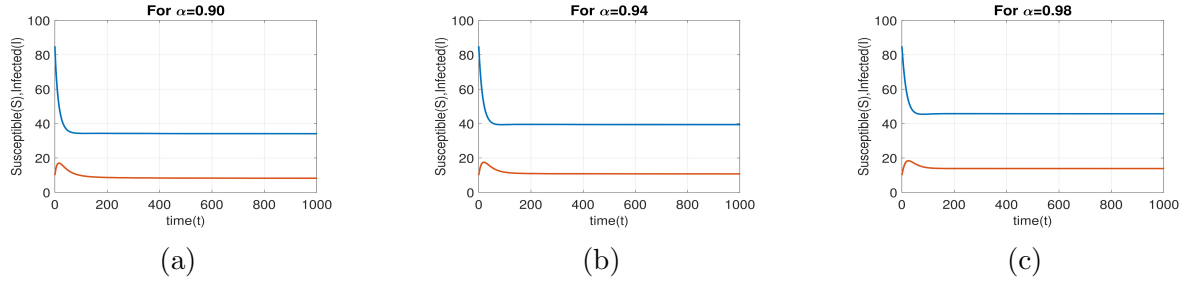


Figure 7.2: Time series solution of all individuals for values of $\alpha = 0.90, 0.94, 0.98$.

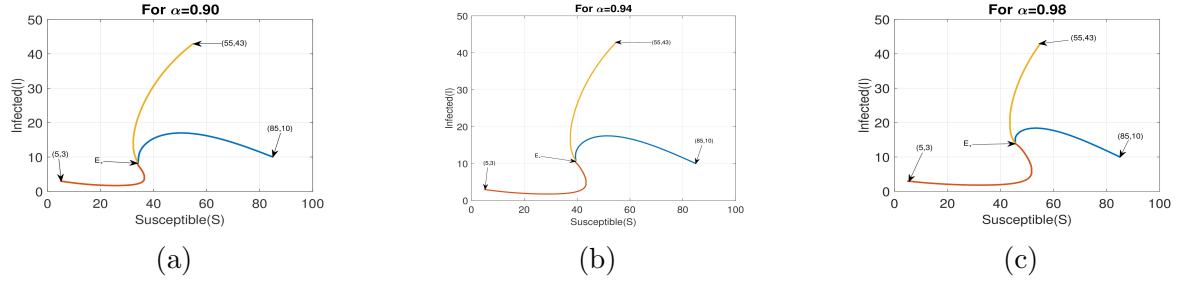


Figure 7.3: Phase portrait diagram for values of $\alpha = 0.90, 0.94, 0.98$.

of the model system (7.2) at E_* with different initial condition taking $\alpha = 0.90, 0.94, 0.98$, confirming our theoretical results.

Case 2: Impact of β on I for $\alpha = 0.95, 0.98$.

The impact of β on infected individuals is depicted in Figures 7.4(a) and 7.4(b). Based on Figure 7.4(a), it may be noted that the individuals of infected increase when β changes from 0.004 to 0.008 for $\alpha = 0.95$. Figure 7.4(b) depicts that the infected individuals decreases initially but after certain time it increases for $\alpha = 0.98$.

Case 3: Nature of I with control and without control for $\alpha = 0.98$.

The infected individuals with and without M-H treatment rates are depicted in Figure 7.5. The figure depicts that when the infected population is treated based on the M-H treatment rate, there are fewer infected people overall, but there are more infected people overall when the M-H cure rate is not taken into account. As a result, the M-H process to improve is crucial in preventing the spread of illness across society.

Case 4: Impact of γ on I for $\alpha = 0.95, 0.98$.

The impact of γ on infected individuals is depicted in Figures 7.6(a) and 7.6(b). Based on the Figure 7.6(a), it may be noted that the infected individuals increases when γ changes from 0.0075 to 0.0035 for $\alpha = 0.95$. Figure 7.6(b) depicts that the infected individuals

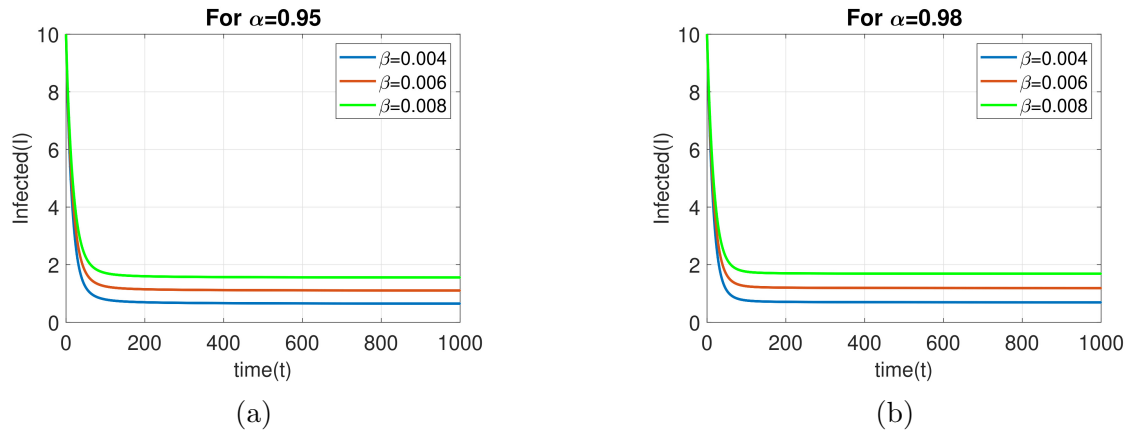


Figure 7.4: Impact of β on I for $\alpha = 0.95, 0.98$.

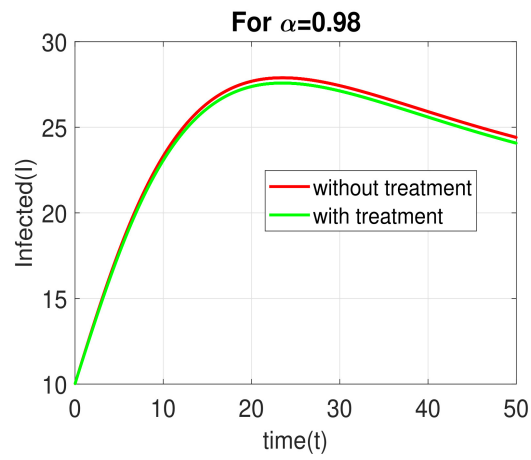


Figure 7.5: Nature of I with control and without control for $\alpha = 0.98$.

decreases with time when γ changes from 0.0035 to 0.0075 for $\alpha = 0.98$.

Case 5: Impact of δ on I for $\alpha = 0.95, 0.98$.

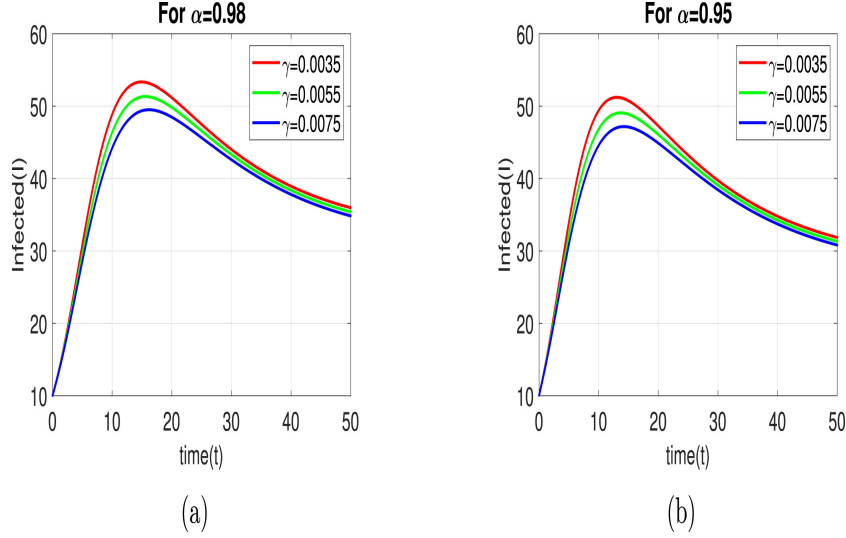


Figure 7.6: Impact of γ on I for $\alpha = 0.95, 0.98$.

The impact of δ on infected individuals is depicted in Figures 7.7(a) and 7.7(b). Based on the Figure 7.7(a), it may be noted that the infected individuals increase initially but after certain time it decreases when δ changes from 0.005 to 0.001 for $\alpha = 0.95$. Figure 7.7(b) depicts that the infected individuals increase initially but after certain time it decreases as γ changes from 0.005 to 0.001 for $\alpha = 0.98$.

Case 6: Contour plots of R_0 for β versus m with $\alpha = 0.87, 0.92$ and 0.97 .

Contour plot shows R_0 with β versus treatment rate m for different fractional order (using Table 7.2). In Figure 7.8, we observed that the value of R_0 decreases for decreasing value of m and β .

7.7 Conclusion

In this chapter, the fractional order SIR model with a Holling type II saturated incidence rate and treatment rate are explored in the Caputo order fractional derivative approach. Investigating how E_0 and E_* behave with regard to stability, it is discovered that the disease-free equilibrium is locally asymptotically stable when $R_0 < 1$ and unstable when $R_0 > 1$. For $R_0 = 1$ at E_0 the model exhibits a forward bifurcation with the parameter $\beta^\alpha = \beta_*^\alpha$. We discovered via numerical simulations that managing the treatment of infectious in accordance with the Holling type II treatment rate can result in more efficient management of the new infection.

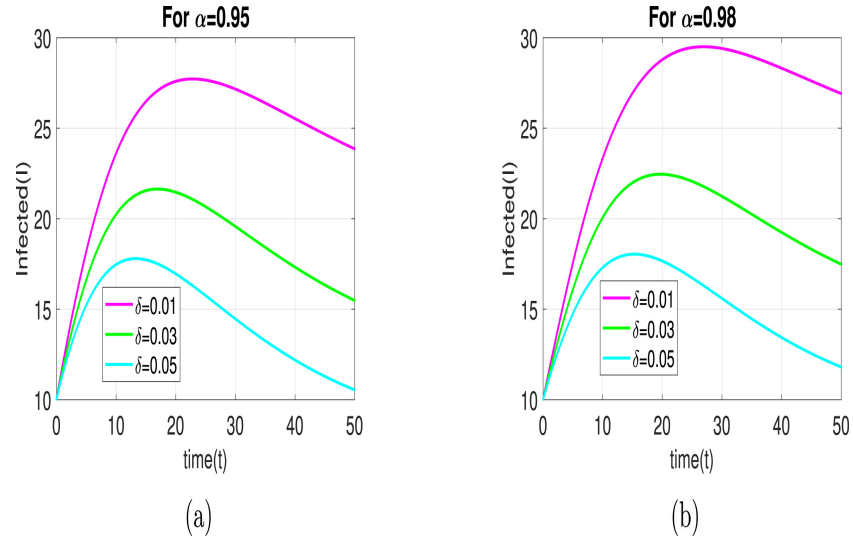


Figure 7.7: Impact of δ on I for $\alpha = 0.95, 0.98$.

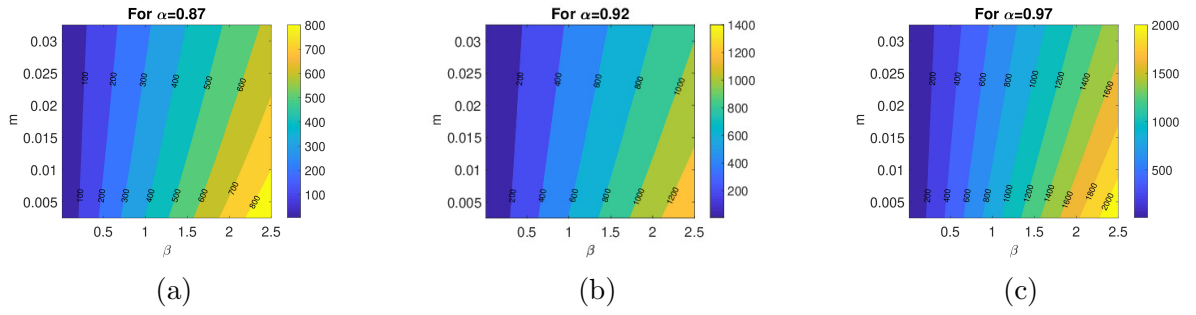


Figure 7.8: Contour plots of R_0 for β versus m with $\alpha = 0.87, 0.92$ and 0.97 .

The stability of the endemic equilibrium in the model has been tested using the Routh-Hurwitz criterion. The simulation results predict that the infection will worsen as the rate of transmission rises, but that it will stabilise due to the accessibility of treatment centres. Additionally, when the amount of inhibition used by the infected increases, infection will also decline. Using simulation results, we also discovered that the population's treatment must be carefully coordinated with the resources that are available in order to completely eradicate the virus. An essential tool for understanding the dynamics of epidemics is epidemic modelling. When there is forward bifurcation, the disease-free equilibrium loses stability as R_0 approaches unity and a stable endemic equilibrium emerges. The graphical depiction of the efficiency of theoretical solutions is displayed by the numerical simulations. Effectively reducing the infection from society will need knowledge, adequate treatment for infectious diseases, and the availability of health resources. Moreover, By using the appropriate Lyapunov function, we were able to show that the equilibrium was globally stable. We have also noticed that fractional order is crucial to population dynamics.

Chapter 8

Study of fractional order SIR model with M-H type treatment rate and its stability analysis

“But in my opinion, all things in nature occur mathematically.”

- Rene Descartes

This chapter is based on the paper

Study of a fractional order SIR model with M-H type treatment rate and its stability analysis. (Communicated).

8.1 Introduction

Epidemiology, sometimes compared to the biological study of public health, focuses on the prevalence and underlying causes of infection susceptibility among the general population. The use of mathematical models to study such communicable diseases makes it easier to comprehend how diseases spread, to identify elements that affect transmission for efficient control efforts, and to assess goals and intervention approaches. Systematically introducing deterministic models for infectious illnesses, Kermack and McKendrick [1, 246]. To better understand the process of disease transmission, a number of researchers have investigated various epidemic systems by looking at various models, such as those developed by SI [247], SIS [281], SIR [25, 31, 32, 148 - 250], SIRS [31], SEIR [25, 123, 251, 282], SIQR [90], SEIRV [97, 100]. Infectious disease management has been harder during the last several decades. One of the most important health measures for avoiding infectious diseases is vaccination because of its safety and cost. Indeed, high vaccination rates have resulted in dramatic reductions or even elimination of a variety of infectious illnesses, such as smallpox [253], SARS-CoV-2 infection [283, 284].

In the modeling of infectious illnesses [285 - 289], the incidence rate is crucial in determining the behavior at phenomena. In 1927, Kermack and McKendrick [23] proposed the transmission rate as βSI . The interaction effect is a linearly rising count of the amount of pathogens in this incidence rate, which is unsuitable for a vast population. As a result, Capasso and Serio [23] proposed a nonlinear occurrence $g(I)S$ for $g'(I) < 0$ that permits for particular “behavioral” effects. With behavioral modifications, Capasso and Serio inspired their approach. The potential damage of infection may become extraordinarily high during times of high occurrence, leading to major behavioral modifications that minimize the actual risk of illness [24]. Goel and Nilam [25], Wei and Chen [26], Capasso et al. [27, 28], Zhang et al. [29], Anderson and May [30], Li et al. [34], including Kumar and Nilam [31, 32]. A few writers [250, 291, 292], have drawn attention to the significance of taking nonlinear incidence rates into account when studying the relationships between infectious transmission and illness. Li et al. [34] presented a SIR model with $f(S, I) = \frac{\beta SI}{1+\gamma I}$.

It is well known that treatment rates are crucial in avoiding and limiting the spread of illnesses. We are aware that the therapy resources in any community are insufficient. As a result, selecting an effective treatment rate is critical for limiting disease transmission. Due to lack of efficient treatment options and vaccinations, epidemic prevention methods focus on efficient preventative measures. Wang and Ruan [35] proposed the following SIR transmission dynamics with a fixed treatment rate:

$$h(I) = \begin{cases} n & \text{for } I > 0, \\ 0 & \text{for } I = 0. \end{cases}$$

Zhang and Liu [36], who also provided a superior treatment rate (Holling type II) as a

continuously differentiable function that populates at the largest benefit, as shown below: $h(I) = \frac{mI}{1+nI}$ for $I \geq 0, m > 0, n > 0$, where m represents the cure rate and n represents the limitation rate in treatment availability. Zhang et al. [267], Zhou et al. [268] and Dubey et al. [251] have investigated this nonlinear saturation treatment rate in a somewhat different manner.

8.1.1 Motivation and Research Background

A particularly useful tool for modelling an infectious disease system that includes past illness states, a memory of past disease patterns, a profile of genetic diversity, etc. is fractional calculus [293 - 296]. When compared to an integer order model, using fractional order derivatives to fine-tune complicated dynamics within a disease system produces a more accurate picture. Because it expands the possibilities of integer-order derivatives, fractional order modelling is a useful tool for analyzing disease features. The integer order derivative is limited to local characteristics, but the fractional order derivative has a broad scope. When the system's consistency domain is improved, the fractional derivative likewise does better. In this chapter, three potential categories using the Caputo technique are studied using the fractional order SIR compartmental model with nonlinear incidence rate and nonlinear treatment rate. The saturated incidence rate of infection is considered as Holling type II and the treatment rate is considered as Monod-Haldane (MH) type. The existence and uniqueness criteria for the new models, as well as the solution's positivity, have been established, among other conclusions. Both at E_0 and E_1 , we have covered the stability analysis of our suggested model. For estimating the system solution, Taylor's approach is also used. We used the MATLAB (2018a) programme to run numerical simulations and analyze the graphical significance.

8.1.2 Chapter structure

We developed the SIR epidemic model in Section 8.2 in an environment of the Caputo derivative. In Section 8.3, the model's solution has been examined in terms of its existence, uniqueness, non-negativity, boundedness criteria, and stability analysis. Using the control parameter treatment rate, we also provide an ideal control strategy for a SIR model in Section 8.4. The suggested model's approximate solution is discussed in Section 8.5 using the fractional-order Taylor's technique in the Caputo derivative. In Section 8.6, the MATLAB-based numerical analysis is presented. Section 8.7 is where the chapter comes to a conclusion.

8.2 Formulation of the model system

We have introduced a mathematical framework that posits the division of the entire population, denoted as $N(t)$, into three distinct categories: susceptible individuals denoted as $S(t)$, infected individuals denoted as $I(t)$, and individuals who have recovered, represented as $R(t)$.

The sub-populations at different times may vary, but the total of all sub-populations remains constant, denoted as N . This can be expressed as $S(t) + I(t) + R(t) = N$. The term $\frac{\beta SI}{1+\gamma I}$ is the Holling type II functional response representing the saturated incidence rate of infection among susceptible where β is the transmission rate between susceptible and infected population. Also the term $\frac{mI}{1+nI^2}$ represents Monod-Haldane type treatment rate, which describes the non-monotonic behavior of the treatment rate due to limitations in the availability of effective treatments. Table 8.1 provides a summary of the symbols used in the proposed model system.

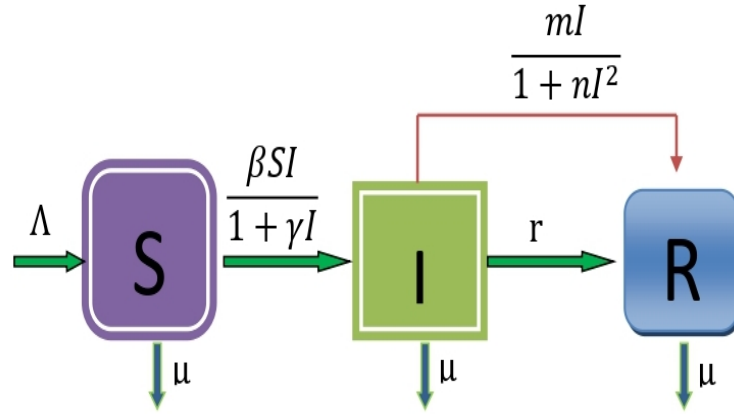


Figure 8.1: The proposed SIR model's flow diagram.

$$\begin{aligned}
 {}^C D_t^\alpha S(t) &= \Lambda - \mu S(t) - \frac{\beta S(t)I(t)}{1 + \gamma I(t)}, S(t)|_{t=0} = S(0) > 0, \\
 {}^C D_t^\alpha I(t) &= \frac{\beta S(t)I(t)}{1 + \gamma I(t)} - \frac{mI(t)}{1 + nI^2(t)} - (\mu + \delta + r)I(t), I(t)|_{t=0} = I(0) > 0, \\
 {}^C D_t^\alpha R(t) &= \frac{mI(t)}{1 + nI^2(t)} + \delta I(t) - \mu R(t), R(t)|_{t=0} = R(0) > 0,
 \end{aligned} \tag{8.1}$$

where $0 < \alpha < 1$, and ${}^C D_t^\alpha$ denotes the Caputo operator.

Parameters	Biological meaning
Λ	recruitment rate
μ	death rate
β	transmission rate
γ	inhabitory rate
m	treatment rate
n	limitation rate in resources availability
δ	recovery rate
r	disease induced mortality rate
S	susceptible population
I	infected population
R	recovered population
N	total population
R_0	basic reproduction number

Table 8.1: Significance of the relevant parameters

8.3 Analysis of the system

8.3.1 Model existence and model uniqueness

Theorem 8.3.1. *The model (8.1), with an initial condition of $(S(t_0), I(t_0), R(t_0))$ belonging to the positive region Γ^+ , invariably exhibits a singular solution within the domain Γ^+ for all time points $t \geq t_0$.*

Proof. Let $\Omega = \{(S, I, R) \in \mathbb{R}^3 : \max(|S|, |I|, |R|) \leq M\}$ where τ and M are finite positive real numbers for the region $\Omega \times [t_0, \tau]$. Let $Y = (S, I, R)$ and $\bar{Y} = (\bar{S}, \bar{I}, \bar{R})$. Consider a mapping $F(Y) = (F_1(Y), F_2(Y), F_3(Y))$, where

$$\begin{aligned}
F_1(Y) &= \Lambda - \mu S(t) - \frac{\beta S(t)I(t)}{1 + \gamma I(t)}, \\
F_2(Y) &= \frac{\beta S(t)I(t)}{1 + \gamma I(t)} - \frac{mI(t)}{1 + nI^2(t)} - (\mu + \delta + r)I(t), \\
F_3(Y) &= \frac{mI(t)}{1 + nI^2(t)} + \delta I(t) - \mu R(t).
\end{aligned}$$

For any $Y, \bar{Y} \in \Omega$:

$$\begin{aligned}
& \|F(Y) - F(\bar{Y})\| \\
&= |F_1(Y) - F_1(\bar{Y})| + |F_2(Y) - F_2(\bar{Y})| + |F_3(Y) - F_3(\bar{Y})| \\
&= \left| \Lambda - \mu S - \frac{\beta SI}{1 + \gamma I} - \left(\Lambda - \mu \bar{S} - \frac{\beta \bar{S} \bar{I}}{1 + \gamma \bar{I}} \right) \right| + \\
& \quad \left| \frac{\beta SI}{1 + \gamma I} - \frac{mI}{1 + nI^2} - (\mu + \delta + r)I - \left(\frac{\beta \bar{S} \bar{I}}{1 + \gamma \bar{I}} - \frac{m\bar{I}}{1 + n\bar{I}^2} \right) + (\mu + \delta + r)\bar{I} \right| + \\
& \quad \left| \frac{mI}{1 + nI^2} + \delta I - \mu R - \left(\frac{m\bar{I}}{1 + n\bar{I}^2} + \delta \bar{I} - \mu \bar{R} \right) \right| \\
&\leq \Lambda |(S - \bar{S})| + 2\beta \left| \left(\frac{SI(t)}{1 + \gamma I} - \frac{\bar{S} \bar{I}}{1 + \gamma \bar{I}} \right) \right| + 2m \left| \left(\frac{I}{1 + nI^2} - \frac{\bar{I}}{1 + n\bar{I}^2} \right) \right| + \\
& \quad (\mu + 2\delta + r) |(I - \bar{I})| + \mu |(R - \bar{R})| \\
&\leq (\Lambda + 2\beta M) |(S - \bar{S})| + (\mu + 2\delta + r + 2mM) |(I - \bar{I})| + \mu |(R - \bar{R})| \\
&\leq G_1 |S - \bar{S}| + G_2 |I - \bar{I}| + G_3 |R - \bar{R}| \\
&\leq G \|Y - \bar{Y}\|, \text{ where } G = \max\{G_1, G_2, G_3\},
\end{aligned}$$

$G_1 = (\Lambda + 2\beta M)$, $G_2 = (\mu + 2\delta + r + 2mM)$ and $G_3 = \mu$.

Thus, $F(Y)$ satisfies Lipschitz's criteria. So $Y(t)$ is a unique solution of the model (8.1), with the help of Lemma 1.4.4.

8.3.2 Boundedness and non-negativity

Theorem 8.3.2. Any solutions originating from the initial condition $(S(t_0), I(t_0), R(t_0))$ in the model (8.1) are characterized by non-negative values.

Proof. Let $Y(t_0) = (S(t_0), I(t_0), R(t_0)) \in \Gamma_+$ be the initial solution of (8.1). Firstly, we shall prove that $S(t) \geq 0$ for all $t \geq 0$. For this, we assume that $S(t) \geq 0$ not true. Then there exists a $\tau > 0$, such that

$$\begin{cases} S(t) > 0 \text{ for } t_0 \leq t < \tau, \\ S(t) = 0 \text{ for } t = \tau, \\ S(t) < 0 \text{ for } \tau < t < \tau + \epsilon \text{ for } \epsilon > 0. \end{cases}$$

With the help of system (8.1), we have

$${}^C_{t_0}D_t^\alpha S(t)|_{S(\tau)=0} = \Lambda > 0.$$

Using Lemma 1.4.5, for any $0 < \epsilon \ll 1$, we have $S(\tau + \epsilon) = S(\tau) + \frac{1}{\alpha} \frac{d^\alpha}{dt^\alpha} S(t) \epsilon^\alpha$.

As a result, $S(\tau + \epsilon) \geq 0$, contradicts our assumption that $S(t) < 0$ for $\tau < t < \tau + \epsilon$.

Therefore, we get $S(t) \geq 0, \forall t \in [t_0, \infty)$. Similarly, we have $I(t) \geq 0$ and $R(t) \geq 0, \forall t \in [t_0, \infty)$.

Theorem 8.3.3. All solutions of system (8.1) are bounded.

Proof. Now $N(t) = S(t) + I(t) + R(t)$, then

$$\begin{aligned} {}^C_{t_0}D_t^\alpha N(t) &= {}^C_{t_0}D_t^\alpha S(t) + {}^C_{t_0}D_t^\alpha I(t) + {}^C_{t_0}D_t^\alpha R(t) \\ &= \Lambda - \mu N(t). \end{aligned}$$

Therefore,

$${}^C_{t_0}D_t^\alpha N(t) + \mu N(t) \leq \Lambda.$$

We get (using Lemma 1.4.1):

$$\begin{aligned} z^\alpha F(z) - z^{\alpha-1}N(0) + \mu F(z) &\leq \frac{\Lambda}{z}, \text{ where } F(z) = \mathcal{L}\{N(t)\} \\ \Rightarrow F(z)(z^{\alpha+1} + z\mu) &\leq z^\alpha N(0) + \Lambda \\ \Rightarrow F(z) &\leq \frac{z^\alpha N(0) + \Lambda}{z^{\alpha+1} + z\mu} \\ &= \frac{z^\alpha N(0)}{z^{\alpha+1} + z\mu} + \frac{\Lambda}{z^{\alpha+1} + z\mu}. \end{aligned}$$

Using inverse Laplace transform:

$$N(t) \leq N(0)E_{\alpha,1}(-\mu t^\alpha) + \Lambda t^\alpha E_{\alpha,\alpha+1}(-\mu t^\alpha).$$

From the properties of Mittag Leffler function [279], we get

$$E_{c,d}(x) = xE_{c,c+d}(x) + \frac{1}{\Gamma(d)}.$$

Hence,

$$N(t) \leq (N(0) - \frac{\Lambda}{\mu})E_{\alpha,1}(-\mu t^\alpha) + \frac{\Lambda}{\mu}.$$

As a result, the system solutions are bounded.

The impact of $R(t)$ on the first two equations in system (8.1) is unaltered. System (8.1) might be converted to a two-dimensional system on the presumption that the whole population N is constant. The third equation of the system (8.1) is traditionally omitted. As a result, we have:

$$\begin{aligned} {}^C_{t_0}D_t^\alpha S(t) &= \Lambda - \mu S(t) - \frac{\beta S(t)I(t)}{1 + \gamma I(t)}, S(t)|_{t=0} = S(0) > 0, \\ {}^C_{t_0}D_t^\alpha I(t) &= \frac{\beta S(t)I(t)}{1 + \gamma I(t)} - \frac{mI(t)}{1 + nI^2(t)} - (\mu + \delta + r)I(t), I(t)|_{t=0} = I(0) > 0. \end{aligned} \quad (8.2)$$

8.3.3 Equilibrium points of the model (8.2)

Let ${}^C_{t_0}D_t^\alpha S(t) = 0$ and ${}^C_{t_0}D_t^\alpha I(t) = 0$. The model (8.2) has two equilibrium points namely,

1. The infection free equilibrium $E_0(\frac{\Lambda}{\mu}, 0)$.
2. The endemic equilibrium $E_1(S^*, I^*)$ where
 $S^* = \frac{\Lambda + I^*(-m - \mu - \delta - r) + I^{*2}(\Lambda n - n(\mu + \delta + r)I^{*3})}{\mu(1 + nI^{*2})}$ and $XI^{*3} + YI^{*2} + ZI^* + W = 0$ where
 $X = n(\mu\gamma + \beta)(\mu + \delta + r)$, $Y = \mu n(\mu + \delta + r) - \beta\Lambda n$,
 $Z = (\mu\gamma + \beta)(m + \mu + \delta + r)$ and $W = \mu(\mu + m + \delta + r) - \Lambda\beta$.

8.3.4 The basic reproduction number

The next-generation matrix [37] technique is used to calculate the model's basic reproduction number R_0 , which may be determined from the largest eigenvalue of the matrix FV^{-1}

where, $F = \begin{bmatrix} \frac{\beta\Lambda}{\mu} & 0 \\ 0 & 0 \end{bmatrix}$ and $V = \begin{bmatrix} m + \mu + \delta + r & 0 \\ \frac{\beta\Lambda}{\mu} & \mu \end{bmatrix}$. Therefore, $R_0 = \frac{\beta\Lambda}{\mu(m + \mu + \delta + r)}$.

8.3.5 Stability analysis at E_0

Let us consider

$J_0(S, I) = F$ where,

$F = \begin{bmatrix} F_{11} & F_{12} \\ 0 & F_{22} \end{bmatrix}$, where

$$F_{11} = -\mu, F_{22} = -(m + \mu + \delta + r), F_{12} = -\frac{\beta\Lambda}{\mu}.$$

Theorem 8.3.4. *The point E_0 of the system (8.2) is locally asymptotically stable.*

Proof. At E_0 the Jacobian matrix is given by

$$J_0\left(\frac{\Lambda}{\mu}, 0\right) = \begin{bmatrix} -\mu & -\frac{\beta\Lambda}{\mu} \\ 0 & -(m + \mu + \delta + r) \end{bmatrix}.$$

The eigenvalues of the system are $\lambda_1 = -\mu, \lambda_2 = -(m + \mu + \delta + r)$. It follows that $|\arg(\lambda_i)| = \pi > \frac{\alpha\pi}{2}$ ($i = 1, 2$) where $0 < \alpha < 1$. Therefore E_0 is asymptotically stable locally by Lemma 1.4.6.

To discuss the global stability at E_0 of system (8.2), first we assume that $G((S(t), I(t)) = \frac{\beta S(t)I(t)}{1+\gamma I(t)}$, is always positive, monotonically increasing and continuously differentiable for all $S > 0$ and $I > 0$. That satisfies the following conditions:

$C1 : G((S(t), I(t)) > 0, G'_S((S(t), I(t)), G'_I((S(t), I(t)))$ for $S > 0$ and $I > 0$.

$C2 : G((S(t), 0) = G((0, I(t)) = 0, G'_S((S(t), 0) = 0, G'_I((S(t), 0) > 0$ for $S > 0$ and $I > 0$.

$C3 : G'_I((S(t), 0)$ is increasing with respect to $S(t) > 0$.

$C4 : \frac{G'_S((S_0, 0))}{G'_I((S(t), 0))} < 1$ for $S(t) > S_0$; $\frac{G'_S((S_0, 0))}{G'_I((S(t), 0))} > 1$ for $S(t) \in (0, S_0)$.

Theorem 8.3.5. *Suppose that (C1) to (C4) are satisfied, the point E_0 of system (8.2) is globally asymptotically stable.*

Proof. Using the appropriate function $L = (S - S_0 - \int_{S_0}^S \lim_{t \rightarrow 0^+} \frac{G(S_0, I)}{G(g, I)} dg) + I$.

The aforementioned function's time derivative is

$$\begin{aligned} {}^{C_{t_0}}D_t^\alpha L &= (1 - \frac{S}{S_0}) {}^{C_{t_0}}D_t^\alpha S + {}^{C_{t_0}}D_t^\alpha I \\ &= -\frac{\mu(S-S_0)^2}{S} + \frac{\beta S_0 I}{1+\gamma I} - \frac{mI}{1+nI^2} - (\mu + \delta + r)I \\ &= \frac{\mu(S - \frac{\Lambda}{\mu})^2}{S} + \frac{(\mu + \delta + r + m)(R_0 - 1)I}{1 + \gamma I} \\ &\quad - \frac{[-\gamma(\mu + \delta + r + m) + mnI - n\gamma(\delta + r + m)I^2]I^2}{(1 + \gamma I)(1 + nI^2)}. \end{aligned}$$

Since all parameters of the system are positive, then ${}^{C_{t_0}}D_t^\alpha L \leq 0$ if $R_0 \leq 1$ and ${}^{C_{t_0}}D_t^\alpha L = 0$ if $S = S_0 = \frac{\Lambda}{\mu}, I = I_0 = 0$.

The point E_0 is asymptotically stable globally.

8.3.6 Stability analysis at E_1

At $E_1(S^*, I^*)$, we get

$$J(S^*, I^*) = \begin{bmatrix} E & F \\ G & H \end{bmatrix}$$

where

$$\begin{aligned} E &= -\mu - \frac{\beta I^*}{1 + \gamma I^*}, \\ F &= -\frac{\beta S^*}{(1 + \gamma I^*)^2}, \\ G &= \frac{\beta I^*}{(1 + \gamma I^*)}, \\ H &= \frac{\beta S^*}{(1 + \gamma I^*)^2} - \frac{m(1 - nI^{*2})}{(1 + nI^{*2})^2} - (\mu + \delta + r). \end{aligned}$$

Theorem 8.3.6. *The point $E_1(S^*, I^*)$ of system (8.2) is asymptotically stable locally.*

Proof. *The characteristic equation is $\lambda^2 + (E + H)\lambda + (EH - FG) = 0$. We have $-(E + H) < 0$ and the roots of the characteristic equation are*

$$\lambda_{1,2} = \frac{-(E + H)}{2} \pm \frac{\sqrt{(E + H)^2 - 4(EH - FG)}}{2}.$$

If $EH > FG$ then $|\arg(\lambda_{1,2})| = \pi > \frac{\alpha\pi}{2}$; $0 < \alpha < 1$, since $(E + H)^2 - 4(EH - FG) = (E - H)^2 + 4FG$. Using Lemma 1.4.6, the point E_1 is locally asymptotically stable in the SI plane.

Theorem 8.3.7. *The point $E_1(S^*, I^*)$ of system (8.2) is globally asymptotically stable.*

Proof. *Let us consider the following hypothesis:*

$$\begin{aligned} H(1) : & \frac{mI^*}{1 + nI^{*2}} + \frac{(1 + I)\beta S^* I^*}{1 + I\gamma I^*} + \frac{m}{1 + nI^{*2}} \\ & \leq \left[\frac{mI}{1 + nI^2} + \frac{\beta S^{*2}}{S + S\gamma I^*} + I^* \left(\frac{S\beta}{1 + \gamma} + \frac{m}{1 + nII^{*2}} \right) \right]. \end{aligned}$$

Since (S^, I^*) is the endemic equilibrium point of model (8.2), then*

$$\Lambda - \mu S^* = \frac{\beta S^* I^*}{1 + \gamma I^*}, \quad \frac{\beta S^* I^*}{1 + \gamma I^*} = \frac{mI^*}{1 + nI^{*2}} + (\mu + \delta + r)I^*.$$

Let us consider the Goh-Volterra form as

$$W(S, I) = \left(S - S^* - S^* \ln \frac{S}{S^*} \right) + \left(I - I^* - I^* \ln \frac{I}{I^*} \right),$$

Now, along the integral curves of (8.2):

$$\begin{aligned}
{}^C D_t^\alpha W(S, I) &\leq \frac{S - S^*}{S} {}^C D_t^\alpha S(t) + \frac{I - I^*}{I} {}^C D_t^\alpha I(t), \text{ (using Lemma 1.4.7)} \\
&= \frac{mI^*}{1 + nI^{*2}} + \frac{(1 + I)\beta S^* I^*}{1 + I\gamma I^*} + \frac{m}{1 + nI^{*2}} \\
&\quad - \left[\frac{mI}{1 + nI^2} + \frac{\beta S^{*2}}{S + S\gamma I^*} + I^* \left(\frac{S\beta}{1 + \gamma} + \frac{m}{1 + nI^2 I^{*2}} \right) \right]
\end{aligned}$$

Hence, by $H(1)$, we have

$${}^C D_t^\alpha W(S, I) \leq 0, \forall (S, I) \in \Omega \quad (3.5)$$

and ${}^C D_t^\alpha W(S, I) = 0$ if $(S, I) = (S^*, I^*)$. So, the point $E_1(S^*, I^*)$ is asymptotically stable globally.

8.4 SIR model with optimal control

One of the most important tools in the fight against infectious illnesses is the treatment rate. On the subject of optimal control theory in fractional derivatives, Ding et al. [50] and Agarwal et al. [51] have contributed. The fractional optimum control principle is fundamentally challenged by Pontryagin's maximum principle [52]. Our goal is to utilise the control measure v ($0 \leq v(t) \leq 1$) to account for the value of immunisation and to choose the optimum control v^* to reduce the cost function $J(v)$ of the control strategy. The cost function:

$$J(v^*) = \min (J(v(t))) \text{ with } J(v) = \left(\int_0^{t_f} [I + A_1 v^2] dt \right), \quad (8.3)$$

subject to

$$\begin{aligned}
{}^C D_t^\alpha S(t) &= \Lambda - \mu S(t) - \frac{\beta S(t)I(t)}{1 + \gamma I(t)}, S(0) > 0, \\
{}^C D_t^\alpha I(t) &= \frac{\beta S(t)I(t)}{1 + \gamma I(t)} - \frac{vI(t)}{1 + nI^2(t)} - (\mu + \delta + r)I(t), I(0) > 0, \\
{}^C D_t^\alpha R(t) &= \frac{vI(t)}{1 + nI^2(t)} + \delta I(t) - \mu R(t), R(t)|_{t=0} = R(0) > 0,
\end{aligned} \quad (8.4)$$

where $0 \leq v(t) \leq 1$.

Theorem 8.4.1. Let $v(t)$ be a measurable control function on $[0, t_f]$, with $v(t) \in [0, 1]$. Then there exists an optimal control v^* to minimize $J(v)$ of (8.3) with $v^* = \max[\min(\bar{v}, 1), 0]$, $\bar{v} = \frac{(\epsilon_2 - \epsilon_3)I}{2A_1(1+nI^2)}$.

Proof. The following method has been used to study the Hamiltonian:

$$H = [I + A_1 v^2] + \epsilon_1(\Lambda - \mu S(t) - \frac{\beta S(t)I(t)}{1+\gamma I(t)}) + \epsilon_2(\frac{\beta S(t)I(t)}{1+\gamma I(t)} - \frac{vI(t)}{1+nI^2(t)} - (\mu + \delta + rI(t)) + \epsilon_3(\frac{vI(t)}{1+nI^2(t)} + \delta I(t) - \mu R(t)),$$

with adjoint variables $\epsilon_i(t), i = 1, 2, 3$ expressed as:

$${}^{RL}D_t^\alpha \epsilon_1(t)(t) = -\frac{\partial H}{\partial S} = -\epsilon_1(-\mu S(t) - \frac{\beta I}{1+\gamma I}) - \epsilon_2 \frac{\beta I}{1+\gamma I},$$

$$\begin{aligned} {}^{RL}D_t^\alpha \epsilon_2(t)(t) &= -\frac{\partial H}{\partial I} = -1 - \epsilon_1(-\frac{\beta S}{(1+\gamma I)^2}) - \epsilon_2(-\frac{\beta S}{(1+\gamma I)^2} - \frac{v(1-nI^2)}{(1+nI^2)^2} - (\mu + \delta + r)) \\ &\quad - \epsilon_3(\frac{v(1-nI^2)}{(1+nI^2)^2} + \delta), \end{aligned}$$

$${}^{RL}D_t^\alpha \epsilon_3(t)(t) = -\frac{\partial H}{\partial R} = \epsilon_3 \mu.$$

As a result, the issue of decreasing the Hamiltonian with regard to the control is now the problem of finding v^* that minimises H in the context of (8.4). The Pontryagin principle is then used to produce the following ideal circumstance:

$$\frac{\partial H}{\partial v} = 2A_1 v + (\epsilon_2 - \epsilon_3)(\frac{I}{1+nI^2}).$$

It may be solved with adjoint variables and state variables to produce:

$$\bar{v} = \frac{(\epsilon_2 - \epsilon_3)I}{2A_1(1+nI^2)}.$$

Consider the control restrictions and the sign of the function $\frac{\partial H}{\partial v}$ for the best control v^* .

As a result, we get

$$v^* = \begin{cases} 0 & \text{if } \frac{\partial H}{\partial v} < 0, \\ \bar{v} & \text{if } \frac{\partial H}{\partial v} = 0, \\ 1 & \text{if } \frac{\partial H}{\partial v} > 0. \end{cases}$$

The ideal circumstance for the model system may be obtained by applying v^* to the equation above (8.3).

8.5 Numerical procedure

The model system (8.2), as stated in Theorem 8.3.1, has a single solution. Taylor's theorem will be used to find the model's numerical solution. Then,

$${}^C_{t_0}D_t^\alpha S(t) = u_1(t, S, I), S(0) = S_0, t > 0. \quad (8.5)$$

Consider the set of points $[0, A]$ as the points on which we are prepared to approximate the system's solution. Actually, we are unable to calculate $S(t)$, which will be the system's necessary solution. We divide $[0, A]$, into P subintervals $[t_j, t_{j+1}]$ of length, i.e., $w = \frac{A}{P}$, using the nodes $t_j = jw$, for $j = 0, 1, 2, \dots, P$. We extend the Taylor's theorem at about $t = t_0$, we have a constant $k \in [0, A]$, so that

$$S(t) = S(t_0) + {}^C_{t_0}D_t^\alpha S(t) \left\{ \frac{w^\alpha}{\Gamma(\alpha+1)} \right\} + {}^C_{t_0}D_t^{2\alpha} [S(t)]_{t=k} \left\{ \frac{w^{2\alpha}}{\Gamma(2\alpha+1)} \right\}.$$

Now substitute ${}^C_{t_0}D_t^\alpha S(t) = u_1(t_0, S(t_0), I(t_0))$ and $t = t_0$ in the above equation which provides

$$S(t_1) = S(t_0) + u_1(t_0, S(t_0), I(t_0)) \left\{ \frac{w^\alpha}{\Gamma(\alpha+1)} \right\} + {}^C_{t_0}D_t^{2\alpha} [S(t)]_{t=k} \left\{ \frac{w^{2\alpha}}{\Gamma(2\alpha+1)} \right\}.$$

If m is small, we ignore the higher terms, then

$$S(t_1) = S(t_0) + u_1(t_0, S(t_0), I(t_0)) \left\{ \frac{w^\alpha}{\Gamma(\alpha+1)} \right\}. \quad \text{A general formula of expanding about } t_j = t_j + w, \text{ provides}$$

$$S(t_j + 1) = S(t_j) + u_1(t_j, S(t_j), I(t_j)) \left\{ \frac{w^\alpha}{\Gamma(\alpha+1)} \right\}.$$

Similarly, we have

$$I(t_j + 1) = I(t_j) + u_1(t_j, S(t_j), I(t_j)) \left\{ \frac{w^\alpha}{\Gamma(\alpha+1)} \right\}.$$

8.6 Numerical discussion

In this part, we evaluate and verify the analytic results of our model system (8.1) using detailed numerical simulations. Although the majority of fractional order differential equations lack accurate analytic solutions, approximation and numerical methods have been devised. Through the mathematical software MATLAB (2018a), we have employed Taylor's theorem in the numerical scheme. Following are several categories for the numerical output of model simulations and the accompanying findings:

Case 1: Dynamical features of all population for different fractional orders

The parameters' values in Table 8.2 are used to examine people's dynamic behaviour. All individuals' behaviour over time for different fractional orders α is shown in Figures 8.2(a) through 8.2(c). The number of susceptible people rises as α moves from 0.90 to 0.98, as seen in Figure 8.2(a). The number of infected people rises over time as α rises, as seen in Figure 8.2(b). When α in Figure 8.2(c) goes from 0.90 to 0.98, there are more people who have been found.

Case 2: Stability analysis of the proposed model

We address in this instance the stability of our proposed model. In this instance, Table

Parameters	Values	Reference
Λ	5	Estimated
μ	0.05	Assumed
β	0.003	Assumed
γ	0.06	Model to fit
m	0.03	Assumed
n	0.04	Assumed
δ	0.002	Model to fit
r	0.02	Assumed

Table 8.2: Parameter values for numerical study.

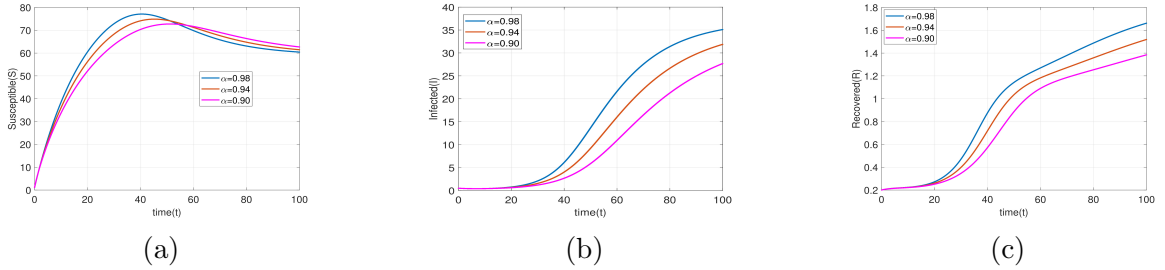


Figure 8.2: The behavior of all individuals for values of $\alpha = 0.90, 0.94, 0.98$.

8.2 contains the parameter values utilised for the numerical simulations. When α changes from 0.90 to 0.98, Figures 8.3(a) to 8.3(f) depict the time series solution of susceptible and infected individuals. From the following figures, we have observed that the system (8.1) is asymptotically stable locally at E_0 , confirming our theoretical results in Theorem 6. Figures 8.4(a) to 8.4(c) depicts the global stability of system (8.1) at E_1 with different initial condition taking $\alpha = 0.90, 0.94, 0.98$, confirming our theoretical results in Theorem 8.3.5.

Case 3: Impact of α on S and I

Figures 8.5(a) and 8.5(b) show the effects of α on susceptible and infected people. It can be shown from Figure 8.5(a) that the number of susceptible persons rises as α increases. Figure 8.5(b) shows that the number of infected people first declines but then rises over time.

Case 4: Mean density of S and I under γ

Plotting the mean densities of S and I with respect to gamma for different fractional orders is shown in Figure 8.6. As seen in Figure 8.6(a), the mean density of susceptible people rises as the value of α rises. Figure 8.6(b) shows that as the values of α fall, the

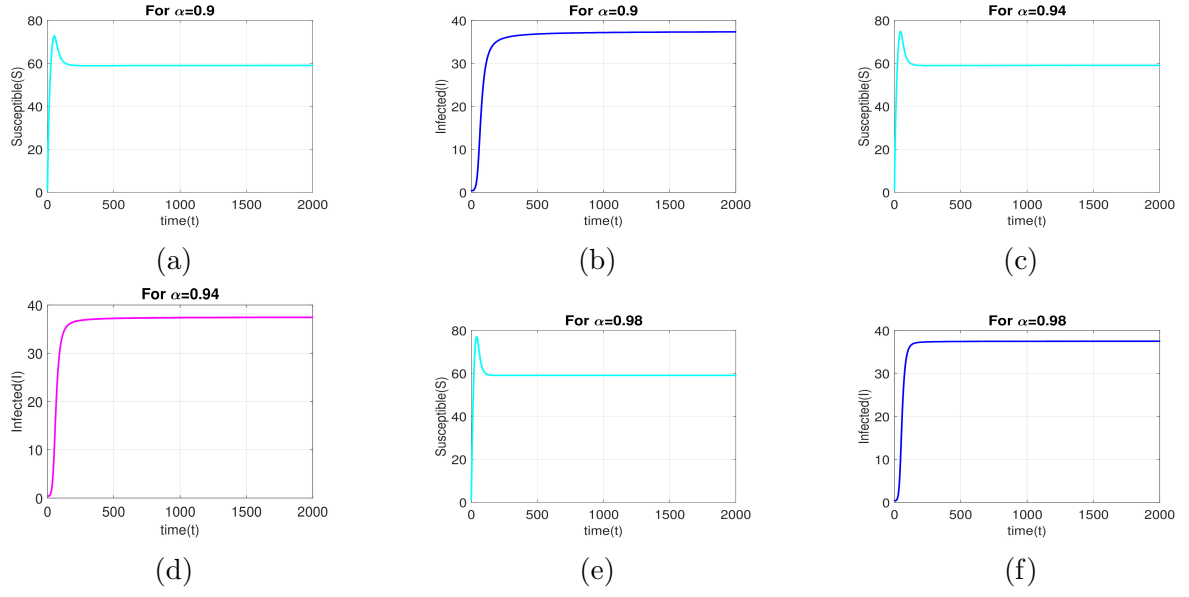


Figure 8.3: Time series solution of all individuals for values of $\alpha = 0.90, 0.94, 0.98$.

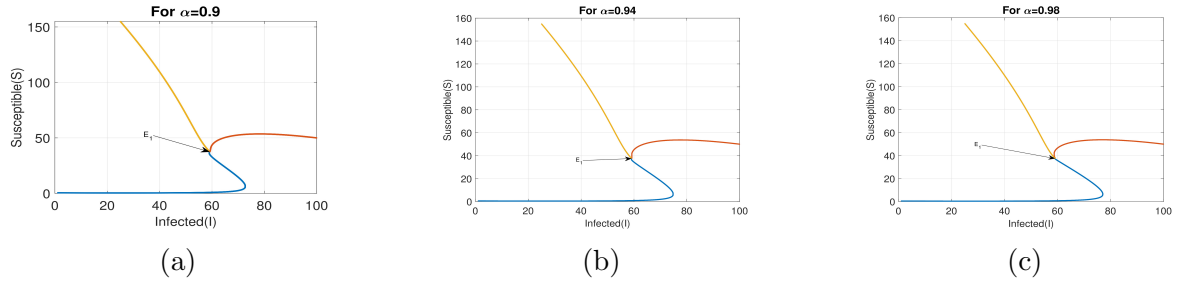


Figure 8.4: Phase portrait diagram for values of $\alpha = 0.90, 0.94, 0.98$.



Figure 8.5: Dynamics of S and I under α .



Figure 8.6: Mean density of S and I under γ for $\alpha=0.90, 0.94, 0.98$.



Figure 8.7: Mean density of S and I under δ for $\alpha=0.90, 0.94, 0.98$.

mean density of infected people rises with regard to γ .

Case 5: Mean density of S and I under δ

Figure 8.7 shows the plot of mean density of S and I with respect to δ for various fractional order. Figure 8.7(a) shows that the mean density of susceptible people rises as the value of α rises. Figure 8.7(b) shows that as the values of α decline, the mean density of infected people rises with regard to δ .

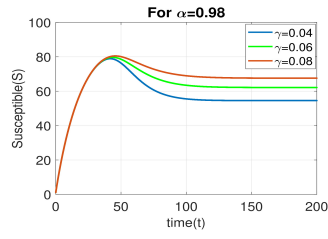
Case 6: Variation of γ under S and I for $\alpha = 0.98$

Figure 8.8 shows the effect of γ on S and I with time for $\alpha=0.98$. Figure 8.8(a) demonstrates a rise in the number of vulnerable people as the inhibitory rate γ drops and reaches its stable state, but the illness is not completely eradicated since it will continue to exist at a much lower level. We noticed that the infected population drops when the inhibitory rate γ rises in Figure 8.8(b). Thus, it is assumed that preventative actions conducted by vulnerable and sick individuals will aid in reducing the spread of illness.

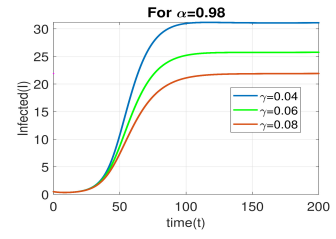
Case 7: Variation of δ under S and I for $\alpha = 0.98$

Figure 8.9 shows the effect of δ on S and I with time for $\alpha=0.98$. As the recovery rate δ declines and reaches its steady state, Figure 8.9(a) depicts a rise in the number of sensitive people. In Figure 8.9(b), we observed that the infected population decreases when recovery rate δ changes from 0.001 to 0.003.

Case 8: Variation of δ under S and I for $\alpha=0.98$

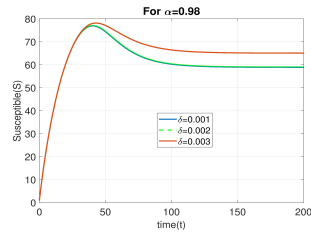


(a)

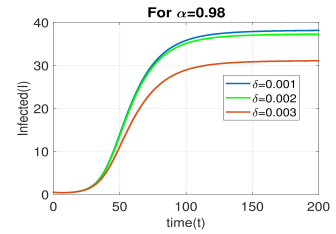


(b)

Figure 8.8: Variation of γ under S and I for $\alpha=0.98$.

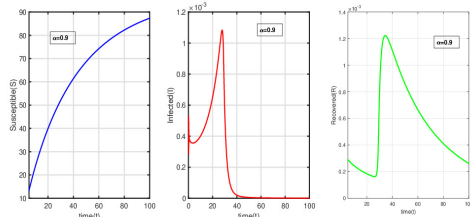


(a)

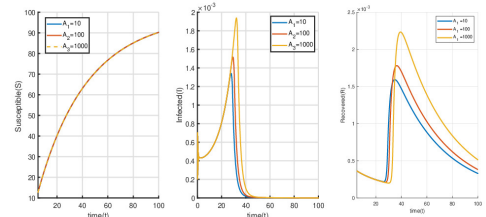


(b)

Figure 8.9: Variation of δ under S and I for $\alpha=0.98$.



(a)



(b)

Figure 8.10: When $\alpha=0.9$, the time series of the model system (8.1) corresponds to Table 8.2.



Figure 8.11: With parameter values matching to Table 8.2 for $\alpha=0.9$, a time series of the ideal control variable v^* and the ideal cost J^* is produced.

Figures 8.10(a) through 8.10(b) depict the time series of people who are vulnerable to infection, those who have been infected, and those who have recovered over a time period of $[0, 100]$, with optimum control using fractional order $\alpha=0.9$. Infectious illness prevention depends heavily on treatment rates, and several theories have been put out in which vaccination rates are seen as very advantageous. The reproduction number R_0 falls as a consequence of the inclusion of the treatment rate parameter. We chose a final time of $t_f=100$ for the simulation of the optimum control problem governed by model (8.1), which corresponds to Table 8.2. The time series of the ideal cost J^* and the ideal control variable v^* are shown in Figure 8.11.

8.7 Conclusion

The mathematical model used in this chapter aims to depict the dynamics of infectious disease when the ratio of infected to susceptible populations is high, taking into account the effects of inhibitory activity, behavioural changes that occur during epidemics, and the limitations of treatment facilities. Analyzing the stability characteristics of equilibrium points corresponding to no infection and sustained infection states, it is shown that the disease-free equilibrium is locally asymptotically stable when $R_0 < 1$ and unstable when $R_0 > 1$.

The R-H criteria has been used to examine the stability of the model's endemic equilibrium. The simulation results predicts that the infection will worsen as the rate of transmission rises, but that it will stabilise due to the accessibility of treatment centres. Furthermore, the prevalence of the infection decreases proportionally when the amount of suppression used by the affected people increases. The results of our simulation also showed that, in order to successfully eradicate the virus, the treatment of the population must be closely coordinated with the resources at hand. Understanding the complexities of disease outbreaks is made possible by the use of epidemic modelling. Numerical

simulations provide the visualisation of the efficacy of theoretical solutions. Comprehensive information, suitable infectious disease treatment methods, and the availability of healthcare services are required for the successful decrease of infection within society. In addition, we showed the global stability of the equilibrium state by choosing an appropriate Lyapunov function.

The importance of fractional order to population dynamics has also been noted. The optimum solution to the optimal control issue must meet certain requirements, which we have established using the Pontryagin's Maximum Principle. It is obvious that the disease's spread can be stopped and eliminated if the control measure v^* is used. Additionally, Theorem 8.4.1 has identified the ideal control value v^* to reduce the cost of vaccination, as shown by $J(v) = \left(\int_0^{t_f} [I + A_1 v^2] dt \right)$. For optimum control, we presume a final time $t_f = 100$. As a consequence, changing the derivatives' order may change the stability requirements for equilibrium locations without changing any other parametric variables. We are unable to analyse our findings using an integer order method since we have achieved so little theoretical advancement in this fractional order framework. We find a variety of biological modelling outcomes based on fractional differential equations in this work.

Chapter 9

Summary and future scopes

In the classical epidemic models, it is assumed that the state of the system at every time is not dependent on the previous history i.e. the system is memoryless. But in reality the memory plays a great role on the evolution of epidemic process. As for example, when a particular area is infected by some highly infectious disease then the human society avoids that area to save themselves from the infection. The memory effect can be incorporated in the epidemic models through fractional calculus. The intent of this thesis was to observe the effect of fractional derivatives in population dynamics and mathematical epidemiology. The theoretical foundations of fractional calculus were laid over a century ago, but the past few decades have witnessed a resurgence of interest due to the discovery of increasing numbers of power-law phenomena in a wide variety of fields. Modelling such phenomena in terms of ordinary differential equations of integer order typically leads to unwieldy sets of equations that come out contrived. On the other hand, differential equations of fractional order tend to naturally capture intrinsic phenomena in complex dynamical systems. These fractional-order equations tell us about the underlying structure of the systems that produce them is, in some cases, yet to be specified. Nevertheless, the evidence suggests that fractional-order dynamic behavior may be related to fractal structure, implying that the multi-scale properties of both structure and function are fundamentally linked. There are many variations of fractional calculus and theories of fractional calculus that are developing day by day. Fractional calculus has made a significant contribution in the field of physical science in few decades and nowadays researchers are concentrating on the application area of fractional calculus in biological fields. Though lack of numerical algorithms have barred the developments of this topic, many accurate and efficient algorithms for numerical simulations strengthen the connection between theoretical studies and real world observations. My wish is to contribute in more complex and advanced field of fractional ordered systems.

Keeping the above perspective, we hope that the following future research works can be

carried out.

- The implications of interface reduction on epidemic dynamic nature are now being investigated. Our goal is to modify the *SEIR* compartmental model to account for the varying levels of population isolation.
- Future studies should use the methodology provided in this work to the third wave of infected patients in Italy to assess the efficacy of existing COVID-19 prevention strategies.
- The present dengue model with fractional order derivatives in Chapter 6 may be extended to further research. Here we have considered exact values of the parameters in the real domain. However, assigning an exact number may seem to be too restrictive in comparison to assignment with a degree of membership or non-membership to the concerned domain. The above notion is the onset of non-standard analysis, which is the future scope of work for this model.
- In our next research, we'll look at how chaotic systems are affected by the generalized Caputo operator. The new operator can also be used to bring additional dynamical properties and features to existing fractional systems or equations that have practical applications.
- The proposed *SIR* model in Chapter 8 may be analyzed further to explore chaotic solutions and various forms of bifurcations by incorporating time delay parameters. More than one control parameter may be used to better understand the treatment strategies and management of the spread of the disease.

List of papers: Published/Communicated

1. Paul S, Mahata A, Mukherjee S, Roy B. Dynamics of SIQR epidemic model with fractional order derivative. *Partial Differ. Equ. Appl. Math.* 5, 100216, 2022.
2. Paul S, Mahata A, Mukherjee S, Roy B, Salimi M, Ahmadian A. Study of Fractional Order SEIR Epidemic Model and Effect of Vaccination on the Spread of COVID-19. *Int. J. Appl. Comput. Math.* 8(237), 2022.
3. Paul S, Mahata A, Mukherjee S, Das M, Roy B. Dynamics of Caputo Fractional Order SEIRV Epidemic Model with Optimal Control and Stability Analysis. *Int. J. Appl. Comput. Math.* 8(1), 1-25, 2022.
4. Paul S, Mahata A, Mukherjee S, Mali P.C, Roy B. Fractional order SEIQRD epidemic model of Covid-19: a case study of Italy, *PLoS ONE* 18(3): e0278880, 2023.
5. Paul S, Mahata A, Mukherjee S, Das M, Mali P.C, Roy B. Optimal Control Analysis of Fractional Order Dengue Model - A Case Study of Singapore. (Under Review).
6. Paul S, Mahata A, Mukherjee S, Mali P.C, Roy B. Dynamical behavior of a fractional order SIR model with stability analysis, *Results in Control and Optimization*, 10, 100212, ISSN 2666-7207, 2023.
7. Paul S, Mahata A, Mukherjee S, Das M, Mali P.C, Roy B. Study of a fractional order SIR model with M-H type treatment rate and its stability analysis. (Under review).
8. Paul S, Mahata A, Ghosh U, Roy B. SEIR epidemic model and scenario analysis of COVID-19 pandemic. *Ecolo. Gene. Genom.* 19, 100087, 2021.
9. Paul S, Mahata A, Mukherjee S, Roy B: Stability analysis and Hopf bifurcation in fractional order SEIRV epidemic model with a time delay in infected individuals. *Partial Differ. Equ. Appl. Math.* 5, 100282, 2022.
10. Paul S, Mahata A, Mukherjee S, Mali P.C, Roy, B. Study of Fractional Order Tri-Tropic Prey-Predator Model with Fear Effect on Prey Population. *Advances in Pure Mathematics*, 12, 652-675, 2022.
11. Paul S, Mahata A, Mukherjee S, Mali P.C, Roy B. Dynamical behavior of fractional order SEIR epidemic model with multiple time delays and its stability analysis. *Examples and Counterexamples*, 100128, 2023.

12. Paul S, Mahata A, Mukherjee S, Chakraborty M, Roy B. Study of Time-Delayed Fractional Order SEIRV Epidemic Model. *Advances in Intelligent Systems and Computing*. AISC, volume 1422, 2022.
13. Paul S, Mahata A, Mukherjee S, Mali P.C, Roy B. Mathematical Model for Tumor-Immune Interaction in Imprecise Environment with Stability Analysis. *Nonlinear Dynamics and Applications*, ISSN 2213-8692, 2022.
14. Paul S, Acharya A, Biswas M.A, Mahata A, Mukherjee S, Mali P.C, Roy B. Mathematical The scenario of COVID-19 pandemic in Brazil using SEIR epidemic model, *Advances in Intelligent Systems and Computing*. AISC, volume 1450, 419-426, 2023.
15. Paul S, Mahata A, Mukherjee S, Mahato, S.K, Salimi, M, Roy, B. Study of Fuzzy Fractional Caputo Order Approach to Diabetes model. *Fuzzy Optimization, Decision-making and Operations Research*. Springer, Cham. 2023.

Paper Presentation

1. Attended and presented paper in 2nd International Conference on Mathematical Modeling and Computational Science [ICMMCS 2021] on Hybrid Mode by Lincoln University College, Malaysia, 29th - 30th October, 2021.
2. Attended and presented paper in 2nd International Conference on Nonlinear Dynamics and Applications [ICNDA 2022] on Hybrid Mode by Sikkim Manipal Institute of Technology (SMIT), Sikkim Manipal University, Majitar, East-Sikkim 737136, India, 9th – 11th March, 2022.
3. Attended and presented paper in 3rd International Conference on Mathematical Modeling and Computational Science [ICMMCS 2023] on Hybrid Mode by Society for Intelligent Systems and Mother Teresa Women's University, Madurai, Tamilnadu, 24th -25th February 2023.
4. Attended and presented paper in Two-day National Seminar on Mathematical Modeling and its Application to Epidemiology [NSMMAE 2022] held in Bangabasi Evening College, Kolkata - 700009 , 10th – 11th November, 2022.

References

1. Martcheva M. An Introduction to Mathematical Epidemiology. Springer, New York, 2015.
2. Jones W. Ed.: Hippocrates collected works I. Cambridge Harvard University Press, Cambridge, 1868.
3. Bernoulli D. An attempt at a new analysis of the mortality caused by smallpox and of the advantages of inoculation to prevent it. *Rev. Med. Virol.* 14, 275-288, 2004.
4. Diez K, Heesterbeek J. Bernoulli's epidemiological model revisited. *Math. Biosci.* 180, 1-21, 2002.
5. Kermack W, Mckendric A. A contribution to mathematical theory of epidemics. *Proc. Roy. Soc. Lond. A Mat.* 115, 700-721, 1927.
6. Kermack W, Mckendric A. A Contributions to the mathematical theory of epidemics-I. *Bull. Math. Biol.* 53, 33-55, 1991.
7. Anderson R.M, May R.M. *Infectious Diseases of Humans: Dynamics and Control.* Oxford University Press, 1998.
8. Murray J.D. *Mathematical Biology.* Springer, New York, 1993.
9. Brauer F, Castillo-Chavez C. *Mathematical Models in Population Biology and Epidemiology.* Springer, New York, 2011.
10. World Health Organization: Pneumonia of unknown cause-China, 2020. <https://www.who.int/csr/don/05-january-2020-pneumonia-of-unkown-cause-china/en/>.
11. World Health Organization: Updated who advice for international traffic in relation to the outbreak of the COVID-19. who, Geneva.
12. World Health Organization: Clinical Management of Severe Acute Respiratory Infection When Infection is Suspected, 2020.
13. Event Horizon-COVID-19: Coronavirus COVID=19 Global Risk Assessment.
14. Li Q, Guan X, Wu P, Wang X, Zhou L, Tong Y, et al. Early transmission dynamics in Wuhan, China, of novel coronavirus-infected pneumonia. *N. Engl. J. Med.* 382(13), 1199-1207, 2020.

15. Chowell G, Fenimore P. W, Castillo-Garsow M. A, et al. SARS outbreak in Ontario, Hong Kong and Singapore: the role of diagnosis and isolation as a control mechanism. Los Alamos Unclassified Report LA-UR-03-2653, 2003.
16. Ma Z, Li J. Dynamical Modelling and Analysis of Epidemics. World Scientific, Singapore, 2009.
17. World Health Organization: Middle East respiratory syndrome coronavirus (MERS-CoV), 2019.
18. Guarner J. Three Emerging Coronaviruses in Two Decades The Story of SARS, MERS, and Now COVID-19. *Am. J. Clin. Pathol.* 153(4), 420-421, 2020.
19. Lin Q, Zhao S, Gao D, Lou Y, Yang S. A conceptual model for the coronavirus disease 2019 (COVID-19) outbreak in Wuhan, China with individual reaction and governmental action. *Int. J. Infect. Dis.* 93, 211-216, 2020.
20. Olson P.E, Hames C.S, Benenson A.S, Genovese E.N. The Thucydides Syndrome: Ebola Déjà Vu? (or Ebola Reemergent?). *Emerg. Infect. Dis.* 2(2), 155-156, 1996.
21. Papagrigorakis M.J, Yapijakis C, Synodinos P.N, Baziotopoulouvalavani E. DNA examination of ancient dental pulp incriminates typhoid fever as a probable cause of the plague of Athens. *Int. J. Infect. Dis.* 10, 206-214, 2006.
22. Alchon S. A pest in the land: New world epidemic in a global perspective. University of New Mexico Press, 2003.
23. Capasso V, Serio G. A generalization of the Kermack–Mckendrick deterministic epidemic model. *Math. Biosci.* 42(12), 43–61, 1978.
24. d’Onofrio A, Manfredi P. Information-related changes in contact patterns may trigger oscillations in the endemic prevalence of infectious diseases. *J. Theo. Biol.* 256(3), 473–8, 2009.
25. Goel K. Nilam. Stability behavior of a nonlinear mathematical epidemic transmission model with time delay. *Nonlinear Dyn.* 98(2), 1501–18, 2019.
26. Wei C, Chen L. A delayed epidemic model with pulse vaccination. *Discret. Dyn. Nat. Soc.* 12, 746951, 2008.
27. Capasso V, Grosso E, Serio G. I modelli matematici nella indagine epidemiologica applicazione all’epidemia Di Colera Verificatasi in Bari Nel 1973. *Annali Sclavo.* 19, 193–208, 1977.

28. Capasso V. Global solution for a diffusive nonlinear deterministic epidemic model. *SIAM J. Appl. Math.* 35(2), 274–84, 1978.
29. Zhang J.Z, Jin Z, Liu Q.X, Zhang Z.Y. Analysis of a delayed SIR model with nonlinear incidence rate. *Discret. Dyn. Nat. Soc.* 2008(636153), 16, 2008.
30. Anderson R.M, May R.M. Regulation and stability of host–parasite population interactions: I. regulatory processes. *J. Anim. Ecol.* 47, 219–67, 1978.
31. Kumar A, Goel K. Nilam. A deterministic time-delayed SIR epidemic model: mathematical modeling and analysis. *Theory Biosci.* 139(1), 67–76, 2019.
32. Kumar A. Nilam. Dynamic behavior of an SIR epidemic model along with time delay; crowley–martin type incidence rate and holling type II treatment rate. *Int. J. Nonlinear Sci. Numer. Simul.* 20(7–8), 757–71, 2019.
33. Kamrujjaman M, Saha P, Islam MS, Ghosh U. Dynamics of SEIR model: A case study of COVID-19 in Italy. *Results Control Optim.* 7, 100119, 2022.
34. Li X.Z, Li W.S, Ghosh M. Stability and bifurcation of an SIR epidemic model with nonlinear incidence and treatment. *Appl. Math. Comput.* 210(1), 141–50, 2009.
35. Wang W, Ruan S. Bifurcation in an epidemic model with constant removal rates of the infective. *J. Math. Anal. Appl.* 21, 775–93, 2004.
36. Zhang X, Liu X. Backward bifurcation of an epidemic model with saturated treatment function. *J. Math. Anal. Appl.* 348, 433–443, 2008.
37. Diekmann O, Heesterbeek J.A.P, Roberts M.G. The Construction of Next-Generation Matrices for Compartmental Epidemic Models. *J. R. Soc. Interface.* 7(47), 873–885, 2009.
38. Caputo M, Fabrizio M. A new definition of fractional derivative without singular kernel. *Prog. Fract. Differ. Appl.* 1(2), 73–85, 2015.
39. Gómez-Aguilar J.F, Yépez-Martínez H, Torres-Jiménez, J, Córdova-Fraga T, Escobar-Jiménez R.F, Olivares-Peregrino V.H. Homotopy perturbation transform method for nonlinear differential equations involving to fractional operator with exponential kernel. *Adv. Differ. Equ.* 68, 2017.
40. Kumar S. A new analytical modelling for fractional telegraph equation via Laplace transform. *Appl. Math. Model.* 38, 3154–3163, 2014.

41. Shaikh A, Tassaddiq A, Nisar K.S, Baleanu D. Analysis of differential equations involving Caputo–Fabrizio fractional operator and its applications to reaction–diffusion equations. *Adv. Differ. Equ.* 178, 2019.
42. Baleanu D, Mousalou A, Rezapour S. The extended fractional Caputo–Fabrizio derivative of order $0 \leq \sigma < 1$ on $R[0, 1]$ and the existence of solutions for two higher-order series-type differential equations. *Adv. Differ. Equ.* 255, 2018.
43. S. Kumar et al., A fractional model for population dynamics of two interacting species by using spectral and hermite wavelets methods. *Numer. Methods Partial Differ. Equ.* 2(37), 1652-1672, 2020.
44. Atangana A. Modelling the spread of COVID-19 with new fractal-fractional operators: Can the lockdown save mankind before vaccination? *Chaos Solitons Fractals*, 136, 109860, 2020.
45. S. Kumar et al., A model for describing the velocity of a particle in Brownian motion by Robotnov function based fractional operator, *Alexandria Eng. J.* 59(3), 1435–1449, 2020.
46. S. Kumar et al., A study of fractional Lotka-Volterra population model using Haar wavelet and Adams-Bashforth-Moulton methods, *Math. Methods Appl. Sci.* 43(8), 5564–5578, 2020.
47. S. Kumar et al., A study on fractional host–parasitoid population dynamical model to describe insect species, *Numer. Methods Partial Differential Eq.* 120, 2020.
48. S. Kumar et al., A wavelet based numerical scheme for fractional order SEIR epidemic of measles by using Genocchi polynomials. *Numer. Methods Partial Differential Equations.* 2(37), 2020.
49. Diethelm K, Ford N.J. Multi-order fractional differential equations and their numerical solution. *Appl. Math Comput.* 154 (3), 621–640, 2004.
50. Ding Y, Wang Z, Ye H. Optimal Control of a Fractional-Order HIV Immune System With Memory, *IEEE Transactions On Control Systems Technology.* 20(3), 763-769, 2012.
51. Agarwal O.P. A general formulation and solution scheme for fractional optimal control problems. *Nonlinear Dyn.* 38(14), 323-337, 2004.
52. Kamocki R. Pontryagin maximum principle for fractional ordinary optimal control problems. *Math. Methods Appl. Sci.* 37(11), 1668-1686, 2014.

53. Garten R, Lai S, Zhang J. Rapid transmission of hepatitis C virus among young injecting heroin users in southern China. *Int. J. Epidemiol.* 33, 182–188, 2004.
54. Tyrrell D.A, Bynoe M.L. Cultivation of viruses from a high proportion of patients with colds. *Lancet* 1966.
55. World Health Organization, Coronavirus who, Available: <https://www.who.int/health-topics/coronavirus> .
56. Bailey N.T.J. The mathematical theory of infectious disease, Griffin, London. 1975.
57. Hethcote, H. W., Lewis, M. A., van den Driessche, P.: An epidemiological model with a delay and a nonlinear incidence rate. *J. Math. Biol.* 27, 49–64, 1989.
58. Blackwood J.C, Childs L.M. An introduction to compartmental modeling for the budding infectious disease modeler. *Lett. Biomath.* 5(1), 195–221, 2018.
59. Shereen M.A, Khan S. COVID-19 Infection: origin, transmission, and characteristics of human coronaviruses. *J. Adv. Res.* 91-98, 2020.
60. Oldham K.B, Spanier J. The fractional calculus Mathematics in Sc. and Eng. Academic Press. 111, 1974.
61. AbbasS. Existence of solutions to fractional order ordinary and delay differential equations and applications. *Electronic J. Diff. Eqs.* 09, 1-11, 2011.
62. Pedersen M.G, Meneghini M. Quantifying undetected COVID-19 cases and effects of containment measures in Italy, preprint 2020.
63. Shaikh A.S, Nisar K.S. Transmission dynamics of fractional order typhoid fever model using Caputo–Fabrizio operator. *Chaos Solit. Fract.* 128, 355–365, 2019.
64. Erturk V.S, Zaman G, Momani S. A numeric analytic method for approximating a giving up smoking model containing fractional derivatives. *Comput. Math. Appl.* 64, 3068–3074, 2012.
65. Abdeljawad T, Al-Mdallal QM. Discrete Mittag-Leffler kernel type fractional difference initial value problems and Gronwalls inequality. *J. Comput. Appl. Math.* 339, 218–230, 2018.
66. Abdeljawad T, Al-Mdallal QM, Jarad F. Fractional logistic models in the frame of fractional operators generated by conformable derivatives. *Chaos Solit. Fract.* 119, 94–101, 2019.

67. Ahmed E, Hashish A, Rihan FA. On fractional order cancer model. *Fract. Calcul. Appl. Anal.* 3, 1–6, 2012.
68. Xu H. Analytical approximations for a population growth model with fractional order. *Commun. Nonlinear Sci. Numer. Simul.* 14, 1978–83, 2009.
69. Keeling MJ, Rohani P. *Modeling infectious diseases*. New Jersey USA: Princeton University Press publisher, 2008.
70. Al-Sulami H, El-Shahed M, Nieto J.J, Shammak W. On fractional order dengue epidemic model. *Math. Probl. Eng.* 2014, 1-6, 456537, 2014.
71. Rihan F.A, Sheek-Hussein M, Tridane A, Yafia R. Dynamics of hepatitis c virus infection: mathematical modeling and parameter estimation. *Math. Model. Nat. Phenom.* 12(5), 33–47, 2017.
72. ÖZalp N, Demirci E. A fractional order SEIR model with vertical transmission. *Math. Comput. Modell.* 54, 1–6, 2011.
73. El-Shahed M, Alsaedi A. The fractional SIRC model and influenza a. *Math. Probl. Eng.* 3, 378–87, 2011.
74. Shaikh A, Sontakke B.R. Impulsive initial value problems for a class of implicit fractional differential equations. *Comput. Methods Differ. Equ.* 8(1), 141–154, 2020.
75. Kumar S, Kumar A, Baleanu D. Two analytical methods for time-fractional nonlinear coupled Boussinesq–Burger’s equations arise in propagation of shallow water waves. *Nonlinear Dyn.* 85, 699–715, 2016.
76. Daftardar-Gejji V, Jafari H. An iterative method for solving nonlinear functional equations. *J. Math. Anal. Appl.* 316, 753–763, 2006.
77. Dutta H, Hattaf K. *Mathematical Modelling and Analysis of Infectious Diseases*, Springer International Publishing, 2020.
78. Zhang Z, Wang Y, Zhang J, Cheng F, Liu F, Ding C. Novel asymptotic stability criterion for fractional-order gene regulation system with time delay. *Asian J. Control.* 1-10, 2021.
79. Wu Z, Wang Z, Zhou T. Global uniform asymptotical stability for fractional-order gene regulatory networks with time-varying delays and structured uncertainties. *Adv. Differ. Equ.* 2021.

80. Zhang Z, Toshimitsu U, Ai Z, Zhang J. Novel stability condition for delayed fractional-order composite systems based on vector Lyapunov function. *Nonlinear Dyn.* 99, 1253 – 1267, 2020.
81. Murray J. *Mathematical Biology I*, third edition, Springer-Verlag, Heidelberg, 2002.
82. Naheed A, Singh M, Lucy D. Numerical study of SARS epidemic model with the inclusion of diffusion in the system. *Appl. Math. Comput.* 229, 480–498, 2014.
83. Billarda L, Dayananda P.W.A. A multi-stage compartmental model for HIV-infected individuals: I waiting time approach. *Math. Biosci.* 249, 92–101, 2014.
84. Upadhyay R.K., Kumari N, Rao V.S.H. Modeling the spread of bird flu and predicting outbreak diversity. *Nonlinear Anal.: Real World Appl.* 9, 1638–1648, 2008.
85. Pongsumpun P, Tang I.M. Dynamics of a new strain of the H1N1 influenza a virus incorporating the effects of repetitive contacts. *Comput. Math. Methods Med.* 487974, 2014.
86. Liu X.X., Hu S, Fong S.J., Crespo R.G., Viedma E.H. Modelling dynamics of coronavirus disease 2019 spread for pandemic forecasting based on Simulink. *Phys. Biol.* 18(4), 2021.
87. Gumel A.B., Mccluskey C., Watmough J. An SVEIR model for assessing potential impact of an imperfect anti-SARS vaccine. *Math. Biosci. Eng.* 3(3), 485-512, 2006.
88. Wang L, Xu R. Global stability of an SEIR epidemic model with vaccination. *Int. J. Biomath.* 9(6), 2016.
89. Ji C, Jiang D, Shi N. Multigroup SIR epidemic model with stochastic perturbation, *Phys. A: Stat. Mech. Appl.* 390(10), 1747–1762, 2011.
90. Paul S, Mahata A, Mukherjee S, Roy B. Dynamics of SIQR epidemic model with fractional order derivative. *Partial Differ. Equ. Appl. Math.* 5, 100216, 2022.
91. Pongkitivanichkul C, Samart D, Tangphati T, Koomhin P, Pimton P, Dam-o P, Payaka A, Channuie P. Estimating the size of COVID-19 epidemic outbreak. *Phys. Scr.* 95, 085206, 2020.
92. Zhu L.H, Wang X.W, Zhang H.H, Shen S.L, Li Y.M, Zhou Y.D. Dynamics analysis and optimal control strategy for a SIRS epidemic model with two discrete time delays. *Phys. Scr.* 95, 035213, 2020.

93. Yu J, Jiang D, Shi N. Global stability of two-group SIR model with random perturbation. *J. Math. Anal. Appl.* 360(1), 235–244, 200.
94. Yuan C, Jiang D, Regan D.O, Agarwal R. P. Stochastically asymptotically stability of the multi-group SEIR and SIR models with random perturbation. *Commun. Nonlinear Sci. Numer. Simul.* 17(6), 2501–2516, 2012.
95. Tang B, Wang X, Li Q, Bragazzi N. L, Tang S, Xiao Y, Wu, J. Estimation of the transmission risk of the 2019-nCoV and its implication for public health interventions. *J. Clin. Med.* 9(2), 462, 2020.
96. Frank T. D, Chiangga S. SEIR order parameters and eigenvectors of the three stages of completed COVID-19 epidemics: with an illustration for Thailand January to May 2020. *Phys. Biol.* 18(4), 2021.
97. Mahata A, Paul S, Mukherjee S, Roy B. Stability analysis and Hopf bifurcation in fractional order SEIRV epidemic model with a time delay in infected individuals. *Partial Differ. Equ. Appl. Math.* 5, 100282, 2022.
98. Vattay G. Forecasting the outcome and estimating the epidemic model parameters from the fatality time series in COVID-19 outbreaks. *Phys. Biol.* 17(6), 2020.
99. Kucharski A, Russell T, Diamond C, Liu Y, Edmunds J, Funk S, Eggo R. Early dynamics of transmission and control of COVID-19: a mathematical modelling study. *Lancet Infect.* 2020.
100. Mahata A, Paul S, Mukherjee S, Das M, Roy B. Dynamics of Caputo Fractional Order SEIRV Epidemic Model with Optimal Control and Stability Analysis. *Int. J. Appl. Comput. Math.* 8(28), 2022.
101. Wang H, Wang Z, Dong Y, Chang R, et al. Phase-adjusted estimation of the number of Coronavirus Disease 2019 cases in Wuhan, China. *Cell. Discov.* 6(10), 2020.
102. Wu J.T, Leung K, Leung G.M. Now casting and forecasting the potential domestic and international spread of the 2019-ncov outbreak originating in wuhan, china: a modelling study. *The Lancet*, 395, 689-697, 2020.
103. Anderson R.M, May R.M. *Infectious Diseases of Humans.* Oxford University Press, Oxford. 1991.
104. Bushnaq S, Khan S, Shah K, Zaman G. Mathematical analysis of HIV/AIDS infection model with Caputo-Fabrizio fractional derivative. *Cogent Math. Stat.* 5, 1432521, 2018.

105. Ghanbari B, Kumar S, Kumar R. A study of behaviour for immune and tumor cells in immune genetic tumour model with non-singular fractional derivative. *Chaos Solitons Fract.* 133, 109619, 2020.
106. Ullah S, Khan M.A, Farooq M, Hammouch Z, Baleanu D. A fractional model for the dynamics of tuberculosis infection using Caputo-Fabrizio derivative. *Discrete Contin. Dyn. Syst. Ser. S* 13(3), 975–993, 2020.
107. Daftardar-Gejji V, Jafari H. An iterative method for solving nonlinear functional equations, *J. Math. Anal. Appl.* 316, 753–763, 2006.
108. Sontakke B.R, Shaikh A.S, Nisar K.S. Approximate solutions of a generalized Hirota–Satsuma coupled KdV and a coupled mKdV systems with time fractional derivatives. *Malaysian J. Math. Sci.* 12(2), 173–193, 2018.
109. Mouaouine A, Boukhouima A, Hattaf K, Yousf N. A fractional order sir epidemic model with nonlinear incidence rate. *Adv. Differ. Equ.* 1, 1–9, 2018.
110. Kumar S. A new analytical modelling for fractional telegraph equation via Laplace transform. *Appl. Math. Model.* 38, 3154–3163, 2014.
111. Shaikh A, Tassaddiq A, Nisar K.S, Baleanu D. Analysis of differential equations involving Caputo–Fabrizio fractional operator and its applications to reaction–diffusion equations. *Adv. Differ. Equ.* 178, 2019.
112. Akdim K, Ez-Zetouni A, Zahid M. The influence of awareness campaigns on the spread of an infectious disease: a qualitative analysis of a fractional epidemic model. *Model. Earth Syst. Environ.* 8, 1311–1319, 2022.
113. Raza A, Ch, Y.M, Bajuri M.Y, Ahmadian A, Ahmed N, Rafiq M, Salahshour S. Dynamical and nonstandard computational analysis of heroin epidemic model. *Results Phys.* 34, 105245, 2022.
114. Zhou J.C, Salahshour S, Ahmadian A, Senu N. Modeling the dynamics of COVID-19 using fractal-fractional operator with a case study. *Results Phys.* 33, 105103, 2022.
115. Shloof A.M, Senu N, Ahmadian A, Salahshour S. An efficient operation matrix method for solving fractal–fractional differential equations with generalized Caputo-type fractional–fractal derivative. *Math. Comput. Simul.* 188, 415–435, 2021.
116. Ahmed N, Raza A, Rafiq M, Ahmadian A, Batool N, Salahshour S. Numerical and bifurcation analysis of SIQR model. *Chaos Solit. Fract.* 150, 111133, 2021.

117. Salahshour S, Ahmadian A, Allahviranloo T. A new fractional dynamic cobweb model based on nonsingular kernel derivatives. *Chaos Solit. Fract.* 145, 110755, 2021.
118. Salahshour S, Ahmadian A, Pansera B.A, Ferrara M. Uncertain inverse problem for fractional dynamical systems using perturbed collage theorem. *Commun. Nonlinear Sci. Numer. Simul.* 94, 105553, 2021.
119. Salahshour S, Ahmadian A, Abbasbandy S, Baleanu D. M-fractional derivative under interval uncertainty: Theory, properties and applications. *Chaos Solit. Fract.* 117, 84-93, 2018.
120. Ahmad S.W, Sarwar M, Shah K, Ahmadian A, Salahshour S. Fractional order mathematical modeling of novel corona virus (COVID-19). *Math. Meth. Appl. Sci.* 1-14, 2021.
121. www.mohfw.gov.in: Retrieved 28th April, 2021.
122. www.cowin.gov.in: Retrieved 21 March 2021.
123. Paul S, Mahata A, Ghosh U, Roy B. SEIR epidemic model and scenario analysis of COVID-19 pandemic. *Ecol. Gene. Genom.* 19, 100087, 2021.
124. Mwalili S, Kimathi M, Ojiambo V, Gathungu D, Mbogo R. SEIR model for COVID-19, dynamics incorporating the environment and social distancing. *BMC Research Notes.* 13(1), 2020.
125. Losada J, Nieto J.J. Properties of the new fractional derivative without singular kernel. *Prog. Fract. Differ. Appl.* 1(2), 87–92, 2015.
126. Samko S.G, Kilbas A.A, Marichev O.I. *Fractional Integrals and Derivatives: Theory and Applications.* Gordon and Breach, Philadelphia. 1993.
127. Kilbas A, Srivastava H, Trujillo J. *Theory and Applications of Fractional Differential Equations,* North-Holland Mathematics Studies. 204, 2006.
128. Odibat Z. M, Shawagfeh N. T. Generalized taylor's formula. *Appl. Math. Comput.* 186, 286 – 293, 2007.
129. Perko L. *Differential Equations and Dynamical Systems.* Springer, New York. 2000.
130. Li M.Y, Smith H.L, Wang L. Global dynamics of an SEIR epidemic model with vertical transmission. *SIAM J Appl. Math.* 62, 58, 2001.

131. <https://www.worldometers.info/coronavirus/>
132. India COVID-19 Tracker. <https://www.covid19india.org/2020>. Retrieved: 2021-05-17
133. Wang C, Horby P. W, Hayden F. G, Gao G. F. A novel coronavirus outbreak of global health concern, *The Lancet*. 395(10223), 470-473, 2020.
134. “Centers for disease control and prevention: 2019 novel coronavirus.”
135. Dietz K, Heesterbee J.A. Bernoulli was ahead of modern epidemiology. *Nature*. 408(6812), 513–514, 2000.
136. Das P, Upadhyay R.K, Misra A.K, Rihan F.A, Das P, Ghosh D. Mathematical model of COVID-19 with comorbidity and controlling using non-pharmaceutical interventions and vaccination. *Nonlinear Dyn.* 106, 1213–1227, 2021.
137. Das P, Nadim S.S, Das S, Das P. Dynamics of COVID-19 transmission with comorbidity: a data driven modelling based approach. *Nonlinear Dyn.* 106, 1197–1211, 2021.
138. Garrappa R. On linear stability of predictor–corrector algorithms for fractional differential equations. *Int. J. Comput. Math.* 87:10, 2281–2290, 2010.
139. Das M, Samanta G.P. A prey-predator fractional order model with fear effect and group defense. *Int. J. Dyn. Contr.* 9, 334–349, 2020.
140. Baleanu D, Sajjadi S.S, Jajarmi A, Deftarli O, Asad J.H. The fractional dynamics of a linear triatomic molecule. *Rom. Rep. Phys.* 73(1), 105, 2021.
141. Ucar S. Analysis of a basic SEIRA model with Atangana–Baleanu derivative. *AIMS Math.* 5(2), 1411–1424, 2020.
142. Baleanu D, Sajjadi S.S, Jajarmi A, Deftarli O. On a nonlinear dynamical system with both chaotic and non-chaotic behaviours: a new fractional analysis and control. *Adv. Differ. Equ.* 234, 2021.
143. Baleanu D, Zibaei S, Namjoo M, Jajarmi A. A nonstandard finite difference scheme for the modelling and nonidentical synchronization of a novel fractional chaotic system. *Adv. Differ. Equ.* 308, 2021.
144. Baleanu D, Sajjadi S.S, Asad J.H, Jajarmi A, Estiri E. Hyperchaotic behaviours, optimal control, and synchronization of a nonautonomous cardiac conduction system. *Adv. Differ. Equ.* 2021. 157, 2021.

145. Kilbas A, Srivastava H, Trujillo J. Theory and Applications of Fractional Differential Equations. North-Holland Mathematics Studies. 204, 2006.
146. Losada J, Nieto J.J. Properties of the new fractional derivative without singular kernel. Prog. Fract. Differ. Appl. 1(2), 87–92, 2015.
147. Kexue L, Jigen P. Laplace transform and fractional differential equations. Appl. Math. Lett. 24, 2019–2023, 2011.
148. Petras I. Fractional-Order Nonlinear Systems: Modeling Aanlysis and Simulation; Higher Education Press: Beijing, China. 2011.
149. Liang S, Wu R, Chen L. Laplace transform of fractional order differential equations. Electron. J. Differ. Equ. 2015(139), 1-15, 2015.
150. Li Y, Chen Y, Podlubny I. Stability of fractional-order nonlinear dynamic systems: Lyapunov direct method and generalized Mittag-Leffler stability. Comput. Math. Appl. 59, 1810–1821, 2010.
151. Zhang Z, Kundu S, Tripathi J.P, Bugalia S. Stability and Hopf bifurcation analysis of an SVEIR epidemic model with vaccination and multiple time delay. Chaos Solit. Fract. 131(C), 2019.
152. Upadhyay R.K, Kumari S, Misra A.K. Modeling the virus dynamics in computer network with SVEIR model and nonlinear incident rate. J. Appl. Math. Comput. 54, 485–509, 2017.
153. Dokoumetzidis A, Magin R, Macheras P. A commentary on fractionalization of multi-compartmental models. J. Pharmacokinet Pharmacodyn . 37, 203–207, 2010.
154. Pongkitivanichkul C, Samart D, Tangphati T, Koomhin P, Pimton P, Dam-o P, Payaka A and Channuie P, Estimating the size of COVID-19 epidemic outbreak, Phys. Scr. 95 085206, 2020.
155. Gaff H, Schaefer E. Optimal control applied to vaccination and treatment strategies for various epidemiological models. Math. Biosci. Eng. 6, 469–492, 2009.
156. <https://data.worldbank.org/indicator/SP.DYN.CBRT.IN?locations=IN>
157. Rothan H.A, Byraredddy S.N. The epidemiology and pathogenesis of coronavirus disease (COVID-19) outbreak. J. Autoimmun.. 109:102433, 2020.
158. Bai Y, Yao L, Wei T, et al. Presumed asymptomatic carrier transmission of COVID-19. JAMA. 323(14), 1406-07, 2020.

159. Australian. Health Protection Principal Committee (AHPPC) coronavirus (COVID-19) statement on April 16, 2020, Australian Government Department of Health.
160. Khan M.A, Atangana A. Modeling the dynamics of novel coronavirus (2019-ncov) with fractional derivative. *Alexandria Eng. J.* 59(4): 2379–2389, 2020.
161. <https://covid19.who.int/> Accessed 20th February, 2022.
162. <https://www.worldometers.info/coronavirus/> Accessed 20th February, 2022.
163. L´opez L, Rodo X. A modified SEIR model to predict the covid-19 outbreak in spain and italy: simulating control scenarios and multi-scale epidemics. *Results Phys.* 21: 103746, 2021.
164. Rodriguez OT, Conde-Guti´errez RA, Hern´andez-Javier RA. Modeling and prediction of covid-19 in mexico applying mathematical and computational models. *Chaos Solit. Fract.* 138, 109946, 2020.
165. Kumar S, Kumar R, Osman MS, Samet B. A wavelet based numerical scheme for fractional order SEIR epidemic of measles by using Genocchi polynomials. *Numer. Methods Partial Differ. Equ.* 37(2): 1250–68, 2021.
166. Nyabadza F, Chirove F, Chukwu CW, Visaya MV. Modelling the potential impact of social distancing on the covid-19 epidemic in south africa. *Comput Math Methods Med.* 2020.
167. Chu YM, Ali A, Khan MA, Islam S, Ullah S. Dynamics of fractional order covid-19 model with a case study of saudiarabia. *Results Phys.* 21: 103787, 2021.
168. Adiga A, Dubhashi D, Lewis B, Marathe M, Venkatramanan S, Vullikanti A. Mathematical models for covid-19 pandemica comparative analysis. *J. Indian Inst. Sci.* 1–15, 2020.
169. Higazy M. Novel fractional order sidarthe mathematical model of covid-19 pandemic. *Chaos Solit. Fract.* 138: 110007, 2020.
170. Arqub O.A, Osman M.S, Abdel-Aty A.H, Mohamed A.B, Momani S. A numerical algorithm for the solutions of ABC singular LaneEmden type models arising in astrophysics using reproducing kernel discretization method. *Mathematics.* 8(6): 923, 2020.
171. Shah K, Arfan M, Mahariq I, Ahmadian A, et al. Fractal-Fractional Mathematical Model Addressing the Situation of Corona Virus in Pakistan. *Results Phys.* 19: 103560, 2020.

172. Din A, Shah K, Seadawy A, Alrabaiah H, Baleanu D. On a new conceptual mathematical model dealing the current novel coronavirus-19 infectious disease. *Results Phys.* 19: 103510, 2020.
173. Khan A, Shah K, Abdeljawad T, Alqudah M.A. Existence of results and computational analysis of a fractional order two strain epidemic model. *Results Phys.* 39: 105649, 2022.
174. Shah K, Irfan M, Ullah A, Mdallal Q, Ansari K, et al. Computational study on the dynamics of fractional order differential equations with application. *Chaos Solit. Fract.* 157 (4):1813-37, 2022..
175. Kumar A, Prakash A, Baskonus HM. The epidemic COVID-19 model via Caputo–Fabrizio fractional operator. *Taylor and Francis.* 1-15, 2022.
176. Gao W, Veeresha P, Cattani C, Baishya C, Baskonus HM. Modified Predictor–Corrector Method for the Numerical Solution of a Fractional-Order SIR Model with 2019-nCoV. *Fractal and Fractional.* 6(2), 92, 2022.
177. Gao W, Baskonus HM. Deeper investigation of modified epidemiological computer virus model containing the Caputo operator. *Chaos Solit. Fract.* 158: 112050, 2022.
178. Wan H, Cui JA, Yang GJ. Risk estimation and prediction by modeling the transmission of the novel coronavirus (COVID-19) in mainland China excluding Hubei province. *medRxiv.* 2020.
179. Boudaoui A, El hadj Moussa Y, Hammouch Z, Ullah S. A fractional-order model describing the dynamics of the novel coronavirus (COVID-19) with nonsingular kernel. *Chaos Solit. Fract.* 146(1): 110859, 2021.
180. Sahoo P, Mondal HS, Hammouch Z, Abdeljawad T, Mishra D, Reza M. On the necessity of proper quarantine without lock down for 2019-nCoV in the absence of vaccine. *Results Phys.* 1(25), 104063, 2021.
181. Ahmad S.W, Sarwar M, Shah K, Ahmadian A, Salahshour S. Fractional order mathematical modeling of novel corona virus (COVID-19). *Math. Meth. Appl. Sci.* 1-14, 2021.
182. Zamir M, Nadeem F, Abdeljawad T, Hammouch Z. Threshold condition and non pharmaceutical interventions control strategies for elimination of COVID-19. *Results Phys.* 1(20), 103698, 2021.

183. Shloof A.M, Senu N, Ahmadian A, Salahshour S. An efficient operation matrix method for solving fractal–fractional differential equations with generalized Caputo-type fractional–fractal derivative. *Math. Comput. Simul.* 188, 415–435, 2021.
184. Katugampola U.N. New approach to a generalized fractional integral. *Appl. Math. Comput.* 218(3), 860–865, 2011.
185. Atangana A, Baleanu D. New fractional derivatives with non-local and non-singular kernel theory and application to heat transfer model. *Therm. Sci.* 20(2), 763–769, 2016.
186. Naik PA, Yavuz M, Qureshi S, Zu J, Townley S. Modeling and analysis of COVID-19 epidemics with treatment in fractional derivatives using real data from Pakistan. *Eur. Phys. J. Plus.* 135(10), 795, 2020.
187. Daşbaşı B. Stability analysis of an incommensurate fractional-order SIR model. *Mathematical Modelling and Numerical Simulation With Applications.* 1(1), 44–55, 2021.
188. Yavuz M, Coşar F, Günay F, Özdemir F. A New Mathematical Modeling of the COVID-19 Pandemic Including the Vaccination Campaign. *Open Journal of Modelling and Simulation.* 9, 299–321, 2021.
189. Allegretti S, Bulai IM, Marino R, Menandro MA, Parisi K. Vaccination effect conjoint to fraction of avoided contacts for a Sars-Cov-2 mathematical model. *Mathematical Modelling and Numerical Simulation With Applications.* 1(2), 56–66, 2021.
190. Ikram R, Khan A, Zahri M, Saeed A, Yavuz M, Kumam P. Extinction and stationary distribution of a stochastic COVID-19 epidemic model with time-delay. *Comput. Biol. Med.* 141, 105115, 2022.
191. Kumar P, Erturk V.S. Dynamics of cholera disease by using two recent fractional numerical methods. *Mathematical Modelling and Numerical Simulation With Applications.* 1(2), 102–111, 2021.
192. Joshi H, Jha BK. Chaos of calcium diffusion in Parkinson’s infectious disease model and treatment mechanism via Hilfer fractional derivative. *Mathematical Modelling and Numerical Simulation With Applications.* 1(2), 84–94, 2021.
193. Özköse F, Şenel MT, Habbireeh R. Fractional-order mathematical modelling of cancer cells-cancer stem cells-immune system interaction with chemotherapy. *Mathematical Modelling and Numerical Simulation With Applications.* 1(2), 67–83, 2021.

194. Zamir M, Nadeem F, Abdeljawad T, Hammouch Z. Threshold condition and non pharmaceutical interventions control strategies for elimination of COVID-19. *Results Phys.* 1(20), 103698, 2021.
195. Diethelm KA. *The Analysis of Fractional Differential Equations*. Springer. Berlin. 2010.
196. World-population. Italy. <https://www.worldometers.info/world-population/italy-population>.
197. Statistics. Birth rate in Italy. <https://www.statista.com/statistics/567936/birth-rate-in-italy>.
198. Das M, Samanta G. Stability analysis of a fractional ordered COVID-19 model. *Comput. Math. Biophys.* 9(1), 22-45, 2021.
199. World Health Organization (WHO), 2018. Dengue. <http://www.who.int/dengue-control/epidemiology/en>.
200. Bhatt S, Gething P.W, Brady O.J, et al. The global distribution and burden of dengue. *Nature.* 496(7446), 504–507, 2013.
201. Shekhar C, Deadly dengue: new vaccines promise to tackle this escalating global menace. *Chem. Biol.* 14(8), 871–872, 2007.
202. Brady O.J, Gething P.W, Bhatt S, et al. xRefining the global spatial limits of dengue virus transmission by evidence-based consensus. *PLoS Negl. Trop. Dis.* 6(8), e1760, 2012.
203. Derouich M, Boutayeb A. Dengue fever: mathematical modelling and computer simulation. *Appl. Math. Comput.* 177(2), 528–544, 2006.
204. Esteva L, Vargas C, Influence of vertical and mechanical transmission on the dynamics of dengue disease. *Math. Biosci.* 167(1), 51–64, 2000.
205. Rodrigues H.S, Monteiro M.T.M, Torres F.M.D. Vaccination models and optimal control strategies to dengue. *Math. Biosci.* 247, 1–12, 2014.
206. Sardar T, Rana S, Chattopadhyay J. A mathematical model of dengue transmission with memory. *Commun. Nonlinear Sci. Numer. Simul.* 22(13), 511–525, 2015.
207. Qureshi S, Atangana A. Mathematical analysis of dengue fever outbreak by novel fractional operators with field data. *Phys. A. Stat. Mech. Appl.* 526, 121127, 2019.

208. Derouich M, Outayeb A, Twizell E.H. A model of dengue fever. *BioMedical Journal on Line Central*. 2(1), 1-10, 2003.
209. Esteva L, Vargas C. Analysis of a dengue disease transmission model. *Math. Biosci.* 150(2), 131-151, 1998.
210. Esteva L, Vargas C. A model for dengue disease with variable human population. *J. Math. Biol.* 38(3), 220-240, 1999.
211. Phaijoo G.R, Gurung D.B. Mathematical study of dengue disease transmission in multi-patch environment. *Appl. Math.* 7(14), 1521-1533, 2016.
212. Pinho S.T.R, Ferreira C.P, Esteva L, Barreto F.R.K, et al. Modelling the dynamics of dengue real epidemics. *Phil. Trans. R. Soci.* 368(1933), 5679- 5693, 2010.
213. Sardar T, Rana S, Chattopadhyay J. A mathematical model of dengue transmission with memory. *Commun. Nonlinear Simmulat.* 22(1), 511-525, 2015.
214. Soewono E, Supriatna A.K. A two - dimensional model for the transmission of dengue fever disease. *Bull. Malaysian Math. Sc. Soc.* 24(1), 49-57, 2001.
215. Chan M, Johansson M.A, The Incubation periods of dengue viruses. *PLoS ONE*. 7(11), e50972, 2012.
216. Parand K, Razzaghi M. Rational Legendre approximation for solving some physical problems on semi-infinite intervals. *Phys. Scr.* 69, 353, 2004.
217. Side S, Noorani M.S.M. SEIR model for transmission of dengue fever. *Int. J. Adv. Sci. Eng. Inf. Techno.* 2(5), 380-389, 2012.
218. Zulqurnain S, et al. Numerical treatment for the nonlinear fifth kind of multi-singular differential model: a neuro-swarving approach. *Phys. Scr.* 97, 075203, 2022.
219. Khan T, et al. Modeling the dynamics of the SARS-CoV-2 virus in a population with asymptomatic and symptomatic infected individuals and vaccination. *Phys. Scr.* 96, 104009, 2021.
220. Senapati A, Sardar T, Ganguly K.S, Chattopadhyay A.K, Chattopadhyay J. Impact of adult mosquito control on dengue prevalence in a multi-patch setting: a case study in Kolkata. *J. Theor. Biol.* 478, 139–152, 2019.

221. Olaniyi S, Alade T.O, Chuma F.M, Ogunsola A.W, Aderele O.R, Abimbade S.F. A fractional-order nonlinear model for a within-host chikungunya virus dynamics with adaptive immunity using Caputo derivative operator, *Healthc. Anal.* 4, 2023.
222. Cosner C, Beier J.C, Cantrell R.S, Impoinvil D, Kapitanski L, Potts M.D, Troyo A, Ruan S. The effects of human movement on the persistence of vector-borne diseases. *J. Theor. Biol.* 258 (4), 550–560, 2009.
223. Thabet H, Kendre S. A fractional mathematical model with nonlinear partial differential equations for transmission dynamics of severe acute respiratory syndrome coronavirus 2 infection. *Healthc. Anal.* 4, 100209, 2023.
224. Shaikh A, Sontakke B.R. Impulsive initial value problems for a class of implicit fractional differential equations. *Comput. Methods Differ. Equ.* 8(1), 141–154, 2020.
225. Alaje A. I, Olayiwola M. O. A fractional-order mathematical model for examining the spatiotemporal spread of COVID-19 in the presence of vaccine distribution. *Healthc. Anal.* 4, 100230, 2023.
226. Paul S, Mahata A, Mukherjee S, Mali P.C, Roy B. Fractional order SEIQRD epidemic model of Covid-19: A case study of Italy. *PLoS ONE.* 18(3). e0278880, 2023.
227. Khan M.A, Fatmawati. Dengue infection modeling and its optimal control analysis in East Java, Indonesia. *Heliyon.* 7(1), e06023, 2021.
228. Communicable Diseases Division, Ministry of Health, Singapore.
229. Vijayalakshmi G.M, Roselyn B.P. Vaccination control measures of an epidemic model with long-term memristive effect. *J. Comput. Appl. Math.* 419, 114738, 2023.
230. Baba I.A, Hincal E. A model for influenza with vaccination and awareness. *Chaos Solit. Fract.* 106, 9-55, 2018.
231. Abioye A. I, Peter O. J, et al. A fractional-order mathematical model for malaria and COVID-19 co-infection dynamics. *Healthc. Anal.* 4, 100210, 2023.
232. Podlubny I. *Fractional Differential Equations.* Academic Press, San Diego, 1999.
233. Lian W, Liu X. Non-Convex Fractional-Order TV Model for Impulse Noise Removal. *J. Comput. Appl. Math.* 417, 114615, 2023.

234. Diethelm K. A fractional calculus based model for the simulation of an out-break of dengue fever. *Nonlinear Dyn.* 71(4), 613-619, 2012.
235. Prosper O, Ruktanonchai N, Martcheva M. Assessing the role of spatial heterogeneity and human movement in malaria dynamics and control. *J. Theor. Biol.* 303, 1–14, 2012.
236. Khan A, Khan H, Gomez-Aguilar J.F, Abdeljawad T. Existence and Hyers-Ulam stability for a nonlinear singular fractional differential equations with Mittag-Leffler kernel. *Chaos Solit. Fract.* 127, 422-427, 2019.
237. Annas S, Pratama M.I, Rifandi M, Sanusi W, Side S. Stability Analysis and Numerical Simulation of SEIR Model for pandemic COVID-19 spread in Indonesia. *Chaos Solit. Fract.* 139, 110072, 2020.
238. Jajarmi A, Baleanu, D. A new fractional analysis on the interaction of HIV with CD4+ T-cells. *Chaos Solit. Fract.* 113, 221–229, 2018.
239. Evirgen F. Transmission of Nipah virus dynamics under Caputo fractional derivative. *J. Comput. Appl. Math.* 418, 114654, 2023.
240. Zheng T.T, Nie L.F. Modelling the transmission dynamics of two-strain Dengue in the presence awareness and vector control. *J. Theor. Biol.* 443, 82–91, 2018.
241. Abboubakar H, Kamgang J.C, Nkamba L.N, et al. Bifurcation thresholds and optimal control in transmission dynamics of arboviral diseases. *J. Math. Biol.* 76, 379–427, 2018.
242. Pandey A, Mubayi A, Medlock J. Comparing vector-host and SIR models for dengue transmission. *J. Math. Biol.* 246(2), 252–259, 2013.
243. Feng Z, Velasco-Hernandez J.X. Competitive exclusion in a vector-host model for the dengue fever. *J. Math. Biol.* 35(5), 523–544, 1997.
244. Dumont Y, Chiroleu F. Vector control for the Chikungunya disease. *Math. Biosci. Eng.* 7, 313–345, 2010.
245. <https://www.moh.gov.sg/resources-statistics/infectious-disease-statistics/2020>.
246. Kermack WO, McKendrick AG. Contributions to the mathematical theory of epidemics. II. The problem of endemicity. *Proc R Soc Lond Ser A.* 138(834), 55–83, 1932.

247. Mukherjee D. Stability analysis of an S-I epidemic model with time delay. *Math Comput. Model.* 24(9), 63–68, 1996.
248. d’Onofrio A, Manfredi P, Salinelli E. Vaccinating behaviour, information, and the dynamics of SIR vaccine preventable diseases. *Theor Popul Biol.* 71(3), 301–317, 2007.
249. Buonomo B, d’Onofrio A, Lacitignola D. Global stability of an SIR epidemic model with information dependent vaccination. *Math Biosci.* 216(1), 9–16, 2008.
250. Hattaf K, Lashari AA, Louartassi Y, Yousfi N. A delayed SIR epidemic model with general incidence rate. *Electron J Qual Theory Differ Equ.* 3, 1–9, 2008.
251. Dubey B, Patra A, Srivastava PK, Dubey US. Modeling and analysis of an SEIR model with different types of nonlinear treatment rates. *J Biol. Syst.* 21(3), 1350023, 2013.
252. Tipsri S, Chinviriyasit W. Stability analysis of SEIR model with saturated incidence and time delay. *Int. J. Appl. Phys. Math.* 4(1), 42–45, 2014.
253. Henderson DA. Smallpox-the death of a disease. Prometheus Books, Amherst. 2009.
254. Li B, Liang HJ, Shi L, He QZ. Complex dynamics of Kopel model with non symmetric response between oligopolists. *Chaos Solit. Fract.* 156, 111860, 2022.
255. Yunshen CW, Ming Y, UR RM, Ibrahim M, Anwar Z. Mathematical analysis of HBV and HCV co-infection model under non-singular fractional order derivative. *Results Phys.* 28, 104582, 2021.
256. Li B, Liang HJ, Shi L, He QZ. Multiple and generic bifurcation analysis of a discrete Hindmarsh-Rose model. *Chaos Solit. Fract.* 146, 110856, 2021.
257. Xu C, Rahman M, Baleanu D. On fractional-order symmetric oscillator with offset-boosting control. *Nonlinear Analysis: Modelling and Control.* 27(5), 994-1008, 2022.
258. Eskandari Z, Avazzadeh Z, Khoshsiar GR, Li B. Dynamics and bifurcations of a discrete-time Lotka–Volterra model using nonstandard finite difference discretization method. *Math Meth. Appl. Sci.* 1- 16, 2022.
259. Li R, He Z. Stability analysis of time-delay differential systems with impulsive effect suffered by logic choice. *Results Control Optim.* 4, 100026, 2021.

260. Panja P, Gayen S, Kar T, Jana DK. Complex dynamics of a three species predator–prey model with two nonlinearly competing species. *Results Control Optim.* 8, 1000153, 2022.
261. Ranjan A, Mehta U. Fractional filter IMC-TDD controller design for integrating processes. *Results Control Optim.* 8, 100155, 2022.
262. Khan H, Gomez-Aguilar JF, Abdeljawad T, Khan A. Existence results and stability criteria for abc-fuzzy-volterra integro-differential equation. *Fractals.* 28(8), 1-9, 2020.
263. Khan A, Alshehri HM, Gomez-Aguilar JF. et al. A predator–prey model involving variable-order fractional differential equations with Mittag-Leffler kernel. *Adv. Differ. Equ.* 183, 2021.
264. Khan H, Tun c C, Khan A. Stability results and existence theorems for nonlinear delay-fractional differential equations with (P -operator[J]). *J. Appl. Anal.* 10(2), 584-597, 2020.
265. Wang W, Ruan S. Bifurcation in an epidemic model with constant removal rates of the infective. *J. Math. Anal. Appl.* 21, 775–793, 2004.
266. Zhang X, Liu X. Backward bifurcation of an epidemic model with saturated treatmentFunction. *J. Math. Anal. Appl.* 348, 433–443, 2008.
267. Zhang Z, Suo S. Qualitative analysis of a SIR epidemic model with saturated treatment rate, *J. Appl. Math. Comput.* 34, 177–194, 2010.
268. Zhou L, Fan M. Dynamics of a SIR epidemic model with limited medical resources revisited, *Nonlinear Anal.: RWA.* 13, 312–324, 2012.
269. Seidu B, Asamoah J.K.K, Wiah E.N, Ackora-Prah J. A comprehensive cost-effectiveness analysis of control of maize streak virus disease with Holling’s Type II predation form and standard incidence. *Results Phys.* 40, 105862, 2022.
270. Asamoah J.K.K, Okyere E, Yankson E, Opoku AA, Adom-Konadu A, Acheampong E, Dissou Arthur Y. Non-fractional and fractional mathematical analysis and simulations for Q fever. *Chaos Solit. Fract.* 156, 111821, 2022.
271. Addai E, Zhang L, Preko A.K, Asamoah J.K.K. Fractional order epidemiological model of SARS-CoV-2 dynamism involving Alzheimer’s disease. *Healthc. Anal.* 2, 100114, 2022.

272. Zhang L, Addai E, Ackora-Prah J, Arthur Y.D, Asamoah J.K.K. Fractional-Order Ebola-Malaria Coinfection Model with a Focus on Detection and Treatment Rate. *Comput. Math Methods Med.* 6502598, 2022.
273. Asamoah J.K.K. Fractal-fractional model and numerical scheme based on Newton polynomial for Q fever disease under Atangana-Baleanu derivative. *Results Phys.* 34, 105189, 2022.
274. Okyere E, Seidu B, Nantomah K, Joshua Kiddy K. Asamoah JKK. Fractal-fractional SIRS epidemic model with temporary immunity using Atangana-Baleanu derivative. *Commun. Math. Biol. Neurosci.* 72, 2022.
275. Das M, Samanta G, De la Sen M. A Fractional Ordered COVID-19 Model Incorporating Comorbidity and Vaccination. *Mathematics.* 9, 2806, 2021.
276. Veisi A, Delavari H. A novel fractional-order feedback management of COVID-19 prevalence. *Journal of Statistics and Management Systems.* 25(6), 1345-1359, 2022.
277. Odibat Z, Shawagfeh N. Generalized Taylor's formula. *Appl. Math. Comput.* 186, 286-293, 2007.
278. Mainardi F. On some properties of the Mittag-Leffler function completely monotone for $t > 0$ with $0 < \alpha < 1$, *AIMS.* 19(7): 2267-2278, 2014.
279. Mohammad J, Nemat N. A fractional-order toxin producing phytoplankton and zoo-plankton system. *International Journal of Biomathematics.* 7:1450039, 2014.
280. Sastry S. *Analysis, Stability and Control*, Springer, New York. 1999.
281. Hethcote H.W, Driessche P.V.D. An SIS epidemic model with variable population size and a delay. *J. Math. Biol.* 34(2), 177–194, 1995.
282. Paul S, Mahata A, Mukherjee S, Roy B, Salimi M, Ahmadian A. Study of Fractional Order SEIR Epidemic Model and Effect of Vaccination on the Spread of COVID-19. *Int. J. Appl. Comput. Math.* 8, 237, 2022.
283. Samui P, Mondal J, Ahmad B, et al. Clinical effects of 2-DG drug restraining SARS-CoV-2 infection: A fractional order optimal control study. *J. Biol. Phys.* 2022.
284. Shekhawat U, Chowdhury R, Chakravarty A. Computational and comparative investigation of hydrophobic profile of spike protein of SARS-CoV-2 and SARS-CoV. *J. Biol. Phys.* 2022.

285. Allegretti S, Bulai I.M, Marino R, Menandro M.A, Parisi K. Vaccination effect conjoint to fraction of avoided contacts for a Sars-Cov-2 mathematical model. *Mathematical Modelling and Numerical Simulation with Applications*. 1(2), 56-66, 2021.
286. Nindjin A.F, Aziz-Alaoui M.A. Persistence and global stability in a delayed Leslie-Gower type three species food chain. *J. Math. Anal. Appl.* 340, 340–357, 2008.
287. Iwa L. L, Nwajeri U. K, Atede A. O, Panle A.B, Egeonu K. U. Malaria and cholera co-dynamic model analysis furnished with fractional-order differential equations. *Mathematical Modelling and Numerical Simulation with Applications*. 3(1), 33-57, 2023.
288. Barman D, Roy J, Alam S, Trade-off between fear level induced by predator and infection rate among prey species. *J. Appl. Math.* 64 (1), 635–663, 2020.
289. Das S, Das P, Das P. Optimal control of behaviour and treatment in a non-autonomous SIR model. *Int. J. Dyn. Syst. Differ. Equ.* 11(2), 108-130, 2021.
290. Hammouch Z, Yavuz M, Ozdemir N. Numerical solutions and synchronization of a variable-order fractional chaotic system. *Mathematical Modelling and Numerical Simulation with Applications*. 1(1), 11-23, 2021.
291. Dasbası B. Stability analysis of an incommensurate fractional-order SIR model. *Mathematical Modelling and Numerical Simulation with Applications*. 1(1), 44-55, 2021.
292. Gholami M, Ghaziani R.K, Eskandari Z. Three-dimensional fractional system with the stability condition and chaos control. *Mathematical Modelling and Numerical Simulation with Applications*. 2(1), 41-47, 2022.
293. Diethelm K, Ford N.J. Analysis of Fractional Differential Equations. *J. Math. Anal. Appl.* 265(2), 229-248, 2002.
294. Rahaman M, Mondal S.P, Alam S, Metwally A.S.M, Salahshour S, Salimi M. Manifestation of interval uncertainties for fractional differential equations under conformable derivative. *Chaos Solit. Fract.* 165, 11275, 2022.
295. Barman D, Roy J, Alrabaiah H, Panja P, Mondal S.P, Alam S. Impact of predator incited fear and prey refuge in a fractional order prey predator model. *Chaos Solit. Fract.* 142, 110420, 2021.
296. Nguyen T.T.H, Nguyen N.T, Tran M.N. Global fractional Halanay inequalities approach to finite-time stability of nonlinear fractional order delay systems. *J. Math. Anal. Appl.* 525(1), 127145, 2023.